

NILOOFAR OKATI

# Modeling and Analysis of Massive Low Earth Orbit Communication Networks



NILOOFAR OKATI

# Modeling and Analysis of Massive Low Earth Orbit Communication Networks

ACADEMIC DISSERTATION

To be presented, with the permission of  
the Faculty of Information Technology and Communication Sciences  
of Tampere University,

for public discussion in the Auditorium TB109  
of the Tietotalo building, Korkeakoulunkatu 1, Tampere,  
on 14<sup>th</sup> of April 2023, at 12 o'clock.

## ACADEMIC DISSERTATION

Tampere University, Faculty of Information Technology and Communication Sciences  
Finland

*Responsible  
supervisor  
and Custos*

Associate Professor  
Taneli Riihonen  
Tampere University  
Finland

*Pre-examiners*

Professor  
Harpreet S. Dhillon  
Virginia Tech  
USA

Associate Professor  
Güneş Karabulut Kurt  
Polytechnique Montréal  
Canada

*Opponent*

Professor  
François Baccelli  
Institut national de recherche en  
informatique et en automatique (INRIA)  
France

The originality of this thesis has been checked using the Turnitin OriginalityCheck service.

Copyright ©2023 author

Cover design: Roihu Inc.

ISBN 978-952-03-2811-5 (print)

ISBN 978-952-03-2812-2 (pdf)

ISSN 2489-9860 (print)

ISSN 2490-0028 (pdf)

<http://urn.fi/URN:ISBN:978-952-03-2812-2>



Carbon dioxide emissions from printing Tampere University dissertations have been compensated.

PunaMusta Oy – Yliopistopaino  
Joensuu 2023



*To all the genuine mentors in my life*



# PREFACE

This thesis presents a summary of the research work conducted during the years 2018–2022 at Tampere University, Tampere, Finland; a journey that not only contributed to several original publications but also to the author’s personal growth. I would like to acknowledge the financial support received from the Faculty of Information Technology and Communication Sciences, Tampere University, Nokia University Donation, the Academy of Finland, Tampere University Industrial Fund, Nokia Foundation, and DELTA network. Obviously, this work could not be accomplished without their support.

First of all, I would like to express my sincere gratitude to my exceptional supervisor Prof. Taneli Riihonen for his unreserved and wholehearted support. The knowledge and skills he imparted upon me will have a profound and ever-lasting impact on both my professional development as a researcher and shaping me as a person. I believe that I gained an unwavering confidence built upon the lessons I learnt from him that will remain with me beyond my Ph.D. journey.

Next, I would like to gratefully thank my pre-examiners, Prof. Gunes Karabulut Kurt from Polytechnique Montréal and Prof. Harpreet S. Dhillon from Virginia Tech for their invaluable comments and feedback that helped me to improve the quality of this thesis. I also wish to express my appreciation to Prof. François Baccelli for agreeing to serve as my opponent during the public examination of this thesis.

I would like to also appreciate my collaborators throughout this journey for all their inspiration and support. Especially, I would like to thank Prof. Risto Wichman and M.Sc. Ilari Angervuori from Aalto University, and D.Sc. Dani Korpi from Nokia Bell labs for their contributions and invaluable feedback in our co-authored publications. I also enjoyed collaborating with M.Sc. Anastasia Yastrebova, D.Sc. Mikko Vehkaperä, and Prof. Marko Höyhty from VTT Technical Research Centre of Finland Ltd., for shared insights and feedback on a co-authored paper. I must also extend my thanks to Prof. Simona Lohan for always providing insightful discussions

during the Graduate Research Seminar in Communications Engineering.

I must extend my heartfelt thanks to all my colleagues at Tampere University, especially, Islam Tanash, Nachiket Ayir, Sahan Liyanaarachchi, Ruben Morales Ferre, Wenbo Wang, Selahattin Gökceli, and Karel Pärlin for being a great source of inspiration and making the Ph.D. journey a truly enjoyable one for me. I consider myself fortunate for receiving support from these individuals in all forms during my time at the university.

Last and foremost, I would like to express my deepest and the most heartfelt appreciation to Mehrdad, who walked this path alongside me since the start, providing a constant source of support and comfort throughout this journey. I am also highly grateful to my loving parents, Mehri and Haji, who always had faith in me and taught me that the sky is the limit. I am also deeply thankful to my adoring siblings, Nastaran and Nazanin, who are the endless source of happiness in my life. You are all the meaning of any achievement in my life!

Tampere, February 2023

Niloofar Okati

# ABSTRACT

Non-terrestrial networks are foreseen as a crucial component for developing 6th generation (6G) of wireless cellular networks by many telecommunication industries. Among non-terrestrial networks, low Earth orbit (LEO) communication satellites have shown a great potential in providing global seamless coverage for remote and under-served regions where conventional terrestrial networks are either not available or not economically justifiable to deploy. In addition, to the date of writing this summary, LEO communication networks have become highly commercialized with many prominent examples, compared to other non-terrestrial networks, e.g., high altitude platforms (HAPs) which are still in prototyping stage.

Despite the rapid promotion of LEO constellations, theoretical methodologies to study the performance of such massive networks at large are still missing from the scientific literature. While commercial plans must obviously have been simulated before deployment of these constellations, the deterministic and network-specific simulations rely on instantaneous positions of satellites and, consequently, are unable to characterize the performance of massive satellite networks in a generic scientific form, given the constellation parameters.

In order to address this problem, in this thesis, a generic tractable approach is proposed to analyze the LEO communication networks using stochastic geometry as a central tool. Firstly, satellites are modeled as a point process which enables using the mathematics of stochastic geometry to formulate two performance metrics of the network, namely, coverage probability and data rate, in terms of constellation parameters. The derivations are applicable to any given LEO constellation regardless of satellites' actual locations on orbits. Due to specific geometry of satellites, there is an inherent mismatch between the actual distribution of satellites and the point processes that are used to model their locality. Secondly, different approaches have thus been investigated to eliminate this modeling error and improve the accuracy of the analytical derivations.

The results of this research are published in seven original publications which are attached to this summary. In these publications, coverage probability and average achievable data rate of LEO satellite networks are derived for several communication scenarios in both uplink and downlink directions under different propagation models and user association techniques. Moreover, the analysis was generalized to cover the performance analysis of a multi-altitude constellation which imitates the geometry of some well-known commercial constellations with satellites orbiting on multiple altitude levels. While direct communication between the satellites and ground terminals is the main studied communication scenario in this thesis, the performance of a LEO network as a backhaul for aerial platforms is also addressed and compared with terrestrial backhaul networks.

Finally, all analytical derivations, obtained from stochastic modeling of the LEO constellations, are verified through Monte Carlo simulations and compared with actual simulated constellations to ensure their accuracy. Through the numerical results, the performance metrics are evaluated in terms of different constellation parameters, e.g., altitude, inclination angle, and total number of satellites, which reveals their optimal values that maximize the capacity and/or coverage probability. Therefore, other than performance analysis, several insightful guidelines can be also extracted regarding the design of LEO satellite networks based on the numerical results.

Stochastic modeling of a LEO satellite network, which is proposed for the first time ever in this thesis, extends the application of stochastic geometry in wireless communication field from planar two-dimensional (2D) networks to highly heterogeneous three-dimensional (3D) spherical networks. In fact, the results show that stochastic modeling can also be utilized to precisely model the networks with deterministic nodes' locations and specific distribution of nodes over the Euclidean space. Thus, the proposed methodology reported herein paves the way for comprehensive analytical understanding and generic performance study of heterogeneous massive networks in the future.

# CONTENTS

1	Introduction . . . . .	1
1.1	Background and motivation . . . . .	1
1.2	Objectives and scope of the thesis . . . . .	3
1.3	Contributions . . . . .	4
1.4	Author's contributions to the publications . . . . .	5
1.5	Thesis structure . . . . .	6
2	Overview of the massive LEO communication networks . . . . .	9
2.1	Background . . . . .	9
2.2	Constellation design and Keplerian elements . . . . .	12
2.3	System model . . . . .	14
2.4	Performance analysis . . . . .	23
3	Stochastic geometry analysis of wireless networks . . . . .	25
3.1	Stochastic Geometry . . . . .	25
3.1.1	Point processes . . . . .	26
3.1.2	Random measures and void probability . . . . .	27
3.2	The application of stochastic geometry in wireless communication . . . . .	28
3.2.1	Two-dimensional networks . . . . .	29
3.2.2	Three-dimensional networks . . . . .	30
4	Stochastic modeling of massive LEO communication networks . . . . .	33
4.1	Physical constellation vs. stochastic constellation . . . . .	33
4.2	Binomially distributed vs. Poissonly distributed constellation . . . . .	34
4.2.1	Serving distance distribution for BPP . . . . .	34
4.2.2	Effective number of satellites . . . . .	35
4.2.3	Serving distance distribution for NPPP . . . . .	37
4.2.4	Interference characterization . . . . .	40

4.3	Single-altitude vs. multi-altitude constellation. . . . .	42
4.4	LEO backhaul for airborne networks. . . . .	44
4.4.1	Overview of the related works . . . . .	44
4.4.2	Serving distance distribution . . . . .	45
5	Performance analysis . . . . .	47
5.1	Coverage probability . . . . .	47
5.1.1	Coverage probability for BPP distributed satellites. . . . .	47
5.1.1.1	Rayleigh fading. . . . .	49
5.1.1.2	Static channels . . . . .	51
5.1.1.3	Nakagami- $m$ fading . . . . .	52
5.1.1.4	Noise-limited system. . . . .	54
5.1.2	Coverage probability for NPPP distributed satellites . . . . .	56
5.1.2.1	Nakagami- $m$ fading . . . . .	56
5.1.2.2	Noise-limited system. . . . .	57
5.1.3	Global coverage probability. . . . .	58
5.2	Average achievable data rate. . . . .	58
5.2.1	Data rate for BPP distributed satellites . . . . .	58
5.2.2	Data rate for NPPP distributed satellites . . . . .	61
5.3	Numerical results and discussion . . . . .	62
5.3.1	Corroboration of analysis by simulations . . . . .	63
5.3.2	Effect of satellites' altitude . . . . .	67
5.3.3	Effect of ground terminal/user's latitude . . . . .	68
5.3.4	Effect of user association policy. . . . .	72
5.3.5	Performance of LEO backhaul network . . . . .	73
5.3.6	Summary of the results . . . . .	74
6	Conclusions . . . . .	77
6.1	Stochastic analysis of LEO Internet networks . . . . .	77
6.2	Future directions . . . . .	78
	References . . . . .	81
	Publication 1 . . . . .	95
	Publication 2 . . . . .	113



Publication 3 . . . . .	121
Publication 4 . . . . .	129
Publication 5 . . . . .	145
Publication 6 . . . . .	153
Publication 7 . . . . .	161

*List of Figures*

2.1	A sketch of the Walker constellation. . . . .	15
2.2	A sketch of the considered system model, where satellites are at altitude $r_{\oplus} + a_s$ and a ground user is located on Earth’s surface. . . . .	16
2.3	Relationship between the minimum required inclination angle and altitude to obtain global coverage. . . . .	17
2.4	Comparison of clutter layer losses versus the elevation angle for excess path loss model given in [47] and log-normal shadowing presented in this thesis. . . . .	21
3.1	Examples of Voronoi diagrams with points distributed randomly according to a BPP on a flat plane (a) and a sphere (b). . . . .	28
4.1	A sketch of the considered system model in [P1–P5]. . . . .	35
4.2	Effective number of satellites obtained from (4.3) for a LEO constellation comprised of 1000 and 2000 satellites. . . . .	37
4.3	Corroboration of serving distance distribution obtained from stochastic modeling for a constellation with 2000 satellites orbiting at altitude of 500 km. . . . .	39
4.4	A multi-altitude network consisting of satellites deployed at different altitudes ranging from $a_{\min}$ to $a_{\max}$ . . . . .	42
4.5	Schematic of an airborne network which can be backhauled by either LEO satellites or terrestrial BSs for uplink and/or downlink directions. . . . .	46

5.1	Distribution of population on different latitudes [101]. The maximum density of population can be observed at $26^\circ$ . . . . .	59
5.2	Global coverage probability for different constellation sizes and altitudes with $\iota = 53^\circ$ and $T = 5$ dB. . . . .	60
5.3	Verification of coverage probability derived in (5.1) with simulations for Rayleigh fading channels and 720 satellites at 1200 km. . . . .	63
5.4	Verification of coverage probability given in (5.19) with simulations for Rician fading channels with fading parameter 100, $\phi_u = 0^\circ$ , $\iota = 70^\circ$ , $a_s \in \{500, 1000, 1500\}$ km, and $\theta_{\min} = 10^\circ$ . . . . .	65
5.5	Verification of (5.22) with simulations when $\phi_u = 25^\circ$ , $\iota = 53^\circ$ , $m \in \{1, 2, 3\}$ , and $\theta_{\min} = 10^\circ$ . Theoretical and simulation results are shown by lines and markers, respectively. . . . .	66
5.6	Effect of the number of frequency bands, $K$ , on average achievable rate and verification of (5.28) for Rayleigh fading channels. . . . .	67
5.7	Verification of (5.35) with simulations when $\phi_u = 25^\circ$ , $\iota = 53^\circ$ , $m \in \{1, 2, 3\}$ , and $\theta_{\min} = 10^\circ$ . Theoretical and simulation results are shown by lines and markers, respectively. . . . .	68
5.8	Effect of altitude on the performance of a LEO network under Nakagami- $m$ fading. Shadowing distribution is assumed to be log-normal, $T = 5$ dB, $\phi_u = \{0^\circ, 25^\circ, 65^\circ\}$ , $\iota = 53^\circ$ , $m = 2$ , and $\theta_{\min} = 10^\circ$ . . . . .	69
5.9	Average rate for different altitudes. Plots are generated using (5.1) for three Walker constellations with $\phi_u = 0^\circ, 30^\circ, 60^\circ$ , and $N_{\text{eff}}(\iota, \phi_u)$ . . . . .	69
5.10	Effect of user's latitude on the performance of a LEO network. The markers are plotted by simulating three Walker constellations with $90^\circ$ , $70^\circ$ and $40^\circ$ inclination angles. . . . .	70
5.11	Effect of user's latitude on the performance of a LEO network for $K = 10$ , $T = 5$ dB, $r_{\min} = 500$ km, $\iota = 53^\circ$ , $m = 2$ , and $\theta_{\min} = 10^\circ$ . . . . .	70
5.12	The effect of user's latitude on the coverage probability for four multi-altitude constellations, given in [P7, Table I], when $T = 5$ and $N_{\text{act}} = 1800$ . The lines and the markers represent the analytical results and simulations, respectively. . . . .	71
5.13	Coverage probability and data rate under BSP and NSP association policies when $K = 10$ , $\phi_u = 25^\circ$ , $r_{\min} = 500$ km, and $\theta_{\min} = 10^\circ$ . . . . .	72

5.14	Effect of BSs' density on coverage probability and data rate of a terrestrial backhaul for an airborne network at different altitudes. . . . .	72
5.15	Effect of aerial platform's altitude on data rate provided by LEO and BS backhaul networks for an airborne network. The total number of LEO satellites and altitude are set to 1000 and 500 km, respectively. . .	74

*List of Tables*

2.1	Existing LEO broadband networks (up to January 2023) . . . . .	13
4.1	Summary of system models and communication scenarios . . . . .	34
5.1	Fading models used for simulations . . . . .	62



# ABBREVIATIONS

2D	two-dimensional
3D	three-dimensional
5G	5th generation
6G	6th generation
AP	aerial platform
BPP	binomial point process
BS	base station
BSP	best server policy
CDF	cumulative density function
DPP	determinantal point process
FCC	Federal Communications Commission
GEO	geostationary Earth orbit
GNSS	global navigation satellite system
GPP	Ginibre point process
HAP	high altitude platform
i.i.d.	independently and identically distributed
ICI	inter-cell interference
IoT	Internet of Things
ITU	International Telecommunication Union
LEO	low Earth orbit
LOS	line-of-sight

MEO	medium Earth orbit
NLOS	non-line-of-sight
NPPP	nonhomogeneous Poisson point process
NSP	nearest server policy
PCP	Poisson cluster process
PDF	probability density function
PP	point process
PPP	Poisson point process
RAAN	right ascension of ascending node
SINR	signal-to- interference-plus-noise ratio
SNR	signal-to-noise ratio
UAV	unmanned aerial vehicle

# SYMBOLS

$\mathcal{A}$	a bounded set in $\mathbb{R}^d$
$a_{\text{AP}}$	altitude of AP
$a_{\text{s}}$	altitude of satellite
$\beta$	level of repulsiveness between points in $\beta$ -GPP
$\bar{C}$	average achievable rate
$c$	speed of light
$\delta(\cdot)$	intensity measure of nonhomogeneous PPP
$\mathbb{E}[\cdot]$	expectation measure
$f_{\text{c}}$	carrier frequency
$f_{\text{d}}$	Doppler shift
$F_X(x)$	CDF of random variable $X$ at point $x$
$f_X(x)$	PDF of random variable $X$ at point $x$
$G$	gravitational constant
$\Gamma(\cdot, \cdot)$	upper incomplete gamma function
$G_n$	the $n$ th satellite's antenna gain
$G_{\text{t}}$	overall antenna gain
$G_{\text{u}}$	user's antenna gain
$\mathcal{H}(\cdot)$	Heaviside step function
$H_n$	fading coefficient of the $n$ th channel
$I$	cumulative interference power
$\iota$	orbital inclination

$K$	number of orthogonal frequency channels
$\lambda$	density of points in a PP
$\Lambda(\cdot)$	intensity measure of PP
$\lambda_s$	satellites's longitude
$\mathcal{L}_X(\cdot)$	Laplace transform of random variable $X$
$M$	mass of Earth
$m$	Nakagami- $m$ shape parameter
$\mathcal{M}(\mathcal{A})$	mean number of points in $\mathcal{A}$
$\mu(\mathcal{A})$	Lebesgue measure of $\mathcal{A}$
$\mu_{\mathcal{X}_n}$	mean of distribution $\mathcal{X}_n$
$\mu_\zeta$	mean of event $\zeta$
$N(\mathcal{A})$	number of point in bounded set $\mathcal{A}$
$N_{\text{act}}$	actual number of satellites
$N_{\text{eff}}$	effective number of satellites
$N_I$	number of interfering satellites
$N_P$	number of orbital plane
$\nu(\cdot)$	void probability
$P_0$	probability of having zero interfering satellites
$P_c$	coverage probability
$\phi_0$	polar angle difference between the serving satellite and a user
$\phi_{\text{AP}}$	AP's latitude
$\phi_s$	satellite's latitude
$\phi_u$	user's latitude
$p_n$	transmit power of the $n$ th satellite
$\mathbb{P}(\cdot)$	probability of the given event
$p_t$	transmit power
$P_V$	visibility probability of satellites to the user



$p_\zeta$	probability of event $\zeta$
$\mathbb{R}^d$	$d$ -dimensional Euclidean space
$r_\oplus$	radius of Earth
$\tilde{R}_0$	nearest effective distance between satellites and a ground user
$r_{\max}$	maximum communicable distance between a user and a satellite
$R_n$	distance from a ground user to the $n$ th satellite
$R_n^{\text{vis}}$	distance between visible satellites and a ground user
$\sigma^2$	additive noise power
$\sigma_{\mathcal{X}_n}^2$	variance of distribution $\mathcal{X}_n$
$\sigma_\zeta^2$	variance of event $\zeta$
$T$	minimum SINR and/or SNR threshold
$\theta$	elevation angle of satellite
$\theta_{\min}$	minimum elevation angle
$\theta_P$	angle between adjacent orbital planes
$\theta_n$	angle between the $n$ th satellite's antenna borsight and its LoS with a user
$\theta_u$	angle between user's antenna borsight and its LoS with a satellite
$U$	true anomaly
$\mathcal{U}(a, b)$	uniform distribution between $a$ and $b$
$\mathcal{X}_n$	shadowing coefficient of the $n$ th channel
$\xi$	a point process



## ORIGINAL PUBLICATIONS

- [P1] N. Okati, T. Riihonen, D. Korpi, I. Angervuori, and R. Wichman, “Downlink Coverage and Rate Analysis of Low Earth Orbit Satellite Constellations Using Stochastic Geometry,” *IEEE Transactions on Communications*, vol. 68, no. 8, pp. 5120–5134, Aug. 2020.
- [P2] N. Okati and T. Riihonen, “Stochastic Analysis of Satellite Broadband by Mega-Constellations with Inclined LEOs,” in *Proc. IEEE 31st Annual International Symposium on Personal, Indoor and Mobile Radio Communications (PIMRC)*, Sep. 2020.
- [P3] N. Okati and T. Riihonen, “Modeling and Analysis of LEO Mega-Constellations as Nonhomogeneous Poisson Point Processes,” in *Proc. IEEE 93rd Vehicular Technology Conference (VTC)*, Apr. 2021.
- [P4] N. Okati and T. Riihonen, “Nonhomogeneous Stochastic Geometry Analysis of Massive LEO Communication Constellations,” *IEEE Transactions on Communications*, vol. 70, no. 3, pp. 1848–1860, Jan. 2022.
- [P5] N. Okati and T. Riihonen, “Coverage and Rate Analysis of Mega-Constellations Under Generalized Serving Satellite Selection,” in *Proc. IEEE Wireless Communications and Networking Conference (WCNC)*, Apr. 2022.
- [P6] N. Okati and T. Riihonen, “Downlink and Uplink Low Earth Orbit Satellite Backhaul for Airborne Networks,” in *Proc. IEEE International Conference on Communications Workshops (ICC Workshops)*, May 2022.
- [P7] N. Okati and T. Riihonen, “Stochastic Coverage Analysis for Multi-Altitude LEO Satellite Networks,” *IEEE Communications Letters*, under review after major revision.



# 1 INTRODUCTION

During the last decades, wireless communications has revolutionized our everyday lives in several ways. The ever-increasing demands on the services and use cases led to significant market growth in telecommunication industry. As a result, the wireless technologies are always developing to provide more ubiquitous connectivity and higher data rates with more energy and spectrum efficient systems.

Several use cases engaged with the 5th generation (5G) of cellular networks and the upcoming 6th generation (6G), require uninterrupted service access in remote and under-served regions, e.g., for Internet of Things (IoT) devices, aircrafts, and maritime vessels. However, ubiquitous and high-capacity connectivity which is needed to meet these requirements cannot be fulfilled by terrestrial networks only [1]. Non-terrestrial networks, comprising airborne or spaceborne components to convey the data, have been taken into consideration to promote the services provided by cellular networks, especially for under-served regions. Therefore, enabling and development of non-terrestrial networks and their integration into the terrestrial networks is envisioned as a crucial part of cellular networks evolution [2]–[4].

In this chapter, a general overview of this research is provided by describing the background and motivation, followed by presenting the scope of the research, the research questions, and objectives of this study. Then, the main contributions to this research area are presented. Finally, the thesis author's contributions to the publications are summarized.

## 1.1 Background and motivation

According to the International Telecommunication Union (ITU), nearly one third of world's population have never accessed Internet, despite the rising demand during the Covid-19 pandemic, when some basic human needs, e.g., education, were tied to having ubiquitous connectivity. Moreover, the requirements of 6G are not only

limited to higher capacity and rate, but also to provide global coverage which ensures every individual's access to the network [5]; the goal that cannot be achieved merely with terrestrial networks as their availability is affected by geographical and economic factors. For instance, the majority of Earth's surface is covered with oceans where the deployment of such networks is not feasible. Furthermore, the deployment of terrestrial networks might not be economically viable at remote non-urban areas [6].

Recently, Low Earth orbit (LEO) communication networks have been developed as a promising solution to provide global Internet coverage especially for underserved regions, e.g., oceans and deserts, and moving vehicles for which a reliable terrestrial connectivity cannot be guaranteed all the time. Furthermore, these networks can provide unblocked Internet for countries with restricted access, and substitute the terrestrial networks temporarily in areas impacted by natural or man-made disasters. Considering the relatively higher latency, lower data rates, and more costly services offered by LEO communication systems compared to the existing cellular networks, this technology is not a reasonable substitution in regions where terrestrial broadband services are reliably available.

Despite the successful commercialization of LEO communication systems, e.g., Starlink, Kuiper, Telesat, their development and design rely solely on system-specific simulations. However, an analytical scientific understanding of these networks in terms of the network parameters, without resorting to orbital simulations, is crucial for their performance evaluation and development. The analytical framework facilitates design modifications of the existing LEO communication networks, acceleration in their development, and precise design guidelines for the future constellations. Other than performance evaluation, the theoretical analysis of these networks can be utilized for optimization of different network parameters which will avoid overestimation of network resources and, consequently, lead to a remarkable drop in the operational costs of LEO communication systems. Moreover, the framework provided in this thesis will significantly impact the investigation on the non-terrestrial and terrestrial networks integration as a promised component for 6G actualization.

This research is motivated by observing the lack of an analytical framework to evaluate the performance of LEO communication systems in the current studies. The analytical derivations enable the performance evaluation and optimization of this game-changing technology in a generic form without limiting the results to some specific networks with fixed number of satellites at known locations.

## 1.2 Objectives and scope of the thesis

The broad scope of this thesis is on physical layer performance analysis of LEO communication networks on both downlink and uplink directions. The performance evaluation of commercial LEO communication networks relies only on simulations since each company has a specific constellation with known predetermined orbital parameters. Thus, by having the complete data on the constellation parameters, a full knowledge on the exact location of each satellite at every time instant and, consequently, the performance of the network can be obtained for a ground terminal at a specific location. Obviously, the acquired performance is not valid for any other time instant due to satellites and users mobility. Moreover, finding the network performance for all possible snapshots of the network is computationally massive and resource consuming.

Concluding from the above discussion, the main research questions that are raised in this thesis are as follows:

- How are the performance metrics, e.g., the coverage probability and data rate, affected by different LEO constellation parameters in presence of interference? How do the user's data rate and its probability to be covered by satellites of a given constellation vary with its geographical position (latitudinal element)? What is the effect of user association techniques on the performance?
- What are the optimum constellation parameters that result in the maximum coverage probability and data rate?
- How does LEO network compare to terrestrial network when serving an airborne network as a backhaul?

To answer the above research questions and overcome the existing challenges in the performance analysis of LEO networks, a general analytical framework to study the performance of these networks regardless of the satellites' actual locality is proposed in this thesis. Stochastic geometry, as a mathematical tool, is utilized to model the LEO network and acquire tractable analytical derivations on its performance in a generic form.

Accordingly, the first and the main objective of this thesis is to obtain generic analytical expressions on the LEO network performance metrics for both uplink

and downlink directions. The generalization of the analysis is not only on constellation parameters, but also on propagation and network parameters, as far as the tractability is maintained. Moreover, this study formulates and includes the effect of user's locality on the performance. Secondly, the thesis provides insights on LEO constellation design by providing practical guidelines on the selection of LEO constellation parameters which can reduce the operational costs considerably through optimizing the network. The last objective of this thesis is to evaluate the performance of LEO networks as a backhaul for airborne networks and compare it with those conventional terrestrial backhaul networks.

### 1.3 Contributions

The summary of contributions on LEO communication networks modeling and performance analysis made by the author of this thesis is as follows.

- An analytical framework is presented in this study for modeling and performance analysis of a massive LEO communication network. Stochastic geometry is utilized as a central tool which enables tractable derivation of the network performance metrics. In particular, the satellites' locality is modeled as a point process (PP) to capture different realization of the network. Thus, by averaging over the point process, the performance metrics of the network can be obtained tractably for any desired constellation regardless of satellites' actual locality over time. The stochastic model also enables characterization of co-channel interference received from transceivers that share the same frequency band with the server.
- Since the satellites are distributed uniformly on orbits in an actual LEO constellation, the density of satellites from a ground user's perspective is not constant along different latitudes, i.e., there are more visible satellites at the inclination limits where several orbits cross. In this study, compensation for this inherent mismatch between stochastic and deterministic constellations has been taken into consideration through two different approaches which are finding the effective number of satellites for every user's latitude, and considering a latitude-dependant density for the stochastic constellation.
- Two performance metrics, namely, coverage probability and average data rate, are derived for both uplink and downlink directions. In uplink scenario, the



performance is also characterized in presence of interference from terrestrial network. Two different user association techniques based on the nearest distance and the highest quality of the received signal are also adopted in this research. All analytical derivations have been corroborated by Monte Carlo simulations in Matlab and compared with reference results from actual deterministic satellite constellations.

- The performance of a LEO communication system as a backhaul for airborne networks is formulated and analyzed in terms of the coverage probability and data rate. The obtained performance was also compared with terrestrial backhaul networks and some criteria on the selection of the best backhaul are provided based on the networks' parameters.
- The performance of a LEO constellation with satellites orbiting on different altitudinal levels is characterized in this thesis. There are several scenarios that correspond to a multi-altitude LEO constellation which will be fully described in the following chapters.

## 1.4 Author's contributions to the publications

A summary on the contributions of the author, which will be referred to as the Author in what follows, to the publications is provided in this subsection. The thesis is based on the author's three peer-reviewed journal papers [P1, P4, P7] and four conference-level papers [P2, P3, P5, P6] published in the proceedings of international conferences.

The original idea of analyzing the performance of LEO communication networks was proposed by Prof. Taneli Riihonen. He contributed to all the publications by providing feedback and sharing his thoughts on technical results as well as the organization and presentation of the manuscripts.

In all the attached publications to this thesis [P1–P7], the Author — as the first author of those publications — was responsible for developing the original ideas, research problem formulation, identifying the appropriate analytical tools, derivation of analytical results, performing simulations, writing, and revising the manuscripts. Other author(s) supported the work mostly by proof-editing and providing guidance to polish the content with the following exceptions: In [P1], Prof. Risto Wichman proposed the idea of extending the results for static fading environment; and for [P2],

Prof. Taneli Riihonen proposed the idea of deriving the effective number of satellites for every user's latitude and assisted its corresponding mathematical derivations.

In addition to the publications attached to this thesis, the Author has collaborated in a closely related research that resulted in a conference publication [7]. The Author contributed to that paper by presenting the system model, writing its corresponding section, proof-editing and providing technical and general feedback.

## 1.5 Thesis structure

The organization of the remainder of this thesis is as follows.

Chapter 2 provides an overview on massive LEO communication networks including their main characteristics, constellation parameters, and some important commercial constellations. The earlier research works on the performance of LEO communication networks are also reviewed in this chapter. Then, a generic system model for a LEO communication network is provided which is used as the basis for all the analyses that have been carried out in this research. Finally, the performance metrics which are considered in this thesis are introduced and formulated based on the described system model.

In Chapter 3, the Author presents the key mathematical tool, i.e., *stochastic geometry*, which was utilized for the first time ever, to the Author's best knowledge, to analyze the performance of a LEO Internet network, while also introducing its applications for modeling and performance analysis of wireless networks in general. Point processes as the central sub-field of stochastic geometry with their characteristics and applications are also discussed in this chapter.

Chapter 4 highlights more specifically how stochastic geometry is implemented in this thesis to model a LEO communication network. Two point processes, i.e., binomial point process (BPP) and nonhomogeneous Poisson point process (NPPP) are introduced to model the satellites' locality, alongside with compensating the inherent mismatch between the actual physical constellation and those modeled by a point process. Finally, the distance statistics are derived based on the stochastic model which are essential to characterize signal-to-noise-ratio (SINR) and, consequently, the performance metrics.

Based on the modeling and distance distributions derived in Chapter 4, coverage probability and data rate are characterized for a LEO network in Chapter 5 in a

generic form, considering different channel models and user association techniques. To evaluate the network performance regardless of the user's location, global coverage probability and data rate are also presented in this chapter. Moreover, the coverage probability and data rate of a LEO backhaul network is derived when serving an aerial platform at an arbitrary altitude above the ground. Finally, the conclusions, insightful guidelines on LEO satellite network design, and directions for future studies are presented in Chapter 6.



## 2 OVERVIEW OF THE MASSIVE LEO COMMUNICATION NETWORKS

This chapter provides the essential background and preliminaries on massive LEO communication networks and their characteristics, including the research works and developments on the performance analysis of LEO networks, constellation design, and LEO commercial projects. The system model, which will be used as the basis of the performance analysis provided in the following chapters, is also specified in details. Finally, the performance metrics which are analyzed for a LEO communication network in this thesis, are defined at the end of this chapter.

### 2.1 Background

After a serious setback of several LEO Internet constellations in 1990s, interests in providing global connectivity through these networks reemerged in 2010s due to the increasing demands for broadband services and decreasing the launch costs [8]. Large satellite constellations, which are sometimes referred to as mega-constellations, are comprised of hundreds or thousands of satellites orbiting on polar or inclined orbits with an altitude of typically between 500 km and 2000 km. The altitude range is selected in such a way that it is high enough to minimize the orbital decay due to atmospheric drag, and low enough to avoid Van Allen radiation belts<sup>1</sup> [9]. There are also other factors that affect the altitude selection including the propagation path loss, satellites' visibility time, and their coverage areas. Obviously, altitude also determines the total number of satellites required to provide a full coverage on Earth, i.e., the higher the altitude, the fewer number of satellites are needed. LEO satellites provide Internet coverage for all over the globe with relatively smaller propagation delay,

---

<sup>1</sup>A zone of energetic charged particles, which originate mostly from the solar wind. The particles are captured by and held around Earth's magnetosphere. The radiation in this zone can damage the electronic components of the satellites.

compared to geostationary Earth orbit (GEO) satellites, due to their lower altitudes.

The studies on several aspects of nongeostationary satellite networks, e.g., performance analysis, handover management, resource allocation and optimization, and their integration with other network platforms, etc. have attracted the researchers' attention since 90s. In [10], the uplink outage probability, as a function of the carrier-to-interference power ratio, in the presence of co-channel terrestrial interference was evaluated for two LEO constellations using time-domain simulations. The results are compared with other medium Earth orbit (MEO) and GEO networks considering several interference mitigation techniques.

One of the early developments of LEO communication systems is Iridium satellite constellation [11], which has become operational since 1998. The constellation is comprised of 66 satellites orbiting on 6 planes at 780 kilometer altitude. Different performance metrics for Iridium constellation were simulated in [12] as a function of constellation parameters, satellites speed, cell size, and average transaction duration. In [13], the outage probability is derived in closed form when the data is relayed to the ground stations through LEO satellites, by assuming only few number of satellites at predetermined locations. In [14] and [15], performance analysis of LEO satellite network has been investigated using stochastic reward net-based and stochastic Petri net models to simplify the characteristics of the LEO satellite networks. Signal-to-interference ratio was evaluated in [16] under traffic non-uniformity by assuming hexagonal coverage regions for satellites.

Different teletraffic performance parameters, i.e., blocking probability, handover failure probability, noncompletion probability, and forced termination probability were estimated for a mobile LEO satellite system in [17]. A general expression for visibility time of a LEO satellite is provided in [18], based on deterministic modeling which cannot conclude the general distribution of visibility periods for an arbitrarily positioned user. The deterministic model in [18] was then developed by statistically analyzing the coverage time per satellite visit in a mobile LEO network [19].

In [20], a LEO-based Internet of Things (IoT) architecture is overviewed in order to provide network access for IoT devices distributed in remote areas. To mitigate the severe path loss caused by large traveling distances between the LEO satellites and IoT devices, a novel architecture for IoT networks is proposed based on utilization of reconfigurable intelligent surfaces on LEO satellites [21]. In [22], resource control of a hybrid satellite-terrestrial network was studied to maximize the delay-limited

capacity and minimize the outage probability in uplink direction. The effect of interference is included in the optimization problem as a constraint. Considering only a single spotbeam, in [23], [24], a hybrid satellite–terrestrial network was analyzed to assist 5G network infrastructure. A comprehensive survey on network design, resource allocation, performance analysis and optimization of space-air-ground integrated network was provided in [25].

As LEO satellites revolve around the Earth at much higher velocities compared to GEO satellites, the Doppler shift is significant and needs to be compensated at the transceivers to mitigate their leakage to the neighboring frequency channels. The maximum Doppler shift induced by the motion of a LEO satellite with altitude  $a_s$  and elevation angle  $\theta$  at a fixed ground terminal located on the ground track of the satellite is

$$f_d = \frac{f_c}{c} \sqrt{\frac{GM}{a_s + r_\oplus}} \cos(\theta), \quad (2.1)$$

where  $G = 6.673 \times 10^{-11}$  N.m<sup>2</sup>/kg<sup>2</sup> is the gravitational constant,  $M$  is the mass of Earth (the central body around which the satellite orbits),  $f_c$  is the carrier frequency,  $c$  is the speed of light, and  $r_\oplus$  is the Earth’s radius.

One approach to compensate the Doppler shift in LEO satellite networks is by utilizing global navigation satellite system (GNSS) receiver at the ground terminals and using the data of satellites’ ephemeris to obtain the location and velocity information [26]. However, the Doppler can be fully compensated only for some known locations within the satellite’s cell (typically the center of the cell) which results in some error for other terminals in the cell. Moreover, an error may also occur in the acquired data from GNSS. As a result, some terminals in the cell might experience residual Doppler shift due to the deviation between the estimated and the actual Doppler shift. Doppler variation estimation and characterization are addressed in downlink LEO communication in [27]. In [28], assuming a single spotbeam for LEO satellites, the Doppler shift magnitude of a LEO network is characterized by utilizing the tools from stochastic geometry.

Among many companies that applied to the Federal Communications Commission (FCC) to deploy massive LEO constellations, the most prominent companies are SpaceX, OneWeb, and Telesat [8]. Starlink constellation, manufactured by SpaceX, is aiming at launching up to 12000 satellites on low Earth orbits, with

approximately 2000 satellites already launched up to the date of writing this summary, on  $53^\circ$ ,  $70^\circ$ , and  $97^\circ$ , at an altitude ranging from 540 to 570 km. OneWeb and Telesat provide global services with relatively fewer number of satellites, i.e., 648 and 298, respectively. SpaceX and Telesat use Ku- and Ka-bands while OneWeb uses only Ka-band. SpaceX and Telesat have circularly shaped steerable and shapeable beams while OneWeb has highly elliptical fixed beams.

A comparison between the three aforementioned constellations is provided in [8], in terms of orbital parameters, bandwidth allocation, beam characteristics, and beam link budgets which are either directly extracted from FCC filings or estimated by using the link budget equations. Other well-known LEO broadband services are Kuiper, Iridium, and Globalstar. Orbital parameters and the planned number of satellites for these constellations are summarized in Table 2.1. It is worth noting that Iridium and Globalstar which are given as two examples of LEO commercial constellations in Table 2.1, are not under the scope of this research as they are not considered as massive constellations due to their small number of satellites.

Phase array antennas are implemented for ground terminals as well as satellites to produce multiple beams. On the ground terminal side, multiple number of beams support transmitting and/or receiving from several visible satellites simultaneously. Several array geometries for LEO satellite ground terminals are reviewed in [29].

On the satellite side, hybrid beamforming to combine analogue and digital beamforming techniques is proposed as a compromise between the higher energy consumption in digital beamforming and less coverage flexibility and, consequently, limited capacity offered by analogue beamforming. It is worth mentioning that modern commercial LEO satellites support both analogue and digital beam types [30].

## 2.2 Constellation design and Keplerian elements

Keplerian or orbital elements which uniquely discern a specific orbit and the satellite's position in a satellite constellation are as follows.

- **Epoch** specifies a particular time instant at which an orbital parameter is measured.
- **Orbital inclination** ( $i$ ) indicates how much the orbital plane position is tilted w.r.t. the equatorial plane.
- **Right ascension of ascending node (RAAN) or longitude of ascending node**



**Table 2.1** Existing LEO broadband networks (up to January 2023)

Systems	Altitude(s) (km)	Total number of satellites	Inclination angle(s)	Number of planes
Starlink	540	1584	53.2°	72
	550	1584	53°	72
	560	348	97.6°	10
	570	720	70°	36
Oneweb	1200	720	87.9°	18
Telesat	1015	78	99.5°	6
	1325	220	37.4°	20
Kuiper	590	784	33°	28
	610	1296	42°	36
	630	1156	51.9°	34
Iridium	780	66	86.4°	11
Globalstar	1400	48	52°	8

is measured in the equatorial plane and is defined as the angle between a reference point in the sky, namely vertical equinox (RAAN= 0), and the ascending node, where satellites cross the equator going from south to north. Inclination angle and RAAN together can fully specify an orbital plane.

- **Argument of perigee** specifies the angle between the ascending node and perigee, the point where satellite is closest to Earth, measured from the center of Earth. It is trivial that argument of perigee is zero for circular orbits as perigee is at the ascending node.
- **Eccentricity** characterizes the shape of elliptical orbits and is defined as the ratio of the distance between the center of orbits and either of its foci to the semi-major axis. This parameter varies between zero to one with zero corresponding to the circular orbits.
- **Orbital period** is simply defined as the time needed to go once around an orbit. This parameter is directly related to the distance of a satellite from Earth through Kepler's third law of orbital motion which states that orbital period is proportional to the semi-major axis of its orbits.

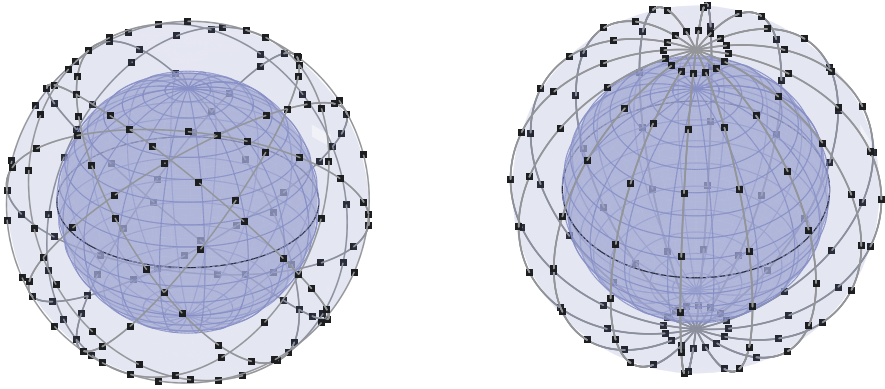
- **True anomaly** defines the position of a satellite in the orbit at the epoch w.r.t. perigee, i.e., the angle between perigee and the position of a satellite measured in the orbital plane.

To briefly summarize the above Keplerian elements, the orientation of orbital planes is determined by inclination and right ascension of ascending node, the orientation of the elliptical orbits, their shape and size are specified by argument of perigee, eccentricity, and orbital period, respectively. Finally, the position of a satellite in the orbit is determined by true anomaly.

Different combinations of Keplerian parameters result in huge number of constellation design possibilities. However, the elements must be selected in such way to lead to an optimal constellation, i.e., providing the global coverage with minimum number of satellites [31]. Optimal constellation design can significantly affect the performance of satellite communication networks while decreasing the manufacturing and launch costs. A very popular LEO constellation for circular orbits with the same inclination angle is Walker constellation which has two types depending on the inclination angle: Walker Delta constellation with inclined orbits and Walker Star constellation with near-polar orbits, shown in Fig. 2.1(a) and Fig. 2.1(b), respectively. Walker Delta can adjust the overlapping coverage footprints of satellites by varying the inclination angle. However, it is more challenging to establish inter-satellite links with Delta constellation as the relative distances between the satellites in adjacent orbits change constantly [32]. Walker constellation is defined as  $\iota : N_{act}/N_P/\theta_P$ , where  $N_{act}$  is the total number of satellites,  $N_P$  determine the number of equally spaced orbital planes, and  $\theta_P$  is the angle between adjacent orbital planes.

## 2.3 System model

In this subsection, we provide some detailed specifications on the studied system model, i.e., a massive LEO constellation. First, the geometry of the network is described in terms of constellation size, distribution of satellites on orbits, inclination angle, constellation altitude, and the minimum required elevation angle. Then system specifications on frequency reuse, antennas, and user association techniques are provided which are followed by an overview of the characteristics of propagation channels in terms of their fading and shadowing distributions. The details on each



(a) A Walker Delta constellation  $53^\circ : 160/8/0$ . (b) A Walker Star constellation (polar orbits)  $90^\circ : 160/8/0$ .

**Figure 2.1** A sketch of the Walker constellation.

item are described as below.

- Geometry of a LEO satellite network is shown in Fig. 2.2. The satellite network comprises  $N_{\text{act}}$  satellites distributed uniformly on circular inclined orbits with altitude and inclination angle denoted by  $a_s$  and  $\iota$ , respectively. The subscript "act" is chosen to refer to the actual number of satellites in the physical constellation and to distinguish it from  $N_{\text{eff}}$ , the effective number of satellites, which will be defined later. The ground user is assumed to be on Earth's surface which is approximated as a perfect sphere with radius  $r_\oplus$ .

In this thesis, we refer to the node that the user is assigned to as the serving node (satellite). The distances from the user to the satellites are denoted by  $R_n$ ,  $n = 0, 1, 2, \dots, N_{\text{act}} - 1$ , where the subscript zero is reserved for the serving link. The satellites must be elevated above the user's horizon at least to an angle of  $\theta_{\text{min}} > 0$ , so that they are visible to the user. Therefore, given the altitude of the constellation, the maximum distance that a satellite and a user terminal are able to communicate is a function of the minimum elevation angle and is obtained from basic geometry as

$$r_{\text{max}} = \sqrt{a_s^2 + 2 a_s r_\oplus + r_\oplus^2 \sin^2(\theta_{\text{min}})} - r_\oplus \sin(\theta_{\text{min}}). \quad (2.2)$$

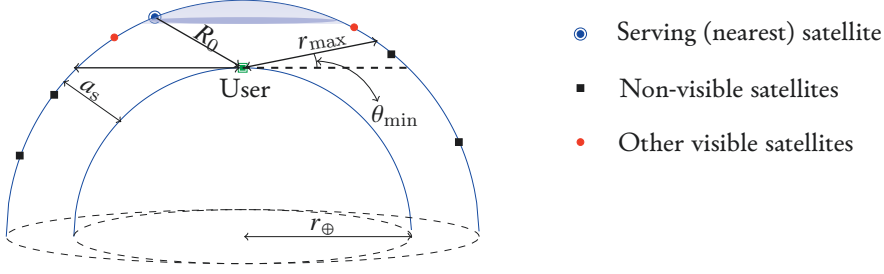


**Figure 2.2** A sketch of the considered system model, where satellites are at altitude  $r_{\oplus} + a_s$  and a ground user is located on Earth's surface.

Conversely, the upper limit for user's latitudes where the user is able to establish a connection with a satellite (at least one satellite is visible to the user) is given by

$$|\phi_u| \leq \iota + \cos^{-1} \left( \frac{r_{\oplus}^2 + r_{\oplus} a_s + (a_s^2 - r_{\max}^2) / 2}{r_{\oplus} (r_{\oplus} + r_{\min})} \right). \quad (2.3)$$

Using (2.3), the minimum altitude which provides global coverage (full coverage on all latitudes from the equator to the poles) is given as

$$a_s \geq \frac{r_{\oplus} \cos(\theta_{\min})}{\sin(\iota - \theta_{\min})} - r_{\oplus}. \quad (2.4)$$

Figure 2.3 provides results on the minimum required inclination angle and altitude to obtain global coverage given the altitude and inclination of the constellation, respectively, for different minimum elevation angles. As it is expected intuitively, the minimum required altitude and inclination angle for a global coverage decrease as the inclination angle and altitude increase, respectively, due to the rise in the visibility probability of satellites.

- Since the frequency spectrum is scarce, the same frequency range must be reused in the same communication system. Using the same frequency channel for different wireless connections may cause co-channel interference (or inter-cell interference (ICI)) due to the reception of signal from other nodes that share the same frequency with the serving node, and are located in its close proximity. Frequency reuse is more efficient for satellite networks as they operate in Ku-band (12–18 GHz) and Ka-band (26–40 GHz) [33], since

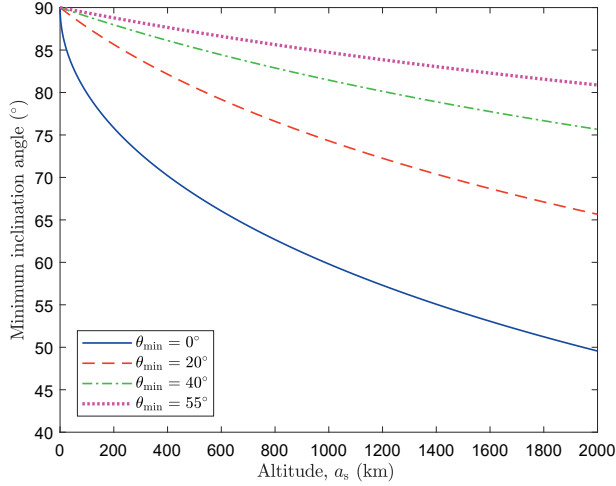


**Figure 2.3** Relationship between the minimum required inclination angle and altitude to obtain global coverage.

attenuation is stronger at higher frequencies which results in lower co-channel interference in the signal reception.

To implement frequency reuse in a satellite network,  $K$  orthogonal frequency channels are considered, with  $K \leq N_{\text{act}}$ , and a subset of  $N_{\text{act}}/K$  satellites is randomly assigned to each channel. Obviously, in real-world practical systems, more efficient channel allocation schemes will be implemented than a random channel allocation. However, random assignment corresponds to the worst-case scenario which can provide lower bounds on the achievable performance. Moreover, random channel allocation preserves the analytical tractability resulted from stochastic geometry [34].

The scheduling ensures that the serving satellite in the constellation uses the channel that is assigned to a user. All the other satellites on the same channel, other than the serving satellite, cause co-channel interference to the user's reception when they are elevated above the horizon to angle greater than  $\theta_{\min}$ .

- Since LEO satellites might be equipped with directional antennas [8], their characteristics are considered in the system model using several approaches. In [P1, P6], the effect of directional antennas is taken into account by assuming that all satellites are equipped with steerable antennas that radiate their main

lobe or the strongest sidelobe towards their serving user, regardless of satellite's elevation angle, while their sidelobes or weaker lobes are radiated towards other users. The effect is approximated by assuming two different power levels for serving and interfering satellites, denoted by  $p_0$  and  $p_n$ , respectively, such that  $p_n \leq p_0$ . In particular, we assume that  $p_0$  is the radiated power of the stronger lobes, while  $p_n$  is the directed power from the side lobes with lower power level. In this model, the users are assumed to be equipped with ideal isotropic antennas.

In order to tractably include the effect of directional antennas with any arbitrary pattern, in [P4, P7], antenna gains of the user and the satellites are formulated as a function of the angle between the antenna boresight and the line-of-sight path, denoted by  $\theta_u$  and  $\theta_n$ , respectively. When the user's antenna boresight is directed towards the sky and the satellites' antennas boresight radiates towards the center of Earth,  $\theta_u$  and  $\theta_n$  can be given in terms of the relative distances as

$$\theta_u(R_n, a_s) = \pi - \cos^{-1} \left( \frac{r_\oplus^2 + R_n^2 - (r_\oplus + a_s)^2}{2r_\oplus R_n} \right) \quad (2.5)$$

and

$$\theta_n(R_n, a_s) = \cos^{-1} \left( \frac{R_n^2 - r_\oplus^2 + (r_\oplus + a_s)^2}{2R_n (r_\oplus + a_s)} \right), \quad (2.6)$$

respectively.

Other than the relative angles between the user and the satellites, the antenna patterns also vary with altitude since a wider beam is required to cover the same area on Earth when satellite is orbiting on lower altitudes. Thus, in the system model,  $G_u(R_n, a_s)$  and  $G_n(R_n, a_s)$  directly represent the user's and the satellites' antenna gains, respectively, with  $G_t(R_n, a_s) = G_u(R_n, a_s)G_n(R_n, a_s)$  being the overall antenna gain.

It is also worth noting that for LEO constellations, highly directional antennas is more preferable at the ground stations due to easier implementation by using mechanically or electronically steering antennas. Considering weight and price

as the two critical factors in LEO antenna design, using directional antennas is more challenging for satellites. Furthermore, the high speed of orbiting in LEO, unlike GEO, may make it practically difficult to beam towards any designated user.

- The signal that travels from the transmitter may reach the destination via several different paths, i.e., direct line-of-sight (LOS) path or non-line-of-sight (NLOS) paths by being reflected at or diffracted by the surrounding obstacles. As the geometry and the medium that radio waves propagate through are completely different for satellite networks compared to terrestrial networks, novel models are required to take account of multi-path fading. Some literature neglected the effect of small-scale fading in satellite networking as the user is assumed to be in remote open areas where there are no obstacles to cause multi-path fading [35], [36].

From the many channel models that have been adopted for land mobile satellite networks, shadowed-Rician is introduced as an accurate model which fits the empirical data [37]–[42]. The model is a modification of Rician model where the amplitude of the LOS component is assumed to follow a Nakagami- $m$  distribution. Two parameters characterize the shadowed-Rician distribution: the Rician factor which denotes the ratio between the average power in the LOS and the diffused components, and the LOS fluctuation level which varies from 0.5 to  $\infty$ , where  $\infty$  corresponds to constant LOS component [43].

As massive LEO satellite networking is a newly developed technology, there are still many limitations for their channel modeling [44] and the current proposed models may be modified and replaced by more precise models. Therefore, in this thesis, the fading statistics are not limited to any specific model for the analytical derivations, except for the serving channel when interference is not neglectable since the analytical tractability can be only fulfilled by considering specific distributions for its channel gain.

As a result, in [P1, P4, P7], no specific distribution is assumed for the fading of the interfering channels since it has no effect on the tractability of the analysis. In [P1], serving channels are assumed to follow Rayleigh and static models. The former is suitable for the case when the received signal is composed of several multi-path components due to low elevation angle of the serving satellite,

each of which form a considerable portion of the received signal. Other than physical justification, Rayleigh assumption makes the analysis more tractable. The latter model holds when the number of satellites is large enough so that it is very likely to have the serving satellite at high elevation. In that case, the transmitted signal is not exposed to significant fading due to existence of a strong LoS component which dominates other reflected and/or scattered fading components.

In [P4, P7], a Nakagami- $m$  fading model is adopted for serving channels, where channel gain, being the square of Nakagami random variable, follows a gamma distribution with  $m$  being its shape parameter and rate parameter. Nakagami- $m$  fading provides the possibility to consider a wide range of multi-path fading patterns with varying NLOS and LOS probabilities. For instance, setting  $m = 1$  corresponds to Rayleigh fading scenario. As the probability of line-of-sight increases, a larger value for  $m$  should be selected. Nakagami- $m$  fading model was also applied in [45], [46] for LEO satellite networks.

For noise-limited communication scenarios in [P2, P3, P5, P6] any fading statistics can be adopted in general for channels as this has no effect on analytical tractability. Obviously, some specific fading distributions need to be opted for channels in order to generate numerical results, although the analytical results are valid for any arbitrary distribution. A stochastic geometry-based analysis is also studied in [39] for a noise-limited system. However, the fading model is specified to shadowed-Rician which limits the generality of the analysis.

- The shadowing attenuation caused by blockage of the received signal by the surrounding objects at the transceiver is a crucial factor to consider in the propagation model. The shadowing effect is not significant if the ground terminal is located in some rural or remote regions. However, in highly dense urban areas the signal may be subject to severe loss, termed as excess path loss in [47], by surrounding obstacles in the last few meters of the signal path (named as clutter). This effect must be considered in the server selection as the conventional association techniques based on the shortest distance may result in full outage if the nearest satellite's signal is blocked on its path [P5]. Excess path loss can be considered by choosing the proper values for parameters of shadowing distribution. In other words, the effect of clutter loss can be embedded in



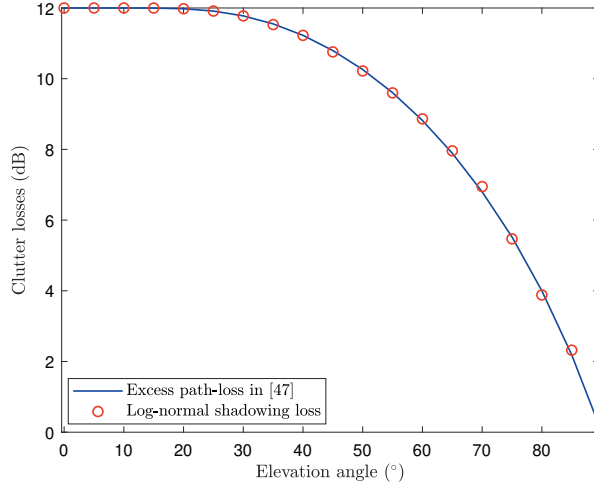


**Figure 2.4** Comparison of clutter layer losses versus the elevation angle for excess path loss model given in [47] and log-normal shadowing presented in this thesis.

the shadowing without making the propagation model too complex by adding extra parameters to it. As plotted in Fig. 2.4, the clutter layer loss modeled in [47] can equivalently be represented by shadowing attenuation considered in our model. The simulation parameters are extracted from [47] to plot the solid line in Fig. 2.4 which shows the excess path loss. To model excess loss, the mean and variance of the shadowing are calculated assuming that it is a weighted sum of two normal distributions given in [47]. Thus, the mean and the variance of the shadowing loss (in dB) are obtained in terms of the probability, mean and variance of the LOS and NLOS components, denoted by  $p_\zeta$ ,  $\mu_\zeta$ , and  $\sigma_\zeta^2$ , respectively, where  $\zeta \in \{\text{LOS}, \text{NLOS}\}$ . The mean and the variance of the shadowing are given as

$$\mu_{X_n} = p_{\text{LoS}}\mu_{\text{LoS}} + p_{\text{NLoS}}\mu_{\text{NLoS}} \quad (2.7)$$

and

$$\sigma_{X_n}^2 = p_{\text{LoS}}\sigma_{\text{LoS}}^2 + p_{\text{NLoS}}\sigma_{\text{NLoS}}^2 + p_{\text{LoS}}p_{\text{NLoS}}(\mu_{\text{LoS}} - \mu_{\text{NLoS}})^2, \quad (2.8)$$

respectively, where  $X_n$ ,  $n = 0, 1, 2, \dots, N_{\text{act}} - 1$ , are the shadowing coefficients

with subscript zero corresponding to the serving channel while other subscripts are reserved for interfering channels (if applicable). The clutter loss obtained from the shadowing model is depicted by markers in Fig. 2.4 and is fairly well matched with excess loss obtained from [47, Eq. 15]. Therefore, the clutter loss can be also modeled by inclusion of shadowing into the propagation model and finding its parameters based on the empirical data and elevation angle. However, to avoid over-complicating the expressions, the shadowing mean and variance are assumed to be constants, yielding an acceptable compromise between varying clutter losses at different elevation angles [P3–P5].

Shadowing model given in [P3–P5] is adopted to have any desired distribution, although in the numerical results the lognormal shadowing is assumed which is represented as  $\mathcal{X}_n = 10^{X_n/10}$ , where  $X_n$  has a normal distribution with mean and standard deviation denoted by  $\mu_{\mathcal{X}_n}$  and  $\sigma_{\mathcal{X}_n}^2$  (in dB), respectively. Thus, the probability density function (PDF) of lognormal shadowing is

$$f_{\mathcal{X}_n}(x) = \frac{10}{\ln(10)\sqrt{2\pi}\sigma_{\mathcal{X}_n}^2} \exp\left(-\frac{1}{2}\left(\frac{10\log_{10}(x) - \mu_{\mathcal{X}_n}}{\sigma_{\mathcal{X}_n}}\right)^2\right). \quad (2.9)$$

Atmospheric attenuation is also another source of potential impairments in the transmission/reception of signal to/from the sky. In [8, Fig. 8], it is shown that atmospheric attenuation for 13.5 GHz frequency exceeds 1 dB only in one percentage of time, which is not comparable to round 170 dB free-space path loss at 500 km. Moreover, the attenuation due to atmospheric gases is insignificant for frequencies below 40 GHz, i.e., Ku and Ka bands [48, Fig. 1].

- User association, namely assigning the user to a particular node in the network to be served by, significantly affects the network performance. Several association techniques can be adopted based on different criteria [49]. The most assumed association technique in wireless networks is the nearest server policy (NSP) which, hence the name, associates the user to the nearest node in the network. Another association technique is the best server policy (BSP) which assigns the ground terminal to a node that provides the highest signal-to-interference-plus-noise ratio (SINR) at the terminal's place. Although, NSP is the most simplistic association technique which results in more tractable derivations on the distribution of the serving distance and, consequently, the

performance metrics of the network, it is rarely used in practice since it is unable to include the effect of the large-scale attenuation, i.e., shadowing, on the variation of the received signal. BSP includes the effect of shadowing on the serving satellite selection which results in a remarkable improvement in the performance of the network.

BSP is frequently used to evaluate the performance of terrestrial networks [50]–[52], and proved to result in more reliable network performance. Moreover, BSP is more in line with practical association techniques since, in reality, the SINR at the receiver is a major criterion to determine the server [52]. Therefore, when implementing NSP and BSP, the serving link must satisfy

$$R_0 = \min_n (R_n | R_n < r_{\max}) \quad (2.10)$$

and

$$\tilde{R}_0 \triangleq \mathcal{X}_0^{-\frac{1}{\alpha}} R_0 = \min_n \left( \mathcal{X}_n^{-\frac{1}{\alpha}} R_n | R_n < r_{\max} \right), \quad (2.11)$$

respectively, where  $\tilde{R}_0$  is referred to as the nearest effective distance from the visible satellites to the user.

## 2.4 Performance analysis

The strength of the desired signal compared to the summation of interference and noise, known as SINR, is an important quantity to evaluate the performance of a communication system. According to the described system model in Section 2.3, SINR at the receiver is given by

$$\text{SINR} = \frac{p_t G_t(R_0, a_s) H_0 \mathcal{X}_0 R_0^{-\alpha}}{I + \sigma^2}, \quad (2.12)$$

where  $p_t$  is the transmit power of satellites, the constant  $\sigma^2$  is the additive noise power, the parameter  $\alpha$  is a path loss exponent, and

$$I \triangleq \sum_{n=1}^{N_I} p_t G_t(R_n, a_s) H_n \mathcal{X}_n R_n^{-\alpha} \quad (2.13)$$

is the cumulative interference power from all  $N_I$  other satellites above the user's horizon that share the same frequency channel with the serving satellite. The fading coefficients are denoted by  $H_n$ ,  $n = 0, 1, 2, \dots, N_{\text{act}} - 1$ , where subscript zero associates the fading parameter to the serving channel while other subscripts are reserved for interfering channels. It is worth noting that the path loss exponent  $\alpha$  is set to 2 for satellite communication since the signal travels through free space for most of its path. If all interfering satellites happen to be invisible to the user, i.e.,  $N_I = 0$ , the SINR in (2.12) is reduced to signal-to-noise ratio (SNR) as

$$\text{SNR} = \frac{p_t G_t(R_0, a_s) H_0 \chi_0 R_0^{-\alpha}}{\sigma^2}, \quad (2.14)$$

and further  $\text{SNR} = 0$  if  $R_0 > r_{\text{max}}$ , i.e., there is no satellite to serve the user.

Coverage probability is an important performance measure to evaluate the quality and reliability of a wireless network. The coverage probability is defined as the probability that the received SINR is higher than the minimum SINR required to ensure successful data transmission. Based on this definition, the coverage probability can be calculated as

$$P_c(T) \triangleq \mathbb{P}(\text{SINR} > T), \quad (2.15)$$

where  $T$  represents the minimum SINR required to successfully transmit the data. In other words, whenever the SINR at the receiver is above the threshold level  $T$ , it is considered to be within the coverage of the network.

The average achievable rate is the ergodic capacity from the Shannon–Hartley theorem over a communication link normalized to unit bandwidth and is defined as

$$\bar{C} \triangleq \frac{1}{K} \mathbb{E}[\log_2(1 + \text{SINR})], \quad (2.16)$$

which is measured in bits/s/Hz.

# 3 STOCHASTIC GEOMETRY ANALYSIS OF WIRELESS NETWORKS

As discussed in Chapter 1, commercial development and design of massive LEO networks is accomplished through some system-specific simulations based on massive time-consuming trial-and-error iterations. Moreover, based on the reviewed literature in Chapter 2, the early studies on performance of LEO networks are limited to considering few satellites with identical coverage footprints on Earth's surface which typically form a regular circular or hexagonal grid. However, actual commercial constellations are extremely massive as they are comprised of hundreds and thousands of satellites. Thus, the assumption of few number of satellites will lead to unrealistic results on the performance of these networks. For instance, the effect of interference on the performance caused by a large number of visible satellites to the user operating on the same frequency band with the serving satellite is ignored in those works. Stochastic geometry, as the main mathematical tool used in this research, enables analytical understanding of massive wireless networks without resorting to hexagonal models. This chapter illuminates an overview on stochastic geometry, its applications in wireless network analysis, and its corresponding mathematical preliminaries.

## 3.1 Stochastic Geometry

Stochastic geometry is a powerful mathematical tool that has been utilized in many fields of science, e.g., biology, material, forestry, astronomy, and wireless communication. Its application to study the wireless networks dates back to 1961 by studying the connectivity in large wireless networks with huge number of nodes [53]. Nodes refer to several elements of a wireless network, e.g., users, base stations (BSs), ground stations, wireless terminals, and access points. In fact, for wireless networks, stochastic geometry is used to average over different realization of nodes in a network [54]. Averages can be taken over a large number of nodes' locations or many network

realizations, for different metrics of interest, e.g., coverage probability and data rate. More particularly, the locations of nodes are modeled as a point process which captures the characteristics of nodes distribution, e.g., their density and the relative distances. In the following subsection, after defining the point processes, some typical point processes that are used to model location of nodes in a wireless network are introduced.

### 3.1.1 Point processes

In stochastic and probability theory, a point process is defined as a random, finite or countably-infinite collection of points located in a  $d$ -dimensional Euclidean space, denoted by  $\mathbb{R}^d$  [55]. It is worth noting that the definitions provided herein are restricted to the  $d$ -dimensional Euclidean space as it is the area of interest in wireless communication. In other words, a PP is defined as a mapping from a probability space to configurations of points in  $\mathbb{R}^d$ . In stochastic geometry analysis of wireless networks, the nodes are modeled as a PP that captures the properties of the network. The simplicity and tractability of Poisson point process (PPP) and BPP made them the most widely used point processes for modeling a wireless network.

A point process is a PPP if the number of points inside any bounded set is a Poisson random variable, and the number of points in disjoint sets are independent. A PPP is characterized by its intensity measure defined as  $\Lambda(\mathcal{A}) = \int_{\mathcal{A}} \lambda(x) dx$ , where  $\mathcal{A}$  is a bounded set in  $\mathbb{R}^d$ , i.e.,  $\mathcal{A} \subseteq \mathbb{R}^d$ , and  $\lambda(x)$  is density of points. Intensity can be either a constant value or a function of node's location in the underlying space which correspond to a homogeneous PPP and a nonhomogeneous PPP, respectively.

The probability mass function of a PPP, i.e., the probability to have exactly  $k$  points in the bounded set  $\mathcal{A}$  follows a Poisson distribution as

$$\mathbb{P}[N(\mathcal{A}) = k] = \frac{\Lambda(\mathcal{A})^k}{k!} e^{-\Lambda(\mathcal{A})}. \quad (3.1)$$

In stochastic geometry analysis of wireless networks, a PPP is used to model large-scale networks with infinite number of nodes distributed in a bounded or boundless service area [34], [54], [56]–[59].

A BPP is used when there are known finite number of nodes distributed within a finite region [60]. A PP is a BPP if the number of points inside any compact set follows a binomial distribution and the number of points in disjoint sets are related

through a multinomial distribution. When a PPP is conditional on the total number of points, denoted by  $n$ , it is equivalent to an  $n$ -point BPP. The probability mass function of BPP comprised of  $n$  points distributed over a finite area  $W$  follows a binomial distribution and is given as

$$\mathbb{P} [N(\mathcal{A}) = k] = \binom{n}{k} \left( \frac{\Lambda(\mathcal{A})}{\Lambda(W)} \right)^k \left( 1 - \frac{\Lambda(\mathcal{A})}{\Lambda(W)} \right)^{(n-k)}. \quad (3.2)$$

The above definitions are presented to summarize the main characteristics of each point process and how one can be opted based on the nodes' distributions in the network. More detailed and mathematical definitions can be found in several references including but not limited to [54], [56], [61].

### 3.1.2 Random measures and void probability

In this subsection, essential parameters in order to characterize a PP are defined.

- The mean measure of a point process,  $\xi$ , on  $\mathcal{A}$ , which is a bounded subset of the  $d$ -dimensional space, is given as

$$\mathcal{M}(\mathcal{A}) = \mathbb{E}[\xi(\mathcal{A})]. \quad (3.3)$$

In fact, mean measure  $\mathcal{M}(\mathcal{A})$  denotes the mean number of points in  $\mathcal{A}$ .

- The density or intensity measure of a point process,  $\xi$ , on a bounded subset of the  $d$ -dimensional space,  $\mathcal{A}$ , is defined as

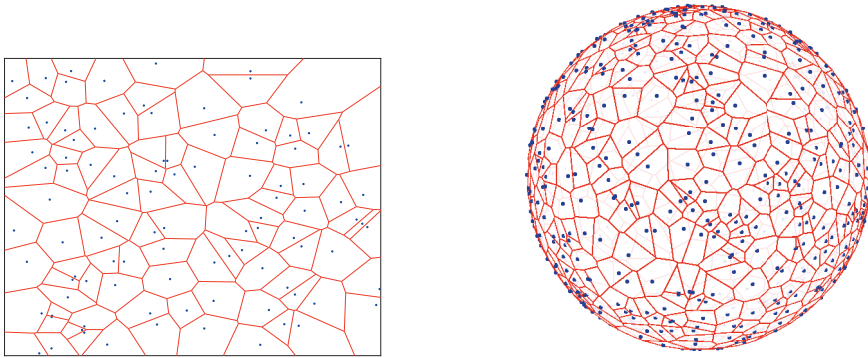
$$\lambda(\mathcal{A}) = \frac{\mathcal{M}(\mathcal{A})}{\mu(\mathcal{A})}, \quad (3.4)$$

where  $\mu(\mathcal{A})$  is the Lebesgue measure of  $\mathcal{A}$ .

- The void or null probability of a point process,  $\xi$ , on a bounded subset of the  $d$ -dimensional space,  $\mathcal{A}$ , is the probability to have no points in  $\mathcal{A}$ . Thus, it is given as

$$v(\mathcal{A}) = \mathbb{P}(\xi(\mathcal{A}) = 0). \quad (3.5)$$

Void probability is an important measure for stochastic analysis of wireless networks as it is used to obtain the distribution of the serving distance. For instance, the cumulative density function (CDF) of the nearest distance be-



(a) Random points on a plane with their Voronoi cells. (b) Random points on a sphere with their Voronoi cells.

**Figure 3.1** Examples of Voronoi diagrams with points distributed randomly according to a BPP on a flat plane (a) and a sphere (b).

tween a node and all other potential transceivers is the complement of the event  $\xi(\mathcal{A}) = 0$ , i.e.,  $F_{R_0}(r_0) = 1 - \mathbb{P}(\xi(\mathcal{A}) = 0)$ , where  $F_{R_0}(r_0)$  denotes the CDF of the nearest distance,  $R_0$ .

- A Voronoi cell of a point  $x \in \xi$  includes all the points in Euclidean space that are closer to  $x$  than to any other point in  $\xi$ . More mathematical definition of a Voronoi cell can be found in [54], [55]. The partitioning of space into Voronoi cells is called a Voronoi diagram or Voronoi tessellation. Examples of two Voronoi diagrams on a flat plane and a sphere are shown in Fig. 3.1.

## 3.2 The application of stochastic geometry in wireless communication

This section provides an overview on different communication networks and scenarios where stochastic geometry is used for performance analysis and/or optimization of the network. According to the geometry of the network, they are divided into two-dimensional (2D) networks, which correspond to planar cellular networks where all nodes—including users—are located on the same 2D surface, and three-dimensional (3D) networks which include several network geometries where com-



municating nodes are on different surfaces in space.

### 3.2.1 Two-dimensional networks

Traditionally, the cellular networks have been modeled as a grid where each cell has a regular hexagonal or square shape with a BS being located at its center. Although these models have been extensively used, they are too ideal for highly heterogeneous dense networks. Moreover, these models lack analytical tractability and need complex time-consuming simulations.

Stochastic geometry has been widely used for analysis of planar 2D networks including heterogeneous [56]–[58], [62], [63], cognitive [56], [64], [65], ad hoc [66]–[69], and vehicular [70], [71] networks. In [56], stochastic geometry-related literature on modeling multi-tier and cognitive cellular networks has been reviewed and a taxonomy based on the network type, the utilized point process, and the performance characterization techniques is provided. The techniques are compared in terms of tractability, accuracy, and practicability. The authors in [34] present one of the seminal works on the utilization of stochastic geometry for performance analysis of a terrestrial cellular network. In that work, the BSs are distributed according to a homogeneous PPP and the coverage and rate are tractably derived. Although the model shows the same accuracy as the conventional grid models, the stochastic model provides a lower band on the coverage and rate of the network. In a recent study [72], PPP is used to model the locations of laser beam directors on the ground, which provide power for an unmanned aerial vehicle (UAV).

When the nodes in a network are distributed as clusters due to some specific network arrangements or users' distribution, they can be modeled as a Poisson cluster process (PCP) [56], [64], [73]. In PCP, first, a set of points are generated according a PPP distribution. Then each point is replaced by a cluster of independently and identically distributed (i.i.d.) points.

Among different point processes used for modeling a wireless network, PPP is the most popular PP which provides tight bounds on the performance of the networks with more tractability and simplicity [56]. However, PPP is not valid when there is a finite-area network with a limited known number of nodes [60]. BPP shows more accuracy to model the characteristics of such networks [61], [74]. The performance for a finite arbitrarily shaped planar network is studied in [74]–[76]. A BPP was used to model a finite network of unmanned aerial vehicles in [77], [78].

Another point process used for modeling the wireless networks is determinantal point process (DPP) which takes into account the possible regularity in the network [79], e.g., repulsion or attraction between nodes. These point processes fit better to the actual properties of the networks since they are not as random as a PPP or as regular as grid models [60]. Among different types of DPPs, Ginibre point process (GPP) and its thinned and re-scaled version ( $\beta$ -GPP) are more popular for wireless network analysis due to their analytical tractability [60], [61], [74], [75], [78]. The parameter  $\beta$  is a real number between zero and 1 that corresponds to the level of repulsiveness or regularity between points.

### 3.2.2 Three-dimensional networks

While stochastic geometry has been widely used for the analysis of planar cellular networks, its application to 3D networks has been also compelling. 3D models can be used to analyze highly heterogeneous urban environments, such as BSs located on both ground and rooftops, UAV swarming, and massive satellite networks.

In [80], the BSs are assumed to be distributed in a 3D space according to a PPP. The model provides a closer bound on the coverage probability as it is more matching with the highly dense and heterogeneous nature of the networks in urban areas. In [77], [78], a downlink performance analysis of a UAV network is provided, where the UAVs are located as a BPP on a disc above the user. Two techniques to share the spectrum between UAV-to-UAV and BS-to-UAV transceivers are analyzed in [81] by modeling both UAVs and BSs as homogeneous PPPs.

Other than UAVs and highly dense heterogeneous networks, 3D stochastic modeling can be also utilized for satellite networks. However, before the journal publication [P1], the utilization of stochastic geometry for these networks was limited to modeling the ground users [23], [82]–[84]. For instance, in [82], stochastic geometry was used to characterize the terrestrial interference and provide user selection criteria for multi-beam satellites which pair each beam with a user. Coverage probability and data rate are derived for a multi-UAV downlink network through assuming PPP distribution for users in [83]. However, due to their channel assignment policy, interference among users and UAVs is neglected. In [84], the performance of a cognitive satellite–terrestrial network is investigated where the secondary terrestrial network shares resources with a primary satellite system network. The users and the secondary terrestrial network are modeled as two independent point processes.

To the best of the Author’s knowledge, the idea of modeling the LEO satellite network as a point process was proposed in [P1] for the first time; the model that enables application of the tools from stochastic geometry for performance analysis of these networks at large. Although the satellites’ positions in every time instant are deterministic for the actual physical satellite network as the satellites orbit on predetermined trajectories (orbits) with fixed spacing between them, due to consistent moving of satellites over the orbits, different realizations of the satellites from a user’s perspective can be seen as a random point process.

In [P1, Fig. 1], four different LEO constellations with their corresponding Voronoi diagrams are depicted. [P1, Figs. 1 (b)–(d)] show a class of regular deterministic Walker constellations with  $87.9^\circ$ ,  $70^\circ$ , and  $40^\circ$  inclination angle, respectively, in which all satellites are evenly spaced on low Earth orbits. Each Voronoi cell represents the coverage area of each satellite wherein all users are served by the satellite, assuming that the users connect to the nearest satellite. On the other hand, [P1, Fig. 1 (a)] depicts a random constellation in which the satellites are distributed as BPP on a spherical shell. As stated in [P1], the Voronoi diagrams formed by the deterministic constellations are not regular and they are more similar to the Voronoi tessellation of the BPP-distributed constellation. It can be also observed that the Voronoi tessellation becomes more irregular as the inclination angles increases. There are several reasons which may result in irregular tessellations formed by coverage area of LEO satellites as listed below:

- Due to the geometry of LEO constellations, the latitudinal density of satellites is not uniform, as there are more satellites around their inclination angle (i.e., the latitude limits) and less in the equatorial regions. This results in a non-uniform Voronoi tessellation with relatively smaller Voronoi cells around the inclination limits and larger cells at the equator. Moreover, in order to provide full coverage all over the globe based on users’ density and their corresponding demands, some commercial LEO constellations are deployed on multiple orbits with different inclination angles. Those varying inclination angles are another source of forming irregular Voronoi coverage cells.
- The continuous moving of satellites on orbits when satellites are moving towards north pole (ascending) and south pole (descending) on adjacent orbits causes the relative distances between the satellites on the neighboring orbits to change continuously. Therefore, satellites’ mutual positions become similar to

those given by a random process (as in [P1, Fig. 1 (a)]).

- Deploying satellites on different altitudes, e.g., in Starlink, or inter-operation of multiple LEO constellations in the future may also result in nonidentical coverage areas for satellites due to their varying transmit power, antenna gains, and orbital speed.
- Adaptive multi-beam and footprint designing to address the varying traffic demand of users as proposed in [85], will also result in more random shapes of Voronoi cells.

Other than the above mentioned specific reasons, the same as the terrestrial networks, modeling the satellite network as a point process provides analytical tractability. Obviously, as it will be illustrated thoroughly in the following chapters, there would be some deviation between the performance of the actual and random networks that can be reduced by adjusting the local density of constellation, i.e., at the ground user's location. In addition, a recent study on this topic [86], evaluates the accuracy of stochastic PPs for modeling a massive LEO network in terms of Wasserstein distance. The results show that under specific constellation parameters, the stochastic models lead to highly accurate results.

The challenges on extending the existing stochastic models for LEO networks stem from geometry of the system as well as the propagation environment of these networks. The geometry of LEO networks is such that the density of satellites is higher at the inclination limits than at the equatorial regions. This will limit the utilization of two widely used PPs, i.e., BPP and homogeneous PPP, since they are unable to capture the uneven distribution of satellites over the latitudes. Another challenge in stochastic geometry analysis of wireless networks is that resorting to Rayleigh fading assumption, which provides less complex derivations [56], is not always possible as the line-of-sight component of the signal is typically more significant than other multi-path components. More details about these challenges and how to remedy them will be given in Chapter 4.

## 4 STOCHASTIC MODELING OF MASSIVE LEO COMMUNICATION NETWORKS

In this chapter, the-state-of-the-art stochastic modeling of satellites in a massive LEO constellation for different network geometries and communication scenarios will be clarified. More specifically, the two point processes used in this thesis with their main features are introduced. Then, all the distance distributions stemmed from those point processes which are required to characterize the SINR function given in (2.12) are derived in terms of constellation parameters. The results and derivations in this chapter are essential in order to contribute expressions for the performance metrics of a LEO network in Chapter 5.

Table 4.1 summarizes different LEO geometries, propagation models, and communication scenarios studied in this thesis as well as the two different point processes used for modeling a massive LEO network.

### 4.1 Physical constellation vs. stochastic constellation

The physical actual constellation which is considered in the Author's publications [P1–P5] is a LEO communication satellite constellation consisting of  $N_{\text{act}}$  satellites launched uniformly on circular inclined orbits and at the same altitude,  $a_s$ , as shown in Fig. 4.1(a). For sake of simplicity, satellites' spherical coordinates are specified in terms of their latitude and longitude denoted by  $(\phi_s, \lambda_s)$ , instead of using the two orbital parameters i.e., true anomaly and right ascension of ascending node.

A user terminal is located arbitrarily on any latitude, denoted by  $\phi_u$ , on the Earth's surface. As stated in Chapter 2, satellites rising above the horizon at least to an angle of  $\theta_{\text{min}}$  are those which are visible to the user and capable of communicating with that. Accordingly, the largest possible distance between a satellite and a ground user is given as in 2.2. In this thesis, two point processes, i.e., BPP and NPPP, were used to model the above-described physical LEO constellation.

**Table 4.1** Summary of system models and communication scenarios

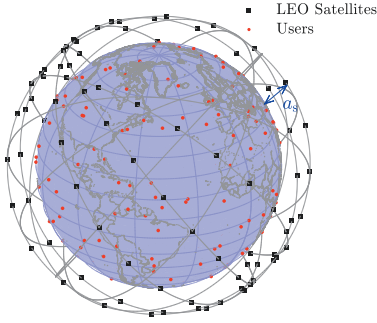
<b>Network model</b>	Single-altitude and inclined orbits
	Multi-altitude and inclined orbits
<b>Network access</b>	Direct and backhaul
<b>Used point process</b>	BPP and NPPP
<b>Fading assumption</b>	Rayleigh, Nakagami- $m$ , static, and arbitrary distribution for the desired links
	Arbitrary distribution for the interfering links
<b>User association</b>	NSP and BSP
<b>Transmission direction</b>	Downlink and Uplink
<b>Compensation for uneven distribution of satellites</b>	Numerical compensation, effective number of satellites, and NPPP

## 4.2 Binomially distributed vs. Poissonly distributed constellation

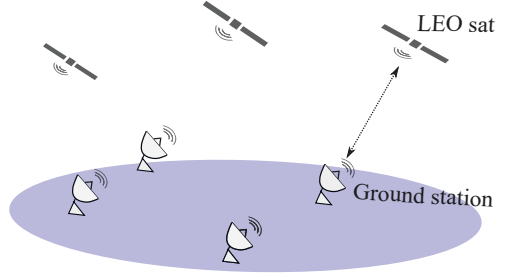
As mentioned earlier in Chapter 3, the first step towards stochastic geometry-based analysis of wireless networks is abstracting the network to an appropriate point process that captures its properties. There is always a compromise on selecting the best PP to obtain the most accurate results while maintaining the tractability [56].

### 4.2.1 Serving distance distribution for BPP

As a known number of satellites are distributed on a finite sphere, namely the spherical shell, a BPP is adopted in [P1, P2] to model the satellites in a massive LEO constellation, i.e., the satellites are assumed to be distributed uniformly on a sphere with radius  $r_{\oplus} + a_s$ . The generic system in [P1] includes both co-channel interference and noise into the analysis while [P2] studies a noise limited system. Upon modeling the satellites as a BPP, the distance distributions of the considered system model that contribute to characterization of SINR or SNR can be derived in terms of their PDF and CDF. By choosing the nearest satellite to the user as the serving satellite, i.e.,



(a) A single-altitude LEO network.



(b) Schematic of the direct access system model.

**Figure 4.1** A sketch of the considered system model in [P1–P5].

NSP association technique, the CDF of the serving distance is given as

$$F_{R_0}(r_0) = 1 - \mathbb{P}(R_0 > r_0) = 1 - \nu(\mathcal{A}) = 1 - \left(1 - \frac{r_0^2 - a_s^2}{4r_\oplus(r_\oplus + a_s)}\right)^{N_{\text{act}}} \quad (4.1)$$

for  $a_s \leq r_0 \leq 2r_\oplus + a_s$  [P1, P2]. The void probability is denoted by  $\nu(\mathcal{A})$ , where  $\mathcal{A}$  is the shaded spherical cap shown in Fig. 2.2 formed by all the points on the satellites' spherical shell which are closer to the user than the serving satellite. By taking the derivative w.r.t.  $r_0$ , the PDF of the serving distance is obtained as

$$f_{R_0}(r_0) = N_{\text{act}} \left(1 - \frac{r_0^2 - a_s^2}{4r_\oplus(r_\oplus + a_s)}\right)^{N_{\text{act}}-1} \frac{r_0}{2r_\oplus(r_\oplus + a_s)} \quad (4.2)$$

for  $a_s \leq r_0 \leq 2r_\oplus + a_s$  while  $f_{R_0}(r_0) = 0$  otherwise. BPP has been used also in later publications [39], [87] to characterize the distance distributions in a LEO network where satellites are distributed on multiple orbital shells with varying radii.

#### 4.2.2 Effective number of satellites

Although BPP provides closed form expressions for contact distance distributions, in practice, satellites are mostly available around their inclination limits while their density decreases as a user moves away from the inclination limits. As a result, the

satellites' distribution is not uniform as modeled by a BPP. In order to compensate for this effect, a new concept, namely *the effective number of satellites*, denoted by  $N_{\text{eff}}$ , has been introduced to remedy the mismatch between the globally uniform density in BPP and non-uniform latitudinal density in actual Walker constellations [P1, P2]. In [P1],  $N_{\text{eff}}$  is determined numerically by mean absolute error minimization between the performance metrics of BPP-distributed constellation and those of the practical Walker constellation for different latitudes. Thus, the serving distance distributions in actual LEO constellations can be obtained by substituting the parameter  $N_{\text{act}}$  in (4.1) and (4.2) with  $N_{\text{eff}}$ .

The effective number of satellites is derived analytically in [P2] for every latitude. The effective number of satellites,  $N_{\text{eff}}$ , can be also defined as the number of satellites that corresponds to a satellite density observed on a specific user's latitude, assuming the same density continues everywhere. Thus, the effective number of satellites is obtained in terms of the latitude of a satellite,  $\phi_s$ , and its PDF,  $f_{\Phi_s}(\phi_s)$ , as

$$N_{\text{eff}} \triangleq \frac{2 f_{\Phi_s}(\phi_s)}{\cos(\phi_s)} \cdot N_{\text{act}}. \quad (4.3)$$

Assuming that the satellites' true anomaly  $U$  has a uniform distribution [88], i.e.,  $U \sim \mathcal{U}(-\frac{\pi}{2}, \frac{\pi}{2})$ ,  $f_{\Phi_s}(\phi_s)$  is given by

$$f_{\Phi_s}(\phi_s) = \frac{\sqrt{2}}{\pi} \cdot \frac{\cos(\phi_s)}{\sqrt{\cos(2\phi_s) - \cos(2\iota)}} \quad (4.4)$$

for  $\phi_s \in [-\iota, \iota]$  while  $f_{\Phi_s}(\phi_s) = 0$  otherwise. Detailed proofs of (4.3) and (4.4) are given in [P2]. It is worth noting that although the density of the point process is adjusted locally for the given user's latitude and the mismatch might increase at other locations, the derived performance metrics will not be affected due to larger distances between the user and those points and, thus, more severe propagation loss. The effective number of satellites using (4.3) is depicted in Fig. 4.2 for three different inclination angles and constellations sizes of 1000 and 2000. As expected based on the geometry of LEO constellations,  $N_{\text{eff}}$  increases drastically near the inclination limits. The difference between the actual number of satellites and the effective number of satellites is more significant for larger user's latitudes. One limitation of applying effective number of satellites to tune the satellites distribution is that it results in zero effective number of satellites, and consequently, a full outage, for user's latitudes



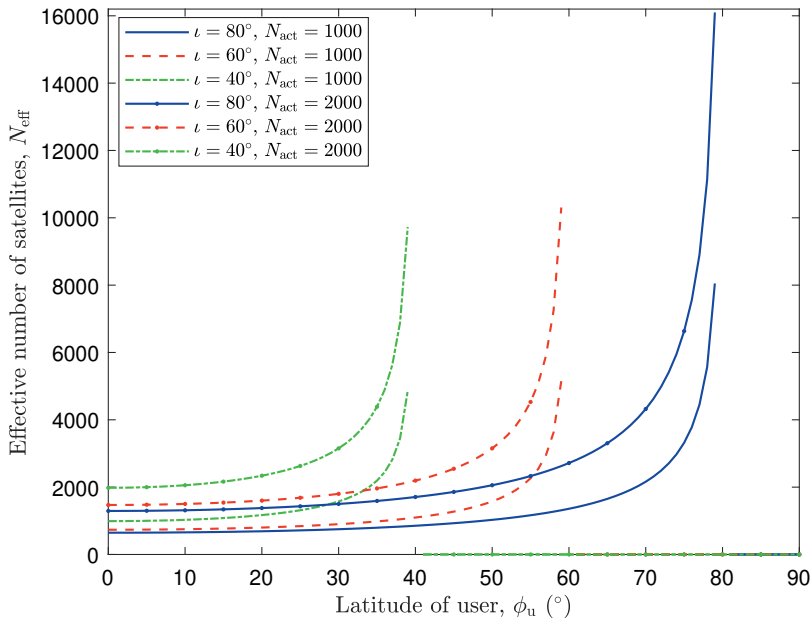


**Figure 4.2** Effective number of satellites obtained from (4.3) for a LEO constellation comprised of 1000 and 2000 satellites.

greater than the constellation inclination angle. However, in reality, when the user is located at latitudes which are slightly greater than the inclination limits, there are still visible satellites to the user at lower elevation angles.

#### 4.2.3 Serving distance distribution for NPPP

Another approach to take into account the effect of uneven distribution of satellites across different latitudes is modeling the satellites as a NPPP [P3–P6]. Unlike in [P1, P2] where the BPP-based derivations need to be compensated to match to the actual distribution of satellites, for NPPP this effect is embedded in the point process. In fact, by setting the intensity of NPPP to the actual latitude-dependent density of satellites on an orbital shell, there is no mismatch between the distance distributions and, consequently, the performance of the NPPP stochastic constellations and actual deterministic LEO networks.

Assuming satellites are distributed uniformly on low circular orbits, the density

of the satellites on an orbital shell element created by  $360^\circ$  spanning of the azimuthal angle on the orbital shell at latitude  $\phi_s$ , is only a function of latitudinal element and is calculated as

$$\delta(\phi_s) = \frac{N_{\text{act}} f_{\Phi_s}(\phi_s) d\phi_s}{2\pi(a_s + r_\oplus)^2 \cos(\phi_s) d\phi_s}, \quad (4.5)$$

which is the ratio of the number of satellites residing on the surface element to the element's surface area. By substituting  $f_{\Phi_s}(\phi_s)$  from (4.4), the density function or, equivalently, the intensity of NPPP is given as

$$\delta(\phi_s) = \frac{N_{\text{act}}}{\sqrt{2}\pi^2(a_s + r_\oplus)^2} \cdot \frac{1}{\sqrt{\cos(2\phi_s) - \cos(2\iota)}}. \quad (4.6)$$

When associating the ground station to the nearest satellite, the CDF of the distance between them is calculated as

$$F_{R_0}(r_0) = 1 - \exp\left(-2(a_s + r_\oplus)^2 \int_{\max(\phi_u - \phi_0, -\iota)}^{\min(\phi_u + \phi_0, \iota)} \delta(\phi_s) \cos(\phi_s) \cos^{-1}\left(\frac{\cos(\phi_0)}{\cos(\phi_s - \phi_u)}\right) d\phi_s\right) \quad (4.7)$$

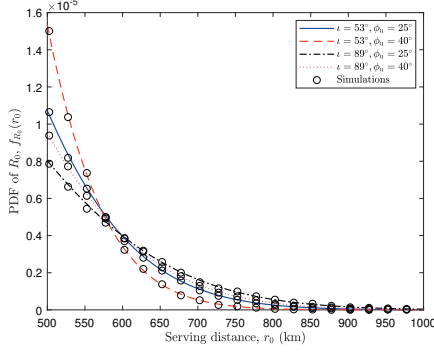
for  $\phi_0 \geq |\phi_u| - \iota$  while  $F_{R_0}(r_0) = 0$  otherwise, where  $\phi_0$  is the polar angle difference between the serving satellite and the ground station given as  $\phi_0 = \cos^{-1}\left(1 - \frac{r_0^2 - a_s^2}{2(a_s + r_\oplus)r_\oplus}\right)$ . Taking the derivative w.r.t.  $r_0$ , the PDF is obtained as

$$f_{R_0}(r_0) = 2r_0 \left(\frac{a_s}{r_\oplus} + 1\right) \exp(-\gamma(r_0)) \int_{\max(\phi_u - \phi_0, -\iota)}^{\min(\phi_u + \phi_0, \iota)} \frac{\delta(\phi_s) \cos(\phi_s)}{\sqrt{\cos^2(\phi_s - \phi_u) - \cos^2(\phi_0)}} d\phi_s, \quad (4.8)$$

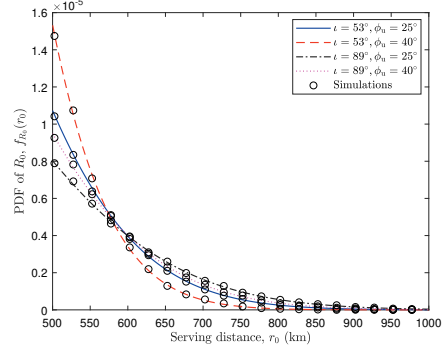
where

$$\gamma(r_0) = 2(a_s + r_\oplus)^2 \int_{\max(\phi_u - \phi_0, -\iota)}^{\min(\phi_u + \phi_0, \iota)} \delta(\phi_s) \cos(\phi_s) \cos^{-1}\left(\frac{\cos(\phi_0)}{\cos(\phi_s - \phi_u)}\right) d\phi_s. \quad (4.9)$$

Figures 4.3(a) and 4.3(b) depict the PDF of the serving distance of a constellation with 2000 satellites for BPP and nonhomogeneous PPP, respectively. The validation of results through Monte Carlo simulations shows a tight match between the actual distributions and the stochastic models. Moreover, both NPPP and compensated BPP result in the same serving distance distribution as the total number of satellites



(a) BPP modeling.



(b) PPP modeling.

**Figure 4.3** Corroboration of serving distance distribution obtained from stochastic modeling for a constellation with 2000 satellites orbiting at altitude of 500 km.

is fixed. To plot the serving distance PDF given in (4.2), the total number of satellites,  $N_{\text{act}}$ , is replaced by  $N_{\text{eff}}$  which calculated for the given inclination angles and user's latitudes. It can be observed that both point processes can precisely model the distance distributions. For lower inclination angles the probability of having the satellite right above the ground station is higher due to distribution of satellites on a relatively smaller spherical shell, which leads to larger density of satellites. The same principle also holds for larger ground user's latitude which results in higher probability density for shorter serving distances.

For a special case of assuming a homogeneous PPP with constant intensity of  $\delta = \frac{N_{\text{act}}}{4\pi(a_s+r_\oplus)^2}$ , the PDF of the serving distance  $R_0$  is

$$f_{R_0}(r_0) = \frac{N_{\text{act}}r_0}{2r_\oplus(a_s+r_\oplus)} \exp\left(-N_{\text{act}}\left(\frac{r_0^2 - a_s^2}{4(a_s+r_\oplus)r_\oplus}\right)\right) \quad (4.10)$$

for  $r_0 \in [a_s, 2r_\oplus + a_s]$  while  $f_{R_0}(r_0) = 0$  otherwise. A parallel study to this thesis, [46], also utilizes homogeneous PPP to model the LEO satellites. The results in that paper show a tight match between the distribution of the number of visible satellites obtained from PPP model and the empirical data obtained from a well-known commercial constellation.

It is worth noting that the Taylor series expansion of (4.10) and the serving dis-

tance distribution given in [P1, P2] are the same for the first two terms. The difference between the serving distance in a uniformly distributed constellation and the homogeneous Poisson point process is insignificant since the argument of exponential function in (4.10), i.e.,  $N_{\text{act}} \left( \frac{r_0^2 - a_s^2}{4(a_s + r_\oplus)r_\oplus} \right)$ , is small.

In [P5], the serving distance distribution is obtained when the ground terminal is associated with a satellite according to BSP. As stated in Chapter 2, BSP considers the effect of shadowing and assigns the user to a satellite that provides the highest received SNR. Thus, a new parameter, namely *the nearest effective distance*, is defined as  $\tilde{R}_0 \triangleq \min_n \mathcal{X}_n^{-\frac{1}{\alpha}} R_n^{\text{vis}}$ . The following expression gives the PDF of  $\tilde{R}_0$  as

$$f_{\tilde{R}_0}(\tilde{r}_0) = \sum_{n=0}^{\infty} n \mathbb{P} [N(\mathcal{A}(r_{\text{max}})) = n] \int_0^{\infty} \alpha z_n^{-\alpha-1} f_{\mathcal{X}_n}(z_n^{-\alpha}) F_{R_n^{\text{vis}}}\left(\frac{\tilde{r}_0}{z_n}\right) dz_n \\ \times \left( 1 - \int_0^{\infty} \alpha z_n^{-\alpha-1} f_{\mathcal{X}_n}(z_n^{-\alpha}) F_{R_n^{\text{vis}}}\left(\frac{\tilde{r}_0}{z_n}\right) dz_n \right)^{n-1}, \quad (4.11)$$

where  $F_{R_n^{\text{vis}}}(\cdot)$  is the CDF of the distances between the visible satellites and the ground user which is given in [P5, Lemma 1]. The PDF of the random variable  $\mathcal{Z}_n \triangleq \mathcal{X}_n^{-\frac{1}{\alpha}}$  is evaluated at point  $z_n$ . The complete proof of (4.11) is given in [P5, Lemma 2].

#### 4.2.4 Interference characterization

As frequency reuse is inevitable in most of communication systems for efficient use of frequency spectrum, co-channel interference from nearby transmitters that share the same frequency band with the server can significantly affect the network performance, especially for massive LEO constellations with such huge constellation sizes. An important outcome of stochastic modeling of a LEO network is facilitating the characterization of co-channel interference. The distribution of the distances from the interfering satellites is obtained by conditioning the distances from all visible satellites to the user on the serving distance,  $R_0$ . Therefore, the PDF of the distance from any interfering satellite to the user is given as

$$f_{R_n|R_0}(r_n|r_0) = \frac{f_R(r_n)}{F_R(r_{\text{max}}) - F_R(r_0)} \quad (4.12)$$

for  $r_0 < r_n \leq r_{\max}$  while  $f_{R_n|R_0}(r_n|r_0) = 0$  otherwise. The PDF and CDF of the distance from any satellite to the user, i.e.,  $f_R(r_n)$  and  $F_R(r_0)$ , is given in [P1, Lemma 1] for BPP distribution of satellites. Using the expression in (4.12), the PDF of interfering distances for a NPPP model is derived as  $f_{R_n|R_0}(r_n|r_0) = \frac{d\gamma(r_n)/dr_n}{\gamma(r_{\max})-\gamma(r_0)}$ .

An auxiliary parameter needed for analyzing coverage probability and rate, is the number of interfering satellites  $N_I$ . When satellites are modeled as a BPP, the number of interfering satellites is a binomial random variable with success probability

$$P_I = \frac{a_s - (r_0^2 - a_s^2)/(2r_\oplus)}{2(r_\oplus + a_s) - (r_0^2 - a_s^2)/(2r_\oplus)}. \quad (4.13)$$

The expression is the ratio of the surface area where satellites are visible to the user (their elevation angle is larger than  $\theta_{\min}$ ) to the total surface area of the spherical shell excluding the shaded cap of Fig. 2.2. Thus, the probability of having zero interfering satellites ( $N_I = 0$ ) is

$$P_0 = \mathbb{P}(N_I = 0) = (1 - P_I)^{\frac{N_{\text{act}}}{K} - 1} = \left(1 - \frac{a_s - (r_0^2 - a_s^2)/(2r_\oplus)}{2(r_\oplus + a_s) - (r_0^2 - a_s^2)/(2r_\oplus)}\right)^{\frac{N_{\text{act}}}{K} - 1} \quad (4.14)$$

for  $r_0 \leq r_{\max}$ , and  $P_0 = 1$  when  $r_0 > r_{\max}$ . Especially, the above probability is a key factor of the presented analysis, since in order to maintain tractability, the two complementary events of having either zero co-channel interference (noise-limited system) or non-zero interference are considered separately as in [P1, P7].

By the definition of a NPPP, the number of points in some bounded region  $\mathcal{A}$  of the orbital shell is a Poisson-distributed random variable. Thereby, the probability of having zero interfering satellites in  $\mathcal{A}$  is given by

$$P_0(\mathcal{A}) = \mathbb{P}(N_I = 0) = \exp\left(-\iint_{\mathcal{A}} \delta(\phi_s, \lambda_s) (a_s + r_\oplus)^2 \cos(\phi_s) d\phi_s d\lambda_s\right), \quad (4.15)$$

where  $\mathcal{A}$  is the spherical cap where viewable interfering satellites to the user exist (cf. the outer one in Fig. 2.2). For the special case when satellites are distributed as a homogeneous PPP, with intensity  $\delta = \frac{N_{\text{act}}}{4\pi(a_s+r_\oplus)^2}$ , the probability given in (4.15) can be expressed in closed form as  $P_0(\mathcal{A}) = \exp\left(-\frac{N_{\text{act}}(r_{\max}^2 - a_s^2)}{4r_\oplus(r_\oplus + a_s)}\right)$ .

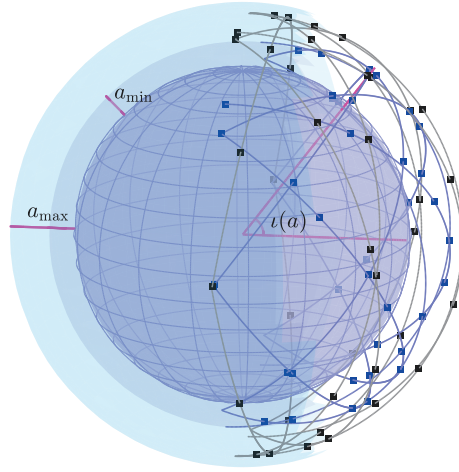


**Figure 4.4** A multi-altitude network consisting of satellites deployed at different altitudes ranging from  $a_{\min}$  to  $a_{\max}$ .

### 4.3 Single-altitude vs. multi-altitude constellation

As illustrated in Table 2.1, most of the commercial constellations are deploying satellites on multiple spherical shells to provide a global coverage over all the latitudes based on the users population and their demands. Other than a single satellite constellation operating at different altitudes, elliptical orbits for which the altitude varies with true anomaly of a satellite as well as the inter-operation of multiple constellations with different altitudes also correspond to a multi-altitude LEO setup.

In [87] and [39], distance distributions are formulated for a multi-altitude LEO networks when satellites are distributed as a BPP on several spheres at known specific altitudes. However, the uneven distribution of satellites on different latitudes and, consequently, the inclination angle of constellation are not considered. Moreover, the results are specific for some known levels of altitudes and, thus, not able to conclude the performance of a multi-altitude network in generic form.

In [P7], the coverage probability for a multi-altitude LEO network is obtained. The analysis is applicable to any generic highly massive LEO network with any number of altitudinal levels without affecting its complexity. Moreover, the inclination angle of satellites as well as the nonuniform density of satellites along different

latitudes are included in the analysis. The physical multi-altitude LEO network, shown in Fig. 4.4, consists of  $N_{\text{act}}$  satellites distributed uniformly on circular orbits with different altitudes ranging from  $a_{\min}$  to  $a_{\max}$ . The inclination angles of orbits, denoted by  $\iota(a_s)$ , can be also varying w.r.t the altitude.

To formulate an analytical expression for coverage performance of a multi-altitude LEO network, the above-mentioned physical network is abstracted and remodeled as a BPP on a sphere with radius  $A+r_{\oplus}$ , where  $A$  is a random variable ranging from  $a_{\min}$  to  $a_{\max}$ . Using the law of total probability, we have  $\mathbb{P}(R \leq r) = \mathbb{E}_A [\mathbb{P}(R \leq r | A = a)]$  where  $\mathbb{P}(R \leq r | A = a)$  is the CDF of  $R$  for a single-altitude network given in [P1, Lemma 1]. Thus, the CDF of the distance  $R$  from the user to any satellite in the multi-altitude network is as follows

$$F_R(r) = \int_l^u \frac{r^2 - a^2}{4r_{\oplus}(r_{\oplus} + a)} f_A(a) da + F_A(\min(a_{\max}, r - 2r_{\oplus})) - F_A(a_{\min}), \quad (4.16)$$

where  $l = \max(a_{\min}, r - 2r_{\oplus})$ ,  $u = \min(a_{\max}, r)$ , and  $f_A(a)$  and  $F_A(a)$  are the PDF and the CDF of the altitude, respectively. Using the Leibniz rule, the corresponding PDF is

$$\begin{aligned} f_R(r) = & \int_l^u \frac{r f_A(a)}{2r_{\oplus}(r_{\oplus} + a)} da + f_A(r - 2r_{\oplus}) \mathcal{H}(a_{\max} - r + 2r_{\oplus}) \\ & + \frac{f_A(u)(r^2 - u^2) \mathcal{H}(a_{\max} - r)}{4r_{\oplus}(r_{\oplus} + u)} - \frac{f_A(l)(r^2 - l^2) \mathcal{H}(r - 2r_{\oplus} - a_{\min})}{4r_{\oplus}(r_{\oplus} + l)}, \end{aligned} \quad (4.17)$$

where  $\mathcal{H}(\cdot)$  is the Heaviside step function. For a special case of having a uniform distribution for altitude, i.e.,  $f_A(a) = \frac{1}{a_{\max} - a_{\min}}$ , the PDF of  $R$  given in (4.17) can be obtained in closed form as

$$f_R(r) = \begin{cases} \frac{r \ln\left(\frac{r_{\oplus} + a_{\max}}{r_{\oplus} + a_{\min}}\right)}{2r_{\oplus}(a_{\max} - a_{\min})}, & r - 2r_{\oplus} \leq a_{\min} \leq a_{\max} \leq r, \\ \frac{r \ln\left(\frac{r_{\oplus} + r}{r_{\oplus} + a_{\min}}\right)}{2r_{\oplus}(a_{\max} - a_{\min})}, & r - 2r_{\oplus} < a_{\min} < r < a_{\max}, \\ \frac{r \ln\left(\frac{r_{\oplus} + a_{\max}}{r - r_{\oplus}}\right) - 2r_{\oplus}}{2r_{\oplus}(a_{\max} - a_{\min})} + \frac{1}{a_{\max} - a_{\min}}, & a_{\min} < r - 2r_{\oplus} < a_{\max} < r, \\ 0, & \text{otherwise.} \end{cases} \quad (4.18)$$

For a single-altitude constellation, i.e.,  $a_{\max} = a_{\min} = a_s$ , the PDF of  $R$  can be

obtained from (4.18) as  $f_R(r) = \frac{r}{2r_\oplus(r_\oplus+a_s)}$  for  $a_s \leq r \leq 2r_\oplus + a_s$  while  $f_R(r) = 0$  otherwise, similar to the derivation in [P1, Lemma 1]. It is worth mentioning that there are also other approaches to model a multi-altitude constellation. For instance, one can distribute BPP over a 3D hollow sphere with  $r_\oplus + a_{\min}$  and  $r_\oplus + a_{\max}$  being the inner and outer radii of the sphere. Another approach could be placing the satellites as a BPP on a sphere with an arbitrary radius and then perturbing the altitude of each point independently according to a uniform distribution ranging from  $r_\oplus + a_{\min}$  to  $r_\oplus + a_{\max}$ . Although these models represent the multi-altitude network more accurately, they lessen the tractability of the analysis without having any impact on the obtained derivations; the reason is that SINR and, consequently, other studied performance metrics are only affected by the relative distances between the satellites and the user. However, when inter-satellite connectivity is considered, the results are affected by the chosen model.

Similar to single-altitude constellation, the PDF of the serving distance  $R_0$  is given as in [P1, Lemma 2] by  $f_{R_0}(r_0) = N_{\text{eff}}(1 - F_R(r_0))^{N_{\text{eff}}-1} f_R(r_0)$  for  $a_{\min} \leq r_0 \leq 2r_\oplus + a_{\max}$  while  $f_{R_0}(r_0) = 0$  otherwise. It is worth emphasizing that  $F_R(r_0)$  and  $f_R(r_0)$  are different for single- and multi-altitude constellations. Moreover, the same as for a single-altitude LEO network, the effect of uneven density of satellites over different latitudes can be compensated by deriving  $N_{\text{eff}}$  as a function of the actual number of satellites,  $N_{\text{act}}$ . The derivation is given in [P7, Proposition 1] as a generalization of the results given in [P2] from single- to multi-altitude networks.

## 4.4 LEO backhaul for airborne networks

As the number of aerial platforms (APs) is growing rapidly, providing seamless Internet connectivity with sufficient data rate is crucial for their communication with other APs and ground terminals. The performance of LEO satellite constellations as a backhaul connection for APs is studied in the following subsections.

### 4.4.1 Overview of the related works

Connecting aerial platforms, e.g., airplanes, UAVs, high altitude platforms (HAPs), etc. to other APs or the ground users is envisioned as a crucial feature for enabling many applications in 6G airborne–terrestrial integrated networks [89]. On one side, APs can improve the link quality and the overall performance of LEO constellation



through relaying the data from satellites to ground terminals [90] or by contributing to the inter-satellite communication [91]. On the other side, as the number of APs is increasing drastically, providing ubiquitous connectivity which satisfies their demands for high data rate and coverage probability is becoming more significant. To satisfy such high demands of APs for data rate, a high quality backhaul connection will ensure the collection of data from/to the APs via the access links.

Traditionally, there are two approaches to provide backhaul access for airborne networks: via GEO satellites or terrestrial BSs. Geostationary satellites provide full sky coverage for most of the regions [92]–[94]. However, the considerable delay and path attenuation caused by traveling the signal over a large distance significantly limits their performance as a backhaul network. Terrestrial BSs can serve as backhaul with considerably smaller latency and path loss attenuation [77], [95]–[97]. The main drawback of the terrestrial backhaul network is the lack of complete sky coverage due to huge under-served regions, e.g., oceans and deserts. Moreover, local terrestrial network operators may restrict their services for some global APs.

Massive LEO networks have a great potential to serve as backhauls for APs due to possessing the advantages of both geostationary satellites and terrestrial networks, i.e., the full sky coverage as well as offering less path attenuation and delay. The application of stochastic geometry on analysis of LEO-backhauled APs has remained unrecognized in the literature, despite its considerable utilization for UAV-to-ground communication analysis [77], [95]–[97].

In [98], the throughput of a LEO backhaul network for both backhaul and access links is jointly maximized through managing the radio resources and optimizing the UAV trajectory. The system model in [98] considers only few satellites orbiting on a single orbit at known positions. In [99], capacity and range of air-to-air and satellite networks, which serve as a backhaul for APs, are simulated. It was shown that integration of air-to-air communication and LEO satellites improves the data rate of APs significantly. Revenue maximization in case of cooperation of LEO satellites with HAPs as a backhaul connection is studied in [35].

#### 4.4.2 Serving distance distribution

In [P6], the performance of both LEO and terrestrial backhaul networks for an AP is derived for uplink and downlink directions, as shown in Fig. 4.5. Obviously, based on the performance, AP may select the best backhaul connection between the

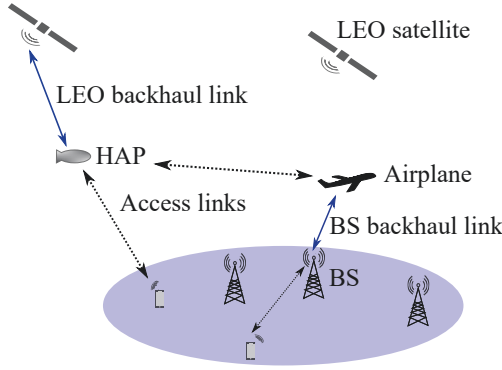


**Figure 4.5** Schematic of an airborne network which can be backhauled by either LEO satellites or terrestrial BSs for uplink and/or downlink directions.

LEO satellite and the terrestrial BS. Each AP is arbitrarily located above the Earth's surface at an altitude and latitude, represented by  $a_{AP}$  and  $\phi_{AP}$ , respectively. Given that  $a_s > a_{AP}$  or actually  $a_s \gg a_{AP}$ , the maximum distance at which an AP may communicate with a LEO satellite (that is when the signal is not blocked by Earth) is

$$r_{\max} = \sqrt{2r_{\oplus}a_s + a_s^2} + \sqrt{2r_{\oplus}a_{AP} + a_{AP}^2}. \quad (4.19)$$

Assuming that satellites are distributed as a NPPP with intensity  $\delta(\phi_s)$ , the distribution of the nearest distance between an AP with  $a_{AP} < a_s$  and a LEO satellite is obtained as

$$f_{R_0}(r_0) = 2r_0 \left( \frac{a_s}{r_{\oplus}} + 1 \right) \exp(-\gamma_{AP}(r_0)) \int_{\max(\phi_{AP}-\phi_{\max}, -\iota)}^{\min(\phi_{AP}+\phi_{\max}, \iota)} \frac{\delta(\phi_s) \cos(\phi_s)}{\sqrt{\cos^2(\phi_s - \phi_{AP}) - \cos^2(\phi_{\max})}} d\phi_s, \quad (4.20)$$

where

$$\gamma_{AP}(r_0) = 2(a_s + r_{\oplus})^2 \int_{\max(\phi_{AP}-\phi_{\max}, -\iota)}^{\min(\phi_{AP}+\phi_{\max}, \iota)} \delta(\phi_s) \cos(\phi_s) \cos^{-1} \left( \frac{\cos(\phi_{\max})}{\cos(\phi_s - \phi_{AP})} \right) d\phi_s, \quad (4.21)$$

and  $r_0 \in [a_s - a_{AP}, r_{\max}]$  while  $f_{R_0}(r_0) = 0$  otherwise. The polar angle difference between the serving satellite and the AP is  $\phi_{\max} = \cos^{-1} \left( \frac{(a_s+r_{\oplus})^2 + (a_{AP}+r_{\oplus})^2 - r_0^2}{2(a_s+r_{\oplus})(a_{AP}+r_{\oplus})} \right)$ .

## 5 PERFORMANCE ANALYSIS

Using the stochastic modeling and the distance distributions obtained in previous chapters, in this chapter, coverage probability and average achievable data rates are derived analytically in terms of LEO constellation and propagation environment parameters. The mathematical expressions show how the performance of a LEO constellation can be characterized analytically using the mathematical models provided by stochastic geometry. The derivations are then verified by simulations and several interesting insights on different constellation parameters, such as constellation's altitude, inclination angle, and the total number of satellites, are provided through the numerical results. Moreover, the effect of user's latitude on the performance metrics is included in the analysis.

### 5.1 Coverage probability

In this section, an analytical expression for coverage probability is derived using the stochastic modeling of a LEO network as a BPP or NPPP. Different uplink and downlink communication scenarios for direct and backhaul connectivity are assumed in characterization of coverage probability. Both single- and multi-altitude constellation geometries are studied for several fading models. The coverage probability is defined as given in (2.15).

#### 5.1.1 Coverage probability for BPP distributed satellites

The coverage probability is expressed as the summation of two terms, each of them representing an important operational case: The first term corresponds to the noise-limited case when there is no co-channel interference; and the second term represents the circumstance when there is at least one interfering satellite. Thus, the coverage

probability is expressed as

$$P_c(T) = P_0 \mathbb{P}(\text{SNR} > T) + (1 - P_0) \mathbb{P}(\text{SINR} > T | N_I > 0), \quad (5.1)$$

where  $P_0$  is given in (4.14). Using the definition of coverage probability for zero interference case given in (2.14), we have

$$\mathbb{P}(\text{SNR} > T) = \int_{a_s}^{r_{\max}} \mathbb{P}\left(H_0 \mathcal{X}_0 > \frac{Tr_0^\alpha \sigma^2}{p_t G_t(r_0, a_s)}\right) f_{R_0}(r_0) dr_0. \quad (5.2)$$

The upper limit for the integral is due to the fact that the satellites with elevation angles lower than  $\theta_{\min}$  are not visible to the user. The details of intermediate steps to derive (5.2) are similar to those given in [P1, Eq. (15)] for zero shadowing case.

For massive LEO constellations with thousands of satellites, it is very likely that multiple satellites are visible to a ground user at the same time. In that case, the reception of the user is subject to co-channel interference from other visible satellites and, thus, the coverage probability is derived as

$$\begin{aligned} & \mathbb{P}(\text{SINR} > T) & (5.3) \\ &= \int_{a_s}^{r_{\max}} \mathbb{E}_I \left[ \int_0^\infty f_{\mathcal{X}_0}(x_0) \left( 1 - F_{H_0} \left( \frac{Tr_0^\alpha (I + \sigma^2)}{p_t G_t(r_0, a_s) x_0} \right) \right) \right] f_{R_0}(r_0) dx_0 dr_0. \end{aligned}$$

The proof to obtain (5.3) is given in [P1, Eqs. (16) and (17)].

In order to complete the derivation of coverage probability from (5.2) and (5.3), some specific assumptions regarding the distribution of  $H_0$  need to be invoked. In fact, in order to maintain the tractability of our analysis, the serving channel must follow some specific fading models while interfering channels may follow any desired arbitrary fading model as it has no effect on the analytical tractability of the derivations. Likewise, the analytical tractability is not affected by shadowing distribution. Therefore,  $f_{\mathcal{X}_n}(x_n)$  can be adopted to any desired distribution without losing the analytical tractability. Assuming arbitrarily distributed fading models for interfering channels leads to timeless results which are valid for any original and novel channel model that may be proposed for land-satellite link in the future.

In this thesis, three different fading models are considered for serving channels, namely Rayleigh, static, Nakagami- $m$ , and Rician. Obviously, in order to generate numerical results, specific fading models need to be adopted for interfering channels

as well. A log-normal shadowing is also assumed in [P3, P4] to produce the numerical results. In the following subsections, coverage probability is derived using (5.2) and (5.3) for the aforementioned fading models.

### 5.1.1.1 Rayleigh fading

Rayleigh fading is adopted to model multi-path fading in a wireless channel when the NLOS components of the received signal are more significant compared to its LOS component. As satellites in a LEO network are deployed at lower altitudes w.r.t. MEO or GEO networks, the NLOS components become more dominant if the number of satellites is small. For such cases, a user can visit a satellite mostly at low elevation angles. In other words, a satellite may be at user's zenith only for a short period of time. As a result, strong NLOS components are more likely available at the user's place. Moreover, the probability of receiving NLOS signals from interfering satellites is even higher due to being at smaller elevation angles w.r.t. the serving satellite. As will be shown in this chapter, Rayleigh fading results in more simplified analytical expressions compared to other fading models.

Normalized Rayleigh fading for the serving channel corresponds to an exponential random variable channel gain with unit mean, i.e.,  $H_0 \sim \text{Exp}(1)$ . Thus, the probabilities of network coverage given in (5.2) and (5.3) for an arbitrarily located user under a Rayleigh-fading serving channel can be derived as

$$\mathbb{P}(\text{SNR} > T) = \frac{N_{\text{eff}}}{2r_{\oplus}(r_{\oplus} + a_s)} \int_{a_s}^{r_{\text{max}}} \int_0^{\infty} f_{\chi_0}(x_0) e^{-\frac{Tr_0^\alpha}{p_t G_t(r_0, a_s)x_0} \sigma^2} \times \left(1 - \frac{r_0^2 - a_s^2}{4r_{\oplus}(r_{\oplus} + a_s)}\right)^{N_{\text{eff}}-1} r_0 dx_0 dr_0 \quad (5.4)$$

and

$$\begin{aligned} & \mathbb{P}(\text{SINR} > T | N_I > 0) \\ &= \int_{a_s}^{r_{\text{max}}} \int_0^{\infty} f_{\chi_0}(x_0) \mathbb{E}_I \left[ \exp \left( -\frac{Tr_0^\alpha}{p_t G_t(r_0, a_s)x_0} (I + \sigma^2) \right) \right] f_{R_0}(r_0) dx_0 dr_0 \end{aligned}$$

$$\begin{aligned}
&= \frac{N_{\text{eff}}}{2r_{\oplus}(r_{\oplus} + a_s)} \int_{a_s}^{r_{\text{max}}} \int_0^{\infty} f_{\chi_0}(x_0) e^{-\frac{Tr_0^\alpha}{p_t G_t(r_0, a_s) x_0} \sigma^2} \\
&\quad \times \mathcal{L}_I \left( \frac{Tr_0^\alpha}{p_t G_t(r_0, a_s) x_0} \right) \left( 1 - \frac{r_0^2 - a_s^2}{4r_{\oplus}(r_{\oplus} + a_s)} \right)^{N_{\text{eff}}-1} r_0 dx_0 dr_0,
\end{aligned} \tag{5.5}$$

respectively. The results for non-shadowing case are given in [P1, Theorem 1]. The PDF of the serving distance when satellites are modeled as a BPP is substituted from (4.2) in (5.4) and (5.5). As described in Chapter 4,  $N_{\text{eff}}$  is the total number of satellites in a constellation that corresponds to a density observed by a user located at a specific latitude. Utilizing  $N_{\text{eff}}$  in the obtained expressions compensates for the inherent mismatch between the BPP-distributed and the actual constellations.  $\mathcal{L}_I(s) \triangleq \mathbb{E}[e^{-sI}]$  is the Laplace transform of cumulative interference power  $I$ .

For a BPP constellation when the serving satellite is at distance  $R_0 \geq a_s$  from the user,  $\mathcal{L}_I(s)$  can be expressed in generic form, i.e., regardless of the fading model, as

$$\begin{aligned}
\mathcal{L}_I(s) &= \sum_{n_I=1}^{\frac{N_{\text{eff}}}{K}-1} \left( \binom{\frac{N_{\text{eff}}}{K}-1}{n_I} P_I^{n_I} (1-P_I)^{\frac{N_{\text{eff}}}{K}-1-n_I} \right. \\
&\quad \left. \times \left( \frac{2}{r_{\text{max}}^4/a_s^2 - r_0^2} \int_{r_0}^{r_{\text{max}}} \int_0^{\infty} f_{\chi_0}(x_0) \mathcal{L}_{H_n}(sp_t G_t(r_n, a_s) x_n r_n^{-\alpha}) r_n dx_0 dr_n \right)^{n_I} \right),
\end{aligned} \tag{5.6}$$

where  $P_I$  is given in (4.13) and  $\mathcal{L}_{H_n}(\cdot)$  is the Laplace transform of the interfering channel gains denoted by the random variable  $H_n$ . The Laplace function for non-shadowing scenario is given in [P1, Lemma 5]. When Rayleigh fading is adopted for interfering channels [P1, Corollary 2], i.e.,  $H_n \sim \text{Exp}(1)$  for  $n = 1, \dots, N_I$ , and, consequently,  $\mathcal{L}_{H_n}(sp_t r_n^{-\alpha}) = \frac{1}{1+sp_t s r_n^{-\alpha}}$ , the Laplace function of interference for a BPP model is expressed as

$$\begin{aligned}
\mathcal{L}_I(s) &= \\
&\sum_{n_I=1}^{\frac{N_{\text{eff}}}{K}-1} \left( \binom{\frac{N_{\text{eff}}}{K}-1}{n_I} P_I^{n_I} (1-P_I)^{\frac{N_{\text{eff}}}{K}-1-n_I} \left( \frac{2}{r_{\text{max}}^4/a_s^2 - r_0^2} \int_{r_0}^{r_{\text{max}}} \left( \frac{r_n}{1+sp_t s r_n^{-\alpha}} \right) dr_n \right)^{n_I} \right).
\end{aligned} \tag{5.7}$$

Assuming some specific values for path loss exponent,  $\alpha$ , (5.7) can be reduced to elementary functions. For instance, for case of assuming  $\alpha = 2$  [P1], which is the most relevant case as the signal travels from the satellite to the ground terminal mostly through the free space, (5.7) can be expressed as

$$\mathcal{L}_I(s) = \sum_{n_I=1}^{\frac{N_{\text{eff}}}{K}-1} \binom{\frac{N_{\text{eff}}}{K}-1}{n_I} P_I^{n_I} (1-P_I)^{\frac{N_{\text{eff}}}{K}-1-n_I} \frac{r_{\text{max}}^2 - r_0^2}{r_{\text{max}}^4/a_s^2 - r_0^2} \left( \frac{p_n s}{r_{\text{max}}^2 - r_0^2} \ln \left( \frac{p_n s + r_0^2}{p_n s + r_{\text{max}}^2} \right) + 1 \right)^{n_I}. \quad (5.8)$$

Assuming  $\alpha = 4$  [P1], (5.7) is simplified into a closed-form expression as

$$\mathcal{L}_I(s) = \sum_{n_I=1}^{\frac{N_{\text{eff}}}{K}-1} \binom{\frac{N_{\text{eff}}}{K}-1}{n_I} P_I^{n_I} (1-P_I)^{\frac{N_{\text{eff}}}{K}-1-n_I} \times \frac{r_{\text{max}}^2 - r_0^2}{r_{\text{max}}^4/a_s^2 - r_0^2} \left( \frac{\sqrt{p_n s}}{r_{\text{max}}^2 - r_0^2} \arctan \left( \frac{\sqrt{p_n s} (r_0^2 - r_{\text{max}}^2)}{p_n s + r_{\text{max}}^2 r_0^2} \right) + 1 \right)^{n_I}. \quad (5.9)$$

The expressions in (5.8) and (5.9) are obtained by rewriting the integral in terms of the Gauss's hyper-geometric function given in [100, Eq. 9.100], and substituting with special arguments  $\alpha = 2$  and 4. The details on these derivations are given in [P1].

### 5.1.1.2 Static channels

Static propagation model is applicable when the satellite constellation is highly massive, so that it is likely to have multiple satellites in LOS propagation range. Consequently, the LOS component of the received signal is more significant than other indirect propagation paths. Moreover, by decreasing the frequency reuse factor, it becomes more likely to receive the interfering signal from the LOS path.

For the static serving channel, the channel gain is set as  $H_0 = 1$ . As mentioned previously, any general fading statistics can be adopted for interfering channels without affecting the analytical tractability. However, interference received from static channels is considered as a special case. Therefore, the coverage probabilities given in (5.2) and (5.3) for an arbitrarily located user under a static serving channel are

given as

$$\mathbb{P}(\text{SNR} > T) = F_{R_0} \left( \left( \frac{p_t G_t(r_0, a_s)}{T\sigma^2} \right)^{\frac{1}{\alpha}} \right) \quad (5.10)$$

and

$$\begin{aligned} \mathbb{P}(\text{SINR} > T | N_I > 0) &= \frac{N_{\text{eff}}}{4\pi r_{\oplus}(r_{\oplus} + a_s)} \int_{a_s}^{r_{\text{max}}} \int_{-\infty}^{\infty} \mathcal{L}_I(j\omega) \\ &\times \left( \frac{e^{j \left( \frac{p_t G_t(r_0, a_s)}{T r_0^{\alpha}} - \sigma^2 \right) \omega} - 1}{j\omega} \right) \left( 1 - \frac{r_0^2 - a_s^2}{4r_{\oplus}(r_{\oplus} + a_s)} \right)^{N_{\text{eff}}-1} r_0 dr_0 d\omega. \end{aligned} \quad (5.11)$$

The proof of (5.10) is straightforward from the definition of coverage probability and setting  $H_0 = 1$ . The detailed proof for (5.11) is given in [P1].

Using the expression given in (5.6), for the special case of having static interfering channels, the Laplace transform of  $I$  is

$$\begin{aligned} \mathcal{L}_I(s) &= \sum_{n_I=1}^{\frac{N_{\text{eff}}}{K}-1} \binom{\frac{N_{\text{eff}}}{K}-1}{n_I} P_I^{n_I} (1 - P_I)^{\frac{N_{\text{eff}}}{K}-1-n_I} \\ &\times \left( \frac{2(sp_n G_t(r_0, a_s))^{2/\alpha}}{\alpha (r_{\text{max}}^4/a_s^2 - r_0^2)} [\Gamma(-2/\alpha, sp_n G_t(r_0, a_s) r_{\text{max}}^{-\alpha}) - \Gamma(-2/\alpha, sp_n G_t(r_0, a_s) r_0^{-\alpha})] \right)^{n_I}, \end{aligned} \quad (5.12)$$

where  $\Gamma(a, x) = \int_x^{\infty} y^{a-1} e^{-y} dy$  denotes the upper incomplete gamma function.

### 5.1.1.3 Nakagami- $m$ fading

Nakagami- $m$  fading model enables considering different propagation environments by changing the Nakagami parameter  $m$ , while preserving the analytical tractability of the derivations. Larger values of  $m$  correspond to availability of a dominant LOS component. For instance,  $m = 1$  is equivalent to Rayleigh fading while  $m \rightarrow \infty$  represents static channels. In addition, Nakagami- $m$  fading can be adopted to model different propagation channels for serving and interfering channels by assuming different values of  $m$  for each channel. In other words, by assuming that the server has a higher elevation angle due to being nearer to the user, the LOS component received from the server is stronger than those coming from the interfering satellites. Thus, a larger value of  $m$  can be opted for serving link to consider this effect.



Considering a Nakagami- $m$  fading model for the serving channels, the channel gain  $H_0$ , being the square of a Nakagami random variable, follows a gamma distribution with both rate and shape parameters set to  $m$ . Using the definition of coverage probability for the case of having non-zero interference, i.e., (5.3), we have

$$\begin{aligned}
\mathbb{E}_{R_0} [\mathbb{P}(\text{SINR} > T | R_0 = r_0)] &= \int_{a_s}^{r_{\max}} f_{R_0}(r_0) \mathbb{P}\left(H_0 > \frac{Tr_0^\alpha (I + \sigma^2)}{p_t G_t(r_0, a)}\right) dr_0 \\
&\stackrel{(a)}{=} \int_{a_s}^{r_{\max}} f_{R_0}(r_0) \mathbb{E}_I \left[ \frac{\Gamma\left(m, m \frac{Tr_0^\alpha (I + \sigma^2)}{p_t G_t(r_0, a_s)}\right)}{\Gamma(m)} | I > 0 \right] dr_0 \\
&\stackrel{(b)}{=} \int_{a_s}^{r_{\max}} f_{R_0}(r_0) e^{-\frac{mTr_0^\alpha \sigma^2}{p_t G_t(r_0, a)}} \mathbb{E}_I \left[ e^{-\frac{mTr_0^\alpha I}{p_t G_t(r_0, a)}} \sum_{k=0}^{m-1} \frac{\sum_{l=0}^k \binom{k}{l} \left(\frac{mTr_0^\alpha \sigma^2}{p_t G_t(r_0, a)}\right)^l \left(\frac{mTr_0^\alpha I}{p_t G_t(r_0, a)}\right)^{k-l}}{k!} \right] dr_0,
\end{aligned} \tag{5.13}$$

where (a) follows from the distribution of gamma random variable  $H_0$ , and (b) is calculated using the definition of incomplete gamma function for integer values of  $m$ . The coverage probability for case of zero interference given in (5.2), i.e.,  $\mathbb{P}(\text{SNR} > T)$ , can be trivially derived using (5.13) and setting  $I = 0$ . Thus, for an arbitrarily located user, the coverage probabilities given in (5.2) and (5.3) under a Nakagami- $m$  fading serving channel are

$$\mathbb{P}(\text{SNR} > T) = \int_{a_s}^{r_{\max}} f_{R_0}(r_0) e^{-s\sigma^2} \sum_{k=0}^{m-1} \frac{(s\sigma^2)^k}{k!} dr_0, \tag{5.14}$$

with  $s = \frac{mTr_0^\alpha}{p_t G_t(r_0, a_s)}$ , and

$$\mathbb{P}(\text{SINR} > T | I > 0) = \int_{a_s}^{r_{\max}} f_{R_0}(r_0) e^{-s\sigma^2} \sum_{k=0}^{m-1} \frac{\sum_{l=0}^k \binom{k}{l} (s\sigma^2)^l (-s)^{k-l} \frac{\partial^{k-l}}{\partial s^{k-l}} \mathcal{L}_I(s)}{k!} dr_0, \tag{5.15}$$

where  $\mathcal{L}_I(s)$  follows the general form given in (5.6). Assuming that interfering channels also follow a Nakagami- $m$  fading model, the Laplace function of interfering

is given as

$$\begin{aligned} \mathcal{L}_I(s) = & \sum_{n_I=1}^{\frac{N_{\text{eff}}}{K}-1} \left( \binom{\frac{N_{\text{eff}}}{K}-1}{n_I} P_I^{n_I} (1-P_I)^{\frac{N_{\text{eff}}}{K}-1-n_I} \right. \\ & \left. \times \left( \frac{2}{r_{\text{max}}^4/a_s^2 - r_0^2} \int_{r_0}^{r_{\text{max}}} \int_0^\infty f_{X_0}(x_0) \frac{m^m}{(m + s p_t G_t(r_n, a_s) x_n r_n^{-\alpha})^m} r_n dx_0 dr_n \right)^{n_I} \right). \end{aligned} \quad (5.16)$$

The expression is obtained by substituting the Laplace transform of a gamma random variable, i.e.,  $\mathcal{L}_{H_n}(z) = \frac{m^m}{(m+z)^m}$  in (5.6).

The results for a BPP distributed constellation assuming Nakagami- $m$  fading channels are generalized in [P7] for a multi-altitude constellation where satellites are distributed according to a BPP on several spherical shells. For that case, the coverage probability given in (5.14) and (5.15) are averaged over the altitude ranging from  $a_{\text{min}}$  to  $a_{\text{max}}$ . It is worth noting that the upper limit of the integral,  $r_{\text{max}}$ , when integrating over the distance varies with altitude for a given minimum elevation angle. Thus, (5.14) and (5.15) for a multi-altitude constellation can be written as [P7, Proposition 2]

$$\mathbb{P}(\text{SNR} > T) = \int_{a_{\text{min}}}^{a_{\text{max}}} \int_{a_{\text{min}}}^{r_{\text{max}}} f_A(a) f_{R_0}(r_0) e^{-s\sigma^2} \sum_{k=0}^{m-1} \frac{(s\sigma^2)^k}{k!} dr_0 da, \quad (5.17)$$

with  $s = \frac{mTr_0^\alpha}{p_t G_t(r_0, a)}$ , and

$$\begin{aligned} \mathbb{P}(\text{SINR} > T | I > 0) = & \int_{a_{\text{min}}}^{a_{\text{max}}} \int_{a_{\text{min}}}^{r_{\text{max}}} f_A(a) f_{R_0}(r_0) e^{-s\sigma^2} \sum_{k=0}^{m-1} \frac{\sum_{l=0}^k \binom{k}{l} (s\sigma^2)^l (-s)^{k-l} \frac{\partial^{k-l}}{\partial s^{k-l}} \mathcal{L}_I(s)}{k!} dr_0 da, \end{aligned} \quad (5.18)$$

where  $\mathcal{L}_I(s)$  is given in [P7, Lemma 3] for a multi-altitude LEO network.

#### 5.1.1.4 Noise-limited system

A noise-limited system has been considered in [P2, P3, P5, P6]. The assumption holds when some co-channel interference mitigation techniques are implemented

properly so that the performance becomes noise-limited. For instance, by virtue of having narrow steerable and shapeable antenna beams and dynamic bandwidth channelization as have already been implemented in the two prominent LEO satellite constellation systems, i.e., Starlink and Telesat [8], the co-channel interference becomes significantly small.

Exclusion of interference results in more simplified results for the performance metrics of the LEO network which are valid for both uplink and downlink direction scenarios. Moreover, when the system is noise-limited, a general fading distribution can be adopted for the serving channel without losing the analytical tractability. Thus, for a noise-limited LEO network, when satellites are distributed as BPP, the uplink and downlink probability of coverage for an arbitrarily located user is given as [P2]

$$P_c(T) = \frac{N_{\text{eff}}}{2r_{\oplus}(r_{\oplus} + a_s)} \int_{a_s}^{r_{\text{max}}} \left(1 - F_{H_0}\left(\frac{Tr_0^\alpha \sigma^2}{p_0}\right)\right) \left(1 - \frac{r_0^2 - a_s^2}{4r_{\oplus}(r_{\oplus} + a_s)}\right)^{N_{\text{eff}}-1} r_0 dr_0, \quad (5.19)$$

where  $F_{H_0}(\cdot)$  is the CDF of the serving channel gain  $H_0$ . It is also shown in [P2] that the coverage probability given in (5.19) is upper bounded by the probability of observing at least one satellite by the user. In other words, the maximum coverage probability is affected only by the geometry of the constellation. Thus, by setting  $T = 0$  for a noise-limited scenario given in [P2], the upper bound for coverage probability is obtained as

$$P_c(T) \leq F_{R_0}(r_{\text{max}}) - F_{R_0}(a_s) = 1 - (1 - P_V)^{N_{\text{eff}}}, \quad (5.20)$$

where  $P_V$  is the visibility probability of satellites to the user and is expressed as

$$P_V = \frac{a_s - r_{\text{max}} \sin(\theta_{\text{min}})}{2(r_{\oplus} + a_s)}. \quad (5.21)$$

Due to uniform distribution of satellites, the expression in (5.21) is directly obtained as the ratio of the surface area of the spherical cap where satellites are visible to the ground user, to the total surface area of the satellites' spherical shell. As it can be observed, channel characteristics have no effect on the upper bound given in (5.20).

## 5.1.2 Coverage probability for NPPP distributed satellites

As mentioned in Chapter 4, NPPP can be also used to model the satellites' locality in a constellation. NPPP not only preserves the tractability of the analytical derivations, but also takes into account the uneven distribution of satellites along different latitudes by setting its intensity to the function given in (4.6). The same as for the BPP distribution, when co-channel interference is non-zero, specific assumptions regarding the fading model of serving channels are needed to derive the performance metrics. In the following subsections, the expressions obtained for the coverage probability of a NPPP constellation assuming Nakagami- $m$  fading model and noise-limited system.

### 5.1.2.1 Nakagami- $m$ fading

The results provided in this subsection are based on Publication [P4]. Under a Nakagami- $m$  fading serving channel while both shape parameter and rate parameter of gamma distribution are  $m$ , the coverage probability for an arbitrarily located ground terminal is

$$P_c(T) = \int_{a_s}^{r_{\max}} \int_0^{\infty} f_{\chi_0}(x_0) f_{R_0}(r_0) \times \left[ e^{-s\sigma^2} \sum_{k=0}^{m-1} \frac{\sum_{l=0}^k \binom{k}{l} (s\sigma^2)^l (-s)^{k-l} \frac{\partial^{k-l}}{\partial s^{k-l}} \mathcal{L}_I(s)}{k!} \right]_{s=\frac{mT r_0^\alpha}{\rho_t G_t(r_0, a_s) x_0}} dx_0 dr_0, \quad (5.22)$$

where the PDF  $f_{R_0}(r_0)$  is given in (4.8) and  $\mathcal{L}_I(s)$  is the Laplace transform of interference power  $I$  which is calculated as

$$\mathcal{L}_I(s) = \sum_{n=0}^{\infty} P_n(\mathcal{A}(r_{\max}) - \mathcal{A}(r_0)) \times \left( \int_{r_0}^{r_{\max}} \int_0^{\infty} \mathcal{L}_{H_n}(s \rho_t G_t(r_n, a_s) x_n r_n^{-\alpha}) f_{\chi_n}(x_n) f_{R_n|R_0}(r_n|r_0) dx_n dr_n \right)^n, \quad (5.23)$$

where  $\mathcal{A}(r_{\max})$  represents the spherical cap where all visible satellites to the user exist while  $\mathcal{A}(r_0)$  is the cap above the user, with the serving satellite on its border (base of the cap) and no satellite within its surface.  $P_n(\cdot)$  represents the probability

to have  $n$  satellites in the above mentioned region. The function  $f_{\chi_n}(x_n)$  denotes the PDF of shadowing for the  $n$ th interfering channel.

Considering some special cases, the Laplace function can be reduced to simpler expressions. For instance, when interfering channels experience Nakagami- $m$  fading, the Laplace function of interference is given as in [P4, Corollary 1]. More simplified Laplace functions can be obtained as given in [P4, Corollaries 2 and 3] when assuming that satellites are distributed as a homogeneous PPP with constant intensity  $\delta = \frac{N_{\text{act}}}{4\pi(a_s+r_\oplus)^2}$ . Assuming free-space path loss exponent, i.e.,  $\alpha = 2$ , and Rayleigh fading channels with no shadowing i.e.,  $m = 1$ , the Laplace function can be expressed in terms of elementary functions as

$$\mathcal{L}_I(s) = \sum_{n=0}^{\infty} \frac{1}{n!} \left( \frac{N_{\text{act}} (r_{\text{max}}^2 - r_0^2)}{4r_\oplus (r_\oplus + a_s)} \right)^n \exp \left( -\frac{N_{\text{act}} (r_{\text{max}}^2 - r_0^2)}{4r_\oplus (r_\oplus + a_s)} \right) \left( 1 + \frac{sp_t G_t(r_n, a_s)}{(r_{\text{max}}^2 - r_0^2)} \ln \left( \frac{k + r_0^2}{k + r_{\text{max}}^2} \right) \right). \quad (5.24)$$

### 5.1.2.2 Noise-limited system

As denoted in the previous section for a BPP-distributed constellation, a noise-limited system enables providing more generic results, i.e., independent of the fading distribution. In [P3], the uplink and downlink probability of coverage for an arbitrarily located user when satellites are distributed as a NPPP is given as

$$P_c(T) = \int_{a_s}^{r_{\text{max}}} \int_0^{\infty} f_{\chi_0}(x_0) f_{R_0}(r_0) \left( 1 - F_{H_0} \left( \frac{Tr_0^\alpha \sigma^2}{p_t G_t(r_0, a_s) x_0} \right) \right) dx_0 dr_0, \quad (5.25)$$

where  $f_{R_0}(r_0)$  is given in (4.8). In [P5], the probability of coverage is calculated for a noise-limited system assuming that the ground terminal associates to the satellite that provides the highest SNR at the receiver (i.e., BSP user association). The probability of coverage is given as

$$P_c(T) = \int_0^{\infty} \left( 1 - F_{H_0} \left( \frac{T\tilde{r}_0^\alpha \sigma^2}{p_0} \right) \right) f_{\tilde{R}_0}(\tilde{r}_0) d\tilde{r}_0, \quad (5.26)$$

where  $f_{\tilde{R}_0}(\tilde{r}_0)$  is the PDF of the effective serving distance given in (4.11). Note that for BSP association technique, the effect of shadowing is embedded in the PDF, i.e.,  $f_{\tilde{R}_0}(\tilde{r}_0)$ .

### 5.1.3 Global coverage probability

Another performance metric that has been evaluated in this thesis is the global coverage probability. The metric is defined as the weighted summation of coverage probability over the latitudes. The weights are selected from the population distribution over different latitudes. The mathematical definition of global coverage probability is given as

$$P_c^{\text{Global}} = \int_{\phi_u = -\pi/2}^{\pi/2} P_c(\phi_u) f_{\phi_u}(\phi_u) d\phi_u. \quad (5.27)$$

Global coverage probability enlightens how a LEO constellation can provide worldwide connectivity for the users, regardless of the user's location or, more specifically, its latitude. The data on the population distribution over different latitudes is collected from NASA's socioeconomic data and applications center [101] as shown in Fig. 5.1. Global coverage probability over different constellation sizes and altitudes is depicted in Figs. 5.2(a) and (b), respectively. The theoretical results are verified by simulations.

## 5.2 Average achievable data rate

Similar to Subsection 5.1, analytical derivations on the average achievable data rate are provided for several communication scenarios, satellite geometries, and propagation models using BPP and NPPP models. The definition of data rate is given in (2.16).

### 5.2.1 Data rate for BPP distributed satellites

The downlink data rate (in bits/sec/Hz) of a LEO network, when satellites are distributed as a BPP is given as

$$\bar{C} \triangleq \frac{P_0}{K} \mathbb{E} [\log_2 (1 + \text{SNR})] + \frac{1 - P_0}{K} \mathbb{E} [\log_2 (1 + \text{SINR}) | N_I > 0]. \quad (5.28)$$

For the case of having non-zero interference, i.e., the second term in (5.28), the expression can be obtained using the definition of SINR and averaging over the spatial

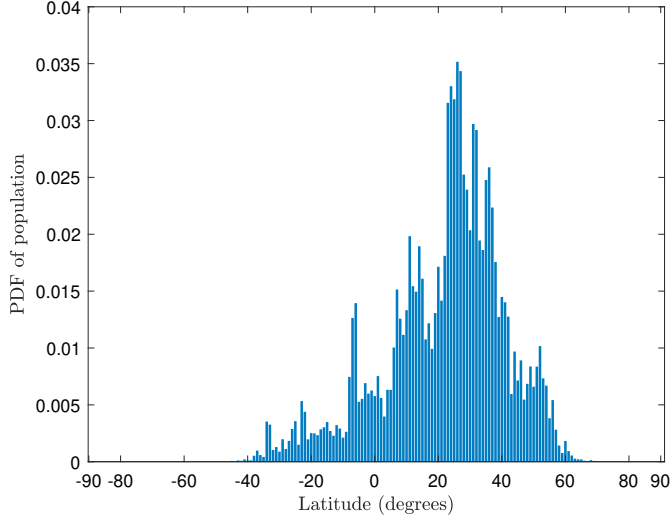


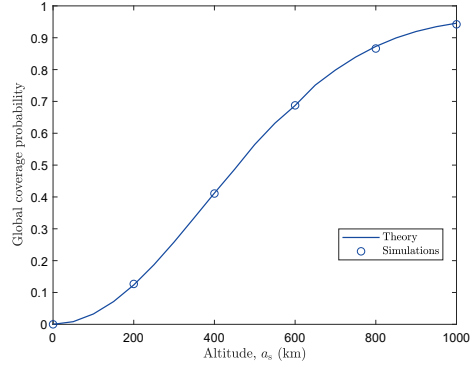
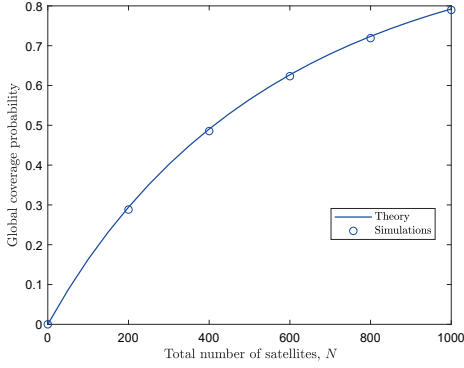
**Figure 5.1** Distribution of population on different latitudes [101]. The maximum density of population can be observed at  $26^\circ$ .

BPP and the fading distribution of the serving channel as

$$\begin{aligned}
& \mathbb{E}_{I, H_0, R_0} [\log_2 (1 + \text{SINR}) | N_I > 0] \\
&= c_0 \int_{a_s}^{r_{\max}} \int_{t>0} \mathbb{P} \left( H_0 > \frac{r_0^\alpha}{p_t G_t(r_0, a_s)} (\sigma^2 + I) (e^t - 1) \mid N_I > 0 \right) \\
&\quad \times \left( 1 - \frac{r_0^2 - a_s^2}{4r_\oplus(r_\oplus + a_s)} \right)^{N_{\text{eff}}-1} r_0 dt dr_0, \tag{5.29}
\end{aligned}$$

where  $c_0 = \frac{N_{\text{eff}}}{2 \ln(2) r_\oplus (r_\oplus + a_s)}$ . The complete proof of (5.29) as well as the details of the intermediate steps can be found in [P1, Theorem 3]. Following the same approach to obtain (5.29), the average data rate for the noise limited scenario [P2, Proposition 2] can be obtained as follows:

$$\begin{aligned}
\mathbb{E} [\log_2 (1 + \text{SNR})] &= \frac{N_{\text{eff}}}{2 \ln(2) r_\oplus (r_\oplus + a_s)} \\
&\times \int_{a_s}^{r_{\max}} \int_0^\infty \ln \left( 1 + \frac{p_t G_t(r_0, a_s) h_0 r_0^{-\alpha}}{\sigma^2} \right) \left( 1 - \frac{r_0^2 - a_s^2}{4r_\oplus(r_\oplus + a_s)} \right)^{N_{\text{eff}}-1} f_{H_0}(h_0) r_0 dh_0 dr_0, \tag{5.30}
\end{aligned}$$



(a) Global coverage probability for different constellation sizes when  $a_s = 500$ .

(b) Global coverage probability for different constellation altitudes and  $N_{\text{act}} = 500$ .

**Figure 5.2** Global coverage probability for different constellation sizes and altitudes with  $\iota = 53^\circ$  and  $T = 5$  dB.

where  $f_{H_0}(h_0)$  represents the PDF of channel gain  $H_0$ . Under Rayleigh fading assumption and invoking the PDF and CDF of serving channel gain, (5.29) and (5.30) can be written as

$$\mathbb{E} [\log_2 (1 + \text{SNR})] = \frac{N_{\text{eff}}}{2 \ln(2) r_{\oplus} (r_{\oplus} + a_s)} \int_{a_s}^{r_{\text{max}}} \int_0^{\infty} -\frac{r_0^\alpha \sigma^2}{p_t G_t(r_0, a_s)} (e^t - 1) \quad (5.31)$$

$$\times e^{-\frac{r_0^\alpha \sigma^2}{p_t G_t(r_0, a_s)} (e^t - 1)} \ln \left( 1 + \frac{p_t G_t(r_0, a_s) h_0 r_0^{-\alpha}}{\sigma^2} \right) \left( 1 - \frac{r_0^2 - a_s^2}{4 r_{\oplus} (r_{\oplus} + a_s)} \right)^{N_{\text{eff}} - 1} r_0 dh_0 dr_0$$

and

$$\mathbb{E} [\log_2 (1 + \text{SINR}) | N_I > 0]$$

$$= c_0 \int_{a_s}^{r_{\text{max}}} \int_{t>0} \mathbb{E}_I \left[ e^{-\frac{r_0^\alpha}{p_t G_t(r_0, a_s)} (I + \sigma^2)} (e^t - 1) \middle| N_I > 0 \right] \left( 1 - \frac{r_0^2 - a_s^2}{4 r_{\oplus} (r_{\oplus} + a_s)} \right)^{N_{\text{eff}} - 1} r_0 dt dr_0$$

$$= c_0 \int_{a_s}^{r_{\text{max}}} \int_{t>0} e^{-\frac{r_0^\alpha}{p_t G_t(r_0, a_s)} \sigma^2} (e^t - 1)$$

$$\times \mathcal{L}_I \left( \frac{r_0^\alpha}{G_t(r_0, a_s)} (e^t - 1) \right) \left( 1 - \frac{r_0^2 - a_s^2}{4 r_{\oplus} (r_{\oplus} + a_s)} \right)^{N_{\text{eff}} - 1} r_0 dt dr_0$$



where  $\mathcal{L}_I(\cdot)$  can be calculated using (5.6). Assuming static serving channels, (5.29) and (5.30) are given in [P1, Theorem 4] as

$$\mathbb{E} [\log_2 (1 + \text{SNR})] = \frac{1}{\ln(2)} \int_{t>0} F_{R_0} \left( \left( \frac{p_t}{(e^t - 1) \sigma^2} \right)^{\frac{1}{\alpha}} \right) dt \quad (5.32)$$

and

$$\begin{aligned} \mathbb{E} [\log_2 (1 + \text{SINR} | N_I > 0)] &= \frac{N_{\text{act}}}{4\pi \ln(2) r_{\oplus} (r_{\oplus} + a_s)} \int_{a_s}^{r_{\text{max}}} \int_{t>0} \int_{-\infty}^{\infty} \mathcal{L}_I(j\omega) \\ &\times \left( \frac{e^{j \left( \frac{p_t}{r_0^\alpha (e^t - 1)} - \sigma^2 \right) \omega} - 1}{j\omega} \right) \left( 1 - \frac{r_0^2 - a_s^2}{4r_{\oplus} (r_{\oplus} + a_s)} \right)^{N_{\text{act}} - 1} r_0 d\omega dt dr_0. \end{aligned} \quad (5.33)$$

For Nakagami- $m$  fading which covers the aforementioned fading models by varying the fading parameter,  $m$ , the data rate for a BPP-distributed constellation is given as

$$\begin{aligned} \bar{C} &= \frac{N_{\text{eff}}}{2K \ln(2) r_{\oplus} (r_{\oplus} + a_s)} \int_{a_s}^{r_{\text{max}}} \int_0^{\infty} \left( 1 - \frac{r_0^2 - a_s^2}{4r_{\oplus} (r_{\oplus} + a_s)} \right)^{N_{\text{act}} - 1} \\ &\times \left[ e^{-s\sigma^2} \sum_{k=0}^{m-1} \frac{\sum_{l=0}^k \binom{k}{l} (s\sigma^2)^l (-s)^{k-l} \frac{\partial^{k-l}}{\partial s^{k-l}} \mathcal{L}_I(s)}{k!} \right]_{s = \frac{m(2^t - 1)r_0^\alpha}{p_t G_t(r_0, a_s)}} dt dr_0. \end{aligned} \quad (5.34)$$

As mentioned earlier for the coverage probability in previous subsections, for noise-limited system, there is no need to limit the results to some specific fading model and the data rate can be obtained in generic form using (5.30) as given in [P2].

## 5.2.2 Data rate for NPPP distributed satellites

The derivations on the average data rate of a NPPP constellation follow the same approach as for the coverage probability. To make this summary more concise, the intermediate steps and detailed proofs given in [P3, P4, P5] are excluded here. Two important propagation models, i.e., Nakagami- $m$  fading and noise-limited transmission scenarios are given as in the below expressions.

The downlink average data rate of a NPPP LEO constellation under a Nakagami- $m$  fading serving channel and arbitrarily distributed fading or shadowing for inter-

**Table 5.1** Fading models used for simulations

Fading model	Channel gain distribution	Publications
Rayleigh	Exponential	[P1]
Nakagami- $m$	Gamma	[P4, P7]
Rician	Noncentral chi-squared	[P2, P3, P5, P6]
Static	Deterministic	[P1]

fering channels is

$$\bar{C} = \frac{1}{K} \int_{a_s}^{r_{\max}} \int_0^\infty \int_0^\infty f_{\mathcal{X}_0}(x_0) f_{R_0}(r_0) \left[ e^{-s\sigma^2} \sum_{k=0}^{m-1} \frac{\sum_{l=0}^k \binom{k}{l} (s\sigma^2)^l (-s)^{k-l} \frac{\partial^{k-l}}{\partial s^{k-l}} \mathcal{L}_I(s)}{k!} \right]_{s=\frac{m(2^t-1)r_0^\alpha}{p_t G_t(r_0, a_s) x_0}} dt dx_0 dr_0, \quad (5.35)$$

where  $\mathcal{L}_I(s)$  will be given in (5.23) and its corresponding special cases given in [P4]. When co-channel interference is zero at the receiver, the data rate for a NPPP model is given as, [P3],

$$\bar{C} = \frac{1}{\ln(2)} \int_{r_{\min}}^{r_{\max}} \int_0^\infty \int_0^\infty f_{\mathcal{X}_0}(x_0) \left( 1 - F_{G_0} \left( \frac{r_0^\alpha \sigma^2}{p_t G_t(r_0, a_s)} (e^t - 1) \right) \right) f_{R_0}(r_0) dx_0 dt dr_0. \quad (5.36)$$

### 5.3 Numerical results and discussion

In this section, the derivations on the performance metrics of a LEO communication network based on the two point processes, i.e., BPP and NPPP, are validated through Monte Carlo simulations. The numerical results are then used to interpret the effect of several network parameters, including the satellites' altitude, constellation size, number of orthogonal frequency channels, and latitude of the user or ground terminal, on the performance of a LEO network.

The simulated LEO constellation is similar to what is described in Section 2.3, i.e.,  $N_{\text{act}}$  satellites are distributed uniformly on equally-spaced circular inclined orbits

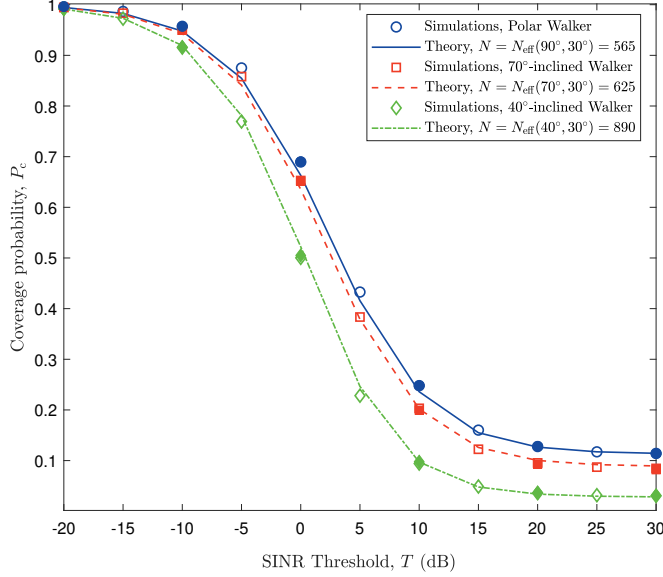


**Figure 5.3** Verification of coverage probability derived in (5.1) with simulations for Rayleigh fading channels and 720 satellites at 1200 km.

distanced  $a_s$  from Earth's surface. To obtain the performance metrics, averages over the satellites' locality as well as the channel gains are taken for a large number of realizations. As satellites move continuously on orbits, the performance is averaged over different realizations of satellites over the time. The averaging is also taken over the channel gains which are modeled as different random variables depending on the fading statistics. Different channel gains which are adopted in the publications are listed in Table 5.1. The shadowing effect included in [P3, P4] is assumed to follow a log-normal distribution for the numerical results.

In the following subsections, the analytical expressions obtained in this chapter are validated through Monte Carlo simulations.

### 5.3.1 Corroboration of analysis by simulations

In [P1, P2], it is shown that the performance deviation between an actual LEO constellation and a randomly modeled constellation can be eliminated by substituting the actual number of satellites with the effective number of satellites,  $N_{\text{eff}}$ . The effective number of satellites is calculated through mean absolute error minimization

between the performance metric derived from the theory and the results from the actual simulated constellations for a given user's latitude in [P1]. Although some specific simulation parameters are used to obtain  $N_{\text{eff}}$ , the value is applicable for other system parameters, i.e., path loss exponent and/or SINR threshold values as well. Likewise, the acquired  $N_{\text{eff}}$  can be also used for other constellation sizes by linearly scaling it accordingly.

Figure 5.3 depicts the coverage probability versus the SINR threshold for three Walker constellations with different inclination angles. The coverage probability is derived theoretically by modeling the satellites as a BPP. As can be seen in the figure, applying  $N_{\text{eff}}$  to the derivations obtained from BPP stochastic modeling compensates for the varying density of satellites along different latitudes and lead to its matching with the performance of the actual constellations. The solid markers on the curves were chosen for finding  $N_{\text{eff}}$  through minimizing the mean absolute error between the coverage probabilities of stochastic and actual constellations. However, the chosen  $N_{\text{eff}}$  also holds for other values that had no contribution on the minimization process. Simulating a constellation comprised of 720 satellites, the corresponding effective number of satellites for  $90^\circ$ ,  $70^\circ$  and  $40^\circ$  inclination angles are 565, 625, and 890, respectively. As the inclination angles decreases, the density of satellites increases as the same number of satellites are distributed on a smaller surface which results in larger values for  $N_{\text{eff}}$ .

Figure 5.4 verifies the theoretical derivations on the coverage probability for a noise-limited communication scenario and two constellation sizes of 648 and 120 given in [P2]. Despite Fig. 5.3, in Fig. 5.4,  $N_{\text{eff}}$  to compensate for the inherent mismatch between the actual and BPP constellations is obtained analytically using (4.3). For fewer number of satellites, e.g.,  $N_{\text{act}} = 120$ , it can be well observed that the performance is upper bounded by the probability of observing at least one satellite above the sky. As a result, the upper bound is enhanced with rising the altitude as better visibility is provided for the ground user. On the other hand, for a larger constellation size, e.g.,  $N_{\text{act}} = 648$ , the coverage probability is affected only by the path loss since all the time there is at least one visible satellite to the user, i.e., the visibility probability approaches one.

Figure 5.5 verifies the coverage probability derived by NPPP modeling given in (5.22) for  $53^\circ$  inclined orbits and a user located at  $25^\circ$  latitude. The constellation size and altitude are set to 2000 and 500 km, respectively. As shown in the figure, the

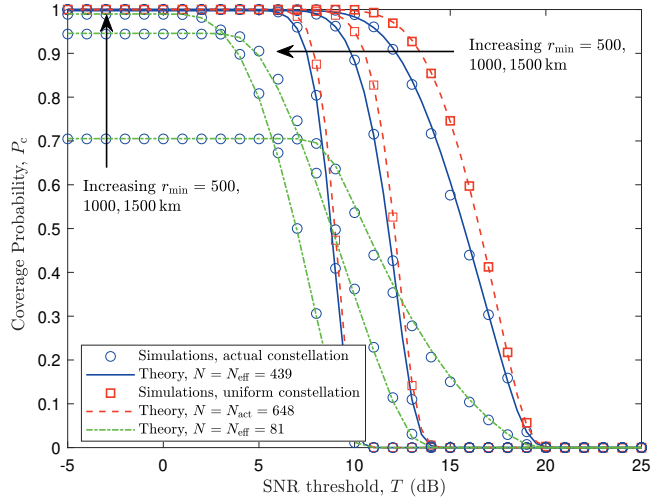


**Figure 5.4** Verification of coverage probability given in (5.19) with simulations for Rician fading channels with fading parameter 100,  $\phi_u = 0^\circ$ ,  $\iota = 70^\circ$ ,  $a_s \in \{500, 1000, 1500\}$  km, and  $\theta_{\min} = 10^\circ$ .

markers that depict the Monte Carlo simulations are fully matched with the solid lines that represent the theoretical expressions.

Shadowing randomness may cause an altering effect on the received SINR at the user's place, i.e., causing an increase or decrease in the received SINR. As a result, an ever-changing shadowing effect on the coverage probability can be observed in Fig. 5.5. The alteration of shadowing effect is affected by its distribution as well as its mean and variance. Nakagami- $m$  is adopted to generate the results given in Fig. 5.5. Larger values of  $m$  correspond to the reception of a stronger LOS component and, consequently, less multi-path distortion, which result in slightly better coverage. However, shadowing masks the effect of fading at large.

The verification of BPP and NPPP models to derive average data rate in (5.28) and (5.35) is depicted in Figs. 5.6 and 5.7, respectively. In Fig. 5.6, the optimal number of frequency channels that maximizes the data rate for each of the Walker constellations decreases by increasing the inclination angle. The selected  $N_{\text{eff}}$  values are slightly different from those in Fig. 5.3 since they correspond to the constellation size that results in the best possible match between the data rate of the random and Walker constellation. Since the density of satellites are lower for polar orbits, a

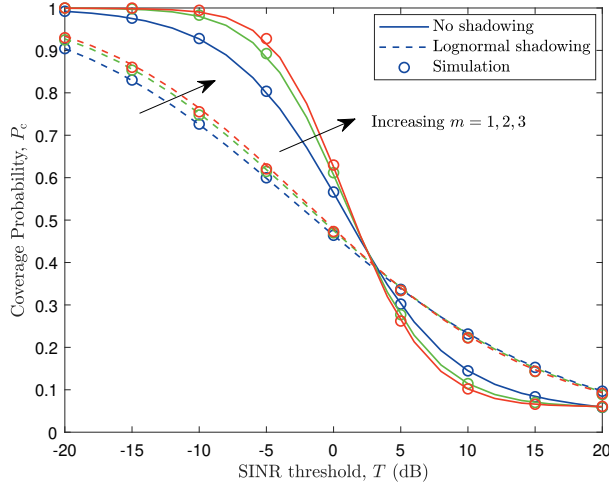


**Figure 5.5** Verification of (5.22) with simulations when  $\phi_u = 25^\circ$ ,  $\iota = 53^\circ$ ,  $m \in \{1, 2, 3\}$ , and  $\theta_{\min} = 10^\circ$ . Theoretical and simulation results are shown by lines and markers, respectively.

slight mismatch is observed between the theoretical and simulation results which indicates an increasing deviation between one snapshot of the point process and the actual LEO constellation with decreasing the density of satellites. In other words, the results provided herein show more accuracy and exactness for high-density satellite networks.

Figure 5.7 verifies the derivation of average data rate given in (5.35) for a user located at latitude  $25^\circ$ . As shown in the figure, the simulation results are perfectly in line with theory. The same as in Fig. 5.3, an optimum value is observed for the number of frequency channels. As the number of orthogonal frequency bands increases, the satellites which operate on the same frequency band and cause interference at the user's reception declines which improves the data rate. On the other hand, by increasing the number of frequency channels, the bandwidth allocated to each shared group of satellites reduces accordingly. Thus, the initial rise in the plot is due to the decrease in the number of interfering satellites, followed by a decline caused by comprising only  $\frac{1}{K}$  of frequency band.

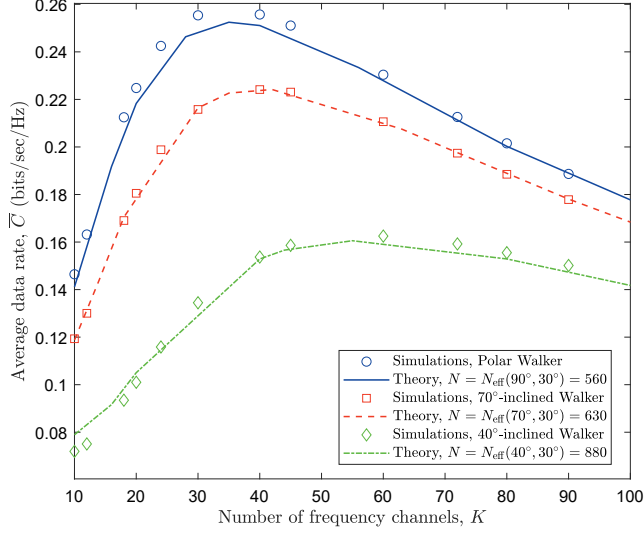


**Figure 5.6** Effect of the number of frequency bands,  $K$ , on average achievable rate and verification of (5.28) for Rayleigh fading channels.

### 5.3.2 Effect of satellites' altitude

Figure 5.8 illustrates the effect of altitude on the coverage probability and data rate under Nakagami fading [P4]. Regardless of the shadowing effect, there is an optimum altitude that maximizes both performance metrics. The optimum value varies with user's latitude. Since constellation density is higher at the inclination limits, the optimum altitude for  $\phi_u = 25^\circ$  is slightly lower than  $\phi_u = 0^\circ$ . This is because of the existence of more interferers at upper latitudes. When user is located at  $\phi_u = 65^\circ$ , i.e., out of the constellation borders ( $\phi_u > \iota = 53^\circ$ ), a larger altitude is required for the user to be served by a satellite. Therefore, both coverage probability and data rate are zero at altitudes below  $\approx 400$  km, as there is no visible satellite to the user.

Effect of altitude on coverage probability and data rate is depicted in Fig. 5.9 (a) and (b), respectively, under Rayleigh fading assumption and zero shadowing. The figure is plotted by substituting  $N_{\text{eff}}$  into the BPP-based derivations given in Theorems 1 and 3 in [P1]. Within the typical LEO satellites' altitude range, i.e., below 500 km, both performance metrics decline with rising the altitude. The optimum altitude, which decreases by increasing the number of satellites, is observed at low altitudes within Earth's atmosphere. Obviously, for commercial constellations, satel-

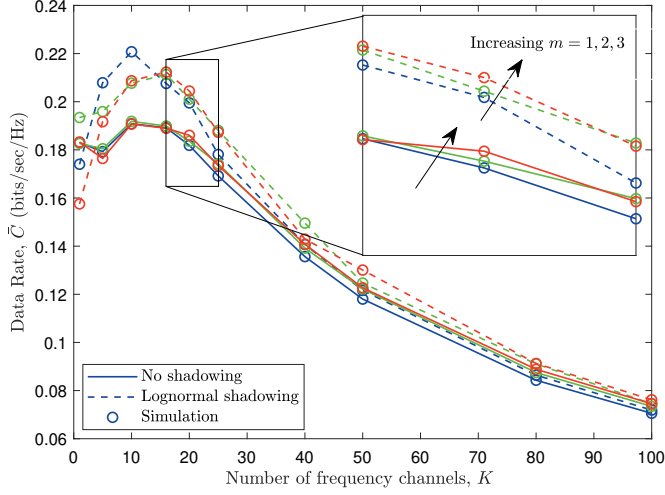


**Figure 5.7** Verification of (5.35) with simulations when  $\phi_u = 25^\circ$ ,  $\iota = 53^\circ$ ,  $m \in \{1, 2, 3\}$ , and  $\theta_{\min} = 10^\circ$ . Theoretical and simulation results are shown by lines and markers, respectively.

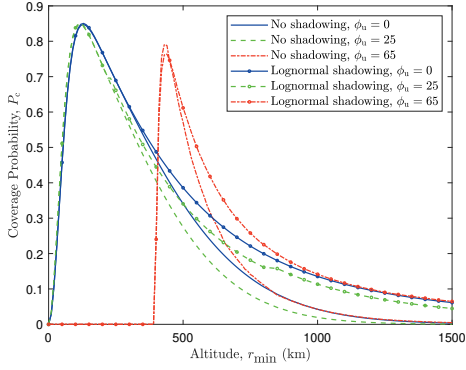
lites are deployed on higher altitudes to avoid atmospheric drag [9].

### 5.3.3 Effect of ground terminal/user's latitude

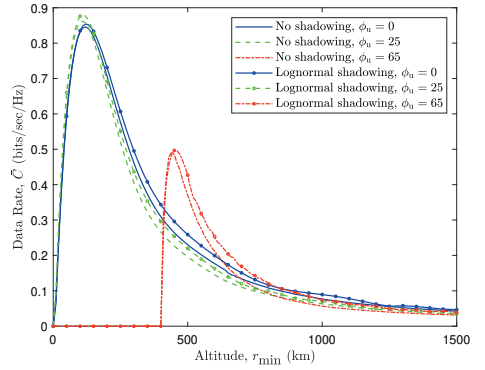
In Fig. 5.10, the effect of user's latitude on coverage probability and data rate is shown for three Walker constellations with different inclination angles under Rayleigh fading. Right side vertical axes show the effective number of satellites obtained numerically to minimize the approximation error in modeling deterministic constellations as a BPP. In this figure, the markers depict the simulation results for the coverage probability and data rate of Walker constellation for polar,  $70^\circ$  and  $40^\circ$  inclined orbits. For a polar constellation, the number of viewable satellites and, consequently, the effective number of satellites increase monotonically from the equator to poles. As a result, the performance degrades accordingly as the user moves from the equator to poles due to viewing more interfering satellites.

The zero coverage probability and data rate for  $40^\circ$ -inclined constellation for latitudes greater than  $75^\circ$  demonstrates the fact that there are no visible satellites to the user at those high latitudes. The solid lines in the figures are generated using (5.1) and (5.28) with  $N_{\text{eff}}(\iota, \phi_u)$  satellites. As can be seen, the solid lines are matched with



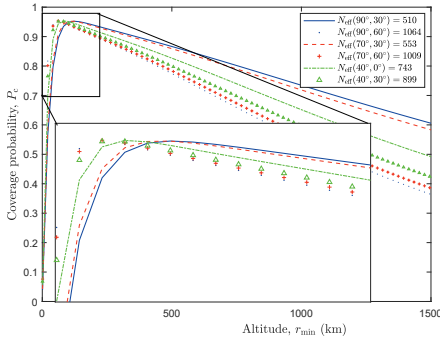


(a) Effect of altitude on coverage probability.

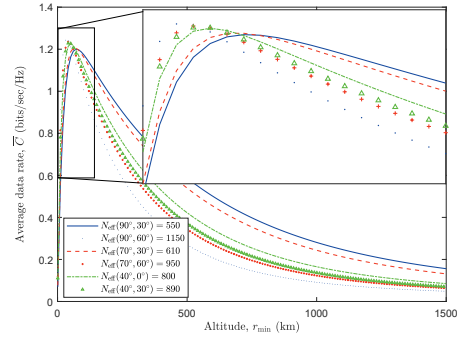


(b) Effect of altitude on data rate.

**Figure 5.8** Effect of altitude on the performance of a LEO network under Nakagami- $m$  fading. Shadowing distribution is assumed to be log-normal,  $T = 5$  dB,  $\phi_u = \{0^\circ, 25^\circ, 65^\circ\}$ ,  $\iota = 53^\circ$ ,  $m = 2$ , and  $\theta_{\min} = 10^\circ$ .



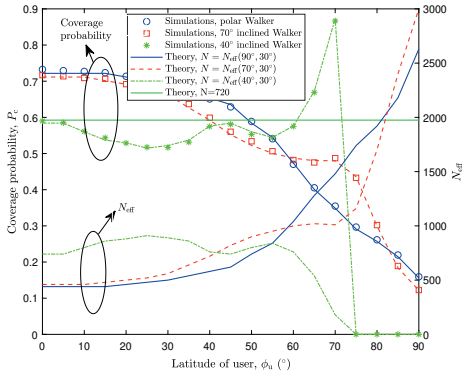
(a) Effect of altitude on coverage probability.



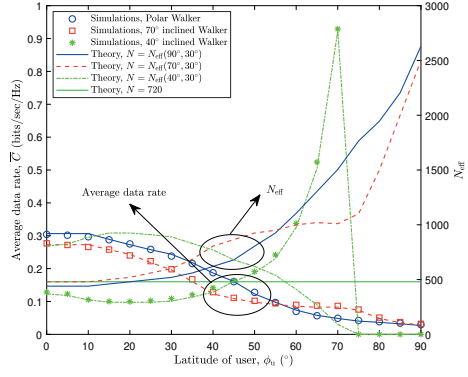
(b) Effect of altitude on data rate.

**Figure 5.9** Average rate for different altitudes. Plots are generated using (5.1) for three Walker constellations with  $\phi_u = 0^\circ, 30^\circ, 60^\circ$ , and  $N_{\text{eff}}(\iota, \phi_u)$ .

the markers obtained from Monte Carlo simulations of Walker constellations for the given  $\phi_u$ . Therefore, using  $N_{\text{eff}}(\iota, \phi_u)$  in (5.1) and (5.28), the varying satellite density along different latitudes is compensated and the performance metrics can be obtained for any desired actual constellation. Most importantly, it can be concluded that the deviation between the performance of deterministic and stochastic constellations can be fairly eliminated by considering the uneven satellite density at different latitudes.

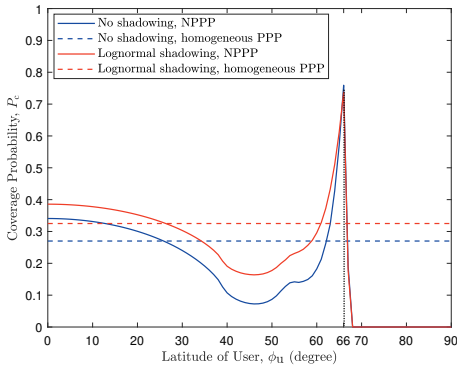


(a) Effect of user's latitude on the coverage probability.

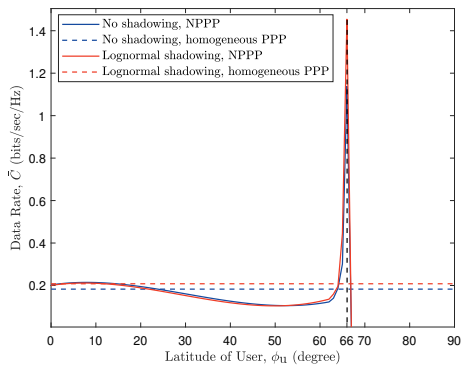


(b) Effect of user's latitude on average data rate.

**Figure 5.10** Effect of user's latitude on the performance of a LEO network. The markers are plotted by simulating three Walker constellations with  $90^\circ$ ,  $70^\circ$  and  $40^\circ$  inclination angles.



(a) Coverage probability on different users' latitudes.



(b) Data rate on different users' latitudes.

**Figure 5.11** Effect of user's latitude on the performance of a LEO network for  $K = 10$ ,  $T = 5$  dB,  $r_{\min} = 500$  km,  $\iota = 53^\circ$ ,  $m = 2$ , and  $\theta_{\min} = 10^\circ$ .

The effect of ground user's latitude on coverage probability and data rate of a LEO constellation is depicted in Fig. 5.11 when satellites are modeled as a NPPP. The performance metrics are shown by solid lines when NPPP intensity function is set to (4.5). As the satellite intensity increases by rising the user's latitude, the performance becomes more unreliable due to presence of more interfering satellites

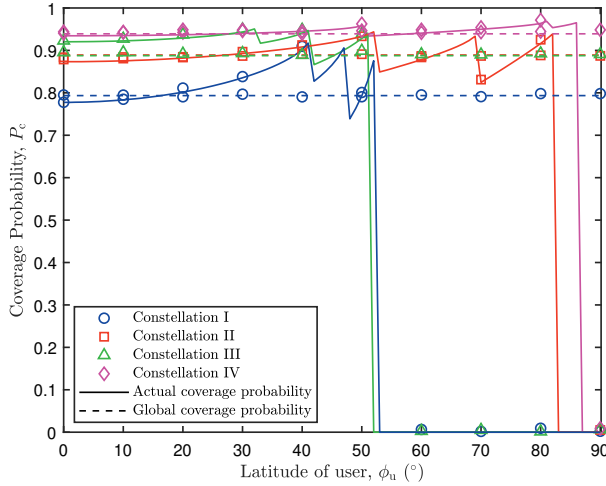
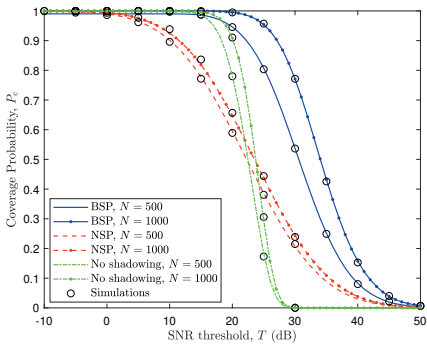


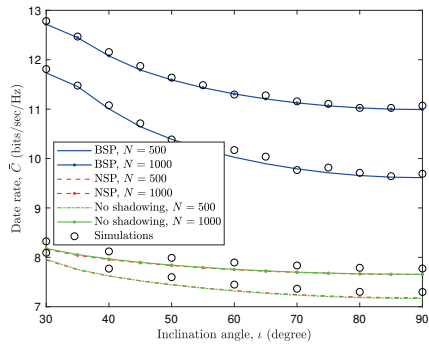
**Figure 5.12** The effect of user's latitude on the coverage probability for four multi-altitude constellations, given in [P7, Table I], when  $T = 5$  and  $N_{\text{act}} = 1800$ . The lines and the markers represent the analytical results and simulations, respectively.

that share the same frequency channel with the serving satellite. At latitudes higher than the constellation inclination limits, the performance increases sharply due to the reduction in the received interference. The performance is maximized at about  $66^\circ$  where the serving satellite is the only visible satellite to the user, i.e., the performance becomes noise-limited. At higher than  $66^\circ$  latitudes, the user will be in full outage and both coverage probability and rate converge to zero. When the intensity of satellites is constant, i.e.,  $\delta = \frac{N_{\text{act}}}{4\pi(a_s+r_\oplus)^2}$ , the performance remains unchanged over all latitudes as shown in the figure by dashed lines.

Four multi-altitude benchmark constellations are considered in [P7] whose satellites are distributed on several orbital shells with varying altitudes and inclination angles. The details on specifications of these constellation can be found in [P7, Table I]. The effect of user's latitude on the coverage probability of multi-altitude constellations is shown in Fig. 5.12. The variations in the plots are justifiable according to the varying density of satellites along different latitudes. A local maxima can be observed at the inclination angle of each orbital shell due to the decrease in the number of interfering satellites which is then followed by a steep local minima caused by losing the connection with the best available server. The drop in coverage probability is more severe at larger inclination angles since the number of visible satellites to



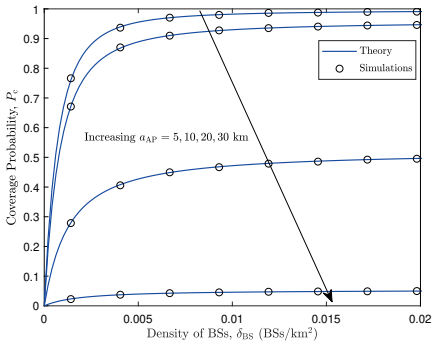
(a) Coverage probability vs. SNR threshold.



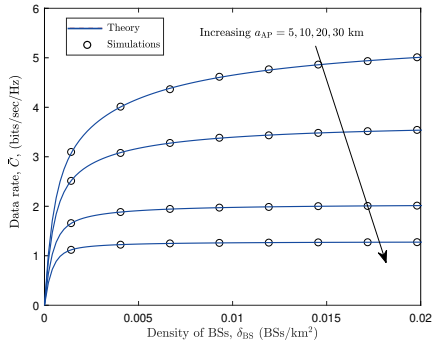
(b) Data rate vs. inclination angle.

**Figure 5.13** Coverage probability and data rate under BSP and NSP association policies when  $K = 10$ ,  $\phi_u = 25^\circ$ ,  $r_{\min} = 500$  km, and  $\theta_{\min} = 10^\circ$ .

the ground user decreases drastically.



(a) Coverage probability



(b) Data rate

**Figure 5.14** Effect of BSs' density on coverage probability and data rate of a terrestrial backhaul for an airborne network at different altitudes.

### 5.3.4 Effect of user association policy

Figure 5.13 depicts how the two association policies, i.e., BSP and NSP, affect the performance of LEO network in terms of coverage probability and data rate for  $N_{\text{act}} = 500$  and 1000 satellites. The fair match between the theory (plotted by

lines) and the simulations (plotted by markers) verifies the derivations in [P5]. As can be seen, the BSP results in a superior performance compared to NSP, since the received SNR is improved by considering the effect of shadowing on user association. Obviously, the two association policies become the same when shadowing is assumed to be zero.

Larger constellation sizes provide higher data rates and coverage probability due to providing a higher probability for the user to connect to a better server. As satellites' density decreases with rising the inclination angle, the data rate slightly decreases accordingly, as shown in Fig. 5.13(b).

### 5.3.5 Performance of LEO backhaul network

In [P5], the performance of a LEO backhaul network is compared to a terrestrial backhaul in order to provide noteworthy criteria on the best backhaul selection for APs which is affected by the LEO constellation parameters, the density of ground BSs, and AP's location in terms of its latitude and altitude. Figure 5.14 depicts the performance of terrestrial backhaul for an airborne network at different altitudes. The terrestrial BSs are distributed on a disc with radius 30 km according to a homogeneous PPP. As can be seen, for lower density of BSs and higher APs' altitudes, the performance of the terrestrial network degrades considerably, especially in terms of the coverage probability.

The effect of AP's altitude on the data rate of both terrestrial and LEO backhaul networks is shown in Fig. 5.15. A slight increase can be observed in data rate of LEO backhaul when rising the AP's altitude which is due to the better visibility and smaller propagation distance at those higher altitudes. However, since the altitude of AP is considerably smaller than the LEO constellation altitude, the variation in the data rate is not significant. The data rate of BS backhaul decreases with increasing the AP's altitude due to the increased path loss. The range of altitude over which the LEO backhaul outperforms the terrestrial backhaul depends on the density of BSs.

Based on the numerical results depicted in Fig. 5.15, it can be concluded that both terrestrial and LEO networks have the potential to serve as the backhaul for the airborne network. Several parameters affect the best backhaul selection such as the LEO network parameters, the terrestrial BS density, and AP's location. For instance, for larger BS densities or higher AP's altitude, terrestrial backhaul provides more promising data rate than LEO satellites. On the other hand, LEO satellites

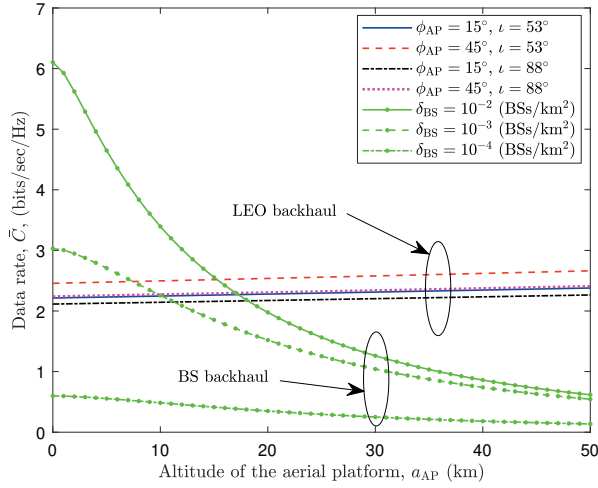


**Figure 5.15** Effect of aerial platform’s altitude on data rate provided by LEO and BS backhaul networks for an airborne network. The total number of LEO satellites and altitude are set to 1000 and 500 km, respectively.

can provide a better backhaul connectivity for extremely low BSs’ densities or excessively high AP’s altitudes. It is also worth mentioning that in highly dense urban areas where the transmitted signal from the terrestrial BSs may be blocked by the surrounding obstacles, a LEO backhaul with a higher probability of LOS can provide better connectivity for APs.

### 5.3.6 Summary of the results

As verified in Subsection 5.3.1, stochastic models can be utilized to accurately model and analyze the massive satellite constellation despite being fully deterministic. Several design guidelines can be directly interpreted from the figures given throughout Section 5.3 on satellites’ altitude, association policies, and the selection of backhaul network. As co-existence of non-terrestrial and terrestrial networks is promised for 6G actualization, the provided analysis provided herein has a great potential for interference modeling and management of such integrated network.

Another key insight is the performance behavior in terms of user’s latitude. As can be seen from Figs. 5.10 – 12, the performance improves close to the inclination limits and, counter intuitively, there could be also coverage for users which are located at higher latitudes than the inclination if satellites can transmit their beams

towards those higher latitudes as well. Moreover, as can be seen throughout the numerical results, the performance is remarkably affected by the used association technique. Finally, some insightful results on the selection of the best backhaul to serve an AP is also provided in this thesis. The outcome suggests that depending on the AP's location, LEO constellation parameters, and the density of BSs on the ground, either a LEO satellite or a ground BS will serve the AP better in terms of achievable data rate.





## 6 CONCLUSIONS

In this dissertation, a tractable analytical framework for physical layer performance analysis of LEO communication networks was studied by stochastic modeling of the network. Such modeling enabled utilizing the tools from stochastic geometry in order to find mathematical derivations on the coverage probability and data rate of any given LEO constellation. This chapter summarizes the main findings of this research while extending the results beyond the immediate scope of the study.

### 6.1 Stochastic analysis of LEO Internet networks

Although LEO satellite networking was studied as the main scope of this research, the analysis also paves the way for extending the application of stochastic geometry to other massive heterogeneous 3D networks, e.g., integrated terrestrial–aerospace networks or massive IoT sensors. Unified and native integration of non-terrestrial network into the existing terrestrial network is foreseen as a key component in 6G. Such integrated network will be highly heterogeneous with BSs extensively distributed over the ground, air, and space. Obviously, stochastic geometry can play a great role in modeling and analysis of such massive 3D network to ensure the required quality of service and its optimal design.

Another key concluding remark is that deterministic networks, e.g., a LEO network with satellites being on predetermined orbits with fixed spacing between them, can be also modeled as a spatial point process. The tight match observed between the performance of actual and stochastic constellations proves the fair accuracy of such models. In fact, despite the terrestrial network for which randomness arises from irregular distribution of nodes, in satellite networks, this randomness is not originated from the satellites' positions, but from different realizations of satellites over the time observed by the user as well as the continuous changing of distances between the satellites in adjacent orbits.

The varying density of satellites over different user's latitudes was taken into account through two different approaches. For BPP, which resulted in more tractable expressions, the error in approximating the LEO constellation as a BPP was compensated through finding the effective number of satellites for each user's latitude. When modeling the LEO network as a NPPP, the non-uniform intensity of satellites is embedded in the intensity function of the point process. A tight match is achieved for this approach without any further compensation at the expense of having less tractability. Therefore, the inherent performance error caused by geometry of satellite constellations is rather minimal when their varying density over the latitudes is considered.

Other than performance analysis, the results can be used to optimize LEO networks in order to provide the same quality of service with fewer resources, e.g., total number of satellites. The optimization will lead to a remarkable drop in the operational and launch costs of LEO networks via minimizing the constellation size.

## 6.2 Future directions

The timely research topic and the novel framework presented in this thesis have inspired many other researchers shortly after the first two publications [P1, P2] to create new results and extend the research line, e.g., in [39], [45], [46], [87], [95], [102]. Obviously, there are still many open lines of research on the modeling and analysis of LEO communication networks as well as other 3D networks. The first research direction would be optimization of LEO communication networks which can accelerate their efficient design and developments. Although performance analysis was the main focus of this thesis, the analytical approach provided herein has a great potential for optimization of different LEO network parameters and resources.

Basic support for integration of non-terrestrial and terrestrial networks has been proposed through Releases 15 to 18 of the third Generation Partnership Project for 5G [103]. However, the fundamental changes will have to wait for 6G for which the non-terrestrial networks are seen as a key component by many mobile industries in their 6G visions. Therefore, the second research direction would be extending the results to an integrated network where the user can be served by the best of both networks. In [P6], this research problem was partially addressed and some insights

on the selection of the best network were provided through the numerical results. However, the analysis on the selection of the best network to serve the users given the network parameters and the performance criteria will remain as an interesting future work. Obviously, the efficient spectrum management (dedicated or shared spectrum) needs to be considered before the integration of the two networks.

The third research direction can be including the inter-satellite links into the current analysis as some commercial constellations have already equipped satellites with laser inter-satellite links. These links can enhance the speed of communication as the data can be relayed by their optical links much faster and through a shorter distance than undersea fiber-optic cables. The first obvious challenge would be modeling the channels and propagation characteristic of such links which are totally different than radio-frequency communication links.

Finally, considering more practical antenna patterns in the analysis which are able to steer the beams towards the actual locations of users on Earth is of great importance as it is in line with the beamforming design of some commercial LEO projects. Moreover, the width of beams can be also adjusted according to the user's demands and population density. To tractably consider beamforming for LEO networks, the distribution of ground terminals needs to be included in the analysis. Moreover, the frequency channel assignment which is performed randomly (uniform) in this thesis, can be included in a more efficient way to optimize the network performance.



## REFERENCES

- [1] H. Xie, Y. Zhan, G. Zeng, and X. Pan, "LEO mega-constellations for 6G global coverage: Challenges and opportunities," *IEEE Access*, vol. 9, pp. 164 223–164 244, Dec. 2021. DOI: 10.1109/ACCESS.2021.3133301.
- [2] M. Giordani and M. Zorzi, "Non-terrestrial communication in the 6G era: Challenges and opportunities," *available online: arxiv.org/abs/1912.10226v2*, 2019.
- [3] Z. Jia, M. Sheng, J. Li, D. Zhou, and Z. Han, "Joint HAP access and LEO satellite backhaul in 6G: Matching game based approaches," *IEEE Journal on Selected Areas in Communications*, Aug. 2020.
- [4] M. Giordani, M. Polese, M. Mezzavilla, S. Rangan, and M. Zorzi, "Toward 6G networks: Use cases and technologies," *IEEE Communications Magazine*, vol. 58, no. 3, pp. 55–61, Mar. 2020.
- [5] H. Xie, Y. Zhan, G. Zeng, and X. Pan, "LEO mega-constellations for 6G global coverage: Challenges and opportunities," *IEEE Access*, vol. 9, pp. 164 223–164 244, Dec. 2021.
- [6] J. L. Grubb, "The traveler's dream come true," *IEEE Communications Magazine*, vol. 29, no. 11, pp. 48–51, Nov. 1991.
- [7] A. Yastrebova, I. Angervuori, N. Okati, M. Vehkaperä, M. Höyhty, R. Wichman, and T. Riihonen, "Theoretical and simulation-based analysis of terrestrial interference to LEO satellite uplinks," in *Proc. IEEE Global Communications Conference*, Dec. 2020.
- [8] I. del Portillo, B. G. Cameron, and E. F. Crawley, "A technical comparison of three low Earth orbit satellite constellation systems to provide global broadband," *Acta Astronautica*, vol. 159, pp. 123–135, Mar. 2019, available online at [www.sciencedirect.com/science/article/pii/S0094576518320368](http://www.sciencedirect.com/science/article/pii/S0094576518320368).

- [9] Y. F. Hu, G. Maral, and E. Ferro, *Service efficient network interconnection via satellite: EU COST Action 253*. John Wiley and Sons, Jan. 2002.
- [10] F. Vatalaro, G. E. Corazza, C. Caini, and C. Ferrarelli, "Analysis of LEO, MEO, and GEO global mobile satellite systems in the presence of interference and fading," *IEEE Journal on Selected Areas in Communications*, vol. 13, no. 2, pp. 291–300, Feb. 1995.
- [11] S. R. Pratt, R. A. Raines, C. E. Fossa, and M. A. Temple, "An operational and performance overview of the iridium low earth orbit satellite system," *IEEE Communications Surveys*, vol. 2, no. 2, pp. 2–10, 1999.
- [12] A. Ganz, Y. Gong, and B. Li, "Performance study of low Earth-orbit satellite systems," *IEEE Transactions on Communications*, vol. 42, no. 234, pp. 1866–1871, Feb. 1994.
- [13] A. K. Dwivedi, S. P. Chokkarapu, S. Chaudhari, and N. Varshney, "Performance analysis of novel direct access schemes for LEO satellites based IoT network," in *Proc. IEEE 31st Annual International Symposium on Personal, Indoor and Mobile Radio Communications*, Sep. 2020.
- [14] Z. Hong, F. Sun, F. Xu, Z. Fan, and G. Zheng, "A stochastic reward net-based performance analysis of LEO satellite networks," in *Proc. IEEE International Conference on Networking, Sensing and Control*, Apr. 2006.
- [15] W. Zeng and Z. Hong, "SPN-based performance analysis of LEO satellite networks with multiple users," in *Proc. International Conference on Machine Learning and Cybernetics*, Jul. 2011.
- [16] H. M. Mourad, A. A. M. Al-Bassiouni, S. S. Emam, and E. K. Al-Hussaini, "Generalized performance evaluation of low Earth orbit satellite systems," *IEEE Communications Letters*, vol. 5, no. 10, pp. 405–407, Oct. 2001.
- [17] G. Ruiz, T. L. Doumi, and J. G. Gardiner, "Teletraffic analysis and simulation for nongeostationary mobile satellite systems," *IEEE Transactions on Vehicular Technology*, vol. 47, no. 1, pp. 311–320, Feb. 1998.
- [18] I. Ali, N. Al-Dhahir, and J. E. Hershey, "Predicting the visibility of LEO satellites," *IEEE Transactions on Aerospace and Electronic Systems*, vol. 35, no. 4, pp. 1183–1190, Oct. 1999.

- [19] Y. Seyedi and S. M. Safavi, "On the analysis of random coverage time in mobile LEO satellite communications," *IEEE Communications Letters*, vol. 16, no. 5, pp. 612–615, May 2012.
- [20] Z. Qu, G. Zhang, H. Cao, and J. Xie, "LEO satellite constellation for Internet of Things," *IEEE Access*, vol. 5, pp. 18 391–18 401, Sep. 2017.
- [21] K. Tekbıyık, G. K. Kurt, and H. Yanikomeroglu, "Energy-efficient RIS-assisted satellites for IoT networks," *IEEE Internet of Things Journal*, pp. 1–1, Sep. 2021. DOI: 10.1109/JIOT.2021.3112881.
- [22] J. Hu, G. Li, D. Bian, L. Gou, and C. Wang, "Optimal power control for cognitive LEO constellation with terrestrial networks," *IEEE Communications Letters*, vol. 24, no. 3, pp. 622–625, Mar. 2020.
- [23] J. Zhang, B. Evans, M. A. Imran, X. Zhang, and W. Wang, "Performance analysis of C/U split hybrid satellite terrestrial network for 5G systems," in *Proc. 20th IEEE International Workshop on Computer Aided Modelling and Design of Communication Links and Networks*, Sep. 2015.
- [24] A. J. Roumeliotis, C. I. Kourogıorgas, and A. D. Panagopoulos, "Optimal dynamic capacity allocation for high throughput satellite communications systems," *IEEE Wireless Communications Letters*, vol. 8, no. 2, pp. 596–599, Apr. 2019.
- [25] J. Liu, Y. Shi, Z. M. Fadlullah, and N. Kato, "Space-air-ground integrated network: A survey," *IEEE Communications Surveys Tutorials*, vol. 20, no. 4, pp. 2714–2741, 2018.
- [26] A. Guidotti, A. Vanelli-Coralli, T. Foggi, G. Colavolpe, M. Caus, J. Bas, S. Cioni, and A. Modenini, "LTE-based satellite communications in LEO mega-constellations," *International Journal of Satellite Communications and Networking*, vol. 37, Jul. 2018. DOI: 10.1002/sat.1258.
- [27] I. Ali, N. Al-Dhahir, and J. Hershey, "Doppler characterization for LEO satellites," *IEEE Transactions on Communications*, vol. 46, no. 3, pp. 309–313, Mar. 1998.
- [28] T. A. Khan and M. Afshang, "A stochastic geometry approach to Doppler characterization in a LEO satellite network," in *Proc. IEEE International Conference on Communications*, 2020.

- [29] G. He, X. Gao, L. Sun, and R. Zhang, "A review of multibeam phased array antennas as LEO satellite constellation ground station," *IEEE Access*, vol. 9, pp. 147 142–147 154, Oct. 2021.
- [30] A. Ivanov, R. Bychkov, and E. Tcatcorin, "Spatial resource management in LEO satellite," *IEEE Transactions on Vehicular Technology*, vol. 69, no. 12, pp. 15 623–15 632, Dec. 2020.
- [31] *Mission Design & Implementation of Satellite Constellations*. Springer, Dordrecht, 1997, available online at arXiv:2102.00588v1. DOI: <https://doi.org/10.1007/978-94-011-5088-0>.
- [32] Y. Su, Y. Liu, Y. Zhou, J. Yuan, H. Cao, and J. Shi, "Broadband leo satellite communications: Architectures and key technologies," *IEEE Wireless Communications*, vol. 26, no. 2, pp. 55–61, Apr. 2019. DOI: 10.1109/MWC.2019.1800299.
- [33] A. F. Molisch, *Wireless communications*. John Wiley & Sons, 2012.
- [34] J. G. Andrews, F. Baccelli, and R. K. Ganti, "A tractable approach to coverage and rate in cellular networks," *IEEE Transactions on Communications*, vol. 59, no. 11, pp. 3122–3134, Nov. 2011.
- [35] Z. Jia, M. Sheng, J. Li, D. Zhou, and Z. Han, "Joint HAP access and LEO satellite backhaul in 6G: Matching game-based approaches," *IEEE Journal on Selected Areas in Communications*, vol. 39, no. 4, pp. 1147–1159, Apr. 2021.
- [36] R. Deng, B. Di, S. Chen, S. Sun, and L. Song, "Ultra-dense LEO satellite offloading for terrestrial networks: How much to pay the satellite operator?" *IEEE Transactions on Wireless Communications*, vol. 19, no. 10, pp. 6240–6254, Oct. 2020.
- [37] A. Abdi, W. Lau, M.-S. Alouini, and M. Kaveh, "A new simple model for land mobile satellite channels: First- and second-order statistics," *IEEE Transactions on Wireless Communications*, vol. 2, no. 3, pp. 519–528, May 2003.
- [38] G. Alfano and A. De Maio, "Sum of squared shadowed-Rice random variables and its application to communication systems performance prediction," *IEEE Transactions on Wireless Communications*, vol. 6, no. 10, pp. 3540–3545, Oct. 2007.



- [39] A. Talgat, M. A. Kishk, and M.-S. Alouini, “Stochastic geometry-based analysis of LEO satellite communication systems,” *IEEE Communications Letters*, Oct. 2020.
- [40] H. Lin, C. Zhang, Y. Huang, R. Zhao, and L. Yang, “Fine-grained analysis on downlink LEO satellite-terrestrial mmWave relay networks,” *IEEE Wireless Communications Letters*, May 2021.
- [41] G. E. Corazza and F. Vatalaro, “A statistical model for land mobile satellite channels and its application to nongeostationary orbit systems,” *IEEE Transactions on Vehicular Technology*, vol. 43, no. 3, pp. 738–742, Aug. 1994.
- [42] F. Vatalaro and G. E. Corazza, “Probability of error and outage in a rice-lognormal channel for terrestrial and satellite personal communications,” *IEEE Transactions on Communications*, vol. 44, no. 8, pp. 921–924, Aug. 1996.
- [43] J. Lopez-Fernandez, J. F. Paris, and E. Martos-Naya, “Bivariate rician shadowed fading model,” *IEEE Transactions on Vehicular Technology*, vol. 67, no. 1, pp. 378–384, Jan. 2018.
- [44] F. Fourati and M.-S. Alouini, “Artificial intelligence for satellite communication: A review,” *Intelligent and Converged Networks*, vol. 2, no. 3, pp. 213–243, Sep. 2021.
- [45] J. Lee, S. Noh, S. Jeong, and N. Lee, “Coverage analysis of LEO satellite downlink networks: Orbit geometry dependent approach,” Aug. 2022, available online at arXiv:2206.09382v1.
- [46] N. L. Jeonghun Park Jinseok Choi, “A tractable approach to coverage analysis in downlink satellite networks,” Aug. 2022, available online at arXiv:arXiv:2111.12851v3.
- [47] A. Al-Hourani, “An analytic approach for modeling the coverage performance of dense satellite networks,” *IEEE Wireless Communications Letters*, vol. 10, no. 4, pp. 897–901, Apr. 2021.
- [48] P. Series, “Attenuation by atmospheric gases and related effects,” *Recommendation ITU-R*, pp. 676–12, 2019.
- [49] D. Liu, L. Wang, Y. Chen, M. Elkashlan, K.-K. Wong, R. Schober, and L. Hanzo, “User association in 5g networks: A survey and an outlook,” *IEEE Communications Surveys Tutorials*, vol. 18, no. 2, pp. 1018–1044, Jan. 2016.

- [50] M. Mühleisen and B. Walke, “Analytical evaluation of LTE uplink performance in the IMT-Advanced Indoor Hotspot scenario,” in *Proc. IEEE 22nd International Symposium on Personal, Indoor and Mobile Radio Communications*, Sep. 2011.
- [51] H. S. Dhillon and J. G. Andrews, “Downlink rate distribution in heterogeneous cellular networks under generalized cell selection,” *IEEE Wireless Communications Letters*, vol. 3, no. 1, pp. 42–45, Nov. 2014.
- [52] D. Ohmann, A. Awada, I. Viering, M. Simsek, and G. P. Fettweis, “Best server sinr models for single- and multi-point transmission in wireless networks,” in *Proc. IEEE Global Communications Conference*, 2015, pp. 1–7. DOI: 10.1109/GLOCOM.2015.7417207.
- [53] E. N. Gilbert, “Random plane networks,” *Journal of the Society for Industrial and Applied Mathematics*, vol. 9, no. 4, pp. 533–543, Dec. 1961.
- [54] F. Baccelli and B. Błaszczyszyn, *Stochastic geometry and wireless networks, volume I—theory, NOW: Foundations and Trends in Networking*, 2009.
- [55] F. Baccelli, B. Błaszczyszyn, and M. Karray, *Random Measures, Point Processes, and Stochastic Geometry*. Jan. Jan. 2020.
- [56] H. ElSawy, E. Hossain, and M. Haenggi, “Stochastic geometry for modeling, analysis, and design of multi-tier and cognitive cellular wireless networks: A survey,” *IEEE Communications Surveys and Tutorials*, vol. 15, no. 3, Jun. 2013.
- [57] H. S. Dhillon, R. K. Ganti, F. Baccelli, and J. G. Andrews, “Modeling and analysis of  $K$ -tier downlink heterogeneous cellular networks,” *IEEE Journal on Selected Areas in Communications*, vol. 30, no. 3, pp. 550–560, Apr. 2012.
- [58] D. Cao, S. Zhou, and Z. Niu, “Optimal combination of base station densities for energy-efficient two-tier heterogeneous cellular networks,” *IEEE Transactions on Wireless Communications*, vol. 12, no. 9, pp. 4350–4362, Sep. 2013, ISSN: 1536-1276.
- [59] H. S. Dhillon, T. D. Novlan, and J. G. Andrews, “Coverage probability of uplink cellular networks,” in *Proc. IEEE Global Communications Conference*, Dec. 2012.

- [60] S. Srinivasa and M. Haenggi, "Distance distributions in finite uniformly random networks: Theory and applications," *IEEE Transactions on Vehicular Technology*, vol. 59, no. 2, pp. 940–949, Feb. 2010.
- [61] Z. Khalid and S. Durrani, "Distance distributions in regular polygons," *IEEE Transactions on Vehicular Technology*, vol. 62, no. 5, pp. 2363–2368, Jun. 2013.
- [62] H. S. Dhillon, R. K. Ganti, and J. G. Andrews, "Load-aware modeling and analysis of heterogeneous cellular networks," *IEEE Transactions on Wireless Communications*, vol. 12, no. 4, pp. 1666–1677, Apr. 2013.
- [63] H. Wei, N. Deng, W. Zhou, and M. Haenggi, "Approximate SIR analysis in general heterogeneous cellular networks," *IEEE Transactions on Communications*, vol. 64, no. 3, pp. 1259–1273, Mar. 2016.
- [64] C.-h. Lee and M. Haenggi, "Interference and outage in Poisson cognitive networks," *IEEE Transactions on Wireless Communications*, vol. 11, no. 4, pp. 1392–1401, Apr. 2012.
- [65] A. H. Sakr and E. Hossain, "Cognitive and energy harvesting-based D2D communication in cellular networks: Stochastic geometry modeling and analysis," *IEEE Transactions on Communications*, vol. 63, no. 5, pp. 1867–1880, May 2015.
- [66] A. Hasan and J. G. Andrews, "The guard zone in wireless ad hoc networks," *IEEE Transactions on Wireless Communications*, vol. 6, no. 3, pp. 897–906, Mar. 2007.
- [67] A. M. Hunter, J. G. Andrews, and S. Weber, "Transmission capacity of ad hoc networks with spatial diversity," *IEEE Transactions on Wireless Communications*, vol. 7, no. 12, pp. 5058–5071, Dec. 2008.
- [68] R. K. Ganti and M. Haenggi, "Interference and outage in clustered wireless ad hoc networks," *IEEE Transactions on Information Theory*, vol. 55, no. 9, pp. 4067–4086, Sep. 2009. DOI: 10.1109/TIT.2009.2025543.
- [69] F. Baccelli, B. Blaszczyszyn, and P. Muhlethaler, "Stochastic analysis of spatial and opportunistic aloha," *IEEE Journal on Selected Areas in Communications*, vol. 27, no. 7, pp. 1105–1119, Sep. 2009.

- [70] V. V. Chetlur and H. S. Dhillon, “On the load distribution of vehicular users modeled by a poisson line cox process,” *IEEE Wireless Communications Letters*, vol. 9, no. 12, pp. 2121–2125, Dec. 2020.
- [71] J. P. Jeyaraj and M. Haenggi, “Cox models for vehicular networks: Sir performance and equivalence,” *IEEE Transactions on Wireless Communications*, vol. 20, no. 1, pp. 171–185, Jan. 2021.
- [72] M.-A. Lahmeri, M. A. Kishk, and M.-S. Alouini, “Stochastic geometry-based analysis of airborne base stations with laser-powered UAVs,” *IEEE Communications Letters*, vol. 24, no. 1, pp. 173–177, Jan. 2020.
- [73] R. K. Ganti and M. Haenggi, “Interference and outage in clustered wireless ad hoc networks,” *IEEE Transactions on Information Theory*, vol. 55, no. 9, pp. 4067–4086, 2009.
- [74] J. Guo, S. Durrani, and X. Zhou, “Outage probability in arbitrarily-shaped finite wireless networks,” *IEEE Transactions on Communications*, vol. 62, no. 2, pp. 699–712, Feb. 2014.
- [75] —, “Performance analysis of arbitrarily-shaped underlay cognitive networks: Effects of secondary user activity protocols,” *IEEE Transactions on Communications*, vol. 63, no. 2, pp. 376–389, Feb. 2015.
- [76] M. Afshang and H. S. Dhillon, “Fundamentals of modeling finite wireless networks using binomial point process,” *IEEE Transactions on Wireless Communications*, vol. 16, no. 5, pp. 3355–3370, May 2017.
- [77] V. V. Chetlur and H. S. Dhillon, “Downlink coverage analysis for a finite 3-D wireless network of unmanned aerial vehicles,” *IEEE Transactions on Communications*, vol. 65, no. 10, pp. 4543–4558, Oct. 2017.
- [78] X. Wang, H. Zhang, Y. Tian, and V. C. M. Leung, “Modeling and analysis of aerial base station-assisted cellular networks in finite areas under LoS and NLoS propagation,” *IEEE Transactions on Wireless Communications*, vol. 17, no. 10, pp. 6985–7000, Oct. 2018.
- [79] M. Haenggi, *Stochastic geometry for wireless networks*. Cambridge University Press, 2012.
- [80] Z. Pan and Q. Zhu, “Modeling and analysis of coverage in 3-D cellular networks,” *IEEE Communications Letters*, vol. 19, no. 5, pp. 831–834, May 2015.

- [81] M. M. Azari, G. Geraci, A. Garcia-Rodriguez, and S. Pollin, "UAV-to-UAV communications in cellular networks," *IEEE Transactions on Wireless Communications*, vol. 19, no. 9, pp. 6130–6144, 2020. DOI: 10.1109/TWC.2020.3000303.
- [82] M. Sellathurai, S. Vuppala, and T. Ratnarajah, "User selection for multi-beam satellite channels: A stochastic geometry perspective," in *Proc. Asilomar Conference on Signals, Systems and Computers*, Nov. 2016.
- [83] S. Zhang and J. Liu, "Analysis and optimization of multiple unmanned aerial vehicle-assisted communications in post-disaster areas," *IEEE Transactions on Vehicular Technology*, vol. 67, no. 12, pp. 12 049–12 060, Dec. 2018.
- [84] O. Y. Kolawole, S. Vuppala, M. Sellathurai, and T. Ratnarajah, "On the performance of cognitive satellite–terrestrial networks," *IEEE Transactions on Cognitive Communications and Networking*, vol. 3, no. 4, pp. 668–683, Dec. 2017, ISSN: 2332-7731. DOI: 10.1109/TCCN.2017.2763619.
- [85] P. J. Honnaiah, N. Maturo, S. Chatzinotas, S. Kisseleff, and J. Krause, "Demand-based adaptive multi-beam pattern and footprint planning for high throughput geo satellite systems," *IEEE Open Journal of the Communications Society*, vol. 2, pp. 1526–1540, Jul. 2021.
- [86] R. Wang, M. A. Kishk, and M.-S. Alouini, "Evaluating the accuracy of stochastic geometry based models for LEO satellite networks analysis," *IEEE Communications Letters*, pp. 1–1, Jul. 2022.
- [87] A. Talgat, M. A. Kishk, and M.-S. Alouini, "Nearest neighbor and contact distance distribution for binomial point process on spherical surfaces," *IEEE Communications Letters*, vol. 24, no. 12, pp. 2659–2663, Dec. 2020.
- [88] Sheng-Yi Li and C. H. Liu, "An analytical model to predict the probability density function of elevation angles for LEO satellite systems," *IEEE Communications Letters*, vol. 6, no. 4, pp. 138–140, Apr. 2002.
- [89] S. Kota and G. Giambene, "6G integrated non-terrestrial networks: Emerging technologies and challenges," in *Proc. IEEE International Conference on Communications Workshops (ICC Workshops)*, Jul. 2021.

- [90] O. Ben yahia, E. Erdogan, G. K. Kurt, I. Altunbas, and H. Yanikomeroglu, "HAPS selection for hybrid RF/FSO satellite networks," *IEEE Transactions on Aerospace and Electronic Systems*, pp. 1–1, 2022, early access.
- [91] E. Erdogan, I. Altunbas, G. K. Kurt, and H. Yanikomeroglu, "Cooperation in space: HAPS-aided optical inter-satellite connectivity with opportunistic scheduling," *IEEE Communications Letters*, vol. 26, no. 4, pp. 882–886, Jan. 2022.
- [92] Y. Zhu, W. Bai, M. Sheng, J. Li, D. Zhou, and Z. Han, "Joint UAV access and GEO satellite backhaul in IoRT networks: Performance analysis and optimization," *IEEE Internet of Things Journal*, vol. 8, no. 9, pp. 7126–7139, May 2021.
- [93] J. Wang, C. Jiang, Z. Wei, C. Pan, H. Zhang, and Y. Ren, "Joint UAV hovering altitude and power control for space-air-ground IoT networks," *IEEE Internet of Things Journal*, vol. 6, no. 2, pp. 1741–1753, Oct. 2019.
- [94] Y. Wang, Y. Xu, Y. Zhang, and P. Zhang, "Hybrid satellite-aerial-terrestrial networks in emergency scenarios: A survey," *China Communications*, vol. 14, no. 7, pp. 1–13, Aug. 2017. DOI: 10.1109/CC.2017.8010971.
- [95] A. Al-Hourani, S. Chandrasekharan, G. Kaandorp, W. Glenn, A. Jamalipour, and S. Kandeepan, "Coverage and rate analysis of aerial base stations," *IEEE Transactions on Aerospace and Electronic Systems*, vol. 52, no. 6, pp. 3077–3081, Dec. 2016.
- [96] M. M. Azari, F. Rosas, K.-C. Chen, and S. Pollin, "Ultra reliable UAV communication using altitude and cooperation diversity," *IEEE Transactions on Communications*, vol. 66, no. 1, pp. 330–344, Jan. 2018.
- [97] P. S. Bithas, V. Nikolaidis, A. G. Kanatas, and G. K. Karagiannidis, "UAV-to-ground communications: Channel modeling and UAV selection," *IEEE Transactions on Communications*, vol. 68, no. 8, pp. 5135–5144, May 2020. DOI: 10.1109/TCOMM.2020.2992040.
- [98] A. H. Arani, P. Hu, and Y. Zhu, "Re-envisioning space-air-ground integrated networks: Reinforcement learning for link optimization," in *Proc. IEEE International Conference on Communications (ICC)*, Aug. 2021.

- [99] M. Vondra, M. Ozger, D. Schupke, and C. Cavdar, "Integration of satellite and aerial communications for heterogeneous flying vehicles," *IEEE Network*, vol. 32, no. 5, pp. 62–69, Sep. 2018. DOI: 10.1109/MNET.2018.1800055.
- [100] I. S. Gradshteyn and I. M. Ryzhik, *Table of Integrals, Series, and Products*. Academic Press, 2014.
- [101] "Gridded population of the world, version 4: Administrative unit center points with population estimates," *Center for International Earth Science Information Network Columbia University, NASA Socioeconomic Data and Applications Center*, 2018, available online at [doi.org/10.7927/H4BC3WMT](https://doi.org/10.7927/H4BC3WMT).
- [102] R. Wang, M. A. Kishk, and M.-S. Alouini, "Ultra-dense LEO satellite-based communication systems: A novel modeling technique," Oct. 2021, available online: <https://arXiv:2110.12938>.
- [103] T. Darwish, G. K. Kurt, H. Yanikomeroğlu, M. Bellemare, and G. Lamontagne, "LEO satellites in 5G and beyond networks: A review from a standardization perspective," *IEEE Internet of Things Journal*, Oct. 2021, available online at [arXiv:2110.08654v1](https://arXiv:2110.08654v1).





## PUBLICATIONS



## PUBLICATION 1

**Downlink Coverage and Rate Analysis of Low Earth Orbit Satellite  
Constellations Using Stochastic Geometry**




N. Okati, T. Riihonen, D. Korpi, I. Angervuori, and R. Wichman

*IEEE Transactions on Communications*, vol. 68, no. 8, pp. 5120–5134

**Publication reprinted with the permission of the copyright holders.**



# Downlink Coverage and Rate Analysis of Low Earth Orbit Satellite Constellations Using Stochastic Geometry

Niloofar Okati , Taneli Riihonen , *Member, IEEE*, Dani Korpi , Ilari Angervuori, and Risto Wichman

**Abstract**—As low Earth orbit (LEO) satellite communication systems are gaining increasing popularity, new theoretical methodologies are required to investigate such networks' performance at large. This is because deterministic and location-based models that have previously been applied to analyze satellite systems are typically restricted to support simulations only. In this paper, we derive analytical expressions for the downlink coverage probability and average data rate of generic LEO networks, regardless of the actual satellites' locality and their service area geometry. Our solution stems from stochastic geometry, which abstracts the generic networks into uniform binomial point processes. Applying the proposed model, we then study the performance of the networks as a function of key constellation design parameters. Finally, to fit the theoretical modeling more precisely to real deterministic constellations, we introduce the effective number of satellites as a parameter to compensate for the practical uneven distribution of satellites on different latitudes. In addition to deriving exact network performance metrics, the study reveals several guidelines for selecting the design parameters for future massive LEO constellations, e.g., the number of frequency channels and altitude.

**Index Terms**—Low Earth orbit (LEO) constellations, massive communication satellite networks, coverage probability, average achievable rate, SINR, stochastic geometry, point processes.

## I. INTRODUCTION

**T**HE challenge for providing affordable Internet coverage everywhere around the world requires novel solutions for ubiquitous connectivity. An emerging technology, which can provide the infrastructure with relatively low propagation delay compared to conventional geostationary satellites and seamless connectivity also at polar regions, is massive low Earth orbit (LEO) satellite networking. Many LEO constellations, e.g., Kuiper, LeoSat, OneWeb, Starlink, Telesat, etc., have secured investors or, even, are already launching pilot satellites. While commercial plans obviously must have been

simulated thoroughly before putting forward, general theoretical understanding on the performance of massive LEO communication constellations at large is still missing in the scientific literature.

In this paper, we apply stochastic geometry to acquire analytical tractable expressions for coverage probability and average data rate of downlink LEO networks. The approach formulated herein for the first time ever to the authors' knowledge paves the way to study the generic performance of satellite networking without relying on explicit orbit simulations and the actual geometry of any specific constellation.

### A. Related Works

In [1], the uplink outage probability in the presence of interference was evaluated for two LEO constellations through time-domain simulations. A performance study of Iridium constellation was presented in [2] in terms of system capacity, the average number of beam-to-beam handoffs and satellite-to-satellite handoffs, the channel occupancy distribution and average call drop probability. The effect of traffic non-uniformity on signal-to-interference ratio was studied in [3] by assuming hexagonal service areas for satellites. A teletraffic analysis of a mobile satellite system based on a LEO constellation was performed in [4]. A general expression for a single LEO satellite's visibility time is provided in [5], but it is incapable of concluding the general distribution of visibility periods for any arbitrarily positioned user.

Stochastic geometry is a powerful mathematical and statistical tool for the modeling, analysis, and design of wireless networks with irregular topologies [6]–[8]. It has been mostly used in the literature to analyze two-dimensional (planar) terrestrial networks [6]–[14]. In [9], a comprehensive review of the literature related to the stochastic geometry modeling of multi-tier and cognitive cellular networks was presented. In [10], the Poisson point process (PPP) was observed to provide lower bounds on the coverage probability and the average transmission rate which are as tight as an upper bound provided by an idealized grid-based model. The work in [10] was extended to multi-tier networks under quality-of-service constraints in [11], [12]. Uplink coverage when base stations and users follow independent PPPs is evaluated in [13].

While stochastic geometry has been extensively applied for the analysis of planar scenarios, its application to three-dimensional networks has started attracting significant attention recently [15], [16]. In [15], modeling and analysis of

Manuscript received October 30, 2019; revised March 4, 2020; accepted April 17, 2020. The work of N. Okati and T. Riihonen was supported by a Nokia University Donation. The associate editor coordinating the review of this paper and approving it for publication was S. Durrani. (*Corresponding author: Niloofar Okati.*)

N. Okati and T. Riihonen are with Unit of Electrical Engineering, Faculty of Information Technology and Communication Sciences, Tampere University, FI-33720 Tampere, Finland (e-mail: niloofar.okati@tuni.fi; taneli.riihonen@tuni.fi).

D. Korpi is with Nokia Bell Labs, Karaportti 3, FI-02610 Espoo, Finland (e-mail: dani.korpi@nokia-bell-labs.com).

I. Angervuori and R. Wichman are with Department of Signal Processing and Acoustics, Aalto University School of Electrical Engineering, FI-00076 Espoo, Finland (e-mail: ilari.angervuori@aalto.fi; risto.wichman@aalto.fi).

Digital Object Identifier 10.1109/TCOMM.2020.2990993

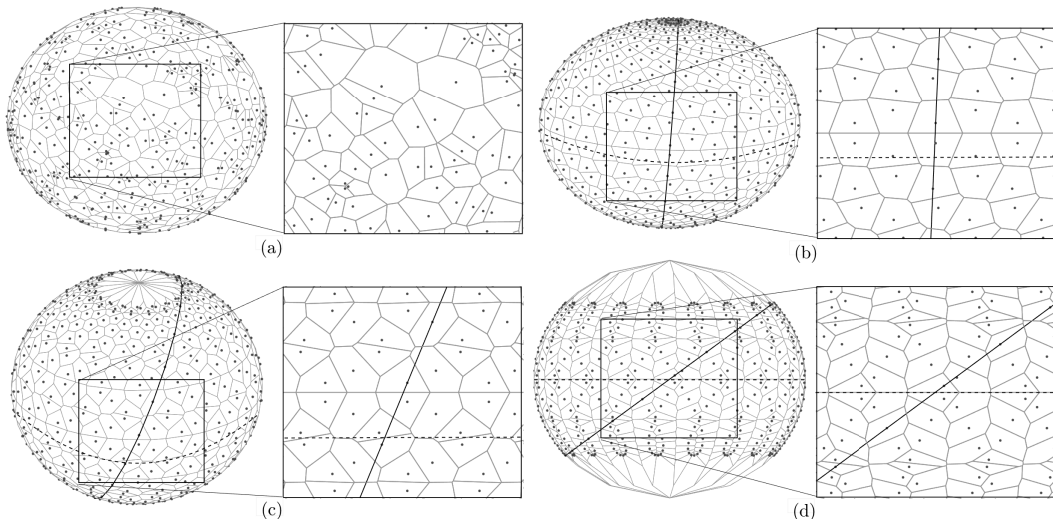


Fig. 1. Example orbits and spherical Voronoi diagrams representing the coverage areas of the nearest satellites with (a) a random constellation, (b) a polar constellation with  $87.9^\circ$  inclination angle, (c) an inclined constellation with  $70^\circ$  inclination angle, and (d) an inclined constellation with  $40^\circ$  inclination angle.

coverage in three-dimensional cellular networks have been investigated using a PPP model. Although PPP has provided tractable and insightful results, it is not valid for modeling a finite-area network with a limited number of nodes [17]. For such cases, binomial point process (BPP) is an appropriate model to capture the characteristics of the network [18], [19]. The performance for an arbitrarily shaped planar network is studied in [18], [20], but the reference transmitter is assumed to be located at a given distance, which can be overcome with two transmitter selection policies from [14]. A BPP modeling for a finite three-dimensional network of unmanned aerial vehicles (UAVs) was developed in [16], [21].

Tools from stochastic geometry have been applied to study satellite communications [22]–[25] only with a limited extent. For instance, in [22], stochastic geometry was used to model the locations of terrestrial users involving multi-beam satellite and terrestrial interference from cellular base stations. The authors in [23] derived coverage probability and data rate of a multi-UAV downlink network through assuming PPP distribution for users where, however, no interference among users and UAVs is considered due to their channel assignment policy. In [24], the performance of a cognitive satellite–terrestrial network is investigated; the secondary terrestrial network and users are modeled as independent point processes and share resources with a primary satellite system. An analysis of coverage times during LEO satellite visits has been conducted in [25] by inclusion of the distribution of users’ positions.

We can conclude from the above that the utilization of stochastic geometry for satellite network analysis is limited to modeling the user’s locality with a low number of satellites. Alternative methods to stochastic geometry are unable to provide a comprehensive analysis that fits to any arbitrary constellation due to being associated with some specific net-

work design parameters. In these models, coverage footprints of satellites are assumed to be identical and typically form a regular circular or hexagonal grid, although uneven distribution of satellites along different latitudes, and differences in transmitted power and/or altitude, create irregular cells. Moreover, there is no analytical tool to model interference in a generic sense.

### B. Contributions and Organization of the Paper

Figure 1(a) demonstrates a random constellation in which a set of satellites is distributed on a sphere according to a uniform point process, while Figs. 1(b)–(d) show a class of regular deterministic Walker constellations with varying inclination angle, in which all satellites are evenly spaced and have the same period and inclination. Each cell represents the coverage area of a satellite wherein it is the closest to and, thus, serving all users located inside the polygon. The set of all coverage cells form a Voronoi tessellation which we can observe to be analogous in the zoomed regions for the random constellation and deterministic Walker constellations. While selecting the inclination angle in practice is based on the service area of interest, we see that smaller inclination results in a more irregular Voronoi tessellation. Furthermore, the inter-operation of multiple LEO constellations, as it might hold in the near future, will make satellites’ mutual positions even more similar to those given by a random process.

Motivated by the above observations, in this paper, we first model the satellite constellation with an appropriate point process, which will then allow us to utilize the tools from stochastic geometry to analyze the performance of generic LEO networks in theory. We consider a network of a given number of satellites whose locations are modeled as a BPP on a sphere at a fixed altitude, which is justifiable due to the

limited number of satellites covering a given finite region [26]. Users are located at some arbitrary locations on Earth and are associated with the nearest satellite while some other satellites above the horizon of a user can cause co-channel interference due to frequency reuse. However, since satellites in Walker constellations are distributed unevenly along different latitudes, i.e., the number of satellites is effectively larger on the inclination limit of the constellation than on the equatorial regions, the density of practical deterministic constellations is typically not uniform like with BPP modeling. Thus, we apply a new parameter in order to compensate for the uneven density w.r.t. practical Walker constellations and create a tight match between the results generated by BPP modeling and those from practical constellation simulations.

Based on the modeling summarized above, we present the following scientific contributions in this paper.

- We derive exact expressions for coverage probability and average achievable data rate of a user in terms of the Laplace transform of interference power distribution.
- We validate our novel theoretical results with numerical simulations and also compare them with reference results from actual deterministic satellite constellations.
- To suppress the performance mismatch between a random network and practical constellations, which mostly stems from uneven distribution of satellites along different latitudes, we define and calculate a new parameter, the effective number of satellites, for every user latitude.
- We show that, with the above compensation, the generic performance of large deterministic constellations can be very accurately analyzed with theoretical expressions that are based on stochastic constellation geometry.
- Finally, the two objectives of coverage and data rate are evaluated for different key design parameters, e.g., the number of frequency channels and satellite altitude.

As for propagation models, we consider two extreme cases, namely Rayleigh fading and static propagation, for the serving channels. The former corresponds to a more drastic fading environment when the received signal is subject to severe multi-path distortion due to the small elevation angle of the transmitting satellite; this case leads to simpler expressions for some specific path loss exponents. The latter represents the typical cases where the serving satellite's elevation is large enough to provide line-of-sight to the user and, thus, weak components from multi-path propagation become insignificant. For interfering channels, any fading statistics can be adopted in general since this has no effect on analytical tractability.

We see that, although increasing the number of frequency bands improves the coverage probability, there is an optimal number of frequency channels that maximizes the data rate depending on the path loss exponent. Assuming a constant effective number of satellites for different altitudes, we observe that the optimum height which maximizes coverage probability or data rate is not within the practical altitude range of LEO networks (i.e., outside Earth's atmosphere), where the performance always declines with increasing the altitude.

The organization of the remainder of this paper is as follows. Section II describes the system model for a randomly distributed satellite network and characterizes some

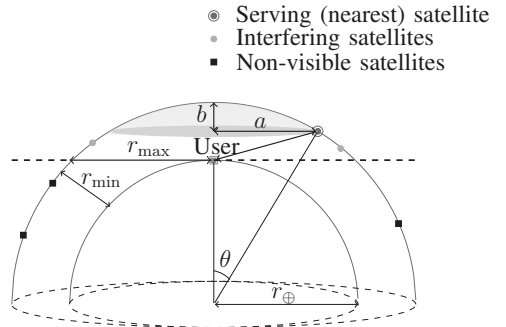


Fig. 2. A sketch of the considered system's stochastic geometry, where satellites are distributed randomly on a sphere with radius  $r_{\oplus} + r_{\min}$  and a user is located on the surface of another cocentric sphere with radius  $r_{\oplus}$ .

baseline probabilities stemming from the stochastic geometry of the system. As for the main results, we derive analytical expressions for downlink coverage probability and average achievable data rate for a terrestrial user in Sections III and IV, respectively. Numerical results are provided in Section V for studying the effect of key system parameters such as satellite altitude and the number of frequency bands allocated for the network. Finally, we conclude the paper in Section VI.

## II. SYSTEM MODEL

Let us consider a downlink network of  $N$  satellite base stations that are uniformly distributed around Earth at the same altitude  $r_{\min}$  forming a BPP on a sphere with radius  $r_{\oplus} + r_{\min}$ , where  $r_{\oplus}$  denotes Earth's radius, as shown in Fig. 2, while user terminals are located on the surface of Earth. The altitude parameter  $r_{\min}$  specifies also the minimum possible distance from a satellite to a user (that is realized when it is directly above the user), hence the name. We assume that wireless transmissions propagate to a user from all and only the satellites that are above its horizon. Correspondingly,  $r_{\max} = \sqrt{2r_{\oplus}r_{\min} + r_{\min}^2}$  denotes the maximum possible distance at which a satellite has any effect on the network service to a user (that is realized when the satellite is at the horizon). The notation followed in this paper is summarized in Table I.

Each user is associated to the nearest satellite that is referred to as the serving satellite in what follows, resulting in spherical Voronoi tessellation for satellites' coverage areas as illustrated in Fig. 1(a). The other satellites may cause co-channel interference to the user because we assume that there are only  $K$ , with  $K \leq N$ , orthogonal frequency channels for the network and randomly assign a subset of  $N/K$  satellites to each channel. The scheduling performed in this way ensures that the nearest satellite in the constellation uses the channel that is assigned to a user. All the other satellites on the same channel, other than the serving satellite, cause interference to the user's reception whenever they are above the horizon.

We suppose that every satellite may be equipped with a directional antenna that radiates its main lobe towards the center of Earth. From the serving satellite, some lobe con-

TABLE I  
SUMMARY OF MATHEMATICAL NOTATION

Notation	Description
$r_{\oplus}; r_{\min}$	Earth radius (6371 km); Altitude of satellites
$R_0; R_n; R$	Serving distance; Distance to the $n^{\text{th}}$ interfering satellite; Distance from the user to any satellite
$G_0; G_n$	Channel fading gain of the serving link; Channel fading gain of the $n^{\text{th}}$ interfering link
$N; K; N_I$	Total number of satellites; Total number of channels; Number of interfering satellites
$p_s$	Transmission power from the serving satellite
$p_i$	Transmission power from interfering satellites
$\sigma^2$	Additive noise power
$\alpha$	Path loss exponent
$T$	SINR threshold
$P_C; \bar{C}$	Coverage probability; Average achievable rate

taining the higher power (but not necessarily the main lobe) is likely directed to the user, while the lobes with lower power levels radiate towards the user from the interfering satellites. In order to approximate the effect of directional transmission, we set differing power levels for serving and interfering satellites which are denoted by  $p_s$  and  $p_i$ , respectively, such that  $p_i \leq p_s$ . If the user is located within the beamwidth of the serving satellite, the transmitted power from it will have the main lobe power level. Considering the main lobe transmitted power from the serving satellite and the largest sidelobe transmitted power from the interfering satellites,  $p_s/p_i$  corresponds to the sidelobe level of the antennas.

The distances from the user to the serving satellite and the other satellites are denoted by random variables  $R_0$  and  $R_n$ ,  $n = 1, 2, \dots, N-1$ , respectively, while  $G_0$  and  $G_n$  represent the corresponding channel gains. Obviously,  $G_n = 0$  if  $R_n > r_{\max}$  for some  $n = 0, 1, \dots, N-1$ , i.e., the satellite is below horizon. For notational convenience, when  $N_I > 0$ , we let indices  $n = 1, 2, \dots, N_I$  correspond to those  $N_I \leq N/K - 1$  satellites (if any) that share the same frequency channel with the serving satellite and are above the user's horizon, so that they cause co-channel interference.

Based on the above modeling, the signal-to-interference-plus-noise ratio (SINR) at the receiver can be expressed as

$$\text{SINR} = \frac{p_s G_0 R_0^{-\alpha}}{I + \sigma^2}, \quad (1)$$

where we assume that the user's receiver is subject to additive noise with constant power  $\sigma^2$ , the parameter  $\alpha$  is a path loss exponent,

$$I = \sum_{n=1}^{N_I} p_i G_n R_n^{-\alpha} \quad (2)$$

is the cumulative interference power from all other satellites above the user's horizon than the serving satellite, and  $N_I$  is a random variable denoting the number of interfering satellites. In the special case of having no interfering satellites, i.e.,  $N_I = 0$ , since they happen to be below the user's horizon, the SINR in (1) is reduced to signal-to-noise ratio (SNR) as

$$\text{SNR} = \frac{p_s G_0 R_0^{-\alpha}}{\sigma^2}, \quad (3)$$

and further SNR = 0 if  $R_0 > r_{\max}$ , i.e., also the nearest satellite that is supposed to be the serving satellite is below horizon.

In order to contribute expressions for coverage probability and average achievable rate in the following sections, we first need to characterize some basic distance distributions that stem from the stochastic geometry of the considered system. In particular, we express the necessary cumulative distribution function (CDF) and probability density functions (PDFs) in the following three lemmas.

**Lemma 1.** *The CDF of the distance  $R$  from any specific one of the satellites in the constellation to the user is given by*

$$F_R(r) \triangleq \mathbb{P}(R \leq r) = \begin{cases} 0, & r < r_{\min}, \\ \frac{r^2 - r_{\min}^2}{4r_{\oplus}(r_{\oplus} + r_{\min})}, & r_{\min} \leq r \leq 2r_{\oplus} + r_{\min}, \\ 1, & r > 2r_{\oplus} + r_{\min}. \end{cases} \quad (4)$$

and the corresponding PDF is given by

$$f_R(r) = \frac{r}{2r_{\oplus}(r_{\oplus} + r_{\min})} \quad (5)$$

for  $r_{\min} \leq r \leq 2r_{\oplus} + r_{\min}$  while  $f_R(r) = 0$  otherwise.

*Proof.* See Appendix A.  $\square$

The above distribution of  $R$  will be a key tool in deriving other distance statistics (i.e., those of the serving and interfering satellites), which are required in turn to characterize the distribution of SINR in (1) using stochastic geometry.

**Lemma 2.** *The PDF of the serving distance  $R_0$  is given by*

$$f_{R_0}(r_0) = N \left( 1 - \frac{r_0^2 - r_{\min}^2}{4r_{\oplus}(r_{\oplus} + r_{\min})} \right)^{N-1} \frac{r_0}{2r_{\oplus}(r_{\oplus} + r_{\min})} \quad (6)$$

for  $r_{\min} \leq r_0 \leq 2r_{\oplus} + r_{\min}$  while  $f_{R_0}(r_0) = 0$  otherwise.

*Proof.* Due to the channel assignment by which the serving satellite is the nearest one among all the  $N$  i.i.d. satellites, the CDF of  $R_0$  can be expressed as  $F_{R_0}(r_0) \triangleq \mathbb{P}(R_0 \leq r_0) = 1 - (1 - F_R(r_0))^N$  with the substitution of (4). The corresponding PDF is obtained by differentiation to complete the proof.  $\square$



**Lemma 3.** *When conditioned on the serving distance such that  $R_0 = r_0$ , the PDF of the distance from any other satellite to the user is given by*

$$f_{R_n|R_0}(r_n|r_0) = \frac{f_R(r_n)}{1 - F_R(r_0)} \quad (7)$$

for  $r_0 < r_n \leq 2r_\oplus + r_{\min}$  while  $f_{R_n|R_0}(r_n|r_0) = 0$  otherwise.

*Proof.* The CDF of  $R_n|R_0=r_0$  is obtained by conditioning  $R$  on  $R_0$  as follows:

$$\begin{aligned} F_{R_n|R_0}(r_n|r_0) &\triangleq \mathbb{P}(R_n < r_n | R_0 = r_0) \\ &= \frac{\mathbb{P}(r_0 \leq R \leq r_n)}{\mathbb{P}(R > r_0)} = \frac{F_R(r_n) - F_R(r_0)}{1 - F_R(r_0)}. \end{aligned} \quad (8)$$

The proof is then completed by taking the derivative of the CDF with respect to  $r_n$  for obtaining the PDF in (7).  $\square$

Furthermore, other auxiliary performance factors, which will be shortly used in analyzing coverage probability and average achievable data rate, are the number of interfering satellites  $N_I$  and the probability  $P_0$  of having an interference-free situation ( $N_I = 0$ ) when  $R_0 = r_0$ . They will be expressed in the following lemma and its corresponding corollary.

**Lemma 4.** *When the serving satellite is at distance  $r_0 \geq r_{\min}$  from the user, the number of interfering satellites, denoted by  $N_I$ , is a binomial random variable with success probability*

$$P_I = \frac{r_{\min} - (r_0^2 - r_{\min}^2)/(2r_\oplus)}{2(r_\oplus + r_{\min}) - (r_0^2 - r_{\min}^2)/(2r_\oplus)}. \quad (9)$$

*Proof.* The expression is directly given by the ratio of the surface area where visible interfering satellites can reside (the spherical cap formed by the intersection of the user's plane and the satellites' sphere) to the total surface area of the satellites' sphere excluding the shaded cap of Fig. 2.  $\square$

It should be noted that there are  $N/K - 1$  satellites sharing the same channel with the serving satellite and potentially causing co-channel interference. The probability of having no interference ( $N_I = 0$ ) then follows from the corollary below.

**Corollary 1.** *When the serving satellite is at distance  $r_0 \geq r_{\min}$  from the user, the probability of having zero co-channel interference is given by*

$$\begin{aligned} P_0 &\triangleq \mathbb{P}(N_I = 0) = (1 - P_I)^{\frac{N}{K} - 1} \\ &= \left( 1 - \frac{r_{\min} - (r_0^2 - r_{\min}^2)/(2r_\oplus)}{2(r_\oplus + r_{\min}) - (r_0^2 - r_{\min}^2)/(2r_\oplus)} \right)^{\frac{N}{K} - 1} \end{aligned} \quad (10)$$

for  $r_0 \leq r_{\max}$ , and  $P_0 = 1$  when  $r_0 > r_{\max}$ .

Especially, the above probability turns out to be a key factor for LEO constellation analysis since, for the derivation of the following performance metrics, we can separately consider the two complementary events of having either zero interference or non-zero interference.

### III. COVERAGE PROBABILITY

In this section, we apply stochastic geometry to derive the downlink coverage probability of the LEO satellite network for a user in an arbitrary location on Earth. The performance measure of coverage probability is defined as

$$P_c(T) \triangleq \mathbb{P}(\text{SINR} > T), \quad (11)$$

where  $T$  represents the minimum SINR required for successful data transmission. In other words, whenever the SINR of the considered user from its nearest satellite is above the threshold level  $T$ , it is considered to be within the coverage of the satellite communication network.

#### A. Coverage Probability under Rayleigh Fading Channel

In this subsection, the propagation model takes into account the large-scale attenuation with path loss exponent  $\alpha$ , as well as the small-scale fading. In particular, the serving channel is assumed to follow normalized Rayleigh fading so that the corresponding channel gain is an exponential random variable with unit mean, i.e.,  $G_0 \sim \text{Exp}(1)$ , while interfering channels are considered to follow general fading (but Rayleigh fading for interfering channels is also analyzed as a special case).

The Rayleigh fading model is applicable when the line-of-sight portion of signals received at the user's place is smaller than that of non-line-of-sight components. Due to lower altitudes in LEO constellations w.r.t. medium Earth or geostationary orbits (MEO/GEO), a strong LoS component is less likely available for the user if the number of satellites is limited. For instance, for constellations with a fewer number of satellites such as Iridium with only 66 satellites, the probability of having even medium elevation angle is rather low [27] that implies very low LoS probability. The probability of receiving LoS signals from interfering satellites is even lower due to their having smaller elevation angles. In addition, due to the shorter orbital period in LEO satellites, the channels vary rapidly with time and location which causes considerable Doppler variation at the user's location.

We express the coverage probability under the Rayleigh fading assumption for the serving channel as follows. In particular, we split the coverage probability into two terms, each of them corresponding to an important operational circumstance: The first term represents the case when there is no interference; and the second term corresponds to the case when there is at least one interfering satellite.

**Theorem 1.** *The probability of network coverage for an arbitrarily located user under a Rayleigh-fading serving channel is*

$$P_c(T) = P_0 \mathbb{P}(\text{SNR} > T) + (1 - P_0) \mathbb{P}(\text{SINR} > T | N_I > 0) \quad (12)$$

with

$$\begin{aligned} \mathbb{P}(\text{SNR} > T) &= \frac{N}{2r_\oplus(r_\oplus + r_{\min})} \int_{r_{\min}}^{r_{\max}} e^{-\frac{r_0^\alpha}{P_s} \sigma^2} \\ &\times \left( 1 - \frac{r_0^2 - r_{\min}^2}{4r_\oplus(r_\oplus + r_{\min})} \right)^{N-1} r_0 dr_0 \end{aligned} \quad (13)$$

and

$$\mathbb{P}(\text{SINR} > T | N_1 > 0) = \frac{N}{2r_{\oplus}(r_{\oplus} + r_{\min})} \int_{r_{\min}}^{r_{\max}} e^{-\frac{Tr_0^\alpha}{p_s} \sigma^2} \\ \times \mathcal{L}_I \left( \frac{Tr_0^\alpha}{p_s} \right) \left( 1 - \frac{r_0^2 - r_{\min}^2}{4r_{\oplus}(r_{\oplus} + r_{\min})} \right)^{N-1} r_0 dr_0, \quad (14)$$

where  $\mathcal{L}_I(s)$  is the Laplace transform of cumulative interference power  $I$  that is expressed in Lemma 5 and  $P_0$  is given in (10) by Corollary 1.

*Proof.* To obtain (13), we start with the definition of coverage probability for the case of having zero interference:

$$\mathbb{E}_{R_0} [\mathbb{P}(\text{SNR} > T | R_0 = r_0)] \\ = \int_{r_{\min}}^{r_{\max}} \mathbb{P}(\text{SNR} > T | R_0 = r_0) f_{R_0}(r_0) dr_0 \\ = \frac{N}{2r_{\oplus}(r_{\oplus} + r_{\min})} \int_{r_{\min}}^{r_{\max}} \mathbb{P} \left( \frac{p_s G_0 r_0^{-\alpha}}{\sigma^2} > T \right) \\ \times \left( 1 - \frac{r_0^2 - r_{\min}^2}{4r_{\oplus}(r_{\oplus} + r_{\min})} \right)^{N-1} r_0 dr_0. \quad (15)$$

The upper limit for the integral is due to the fact that the satellites below the user's horizon are not visible to the user. Invoking the assumption regarding the distribution of  $G_0$ , the expression in (13) is obtained. To prove (14), we first note that there is at least one interfering satellite, so that we have

$$\mathbb{E}_{R_0} [\mathbb{P}(\text{SINR} > T | R_0 = r_0, N_1 > 0)] \\ = \int_{r_{\min}}^{r_{\max}} \mathbb{P}(\text{SINR} > T | R_0 = r_0, N_1 > 0) f_{R_0}(r_0) dr_0 \\ = \frac{N}{2r_{\oplus}(r_{\oplus} + r_{\min})} \int_{r_{\min}}^{r_{\max}} \mathbb{P} \left( \frac{p_s G_0 r_0^{-\alpha}}{I + \sigma^2} > T \mid N_1 > 0 \right) \\ \times \left( 1 - \frac{r_0^2 - r_{\min}^2}{4r_{\oplus}(r_{\oplus} + r_{\min})} \right)^{N-1} r_0 dr_0. \quad (16)$$

When  $G_0 \sim \text{Exp}(1)$ , we can express the first term in the integrand of (16) as

$$\mathbb{P} \left( G_0 > \frac{Tr_0^\alpha (I + \sigma^2)}{p_s} \mid N_1 > 0 \right) \\ = E_I \left[ \mathbb{P} \left( G_0 > \frac{Tr_0^\alpha (I + \sigma^2)}{p_s} \mid N_1 > 0 \right) \right] \\ = E_I \left[ \exp \left( -\frac{Tr_0^\alpha}{p_s} (I + \sigma^2) \right) \right] \\ = e^{-\frac{Tr_0^\alpha}{p_s} \sigma^2} E_I \left[ e^{-\frac{Tr_0^\alpha}{p_s} I} \right] = e^{-\frac{Tr_0^\alpha}{p_s} \sigma^2} \mathcal{L}_I \left( \frac{Tr_0^\alpha}{p_s} \right). \quad (17)$$

Substituting (17) into (16) completes the derivation of (14).  $\square$

It is worth highlighting that, in the case of having  $K = N$  orthogonal channels, the system becomes noise-limited and the coverage probability in (12) will reduce to its first term. In the following lemma, we will obtain the Laplace function of the random variable  $I$  to complete the derivation of (14).

**Lemma 5.** When the serving satellite is at distance  $r_0 \geq r_{\min}$  from the user, the Laplace transform of random variable  $I$  is

$$\mathcal{L}_I(s) = \sum_{n_1=1}^{\frac{N}{K}-1} \left( \binom{\frac{N}{K}-1}{n_1} P_1^{n_1} (1 - P_1)^{\frac{N}{K}-1-n_1} \right) \\ \times \left( \frac{2}{r_{\max}^4/r_{\min}^2 - r_0^2} \int_{r_0}^{r_{\max}} \mathcal{L}_{G_n}(s p_i r_n^{-\alpha}) r_n dr_n \right)^{n_1}, \quad (18)$$

where  $P_1$  is given in (9) by Lemma 4 and  $\mathcal{L}_{G_n}(\cdot)$  is the Laplace transform of the random variable  $G_n$ .

*Proof.* See Appendix B.  $\square$

Consequently, by only specifying  $\mathcal{L}_{G_n}(\cdot)$  at the point  $s p_i r_n^{-\alpha}$ , i.e., assuming some specific fading model, the Laplace transform of interference for any fading distribution can be calculated using Lemma 5. For instance, when  $G_n$  is exponentially distributed,  $\mathcal{L}_{G_n}(s p_i r_n^{-\alpha}) = \frac{1}{1 + p_i s r_n^{-\alpha}}$ . Thus, the Laplace function of interference when interfering channels are assumed to be Rayleigh is given by the following corollary.

**Corollary 2.** When the serving satellite is at distance  $r_0 \geq r_{\min}$  from the user and interfering channels experience Rayleigh fading, i.e.,  $G_n \sim \text{Exp}(1)$  for  $n = 1, \dots, N_1$ , the Laplace transform of random variable  $I$  is

$$\mathcal{L}_I(s) = \sum_{n_1=1}^{\frac{N}{K}-1} \left( \binom{\frac{N}{K}-1}{n_1} P_1^{n_1} (1 - P_1)^{\frac{N}{K}-1-n_1} \right) \\ \times \left( \frac{2}{r_{\max}^4/r_{\min}^2 - r_0^2} \int_{r_0}^{r_{\max}} \left( \frac{r_n}{1 + p_i s r_n^{-\alpha}} \right) dr_n \right)^{n_1}. \quad (19)$$

Consequently, for Rayleigh-fading interfering channels and particular values of the path loss exponent, Lemma 5 will reduce to elementary functions, which will result in a simpler expression for (14). Using [28, Eq. 3.194.5], the integral in (19) can be rewritten as

$$\int \frac{r_n}{1 + p_i s r_n^{-\alpha}} dr_n \\ = -\frac{r_n^2}{2} \left( {}_2F_1 \left( 1, \frac{2}{\alpha}; 1 + \frac{2}{\alpha}; -\frac{r_n^\alpha}{p_i s} \right) - 1 \right), \quad (20)$$

where  ${}_2F_1(\cdot, \cdot; \cdot; \cdot)$  is the Gauss's hyper-geometric function. Using the definition of the function [28, Eq. 9.100] and substituting with special arguments, it is reduced to elementary functions. If  $\alpha = 2$ , we have [28, Eq. 9.121.5]

$${}_2F_1 \left( 1, 1; 2; -\frac{r_n^\alpha}{p_i s} \right) = \frac{p_i s \ln(1 + r_n^2/(p_i s))}{r_n^2} \quad (21)$$

so that (19) can be rewritten as

$$\mathcal{L}_I(s) = \sum_{n_1=1}^{\frac{N}{K}-1} \left( \binom{\frac{N}{K}-1}{n_1} P_1^{n_1} (1 - P_1)^{\frac{N}{K}-1-n_1} \right) \\ \times \left( \frac{r_{\max}^2 - r_0^2}{r_{\max}^4/r_{\min}^2 - r_0^2} \left( \frac{p_i s}{r_{\max}^2 - r_0^2} \ln \left( \frac{p_i s + r_0^2}{p_i s + r_{\max}^2} \right) + 1 \right) \right)^{n_1}. \quad (22)$$

On the other hand, if we assume  $\alpha = 4$ , the Gauss hypergeometric function can be written as [28, Eq. 9.121.27]

$${}_2F_1\left(1, \frac{3}{2}; \frac{5}{2}; -\frac{r_n^4}{p_1 s}\right) = \frac{\sqrt{p_1 s} \arctan\left(\frac{r_n^2/\sqrt{p_1 s}}{r_n^2}\right)}{r_n^2}, \quad (23)$$

by which (19) is simplified into a closed-form expression as

$$\begin{aligned} \mathcal{L}_I(s) &= \sum_{n_1=1}^{\frac{N}{K}-1} \binom{\frac{N}{K}-1}{n_1} P_1^{n_1} (1-P_1)^{\frac{N}{K}-1-n_1} \\ &\times \frac{r_{\max}^2 - r_0^2}{r_{\max}^4/r_{\min}^2 - r_0^2} \left( \frac{\sqrt{p_1 s}}{r_{\max}^2 - r_0^2} \arctan\left(\frac{\sqrt{p_1 s} (r_0^2 - r_{\max}^2)}{p_1 s + r_{\max}^2 r_0^2}\right) + 1 \right)^{n_1}. \end{aligned} \quad (24)$$

### B. Coverage Probability under Non-fading Channels

In this subsection, we derive the coverage probability for non-fading propagation environments. This propagation model is applicable (at least as an accurate approximation) when the number of satellites in a constellation is large enough, so that it is likely to have multiple satellites in LoS propagation range. Consequently, the serving satellite is likely high above the user and potential multi-path fading components are weak compared to the direct propagation path. Moreover, the LoS probability for interfering satellites increases as we decrease the number of frequency channels.

Similar to Theorem 1, the coverage probability is split into two terms. The first one is for the case of having no interference and, in the second term, we assume that there is at least one interfering satellite. As will be seen shortly, other than representing two important communication scenarios, such division is needed to make our approach tractable. For the non-fading serving channel, we denote  $G_0 = 1$ . Like in the previous section, any general fading statistics can be assumed for interfering channels, for which non-fading interference is considered as a special case towards the end of the section.

**Theorem 2.** *The coverage probability of a user with a non-fading serving channel is*

$$P_c(T) = P_0 \mathbb{P}(\text{SNR} > T) + (1 - P_0) \mathbb{P}(\text{SINR} > T | N_I > 0), \quad (25)$$

with

$$\mathbb{P}(\text{SNR} > T) = F_{R_0} \left( \left( \frac{P_s}{T \sigma^2} \right)^{\frac{1}{\alpha}} \right) \quad (26)$$

and

$$\begin{aligned} \mathbb{P}(\text{SINR} > T | N_I > 0) &= \frac{N}{4\pi r_{\oplus} (r_{\oplus} + r_{\min})} \int_{r_{\min}}^{r_{\max}} \int_{-\infty}^{\infty} \mathcal{L}_I(j\omega) \\ &\times \left( \frac{e^{j\left(\frac{P_s}{T r_0^{\alpha}} - \sigma^2\right)\omega} - 1}{j\omega} \right) \left( 1 - \frac{r_0^2 - r_{\min}^2}{4r_{\oplus} (r_{\oplus} + r_{\min})} \right)^{N-1} r_0 dr_0 d\omega. \end{aligned} \quad (27)$$

*Proof.* The derivation of (26) is straightforward by substituting  $G_0 \rightarrow 1$  in (3) and using the definition of a CDF. Excluding zero interference from  $I$  satisfies the sufficient conditions, given in [29, Prop. A.2], for its PDF  $f_I(\cdot)$  to exist (especially,

$I$  is continuous). Substituting  $G_0 \rightarrow 1$  in the first term of the integral in (16), we have

$$\mathbb{P}\left(T r_0^{\alpha} (\sigma^2 + I) < P_s | N_I > 0\right) = \mathbb{P}\left(I < \frac{P_s}{T r_0^{\alpha}} - \sigma^2 | N_I > 0\right) \quad (28)$$

$$= \int_0^{\frac{P_s}{T r_0^{\alpha}} - \sigma^2} f_I(i) di \quad (29)$$

$$= \frac{1}{2\pi} \int_{-\infty}^{\infty} \mathcal{L}_I(s)|_{s=j\omega} \frac{e^{j\left(\frac{P_s}{T r_0^{\alpha}} - \sigma^2\right)\omega} - 1}{j\omega} d\omega. \quad (30)$$

The latter equality follows immediately from the Parseval–Plancherel property and from the fact that the Fourier transform of the square integrable function  $\mathbb{1}(0 \leq t \leq \frac{P_s}{T r_0^{\alpha}} - \sigma^2)$  is  $(1 - e^{-j\left(\frac{P_s}{T r_0^{\alpha}} - \sigma^2\right)\omega})/(j\omega)$  according to [30].  $\square$

The Laplace function  $\mathcal{L}_I(s)$  for general fading can be obtained using Lemma 5 given in the previous section. The following corollary presents the Laplace function when interfering signals experience non-fading propagation as well.

**Corollary 3.** *When the serving satellite is at distance  $r_0 \geq r_{\min}$  from the user, the Laplace transform of  $I$  for non-fading channels is*

$$\begin{aligned} \mathcal{L}_I(s) &= \sum_{n_1=1}^{\frac{N}{K}-1} \binom{\frac{N}{K}-1}{n_1} P_1^{n_1} (1-P_1)^{\frac{N}{K}-1-n_1} \\ &\times \left( \frac{2(s p_1)^{2/\alpha}}{\alpha (r_{\max}^4/r_{\min}^2 - r_0^2)} \left[ \Gamma(-2/\alpha, s p_1 r_{\max}^{-\alpha}) - \Gamma(-2/\alpha, s p_1 r_0^{-\alpha}) \right] \right)^{n_1}, \end{aligned} \quad (31)$$

where  $\Gamma(a, x) = \int_x^{\infty} y^{a-1} e^{-y} dy$  denotes the upper incomplete gamma function.

*Proof.* The first term of the integrand in Lemma 5 will be reduced to an exponential function. As a result, the integral can be expressed in form of the upper incomplete gamma function defined as  $\Gamma(a, x) = \int_x^{\infty} y^{a-1} e^{-y} dy$  by changing integration variable as  $s p_1 r_n^{-\alpha} \rightarrow y$ .  $\square$

## IV. AVERAGE ACHIEVABLE RATE

In this section, we focus on the average achievable data rate. The technical tools and expressions presented in Sections II and III are reused also herein. The average achievable rate (in bit/s/Hz) is defined as

$$\bar{C} \triangleq \frac{1}{K} \mathbb{E} \left[ \log_2 (1 + \text{SINR}) \right], \quad (32)$$

which states the ergodic capacity from the Shannon–Hartley theorem over a fading communication link normalized to the bandwidth of  $1/K$  [Hz].

### A. Average Achievable Rate under Rayleigh Fading Channel

We can calculate the expression for the average rate of an arbitrary user under the assumption of a Rayleigh-fading

serving channel as follows. It is worth noting that the average is taken over both the spatial BPP and fading distribution.

**Theorem 3.** *The downlink average rate (in bits/s/Hz) of an arbitrarily located user and its serving satellite under Rayleigh fading assumption, i.e.,  $G_0 \sim \text{Exp}(1)$ , is*

$$\bar{C} \triangleq \frac{P_0}{K} \mathbb{E} [\log_2(1 + \text{SNR})] + \frac{1 - P_0}{K} \mathbb{E} [\log_2(1 + \text{SINR}) | N_I > 0], \quad (33)$$

with

$$\begin{aligned} & \mathbb{E} [\log_2(1 + \text{SNR})] \\ &= \frac{N}{2 \ln(2) r_\oplus (r_\oplus + r_{\min})} \int_{r_{\min}}^{r_{\max}} \int_{t>0} e^{-\frac{r_0^\alpha}{P_s} \sigma^2 (e^t - 1)} \\ & \times \left( 1 - \frac{r_0^2 - r_{\min}^2}{4r_\oplus (r_\oplus + r_{\min})} \right)^{N-1} r_0 dt dr_0 \end{aligned} \quad (34)$$

and

$$\begin{aligned} & \mathbb{E} [\log_2(1 + \text{SINR}) | N_I > 0] \\ &= \frac{N}{2 \ln(2) r_\oplus (r_\oplus + r_{\min})} \int_{r_{\min}}^{r_{\max}} \int_{t>0} e^{-\frac{r_0^\alpha}{P_s} \sigma^2 (e^t - 1)} \\ & \times \mathcal{L}_I \left( \frac{r_0^\alpha}{P_s} (e^t - 1) \right) \left( 1 - \frac{r_0^2 - r_{\min}^2}{4r_\oplus (r_\oplus + r_{\min})} \right)^{N-1} r_0 dt dr_0. \end{aligned} \quad (35)$$

*Proof.* See Appendix C.  $\square$

The above applies to interfering channels with any fading statistics. However, analogous to the results in Section III, by considering  $G_n \sim \text{Exp}(1)$  for some specific  $\alpha$  values, i.e.,  $\alpha = 2$  and  $\alpha = 4$ , and substituting (22) or (24) into (35) will lead to more simplified expressions for Theorem 3. Moreover, if we allocate  $K = N$  orthogonal channels to the system, the second term in (33) will be eliminated and the network's performance will become noise-limited.

### B. Average Achievable Rate under Non-fading Channels

In this subsection, we derive the average data rate for non-fading serving channels and any fading statistics for interference. The rate expression is again split into two terms to consider zero and non-zero interference conditions separately.

**Theorem 4.** *The downlink average rate of an arbitrary located mobile user and its serving satellite for a non-fading channel is*

$$\bar{C} \triangleq \frac{P_0}{K} \mathbb{E} [\log_2(1 + \text{SNR})] + \frac{(1 - P_0)}{K} \mathbb{E} [\log_2(1 + \text{SINR}) | N_I > 0], \quad (36)$$

with

$$\mathbb{E} [\log_2(1 + \text{SNR})] = \frac{1}{\ln(2)} \int_{t>0} F_{R_0} \left( \left( \frac{P_s}{(e^t - 1) \sigma^2} \right)^{\frac{1}{\alpha}} \right) dt \quad (37)$$

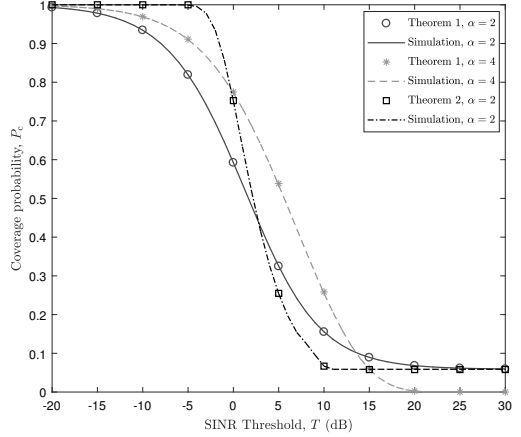


Fig. 3. Verification of coverage probability expressions with simulations for  $N = 720$  satellites. The path loss exponent ( $\alpha$ ) is set to 2 and 4.

and

$$\begin{aligned} & \mathbb{E} [\log_2(1 + \text{SINR}) | N_I > 0] \\ &= \frac{N}{4\pi \ln(2) r_\oplus (r_\oplus + r_{\min})} \int_{r_{\min}}^{r_{\max}} \int_{t>0} \int_{-\infty}^{\infty} \mathcal{L}_I(j\omega) \\ & \times \left( \frac{j \left( \frac{r_0^\alpha P_s}{(e^t - 1) \sigma^2} \right) \omega - 1}{j\omega} \right) \left( 1 - \frac{r_0^2 - r_{\min}^2}{4r_\oplus (r_\oplus + r_{\min})} \right)^{N-1} r_0 d\omega dt dr_0. \end{aligned} \quad (38)$$

*Proof.* See Appendix D.  $\square$

In case of non-fading interfering channels, the Laplace transform in (38) can be calculated from Corollary 3.

## V. NUMERICAL RESULTS

In this section, we verify our expressions for coverage probability and average data rate by comparing them with the results of Monte Carlo simulations. We obtain a new parameter—effective number of satellites ( $N_{\text{eff}}$ )—to compensate for the effect of uneven distribution of satellites along different latitudes. We then illustrate the two performance metrics in terms of different network design parameters such as the number of frequency channels and the satellite altitude.

For numerical verification, we calculate the simulated coverage probability in Monte Carlo manner as follows. First, we randomly place  $N$  satellites with uniform distribution on a sphere centered at Earth's center and distanced  $r_{\min}$  from its surface. At the same time, we also model the channels between the satellites and the user by exponential random variables (to model Rayleigh fading) with unit mean value while, to model a non-fading environment, we set the channel gains to one. Then we calculate the SINR at the receiver and compare it with a pre-defined threshold value to evaluate coverage probability. We repeat this experiment for a large number of realizations to obtain the averaged performance metrics.

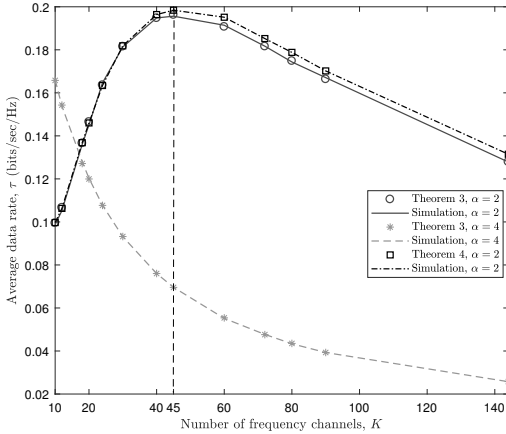


Fig. 4. Effect of the number of frequency bands ( $K$ ) on average achievable rate with Rayleigh and non-fading channels.

Finally, we compare these numerical results with the analytical expressions in Theorems 1–4 to confirm our analysis.

For producing the numerical results, the transmitted power from all satellites is set to  $p_s = p_i = 10$  W. The assumption corresponds to the case where all satellites are equipped with omni-directional antennas. The theory is applicable also to other antenna patterns by adjusting different power levels for the serving and interfering satellites accordingly to take into account that the serving satellite’s transmission would be directed to the user while all interfering transmissions are sent to other, arbitrary and independent, directions. The noise power is assumed to be  $\sigma^2 = -98$  dBm. The number of channels is considered to be  $K = 20$  unless otherwise stated.

#### A. Corroboration of Theorems by Simulations

In this subsection, we validate the coverage probability and the data rate derived in Theorems 1–4 through Monte Carlo simulations. We considered static propagation or Rayleigh fading for serving channels and general fading for interference.

Figure 3 demonstrates the coverage probability for different threshold values assuming  $\alpha$  is 2 and 4. The parameters  $N$  and  $r_{\min}$  are set to 720 and 1200 km, respectively. We find that our theoretical results are perfectly in line with the simulations, which confirms the correctness of the derivations. The transition of coverage probability from one to zero occurs variously depending on path loss exponent and the type of fading. For  $\alpha = 2$ , the coverage probability saturates when  $T > 20$  dB which corresponds to the case when the number of interfering satellites is considerable. As a result, the SINR and, consequently, the second term in Theorem 1 approach zero. For larger path loss exponents, the effect of interference becomes insignificant and the transition from one to zero includes no saturation mode since the difference between SNR and SINR becomes less dominant. All curves tend to zero for thresholds greater than 80 dB although not shown in the figure.

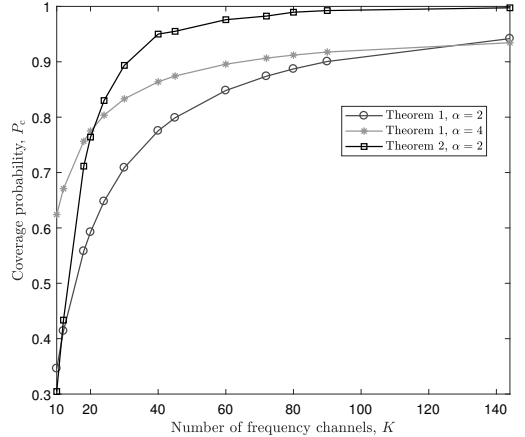


Fig. 5. Effect of frequency reuse on coverage probability for different propagation environments and path loss exponents.

Figure 4 shows average achievable data rate versus the number of frequency bands for Rayleigh fading and non-fading environments. The behavior of the curves can be justified according to two contradictory effects of increasing the number of orthogonal channels on data rate. Allocating more orthogonal channels improves data rate by mitigating the interference but, at the same time, degrades it by making only a portion of the whole band available for each group of satellites. For  $\alpha = 2$ , the former effect dominates for  $K < 45$  as by increasing  $K$ , data rate increases accordingly, while for  $K > 45$ , the latter effects overcomes the interference elimination effect and data rate starts falling.

The effect of increasing the number of channels on the reduced available frequency band dominates the SINR enhancement for  $\alpha = 4$  since the largest average data rate for  $\alpha = 4$  corresponds to the lowest number of frequency channels. This is due to the fact that the larger path loss exponents make the interfering satellites less effective since they transmit from a farther distance. As it can be observed in the figure, for AWGN channel and  $\alpha = 2$ , the behaviour of the data rate is slightly affected by the fading model.

The effect of frequency reuse on coverage probability can be determined from Fig. 5. The channel allocation policy is such that the channel corresponding to the nearest satellite to the user will be selected. As can be observed, the coverage probability rises with increasing the number of frequency bands due to interference mitigation, and all three curves present the same behaviour. However, the effect of the parameter  $K$  is more significant for the smaller path loss exponent as it affects the interference level more significantly. The coverage performance is superior for non-fading environment due to better quality of the serving signal. It can be interpreted from Figs. 4 and 5 that the coverage probability is an increasing function of the number of channels, i.e., the higher number of frequency channels will result in better coverage probability, while there is an optimum number of channels that maximizes the data

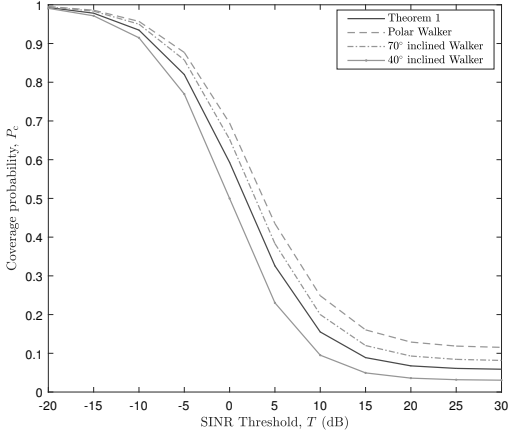


Fig. 6. Comparison of Theorem 1 with actual polar and inclined constellations. The user's latitude is set to  $30^\circ$ .

rate. Therefore, the number of frequency channels should be compromised according to the performance demands of the intended constellation.

### B. Effective Number of Satellites

In this subsection, we provide analysis of deterministic Walker satellite constellations with different inclination angles which are expected to provide global Internet broadband services to users by 720 LEO satellites. In Fig. 6, the coverage probability of the Walker constellation, with inclination angles,  $\phi_i$ , of  $90^\circ$  (polar),  $70^\circ$  and  $40^\circ$  are plotted for comparison to a random constellation. The user's latitude, denoted by  $\phi_u$ , is assumed to be  $30^\circ$ . The slight difference of coverage probability in random and Walker constellations is due to the fact that the latitudinal density of satellites in deterministic constellations is not uniform, as there are more satellites around their inclination angle (i.e., the latitude limits) and less in the equatorial regions. Consequently, the coverage probability changes as we move from the equator to the latitude limits.

In order to compensate for uneven latitudinal density, we introduce a new parameter, entitled as the effective number of satellites, and denote it by  $N_{\text{eff}}(\phi_i, \phi_u)$ , which is the number of satellites for a random uniform constellation that corresponds to the same coverage probability as for a practical non-uniform constellation with inclination angle  $\phi_i$  and at the user latitude  $\phi_u$ . This parameter is approximated by mean absolute error minimization between the coverage probability given in Theorem 1 and the results from practical Walker constellation for a few threshold values on different latitudes. The approximated value for  $N_{\text{eff}}$  is then refined to give the best matching between random and practical constellation based on the target performance metric. Although we used some of the values from simulated results to obtain  $N_{\text{eff}}$ , the same  $N_{\text{eff}}$  can be used for other system parameters, i.e., path loss exponent

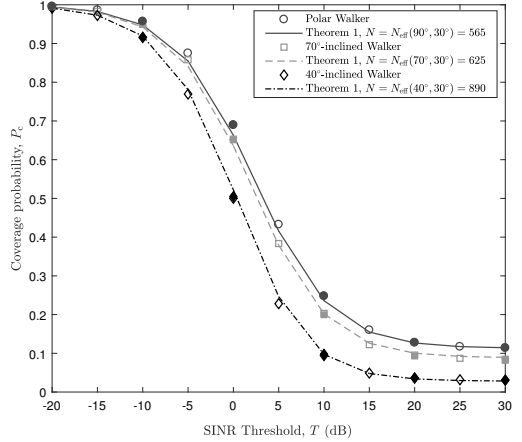


Fig. 7. Effect of using  $N_{\text{eff}}$  in Theorem 1 on providing a better matching between the random and practical constellations. Filled points have been used in mean absolute error minimization process in order to obtain  $N_{\text{eff}}$ .

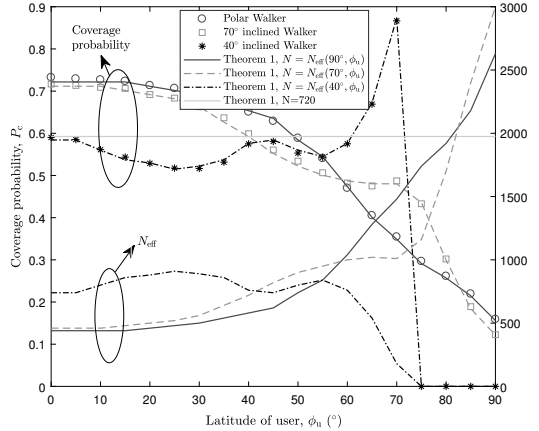


Fig. 8. Effect of latitude on coverage probability. The markers for coverage probability are plotted by simulation of a Walker constellation for  $90^\circ$ ,  $70^\circ$  and  $40^\circ$  inclined orbits. The right axis depicts  $N_{\text{eff}}(\phi_i, \phi_u)$  for different latitudes. The lines are plotted by applying  $N_{\text{eff}}(\phi_i, \phi_u)$  in Theorem 1.

and/or SINR threshold values. Likewise, the acquired  $N_{\text{eff}}$  can be also used for a constellation with different total number of satellites by linearly scaling it accordingly.

In Fig. 7, we eliminated the deviation between Walker and random constellations (cf. Fig. 6) by compensating the non-uniform latitudinal density. The solid markers on the curves were chosen from practical constellation in order to minimize the mean absolute error in coverage probability of a random constellation. As it can be seen, although only a few points are employed for fitting, the selected  $N_{\text{eff}}$  also holds for other values that had no contribution on the minimization process. In other words, applying  $N_{\text{eff}}$  in theorems provided in this paper

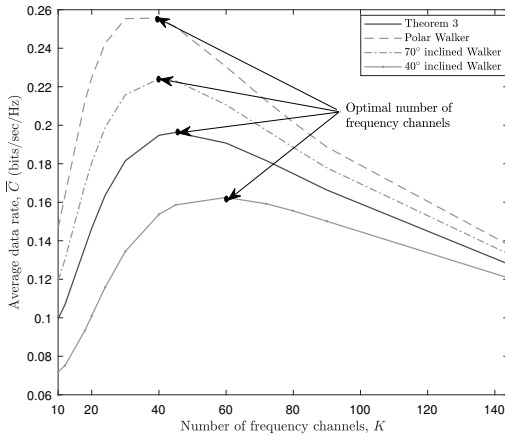


Fig. 9. Comparison of Theorem 3 with actual polar and inclined constellations. The user's latitude is set to  $30^\circ$ .

will lead to more precise results for many system parameters and performance metrics by taking into account only a few input data from the actual network.

In Fig. 8, the effect of latitude of user on coverage probability is shown for three practical constellations. In this figure, we have two groups of data that demonstrate the coverage probability. The first group (depicted by markers) is obtained by simulation of a Walker constellation for polar,  $70^\circ$  and  $40^\circ$  inclined orbits. For a polar constellation, the number of satellites in the view increases monotonically from the equator to poles. As a result, the coverage probability declines as the user moves from the equator to poles due to intensifying interference. On the other hand, for the other two inclination angles, the number of satellites in the view varies non-uniformly due to the network geometry which results in coverage alternation for different latitudes. The zero coverage probability for user latitudes greater than  $75^\circ$  in  $40^\circ$ -inclined Walker results from the fact that there are no visible satellites for those latitudes.

The second group of data (depicted by lines) in Fig. 8 is generated using Theorem 1 with  $N_{\text{eff}}(\phi_i, \phi_u)$  satellites. As can be seen in the figure, coverage probability in Theorem 1 for  $N_{\text{eff}}(\phi_i, \phi_u)$  results in the same coverage from Walker constellation for the given  $\phi_u$ . Therefore, using  $N_{\text{eff}}(\phi_i, \phi_u)$  in Theorem 1, the effect of uneven distribution of satellites along different latitudes is compensated and the coverage probability can be obtained for any actual constellation. Most importantly, we can conclude that the approximation error in modeling deterministic constellations as random ones is actually rather minimal when the varying satellite density at different latitudes is taken into account.

The data rate of a Walker satellite constellation for different inclination angles to compare with a random constellation (viz. Theorem 3) is depicted in Fig. 9. As mentioned for Fig. 6, the difference between the random and Walker constellation is mainly due to the non-uniform density of satellites in Walker constellation. The optimal number of frequency channels that

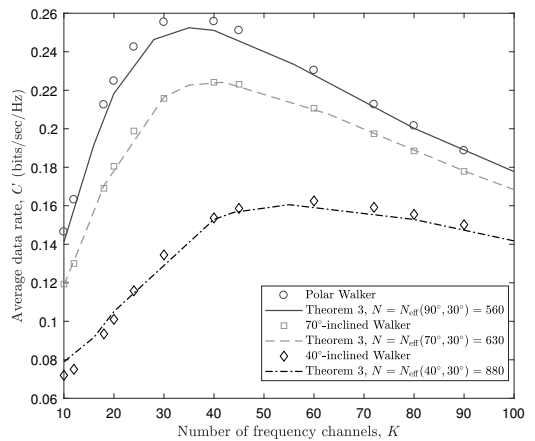


Fig. 10. Effect of using  $N_{\text{eff}}$  in Theorem 3 on providing a better matching between the random and practical constellations.

can be observed in this figure for each of the constellations increases by decreasing the inclination angle. Figure 10 depicts the effect of applying  $N_{\text{eff}}$  to Theorem 3 in eliminating the observed deviation in Fig. 9. The selected  $N_{\text{eff}}$  values are slightly different from those in Fig. 7 since they are refined to create the best possible matching between the data rate of the random and practical constellation.

Figure 11 is a counterpart for Fig. 8 to illustrate the effect of latitude of the user on achievable data rate and  $N_{\text{eff}}(\phi_i, \phi_u)$ . In this figure,  $N_{\text{eff}}(\phi_i, \phi_u)$  is the number of satellites in a random constellation that corresponds to the same data rate as a Walker constellation for the given  $\phi_u$ . Due to different values of  $N_{\text{eff}}(\phi_i, \phi_u)$  in Figs. 8 and 11, we can realize that this value is not only a function of geometrical characteristics of the constellation but also depends slightly on the performance metric. However, the compensation of latitudinal diversity is still applicable to varying system parameters that are different from those used for fitting theoretical expressions to simulations.

### C. The Effect of Satellite Altitude

Coverage probability for different altitudes is then depicted in Fig. 12. The figure is plotted using  $N_{\text{eff}}(\phi_i, \phi_u)$  for Theorem 1. In this figure, we assumed that the total number of satellites varies with altitude so that  $N_{\text{eff}}$  remains constant irrespective of altitude. This balances between a practical constellation design in which the number of satellites (when aiming at covering economically the entire globe) typically decreases with increasing altitude and the direct relationship between altitude and the effective number of satellites. It can be observed from Fig. 12 that, for practical LEO altitudes, the coverage probability declines when altitude increases. Within Earth's atmosphere, there is an impractical optimal altitude, which moves even lower as the number of satellites increases.

Data rate for different altitudes is plotted in Fig. 13. The figure is created using Theorem 3 with  $N_{\text{eff}}(\phi_i, \phi_u)$  that cor-

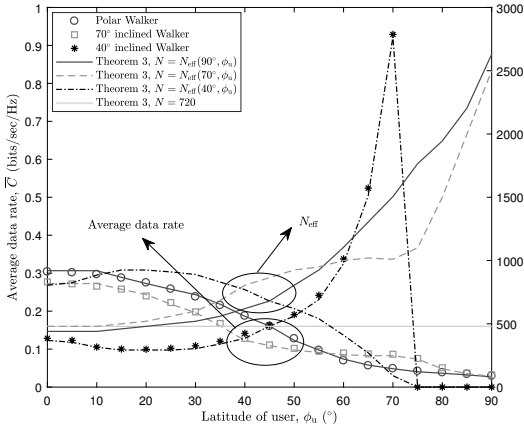


Fig. 11. Effect of latitude on average data rate and  $N_{\text{eff}}(\phi_i, \phi_u)$ . The markers for data rate are plotted by simulation of a Walker constellation for  $90^\circ$ ,  $70^\circ$  and  $40^\circ$  inclined orbits. The lines are plotted by applying  $N_{\text{eff}}(\phi_i, \phi_u)$  in Theorem 3.

responds to a specific latitude  $\phi_u$  for Walker constellations (polar and inclined). The same assumption as for Fig. 12 is also made regarding the invariance of  $N_{\text{eff}}$  w.r.t. altitude. This serves to show that, having  $N_{\text{eff}}(\phi_i, \phi_u)$  at hand, we can use the expressions in Theorems 3 or 4 to analyze the data rate for any given satellite constellation and the approximation error in modeling a deterministic constellation as a binomial point process is insignificant. The same as for Fig. 12, it can be seen that the peak value of data rate does not exist within the LEO practical altitude range outside atmospheric drag.

## VI. CONCLUSIONS

In this paper, we presented a tractable approach for down-link coverage and rate analysis of low Earth orbit satellite networks. Using the concept of stochastic geometry, we modeled the satellite network as a binomial point process. We then applied this model to obtain exact expressions for coverage probability and data rate of an arbitrary user in terms of network parameters and the Laplace transform of interference power. The performance metrics of the random and real constellation match with each other almost perfectly; there is only a slight deviation between them which can be compensated by taking into account the effect of uneven satellite distribution along different latitudes. A frequency reuse approach was also applied to make the network spectral efficiency suitable for commercial operation. Its effect on data rate is more ambivalent than on coverage probability. The proposed framework in this paper paves the way for accurate analysis and design of the future dense satellite networks. The scalable results presented here are not only applicable to a single constellation but also to massive satellite networks that merge several different constellations.

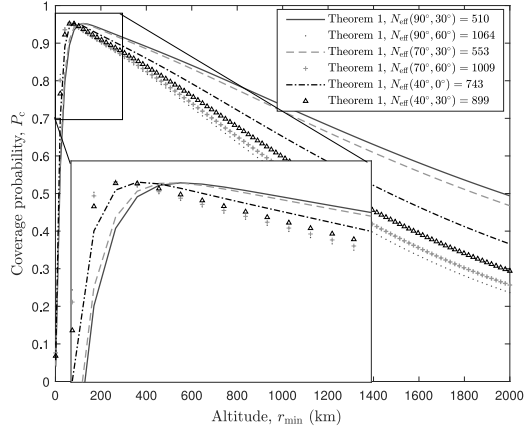


Fig. 12. Coverage probability for different altitudes. Curves are plotted using Theorem 1 for different Walker constellations in  $\phi_u = 0^\circ$ ,  $30^\circ$ , and  $60^\circ$  assuming  $N = N_{\text{eff}}(\phi_i, \phi_u)$ .

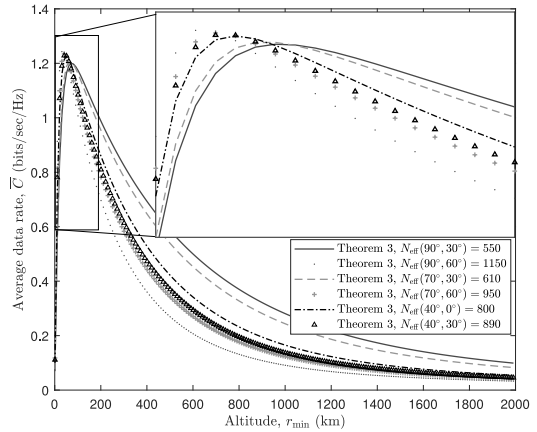


Fig. 13. Average rate for different altitudes. Curves are plotted using Theorem 3 for different Walker constellations in  $\phi_u = 0^\circ$ ,  $30^\circ$ , and  $60^\circ$  assuming  $N = N_{\text{eff}}(\phi_i, \phi_u)$ .

## APPENDIX

### A. Proof of Lemma 1

From basic geometry, the CDF of the surface area of the shaded spherical cap  $A_{\text{cap}}$ , formed by any satellite at distance  $R$  from the user, in Fig. 2 is  $F_{A_{\text{cap}}}(A_i) = \frac{A_i}{4\pi(r_0 + r_{\text{min}})^2}$ . To find the distribution of  $R$ , we need to find a relationship between  $A_{\text{cap}}$  and  $R$ , when know that

$$A_{\text{cap}} = \pi(a^2 + b^2), \quad (39)$$

$$R^2 = (r_{\text{min}} - b)^2 + a^2, \quad (40)$$



for which  $a$  and  $b$  are given in Fig. 2. Combining (39) and (40), we have

$$\begin{aligned} R^2 &= r_{\min}^2 - 2r_{\min}b + b^2 + a^2 = r_{\min}^2 - 2r_{\min}b + \frac{A_{\text{cap}}}{\pi} \\ &= r_{\min}^2 - 2r_{\min}(r_{\oplus} + r_{\min})(1 - \cos\theta) + \frac{A_{\text{cap}}}{\pi}. \end{aligned} \quad (41)$$

Using the formula for the surface area of a spherical cap, i.e.,  $A_{\text{cap}} = 2\pi(r_{\oplus} + r_{\min})^2(1 - \cos\theta)$ , we obtain

$$\begin{aligned} R^2 &= r_{\min}^2 - 2r_{\min}(r_{\oplus} + r_{\min}) \left( \frac{A_{\text{cap}}}{2\pi(r_{\oplus} + r_{\min})^2} \right) + \frac{A_{\text{cap}}}{\pi} \\ &= r_{\min}^2 + \frac{A_{\text{cap}}}{\pi} \left( 1 - \frac{r_{\min}}{r_{\oplus} + r_{\min}} \right). \end{aligned} \quad (42)$$

The CDF can then be deduced as follows:

$$\begin{aligned} \mathbb{P}(R < r) &= \mathbb{P}(R^2 < r^2) \\ &= \mathbb{P}\left(r_{\min}^2 + \frac{A_{\text{cap}}}{\pi} \left( 1 - \frac{r_{\min}}{r_{\oplus} + r_{\min}} \right) < r^2\right) \\ &= \mathbb{P}\left(A_{\text{cap}} < \frac{\pi(r^2 - r_{\min}^2)}{1 - \frac{r_{\min}}{r_{\oplus} + r_{\min}}}\right) \\ &= \frac{\pi(r^2 - r_{\min}^2)}{\left(1 - \frac{r_{\min}}{r_{\oplus} + r_{\min}}\right) 4\pi(r_{\oplus} + r_{\min})^2} \\ &= \frac{r^2 - r_{\min}^2}{4r_{\oplus}(r_{\oplus} + r_{\min})}. \end{aligned} \quad (43)$$

Finally, the corresponding PDF can be derived by differentiating (43) with respect to  $r$ .

### B. Proof of Lemma 5

In this Appendix, we provide the proof to the expression of Laplace function for general fading channels. Using the definition of the Laplace transform yields

$$\begin{aligned} \mathcal{L}_I(s) &\triangleq \mathbb{E}_I[e^{-sI}] = \mathbb{E}_{N_I, R_n, G_n} \left[ \exp\left(-s \sum_{n=1}^{N_I} p_i G_n R_n^{-\alpha}\right) \right] \\ &= \mathbb{E}_{N_I, R_n, G_n} \left[ \prod_{n=1}^{N_I} \exp(-s p_i G_n R_n^{-\alpha}) \right] \\ &\stackrel{(a)}{=} \mathbb{E}_{N_I, R_n} \left[ \prod_{n=1}^{N_I} \mathbb{E}_{G_n} [\exp(-s p_i G_n R_n^{-\alpha})] \right] \\ &\stackrel{(b)}{=} \mathbb{E}_{N_I} \left[ \prod_{n=1}^{N_I} \frac{2}{r_{\max}^4 / r_{\min}^2 - r_0^2} \right. \\ &\quad \times \int_{r_0}^{r_{\max}} \mathbb{E}_{G_n} [\exp(-s p_i G_n r_n^{-\alpha})] r_n dr_n \left. \right] \\ &\stackrel{(c)}{=} \sum_{n_1=1}^{\frac{N}{K}-1} \left( \binom{\frac{N}{K}-1}{n_1} P_1^{n_1} (1-P_1)^{\frac{N}{K}-1-n_1} \left( \frac{2}{r_{\max}^4 / r_{\min}^2 - r_0^2} \right)^{n_1} \right. \\ &\quad \times \int_{r_0}^{r_{\max}} \mathbb{E}_{G_n} [\exp(-s p_i G_n r_n^{-\alpha})] r_n dr_n \left. \right)^{n_1} \\ &\stackrel{(d)}{=} \sum_{n_1=1}^{\frac{N}{K}-1} \left( \binom{\frac{N}{K}-1}{n_1} P_1^{n_1} (1-P_1)^{\frac{N}{K}-1-n_1} \right. \end{aligned}$$

$$\left. \times \left( \frac{2}{r_{\max}^4 / r_{\min}^2 - r_0^2} \int_{r_0}^{r_{\max}} \mathcal{L}_{G_n}(s p_i r_n^{-\alpha}) r_n dr_n \right)^{n_1} \right) \quad (44)$$

where (a) follows from the i.i.d. distribution of  $G_n$  and its further independence from  $N_I$  and  $R_n$ , (b) is obtained using the interfering distance distribution from (7), (c) is the averaging over the binomial random variable  $N_I$  with the success probability  $P_1$ , which is given in Lemma 4, and (d) is the substitution from the definition of Laplace function.

### C. Proof of Theorem 3

We only provide the proof for (35) herein, while the proof for (34) follows the same approach as well. In particular,

$$\begin{aligned} &\mathbb{E}_{I, G_0, R_0} [\log_2(1 + \text{SINR}) | N_I > 0] \\ &= c_0 \int_{r_{\min}}^{r_{\max}} \mathbb{E} \left[ \ln \left( 1 + \frac{P_s G_0 r_0^{-\alpha}}{I + \sigma^2} \right) \middle| N_I > 0 \right] \\ &\quad \times \left( 1 - \frac{r_0^2 - r_{\min}^2}{4r_{\oplus}(r_{\oplus} + r_{\min})} \right)^{N-1} r_0 dr_0 \\ &\stackrel{(a)}{=} c_0 \int_{r_{\min}}^{r_{\max}} \int_{t>0} \mathbb{P} \left( \ln \left( 1 + \frac{P_s G_0 r_0^{-\alpha}}{I + \sigma^2} \right) > t \middle| N_I > 0 \right) dt \\ &\quad \times \left( 1 - \frac{r_0^2 - r_{\min}^2}{4r_{\oplus}(r_{\oplus} + r_{\min})} \right)^{N-1} r_0 dr_0 \\ &= c_0 \int_{r_{\min}}^{r_{\max}} \int_{t>0} \mathbb{P} \left( G_0 > \frac{r_0^\alpha}{P_s} (\sigma^2 + I) (e^t - 1) \middle| N_I > 0 \right) dt \\ &\quad \times \left( 1 - \frac{r_0^2 - r_{\min}^2}{4r_{\oplus}(r_{\oplus} + r_{\min})} \right)^{N-1} r_0 dr_0 \\ &= c_0 \int_{r_{\min}}^{r_{\max}} \int_{t>0} \mathbb{E}_I \left[ e^{-\frac{r_0^\alpha}{P_s} (I + \sigma^2) (e^t - 1)} \middle| N_I > 0 \right] dt \\ &\quad \times \left( 1 - \frac{r_0^2 - r_{\min}^2}{4r_{\oplus}(r_{\oplus} + r_{\min})} \right)^{N-1} r_0 dr_0 \\ &= c_0 \int_{r_{\min}}^{r_{\max}} \int_{t>0} e^{-\frac{r_0^\alpha}{P_s} \sigma^2 (e^t - 1)} \mathbb{E}_I \left[ e^{-\frac{r_0^\alpha}{P_s} (e^t - 1) I} \right] dt \\ &\quad \times \left( 1 - \frac{r_0^2 - r_{\min}^2}{4r_{\oplus}(r_{\oplus} + r_{\min})} \right)^{N-1} r_0 dr_0, \end{aligned} \quad (45)$$

where  $c_0 = \frac{N}{2 \ln(2) r_{\oplus} (r_{\oplus} + r_{\min})}$  and (a) follows from the fact that for a positive random variable  $X$ ,  $\mathbb{E}[X] = \int_{t>0} \mathbb{P}(X > t) dt$ .

### D. Proof of Theorem 4

Assuming  $G_n = 1$ , we have

$$\begin{aligned} &\mathbb{E}_{I, R_0} [\log_2(1 + \text{SINR}) | N_I > 0] \\ &= c_0 \int_{r_{\min}}^{r_{\max}} \mathbb{E} \left[ \ln \left( 1 + \frac{P_s r_0^{-\alpha}}{I + \sigma^2} \right) \middle| N_I > 0 \right] \\ &\quad \times \left( 1 - \frac{r_0^2 - r_{\min}^2}{4r_{\oplus}(r_{\oplus} + r_{\min})} \right)^{N-1} r_0 dr_0 \\ &= c_0 \int_{r_{\min}}^{r_{\max}} \int_{t>0} \mathbb{P} \left( \ln \left( 1 + \frac{P_s r_0^{-\alpha}}{I + \sigma^2} \right) > t \middle| N_I > 0 \right) dt \end{aligned}$$

$$\begin{aligned}
& \times \left(1 - \frac{r_0^2 - r_{\min}^2}{4r_{\oplus}(r_{\oplus} + r_{\min})}\right)^{N-1} r_0 dr_0 \\
= & c_0 \int_{r_{\min}}^{r_{\max}} \int_{t>0} \mathbb{P}\left(p_s > r_0^\alpha (\sigma^2 + I) (e^t - 1) dt \mid N_1 > 0\right) \\
& \times \left(1 - \frac{r_0^2 - r_{\min}^2}{4r_{\oplus}(r_{\oplus} + r_{\min})}\right)^{N-1} r_0 dr_0 \\
= & c_0 \int_{r_{\min}}^{r_{\max}} \int_{t>0} \mathbb{P}\left(0 < I < \frac{p_s}{r_0^\alpha (e^t - 1)} - \sigma^2\right) dt \\
& \times \left(1 - \frac{r_0^2 - r_{\min}^2}{4r_{\oplus}(r_{\oplus} + r_{\min})}\right)^{N-1} r_0 dr_0, \quad (46)
\end{aligned}$$

where  $c_0 = \frac{N}{2\ln(2)r_{\oplus}(r_{\oplus} + r_{\min})}$ . Following the same approach as in (28)–(30) and using Parseval–Plancherel formula will result in (38). The proof for (37) can be obtained easily using the same principles as the above and only by substituting  $I = 0$ .

#### REFERENCES

- [1] F. Vatalaro, G. E. Corazza, C. Caini, and C. Ferrarelli, "Analysis of LEO, MEO, and GEO global mobile satellite systems in the presence of interference and fading," *IEEE Journal on Selected Areas in Communications*, vol. 13, no. 2, pp. 291–300, Feb. 1995.
- [2] A. Ganz, Y. Gong, and B. Li, "Performance study of low Earth-orbit satellite systems," *IEEE Transactions on Communications*, vol. 42, no. 234, pp. 1866–1871, Feb. 1994.
- [3] H. M. Mourad, A. A. M. Al-Bassiouni, S. S. Emam, and E. K. Al-Hussaini, "Generalized performance evaluation of low Earth orbit satellite systems," *IEEE Communications Letters*, vol. 5, no. 10, pp. 405–407, Oct. 2001.
- [4] G. Ruiz, T. L. Doumi, and J. G. Gardiner, "Teletraffic analysis and simulation for nongeostationary mobile satellite systems," *IEEE Transactions on Vehicular Technology*, vol. 47, no. 1, pp. 311–320, Feb. 1998.
- [5] I. Ali, N. Al-Dhahir, and J. E. Hershey, "Predicting the visibility of LEO satellites," *IEEE Transactions on Aerospace and Electronic Systems*, vol. 35, no. 4, pp. 1183–1190, Oct. 1999.
- [6] M. Haenggi, *Stochastic geometry for wireless networks*. Cambridge University Press, 2012.
- [7] B. Błaszczyszyn, M. Haenggi, P. Keeler, and S. Mukherjee, *Stochastic geometry analysis of cellular networks*. Cambridge University Press, 2018.
- [8] M. Haenggi, J. G. Andrews, F. Baccelli, O. Dousse, and M. Franceschetti, "Stochastic geometry and random graphs for the analysis and design of wireless networks," *IEEE Journal on Selected Areas in Communications*, vol. 27, no. 7, pp. 1029–1046, Sep. 2009.
- [9] H. ElSawy, E. Hossain, and M. Haenggi, "Stochastic geometry for modeling, analysis, and design of multi-tier and cognitive cellular wireless networks: A survey," *IEEE Communications Surveys and Tutorials*, vol. 15, no. 3, pp. 996–1019, Jun. 2013.
- [10] J. G. Andrews, F. Baccelli, and R. K. Ganti, "A tractable approach to coverage and rate in cellular networks," *IEEE Transactions on Communications*, vol. 59, no. 11, pp. 3122–3134, Nov. 2011.
- [11] H. S. Dhillon, R. K. Ganti, F. Baccelli, and J. G. Andrews, "Modeling and analysis of k-tier downlink heterogeneous cellular networks," *IEEE Journal on Selected Areas in Communications*, vol. 30, no. 3, pp. 550–560, Apr. 2012.
- [12] D. Cao, S. Zhou, and Z. Niu, "Optimal combination of base station densities for energy-efficient two-tier heterogeneous cellular networks," *IEEE Transactions on Wireless Communications*, vol. 12, no. 9, pp. 4350–4362, Sep. 2013.
- [13] H. S. Dhillon, T. D. Novlan, and J. G. Andrews, "Coverage probability of uplink cellular networks," in *Proc. IEEE Global Communications Conference (GLOBECOM)*, Dec. 2012.
- [14] M. Afshang and H. S. Dhillon, "Fundamentals of modeling finite wireless networks using binomial point processes," *IEEE Transactions on Wireless Communications*, vol. 16, no. 5, pp. 3355–3370, May 2017.
- [15] Z. Pan and Q. Zhu, "Modeling and analysis of coverage in 3-D cellular networks," *IEEE Communications Letters*, vol. 19, no. 5, pp. 831–834, May 2015.
- [16] V. V. Chetlur and H. S. Dhillon, "Downlink coverage analysis for a finite 3-D wireless network of unmanned aerial vehicles," *IEEE Transactions on Communications*, vol. 65, no. 10, pp. 4543–4558, Oct. 2017.
- [17] S. Srinivasa and M. Haenggi, "Distance distributions in finite uniformly random networks: Theory and applications," *IEEE Transactions on Vehicular Technology*, vol. 59, no. 2, pp. 940–949, Feb. 2010.
- [18] J. Guo, S. Durrani, and X. Zhou, "Outage probability in arbitrarily-shaped finite wireless networks," *IEEE Transactions on Communications*, vol. 62, no. 2, pp. 699–712, Feb. 2014.
- [19] Z. Khalid and S. Durrani, "Distance distributions in regular polygons," *IEEE Transactions on Vehicular Technology*, vol. 62, no. 5, pp. 2363–2368, Jun. 2013.
- [20] J. Guo, S. Durrani, and X. Zhou, "Performance analysis of arbitrarily-shaped underlay cognitive networks: Effects of secondary user activity protocols," *IEEE Transactions on Communications*, vol. 63, no. 2, pp. 376–389, Feb. 2015.
- [21] X. Wang, H. Zhang, Y. Tian, and V. C. M. Leung, "Modeling and analysis of aerial base station-assisted cellular networks in finite areas under LoS and NLoS propagation," *IEEE Transactions on Wireless Communications*, vol. 17, no. 10, pp. 6985–7000, Oct. 2018.
- [22] M. Sellathurai, S. Vuppala, and T. Ratnarajah, "User selection for multi-beam satellite channels: A stochastic geometry perspective," in *Proc. Asilomar Conference on Signals, Systems and Computers*, Nov. 2016.
- [23] S. Zhang and J. Liu, "Analysis and optimization of multiple unmanned aerial vehicle-assisted communications in post-disaster areas," *IEEE Transactions on Vehicular Technology*, vol. 67, no. 12, pp. 12 049–12 060, Dec. 2018.
- [24] O. Y. Kolawole, S. Vuppala, M. Sellathurai, and T. Ratnarajah, "On the performance of cognitive satellite–terrestrial networks," *IEEE Transactions on Cognitive Communications and Networking*, vol. 3, no. 4, pp. 668–683, Dec. 2017.
- [25] Y. Seyed and S. M. Safavi, "On the analysis of random coverage time in mobile LEO satellite communications," *IEEE Communications Letters*, vol. 16, no. 5, pp. 612–615, May 2012.
- [26] S. A. Banani, A. W. Eckford, and R. S. Adve, "Analyzing the impact of access point density on the performance of finite-area networks," *IEEE Transactions on Communications*, vol. 63, no. 12, pp. 5143–5161, Dec. 2015.
- [27] N. K. Lyras, C. I. Kourogorgas, and A. D. Panagopoulos, "Cloud free line of sight prediction modeling for low Earth orbit optical satellite networks," 2019. [Online]. Available: <https://doi.org/10.1117/12.2535971>.
- [28] I. S. Gradshteyn and I. M. Ryzhik, *Table of Integrals, Series, and Products*. Academic Press, 2014.
- [29] F. Baccelli and B. Błaszczyszyn, "On a coverage process ranging from the Boolean model to the Poisson–Voronoi tessellation with applications to wireless communications," *Advances in Applied Probability*, vol. 33, no. 2, pp. 293–323, Jun. 2001.
- [30] —, "Stochastic geometry and wireless networks: Volume II applications," *Foundations and Trends® in Networking*, vol. 4, no. 1–2, pp. 1–312, Jan. 2010.



**Niloofer Okati** received the B.E. degree in electrical engineering from Shiraz University of Technology, Iran, in 2013, and M.Sc. degree in communications engineering from Iran University of Science and Technology (IUST), Iran, in 2016. She is currently a Ph.D. researcher at the Faculty of Information Technology and Communication Sciences, Tampere University, Finland. Her research interests include stochastic geometry, wireless communication and satellite networks. She was one of the 200 young researchers in mathematics and computer science selected worldwide to participate in the 7th Heidelberg Laureate Forum (HLF), in 2019.



**Taneli Riihonen** (S'06–M'14) received the D.Sc. degree in electrical engineering (with distinction) from Aalto University, Helsinki, Finland, in August 2014. He is currently an Assistant Professor (tenure track) at the Faculty of Information Technology and Communication Sciences, Tampere University, Finland. He held various research positions at Aalto University School of Electrical Engineering from September 2005 through December 2017. He was a Visiting Associate Research Scientist and an Adjunct Assistant Professor at Columbia University in the

City of New York, USA, from November 2014 through December 2015. He has been nominated eleven times as an Exemplary/Top Reviewer of various IEEE journals and is serving as an Editor for IEEE WIRELESS COMMUNICATIONS LETTERS since May 2017. He has previously served as an Editor for IEEE COMMUNICATIONS LETTERS from October 2014 through January 2019. He received the Finnish technical sector's award for the best doctoral dissertation in 2014 and the EURASIP Best PhD Thesis Award 2017. His research activity is focused on physical-layer OFDM(A), multiantenna, relaying and full-duplex wireless techniques with current interest in the evolution of beyond 5G systems.



**Dani Korpi** received the M.Sc. and D.Sc. degrees (Hons.) in communications engineering and electrical engineering from Tampere University of Technology, Finland, in 2014 and 2017, respectively. Currently, he is a Senior Specialist with Nokia Bell Labs in Espoo, Finland. His doctoral thesis received an award for the best dissertation of the year in Tampere University of Technology, as well as the Finnish technical sector's award for the best doctoral dissertation in 2017. His research interests include inband full-duplex radios, machine learning

for wireless communications, and beyond 5G radio systems.



**Ilari Angervuori** received the B.Sc. and M.Sc. degrees from the University of Helsinki, Finland, in 2016 and 2018. Since 2018, he has been with the School of Electrical Engineering at Department of Signal Processing and Acoustics, Aalto University, where he has been a Doctoral Candidate since 2019. His research interests are in the areas of satellite communications and wireless communication. He has a strong background in applied mathematics and applying stochastic geometry into areas of engineering is in his main focus.



**Risto Wichman** received his M.Sc. and D.Sc. (Tech.) degrees in digital signal processing from Tampere University of Technology, Finland, in 1990 and 1995, respectively. From 1995 to 2001, he worked at Nokia Research Center as a senior research engineer. In 2002, he joined Department of Signal Processing and Acoustics, Aalto University School of Electrical Engineering, Finland, where he is a full professor since 2008. His research interests include signal processing techniques for wireless communication systems.



## PUBLICATION 2

**Stochastic Analysis of Satellite Broadband by Mega-Constellations with  
Inclined LEOs**

N. Okati and T. Riihonen

In *Proc. IEEE 31st Annual International Symposium on Personal, Indoor and Mobile Radio  
Communications (PIMRC)*, Sep. 2020

**Publication reprinted with the permission of the copyright holders.**



# Stochastic Analysis of Satellite Broadband by Mega-Constellations with Inclined LEOs

Niloofer Okati and Taneli Riihonen

Faculty of Information Technology and Communication Sciences, Tampere University, Finland

e-mail: {niloofer.okati, taneli.riihonen}@tuni.fi

**Abstract**—As emerging massive constellations are intended to provide seamless connectivity for remote areas using hundreds of small low Earth orbit (LEO) satellites, new methodologies have great importance to study the performance of these networks. In this paper, we derive both downlink and uplink analytical expressions for coverage probability and data rate of an inclined LEO constellation under general fading, regardless of exact satellites' positions. Our solution involves two phases as we, first, abstract the network into a uniformly distributed network. Secondly, we obtain a new parameter, effective number of satellites, for every user's latitude which compensates for the performance mismatch between the actual and uniform constellations. In addition to exact derivation of the network performance metrics, this study provides insight into selecting the constellation parameters, e.g., the total number of satellites, altitude, and inclination angle.

## I. INTRODUCTION

A constellation of low Earth orbit (LEO) satellites can provide infrastructure for ubiquitous connectivity with low round-trip delay—compared to geostationary satellites—when terrestrial networks are not available or economically reasonable to deploy [1], [2]. Technological advancements along with the need for seamless connectivity have emerged the utilization of massive satellite networks and, consequently, the research around this topic.

The uplink outage probability in the presence of interference was evaluated for two LEO constellations through time-domain simulations in [3]. A performance study of Iridium constellation was presented in [4] in terms of the distribution of the number of handoffs involved in a single transaction duration and the average call drop probability. The effect of traffic non-uniformity was studied in [5] by assuming hexagonal service areas for satellites.

A general expression for a single LEO satellite's visibility time was provided in [6], but it is incapable of concluding the general distribution of visibility periods for any arbitrarily positioned user. The deterministic model in [6] was then developed by a statistical analysis of coverage time in mobile LEO during a satellite visit [7]. In [8], the Doppler shift magnitude of a LEO network is characterized for a single spotbeam by using tools from stochastic geometry. Resource control of a hybrid satellite–terrestrial network was performed in [9] with two objectives of maximizing the delay-limited capacity and minimizing the outage probability. A hybrid

satellite–terrestrial network to assist 5G infrastructure has been analyzed by considering only one spotbeam [10], [11].

In the current literature around communication satellites' performance, the network analysis is limited to deterministic simulation-based studies, simplifying the network by considering specific constellations with a limited number of satellites, and assuming specific coverage footprints for satellites. Therefore, a comprehensive method that fits any constellation with arbitrary parameters is missing from the scientific literature. In our recent study [12], downlink performance of a massive LEO constellation was investigated by assuming uniform distribution for satellites. However, the performance mismatch between actual and uniform constellations was compensated only through numerical mean absolute error minimization.

In this paper, we provide a mathematical framework for downlink and uplink coverage probability and data rate analysis of an inclined LEO constellation under a general fading model. For our derivations, first, we assume the satellites are distributed uniformly on the orbital shell. Later, the mismatch between the actual and uniform constellations is compensated by deriving a new parameter as the effective number of satellites. Finally, the mathematical expressions are verified through simulations and the main findings of this paper are demonstrated for different network parameters, e.g., the total number of satellites, altitude and minimum elevation angle required for a satellite to be visible to the user. The results obtained in this paper are scalable for numerous problems in massive satellite networks.

The organization of the remainder of this paper is as follows. Section II describes the system model for an inclined LEO constellation. As for the main results, in Sections III, we derive analytical expressions for coverage probability and average achievable data rate for a terrestrial user and introduce the concept of effective number of satellites. Numerical results are provided in Section IV for studying the effect of key system parameters. Finally, we conclude the paper in Section V.

## II. SYSTEM MODEL

Let us consider a LEO communication satellite constellation, as shown in Fig. 1, that consists of  $N_{\text{act}}$  satellites, which are placed on low circular orbits with the same inclination angle and altitude denoted by  $\iota$  and  $r_{\text{min}}$ , respectively. The altitude parameter  $r_{\text{min}}$  has the subscript because it specifies also the minimum possible distance between a satellite and a user on Earth (that is realized when it is at the zenith).

This research work was supported by a Nokia University Donation.

User terminals are located on the surface of Earth that is approximated as a perfect sphere. We assume that wireless transmissions propagate to/from a user from/to all and only the satellites that are elevated above the horizon to an angle of  $\theta_s \geq \theta_{\min}$ . Correspondingly,  $r_{\max}$  denotes the maximum possible distance at which a satellite and a user may be able to communicate (that is realized when  $\theta_s = \theta_{\min}$ ), and

$$\frac{r_{\max}}{r_{\oplus}} = \sqrt{\frac{r_{\min}}{r_{\oplus}} \left( \frac{r_{\min}}{r_{\oplus}} + 2 \right) + \sin^2(\theta_{\min})} - \sin(\theta_{\min}), \quad (1)$$

where  $r_{\oplus} \approx 6371$  km denotes Earth's radius. Conversely, the latitudes, where a terrestrial user may be able to establish connection with any satellite at all, are limited by

$$|\phi_u| \leq \iota + \cos^{-1} \left( \frac{r_{\oplus}^2 + r_{\oplus} r_{\min} + (r_{\min}^2 - r_{\max}^2)/2}{r_{\oplus}(r_{\oplus} + r_{\min})} \right). \quad (2)$$

For instance, with satellite altitudes of  $r_{\min} = 500$  km and  $r_{\max} = 2000$  km, global coverage up to poles for  $\theta_{\min} = 0^\circ$  is possible only if  $\iota > 68^\circ$  and  $\iota > 49^\circ$ , respectively. Using (2), the minimum altitude which provides global coverage is given as

$$r_{\min} \geq \frac{r_{\oplus} \cos(\theta_{\min})}{\sin(\iota - \theta_{\min})} - r_{\oplus}. \quad (3)$$

Each user is associated with the nearest satellite that is referred to as the serving satellite in what follows. We assume that co-channel interference mitigation has been implemented properly so that the network performance becomes noise-limited. The distances from the user to the serving satellite and the other satellites are denoted by  $r_0$  and  $r_n$ ,  $n = 1, 2, \dots, N_{\text{act}} - 1$ , respectively, while  $G_0$  and  $G_n$  represent the corresponding channel gains. Obviously,  $G_n = 0$  if  $r_n > r_{\max}$  for some  $n = 0, 1, \dots, N_{\text{act}} - 1$ .

Based on the above modeling, the signal-to-noise ratio (SNR) at the receiver can be expressed as

$$\text{SNR} = \begin{cases} \frac{p_s G_0 r_0^{-\alpha}}{\sigma^2}, & r_0 \leq r_{\max}, \\ 0, & \text{otherwise,} \end{cases} \quad (4)$$

where we assume that the user's receiver is subject to additive white Gaussian noise with constant power  $\sigma^2$ , and the parameter  $\alpha$  is a path loss exponent.

### III. PERFORMANCE ANALYSIS

In order to contribute expressions for coverage probability and average achievable rate of the satellite constellation described in Section II, first, we assume that  $N$  satellites are distributed uniformly on a sphere with radius  $r_{\oplus} + r_{\min}$ . We will shortly compensate for the performance mismatch generated by the distribution difference between the uniform model and the practical constellations.

First, we need to characterize some basic distance distributions that stem from the geometry of the considered system. In particular, we express the necessary cumulative distribution function (CDF) and probability density functions (PDFs) in the following lemmas.

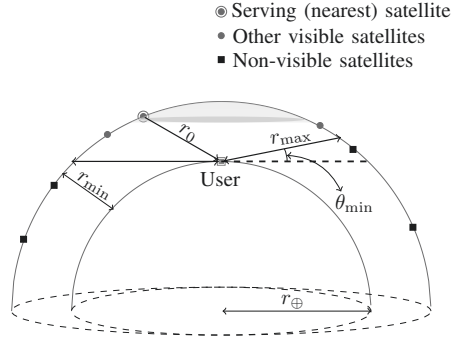


Fig. 1. A sketch of the considered system model, where satellites are distributed uniformly over the inclined orbits.

**Lemma 1.** The PDF of the serving distance  $R_0$  is given by

$$f_{R_0}(r_0) = N \left( 1 - \frac{r_0^2 - r_{\min}^2}{4r_{\oplus}(r_{\oplus} + r_{\min})} \right)^{N-1} \frac{r_0}{2r_{\oplus}(r_{\oplus} + r_{\min})} \quad (5)$$

for  $r_0 \in [r_{\min}, 2r_{\oplus} + r_{\min}]$  while  $f_{R_0}(r_0) = 0$  otherwise.

*Proof.* We first need to derive the CDF of the distance  $R$  from any specific one of the satellites in the constellation to the user. From basic geometry, the CDF of the surface area of the shaded spherical cap  $A_{\text{cap}}$ , formed by any satellite at distance  $R$  from the user, in Fig. 1 is  $F_{A_{\text{cap}}}(a_{\text{cap}}) = \frac{a_{\text{cap}}}{4\pi(r_{\oplus} + r_{\min})^2}$ . Finding a relationship between  $A_{\text{cap}}$  and  $R$ , gives the distribution as

$$F_R(r) = \begin{cases} 0, & r < r_{\min}, \\ \frac{r^2 - r_{\min}^2}{4r_{\oplus}(r_{\oplus} + r_{\min})}, & r_{\min} \leq r \leq 2r_{\oplus} + r_{\min}, \\ 1, & r > 2r_{\oplus} + r_{\min}, \end{cases} \quad (6)$$

and the corresponding PDF is given by

$$f_R(r) = \frac{r}{2r_{\oplus}(r_{\oplus} + r_{\min})} \quad (7)$$

for  $r_0 \in [r_{\min}, 2r_{\oplus} + r_{\min}]$  while  $f_R(r) = 0$  otherwise. Due to the channel assignment by which the serving satellite is the nearest one among all the  $N$  i.i.d. satellites, the CDF of  $R_0$  can be expressed as  $F_{R_0}(r_0) \triangleq \mathbb{P}(R_0 \leq r_0) = 1 - (1 - F_R(r_0))^N$  and, by differentiation, its PDF is  $f_{R_0}(r_0) = N(1 - F_R(r_0))^{N-1} f_R(r)$  which will result in Lemma 1 by substitution from (6) and (7).  $\square$

#### A. Coverage Probability

In this subsection, we derive the coverage probability of the LEO satellite network for a user in an arbitrary location on Earth. The performance measure of coverage probability is defined as the probability of having at least minimum SNR required for successful data transmission. In other words, whenever the SNR of the considered user from its nearest satellite is above the threshold level  $T > 0$ , it is considered to be within the coverage of the satellite communication network.



**Proposition 1.** *The probability of network coverage for an arbitrarily located user under general fading is*

$$P_c(T) \triangleq \mathbb{P}(\text{SNR} > T) = \frac{N}{2r_\oplus(r_\oplus + r_{\min})} \int_{r_{\min}}^{r_{\max}} \left(1 - F_{G_0}\left(\frac{Tr_0^\alpha \sigma^2}{p_s}\right)\right) \times \left(1 - \frac{r_0^2 - r_{\min}^2}{4r_\oplus(r_\oplus + r_{\min})}\right)^{N-1} r_0 dr_0, \quad (8)$$

where  $F_{G_0}(\cdot)$  is the CDF of the channel gain  $G_0$ .

*Proof.* To obtain (8), we start with the definition of coverage probability:

$$P_c(T) = \mathbb{E}_{R_0}[\mathbb{P}(\text{SNR} > T | R_0)] = \int_{r_{\min}}^{r_{\max}} \mathbb{P}(\text{SNR} > T | R_0 = r_0) f_{R_0}(r_0) dr_0 = \frac{N}{2r_\oplus(r_\oplus + r_{\min})} \int_{r_{\min}}^{r_{\max}} \mathbb{P}\left(G_0 > \frac{Tr_0^\alpha \sigma^2}{p_s}\right) \times \left(1 - \frac{r_0^2 - r_{\min}^2}{4r_\oplus(r_\oplus + r_{\min})}\right)^{N-1} r_0 dr_0. \quad (9)$$

The upper limit for the integral is due to the fact that the satellites with smaller than  $\theta_{\min}$  elevation angle have no visibility to the user.  $\square$

The channel characteristics have no effect on the maximum achievable coverage as it is affected only by the geometry of the system model. The following corollary provides the upper bound for coverage probability using Proposition 1.

**Corollary 1.** *Setting  $T = 0$ , Proposition 1 leads to an upper bound for coverage probability as*

$$P_c(T) \leq F_{R_0}(r_{\max}) - F_{R_0}(r_{\min}) = 1 - (1 - P_V)^N, \quad (10)$$

where  $P_V$  is the visibility probability of satellites to the user and is expressed as

$$P_V = \frac{r_{\min} - r_{\max} \sin(\theta_{\min})}{2(r_\oplus + r_{\min})}. \quad (11)$$

The expression in (11) can be directly obtained as the surface area of the spherical cap, where visible satellites can reside, to the total surface area of the satellites' sphere since the satellites are uniformly distributed.

Since the number of visible satellites is a binomial random variable with success probability  $P_V$ , the coverage probability is upper bounded by the probability of observing at least one satellite by the user.

### B. Average Data Rate

In this subsection, we focus on the average achievable data rate. The average achievable rate (in bit/s/Hz) states the ergodic capacity from the Shannon–Hartley theorem over a fading communication link normalized to the bandwidth of 1 Hz. We can calculate the expression for the average rate of an arbitrary user over generalized fading channels as follows.

It is worth noting that the average is taken over both serving distance and fading distributions.

**Proposition 2.** *The average rate (in bits/s/Hz) of an arbitrarily located user and its serving satellite under general fading assumption is*

$$\bar{C} \triangleq \mathbb{E}[\log_2(1 + \text{SNR})] = \frac{N}{2 \ln(2) r_\oplus (r_\oplus + r_{\min})} \times \int_{r_{\min}}^{r_{\max}} \int_0^\infty \ln\left(1 + \frac{p_s g_0 r_0^{-\alpha}}{\sigma^2}\right) f_{G_0}(g_0) \times \left(1 - \frac{r_0^2 - r_{\min}^2}{4r_\oplus(r_\oplus + r_{\min})}\right)^{N-1} r_0 dg_0 dr_0, \quad (12)$$

where  $f_{G_0}(g_0)$  represents the PDF of channel gain  $G_0$ .

*Proof.* Taking the expectation over serving distance and channel gain, we have

$$\bar{C} = \mathbb{E}_{G_0, R_0}[\log_2(1 + \text{SNR})] = c_0 \int_{r_{\min}}^{r_{\max}} \mathbb{E}\left[\ln\left(1 + \frac{p_s G_0 r_0^{-\alpha}}{\sigma^2}\right)\right] \times \left(1 - \frac{r_0^2 - r_{\min}^2}{4r_\oplus(r_\oplus + r_{\min})}\right)^{N-1} r_0 dr_0, \quad (13)$$

where  $c_0 = \frac{N}{2 \ln(2) r_\oplus (r_\oplus + r_{\min})}$ .  $\square$

### C. Effective Number of Satellites

Due to the fact that satellites in practical constellations are distributed unevenly along different latitudes, i.e., the number of satellites is effectively larger on the inclination limit of the constellation than on equatorial regions, the density of practical deterministic constellations is typically not uniform. Thus, we define and calculate a new parameter, the effective number of satellites,  $N_{\text{eff}}$ , for every satellite latitude in order to compensate for the uneven density w.r.t. practical inclined constellations and create a tight match between the results generated by uniform modeling and those from practical constellation simulations.

**Proposition 3.** *Let the effective number of satellites ( $N_{\text{eff}}$ ) be the constellation size that corresponds to a satellite density observed by a user on a specific latitude assuming the same density continues everywhere. The effective number of satellites can then be determined as*

$$N_{\text{eff}} \triangleq \frac{2 f_{\Phi_s}(\phi_s)}{\cos(\phi_s)} \cdot N_{\text{act}}, \quad (14)$$

where random variable  $\Phi_s$  denotes the latitude of a satellite and  $f_{\Phi_s}(\phi_s)$  corresponds to its PDF.

*Proof.* The satellite density observed effectively by a user at any latitude assuming that there are  $N_{\text{eff}}$  uniformly distributed satellites in total is

$$\delta_{\text{eff}} = \frac{N_{\text{eff}}}{4\pi(r_{\min} + r_\oplus)^2}, \quad (15)$$

where the denominator represents the surface area of the satellites' orbital shell. On the other hand, the actual density of the satellites on a ring surface element at latitude  $\phi_s$  can be written as

$$\delta_{\text{act}} = \frac{N_{\text{act}} f_{\Phi_s}(\phi_s) d\phi_s}{2\pi(r_{\min} + r_{\oplus})^2 \cos(\phi_s) d\phi_s}, \quad (16)$$

where the nominator and denominator represent the number of satellites resided in the surface element and the element's surface area, respectively. Setting  $\delta_{\text{eff}} = \delta_{\text{act}}$  and applying some simplifications completes the proof.  $\square$

**Lemma 2.** *When the satellites' argument of latitude  $U$  is a uniform random variable [13], i.e.,  $U \sim \mathcal{U}(-\frac{\pi}{2}, \frac{\pi}{2})$ , the PDF of satellites' latitude with inclination  $\iota$  is given by*

$$f_{\Phi_s}(\phi_s) = \frac{\sqrt{2}}{\pi} \cdot \frac{\cos(\phi_s)}{\sqrt{\cos(2\phi_s) - \cos(2\iota)}} \quad (17)$$

for  $\phi_s \in [-\iota, \iota]$  while  $f_{\Phi_s}(\phi_s) = 0$  otherwise.

*Proof.* Since the distribution of the argument of latitude is known, we need to find the satellite's latitude as a function of the argument of latitude and inclination angle. The satellite's coordinates can be obtained by multiplication of  $\iota$ -degree rotation matrix and satellites' orbital plane:

$$\begin{aligned} \begin{bmatrix} x_s \\ y_s \\ z_s \end{bmatrix} &= \begin{bmatrix} \cos(\iota) & 0 & \sin(\iota) \\ 0 & 1 & 0 \\ -\sin(\iota) & 0 & \cos(\iota) \end{bmatrix} \begin{bmatrix} (r_{\min} + r_{\oplus}) \cos(U) \\ (r_{\min} + r_{\oplus}) \sin(U) \\ 0 \end{bmatrix} \\ &= \begin{bmatrix} (r_{\min} + r_{\oplus}) \cos(U) \cos(\iota) \\ (r_{\min} + r_{\oplus}) \sin(U) \\ -(r_{\min} + r_{\oplus}) \cos(U) \sin(\iota) \end{bmatrix}. \end{aligned} \quad (18)$$

Therefore, the latitude of the satellite is given as

$$\begin{aligned} \Phi_s &= g(U) = \tan^{-1} \left( \frac{z_s}{\sqrt{x_s^2 + y_s^2}} \right) \\ &= \tan^{-1} \left( -\frac{\cos(U) \sin(\iota)}{\sqrt{\cos^2(U) \cos^2(\iota) + \sin^2(U)}} \right). \end{aligned} \quad (19)$$

The PDF of  $\Phi_s$  can be written as

$$f_{\Phi_s}(\phi_s) = f_U(g^{-1}(\phi_s)) \frac{d}{d\phi_s} (g^{-1}(\phi_s)) \quad (20)$$

by the transform of random variables.  $\square$

Thus, when the satellites' argument of latitude is uniform and their inclination is  $\iota$ , the effective number of satellites can be obtained by using Lemma 2 in Proposition 3 as follows:

$$N_{\text{eff}} = \frac{2\sqrt{2}}{\pi} \cdot \frac{1}{\sqrt{\cos(2\phi_s) - \cos(2\iota)}} \cdot N_{\text{act}}. \quad (21)$$

With high orbit inclination, the effective number of satellites matches to the true number of satellites at some latitudes, decreasing monotonically toward the equator and increasing

TABLE I  
SIMULATION PARAMETERS

Parameters	Values
Path loss exponent, $\alpha$	2
Rician factor, $K$	100
CDF of channel gains, $F_{G_n}(g_n)$	$1 - Q_1(\sqrt{2K}, \sqrt{g_n})$
PDF of channel gains, $f_{G_n}(g_n)$	$\frac{1}{2} e^{-\frac{g_n + 2K}{2}} I_0(\sqrt{2Kg_n})$
Transmission power, $p_s$ (W)	10
Noise power, $\sigma^2$ (dBm)	-93
User's latitude, $\phi_u$ (degree)	0

monotonically toward the poles. By setting  $N_{\text{act}} = N_{\text{eff}}$ , we can solve these special latitudes (one for each hemisphere) as

$$\phi_s = \pm \frac{1}{2} \cos^{-1} \left( \frac{8}{\pi^2} + \cos(2\iota) \right), \quad (22)$$

if  $\iota \geq \frac{1}{2} \cos^{-1} \left( 1 - \frac{8}{\pi^2} \right) \approx 39.5^\circ$  and otherwise  $N_{\text{eff}} > N_{\text{act}}$  for all  $\phi_s \leq \iota$ .

In the special case of having polar orbits (i.e.,  $\iota = 90^\circ$ ), the PDF of latitude would be the same as the argument of latitude, i.e.,  $\phi_s = U \sim \mathcal{U}(-\frac{\pi}{2}, \frac{\pi}{2})$  for all  $\phi_s$  values. Thus,  $N_{\text{eff}} = \frac{2/\pi}{\cos(\phi_s)} \cdot N_{\text{act}}$ . For instance, at equator, ( $\phi_s = 0^\circ$ ),  $N_{\text{eff}} \approx 0.64 N_{\text{act}}$  and by increasing the latitude up to  $\phi_s \approx 50.5^\circ$ , we will have  $N_{\text{eff}} \approx N_{\text{act}}$ . Finally  $N_{\text{eff}}$  will approach to infinity at poles where all satellite orbits cross. The authors up north ( $\phi_u = 61.5^\circ$ ) at Tampere, Finland observe effectively 30% more satellites than there are in reality.

#### IV. NUMERICAL RESULTS

The propagation model takes into account the large-scale attenuation with path loss exponent  $\alpha = 2$ , as well as the small-scale fading. To take into account a wider range of fading environments, the channels are assumed to follow Rician fading with parameter  $K = 100$ , where  $K$  is the ratio between the direct path received power and other, scattered, paths. The parameter  $K$  can be determined according to the type of constellation, i.e., higher  $K$  values are suitable when the serving satellite is likely high above the user. As a result, the corresponding channel gains,  $G_n$ , (being the square of the Rice random variable) have a noncentral chi-squared distribution,  $\chi^2$ , with two degrees of freedom and non-centrality parameter  $2K$ . Therefore, the CDF and PDF in Propositions 1 and 2 are

$$F_{G_0}(g_0) = 1 - Q_1(\sqrt{2K}, \sqrt{g_0}), \quad (23)$$

$$f_{G_0}(g_0) = \frac{1}{2} e^{-\frac{g_0 + 2K}{2}} I_0(\sqrt{2Kg_0}), \quad (24)$$

respectively, where  $Q_1(\cdot, \cdot)$  denotes the Marcum Q-function and  $I_0(\cdot)$  is the modified Bessel function of the first kind. For producing the numerical results, the transmitted and noise power are set to  $p_s = 10$  W and  $\sigma^2 = -93$  dBm, respectively. The simulation parameters are summarized in Table I.

For numerical verification, we compute the coverage probability and data rate of an actual LEO constellation through Monte Carlo simulations in Matlab to compare them with analytical results presented in this paper. Figure 2 verifies the coverage expression given in Proposition 1, considering

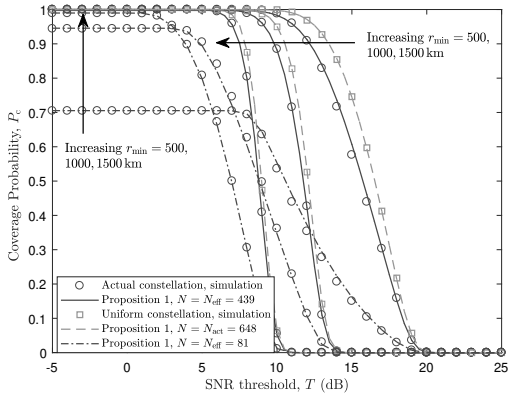


Fig. 2. Verification of Proposition 1 with simulations when  $K = 100$ ,  $\phi_u = 0^\circ$ ,  $\iota = 70^\circ$ ,  $r_{\min} \in \{500, 1000, 1500\}$  km, and  $\theta_{\min} = 10^\circ$ .

different altitudes for  $N_{\text{act}} = 648$  and  $120$ . As shown in this figure, there is a slight deviation between the actual constellation described in Section II and uniform constellation performance due to the non-uniform distribution of satellites along different latitudes in the real constellation. Substituting  $N = N_{\text{eff}} = 439$  and  $81$  in Proposition 1 which corresponds to  $N_{\text{act}} = 648$  and  $120$ , respectively, we can eliminate the mismatch in the coverage.

For a fewer number of satellites, e.g.,  $N_{\text{act}} = 120$ , it can be well observed from Fig. 2 that the upper bound for coverage probability, given in Corollary 1, is limited by the probability of observing at least one satellite above the sky. As a result, the upper bound is enhanced with rising the altitude due to the increase in the visibility probability given in (11). On the other hand, for larger number of satellites, e.g.,  $N_{\text{act}} = 648$ , the performance is affected only by the path loss since the visibility probability approaches one. Verification of data rate in Proposition 2 is shown in Fig. 3 for different minimum elevation angles. The same as for Fig. 2, the mismatch between uniform and actual constellation is omitted by setting  $N = N_{\text{eff}} = 439$ .

Coverage probability versus the total number of satellites for different inclination and minimum required elevation angles is depicted in Fig. 4. For plotting this figure, we applied  $N = N_{\text{eff}}$  in Proposition 1 in order to compensate for the uneven distribution of satellites along different latitudes. The coverage probability declines with  $\theta_{\min}$  as the visibility to the user decreases. However, this effect becomes less dominant as the number of satellites increases since the serving satellite, most probably, will be located above the user. Moreover, within the depicted range, the smaller inclination angles result in superior performance due to the larger density of satellites and, consequently, the existence of a stronger serving channel.

There is an optimum altitude for every constellation, as shown in Fig. 5, which results in maximum coverage probability. The optimum point increases with rising the minimum

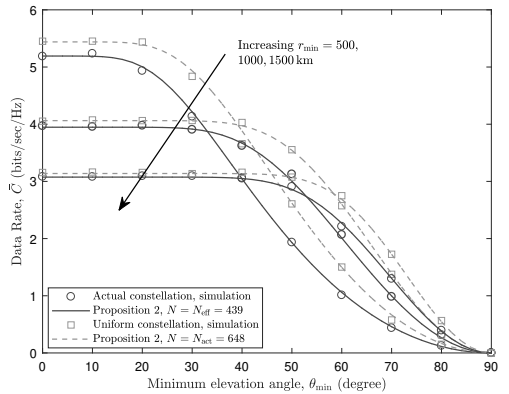


Fig. 3. Verification of Proposition 2 with simulations when  $K = 100$ ,  $\phi_u = 0^\circ$ ,  $\iota = 70^\circ$ , and  $r_{\min} \in \{500, 1000, 1500\}$  km.

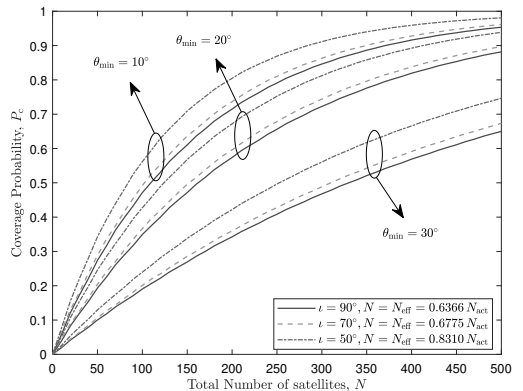


Fig. 4. Coverage probability for different constellation sizes when  $K = 100$ ,  $\phi_u = 0^\circ$ ,  $T = 10$  dB, and  $r_{\min} = 500$  km.

elevation angle while the maximum achieved coverage decreases accordingly. The initial increase in the plot is due to the enhancement in the line-of-sight probability of the serving satellite while it is followed by a decline caused by more severe path loss in higher altitudes.

Above results are repeated in terms of data rate in Figs. 6 and 7 w.r.t. the total number of satellites and satellite altitude, respectively, using Proposition 2 with  $N = N_{\text{eff}}$ . The same as for Fig. 4, lower inclination will result in higher data rates in Fig. 6. However, the impact of both inclination and minimum elevation angle on data rate reduces with increasing the total number of satellites. The same observations as for Fig. 5 can be also seen in Fig. 7, except for the optimum altitude differs for maximum coverage probability and data rate.

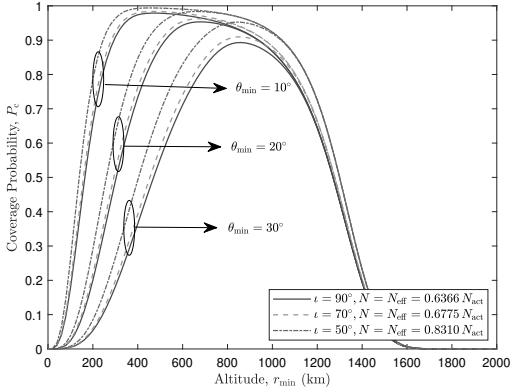


Fig. 5. Coverage probability for different altitudes when  $K = 100$ ,  $\phi_u = 0^\circ$ ,  $T = 10$  dB, and  $N_{act} = 648$ .

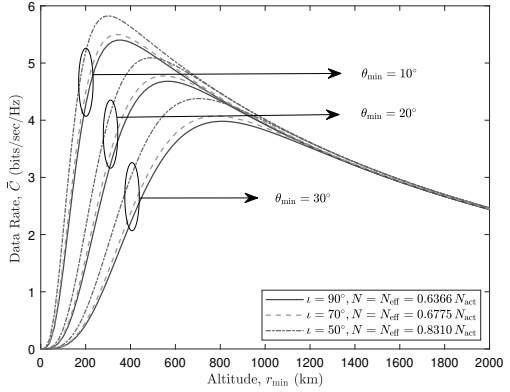


Fig. 7. Data rate for different altitudes when  $K = 100$ ,  $\phi_u = 0^\circ$ , and  $N_{act} = 648$ .

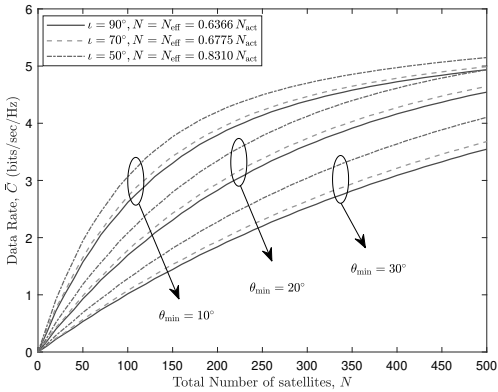


Fig. 6. Data rate for different constellation sizes when  $K = 100$ ,  $\phi_u = 0^\circ$ , and  $r_{min} = 500$  km.

## V. CONCLUSIONS

In this paper, we presented a tractable approach for uplink and downlink coverage and rate analysis of low Earth orbit satellite networks. The satellite network is, first, modeled with a uniform distribution which was then applied to obtain exact expressions for coverage probability and data rate of an arbitrary user in terms of network parameters. The slight deviation between the performance metrics of the uniform and actual constellations was compensated by derivation of a new parameter—effective number of satellites—to take into account the effect of uneven satellite distribution along different latitudes. The proposed framework in this paper paves the way for accurate analysis, optimization and design of the future dense satellite networks.

## REFERENCES

- [1] J. L. Grubb, "The traveler's dream come true," *IEEE Communications Magazine*, vol. 29, no. 11, pp. 48–51, Nov. 1991.
- [2] A. Mokhtar and M. Azizoglu, "On the downlink throughput of a broadband LEO satellite network with hopping beams," *IEEE Communications Letters*, vol. 4, no. 12, pp. 390–393, Dec. 2000.
- [3] F. Vatalaro, G. E. Corazza, C. Caini, and C. Ferrarelli, "Analysis of LEO, MEO, and GEO global mobile satellite systems in the presence of interference and fading," *IEEE Journal on Selected Areas in Communications*, vol. 13, no. 2, pp. 291–300, Feb. 1995.
- [4] A. Ganz, Y. Gong, and B. Li, "Performance study of low Earth-orbit satellite systems," *IEEE Transactions on Communications*, vol. 42, no. 234, pp. 1866–1871, Feb. 1994.
- [5] H. M. Mourad, A. A. M. Al-Bassiouni, S. S. Emam, and E. K. Al-Hussaini, "Generalized performance evaluation of low Earth orbit satellite systems," *IEEE Communications Letters*, vol. 5, no. 10, pp. 405–407, Oct. 2001.
- [6] I. Ali, N. Al-Dhahir, and J. E. Hershey, "Predicting the visibility of LEO satellites," *IEEE Transactions on Aerospace and Electronic Systems*, vol. 35, no. 4, pp. 1183–1190, Oct. 1999.
- [7] Y. Seyedi and S. M. Safavi, "On the analysis of random coverage time in mobile LEO satellite communications," *IEEE Communications Letters*, vol. 16, no. 5, pp. 612–615, May 2012.
- [8] T. A. Khan and M. Afshang, "A stochastic geometry approach to Doppler characterization in a LEO satellite network," in *IEEE International Conference on Communications (ICC)*, 2020, available online: <https://arxiv.org/abs/2005.03205v1>.
- [9] J. Hu, G. Li, D. Bian, L. Gou, and C. Wang, "Optimal power control for cognitive LEO constellation with terrestrial networks," *IEEE Communications Letters*, vol. 24, no. 3, pp. 622–625, Mar. 2020.
- [10] J. Zhang, B. Evans, M. A. Imran, X. Zhang, and W. Wang, "Performance analysis of C/U split hybrid satellite terrestrial network for 5G systems," in *20th IEEE International Workshop on Computer Aided Modelling and Design of Communication Links and Networks (CAMAD)*, Sep. 2015.
- [11] A. J. Roumeliotis, C. I. Kourgiorgas, and A. D. Panagopoulos, "Optimal dynamic capacity allocation for high throughput satellite communications systems," *IEEE Wireless Communications Letters*, vol. 8, no. 2, pp. 596–599, Apr. 2019.
- [12] N. Okati, T. Riihonen, D. Korpi, I. Angervo, and R. Wichman, "Downlink coverage and rate analysis of low Earth orbit satellite constellations using stochastic geometry," *IEEE Transactions on Communications*, 2020, in press.
- [13] S.-Y. Li and C. H. Liu, "An analytical model to predict the probability density function of elevation angles for LEO satellite systems," *IEEE Communications Letters*, vol. 6, no. 4, pp. 138–140, Apr. 2002.

## **PUBLICATION 3**

**Modeling and Analysis of LEO Mega-Constellations as Nonhomogeneous  
Poisson Point Processes**

**N. Okati and T. Riihonen**

*In Proc. IEEE 93rd Vehicular Technology Conference (VTC), Apr. 2021*

**Publication reprinted with the permission of the copyright holders.**



# Modeling and Analysis of LEO Mega-Constellations as Nonhomogeneous Poisson Point Processes

Niloofer Okati and Taneli Riihonen

Faculty of Information Technology and Communication Sciences, Tampere University, Finland  
e-mail: {niloofer.okati, taneli.riihonen}@tuni.fi

**Abstract**—Requirements and technological advancements towards 6th generation (6G) wireless networks lead to enabling and development of massive low Earth orbit (LEO) satellite constellations to provide ubiquitous and high-capacity connectivity, particularly for maritime and airborne platforms. Consequently, new methodologies to study the performance of LEO networks are of great importance. In this paper, we derive both downlink and uplink analytical expressions for coverage probability and data rate of a massive inclined LEO constellation under general shadowing and fading. We model the LEO satellite network as a nonhomogeneous Poisson point process with general intensity in order to take into account uneven distribution of satellites along the latitudes. The results provided in this study facilitate the stochastic evaluation and design of the future massive LEO networks, regardless of satellites’ exact trajectories in orbits.

## I. INTRODUCTION

As 5th generation (5G) cellular networks are becoming fully commercial all around the globe, characterizing 6G challenges and requirements has recently attracted significant attention [1]–[3]. Providing ubiquitous and high-capacity connectivity, as promised in 6G, requires enabling and development of non-terrestrial networks. Among non-terrestrial networks low Earth orbit (LEO) satellite systems have gained increasing popularity due to providing seamless connectivity with lower round-trip delay—compared to geostationary satellites—especially for remote regions where the deployment of terrestrial networks is not economically reasonable [4], [5].

Despite the commercial promotion of massive LEO networks (e.g., Starlink, Kuiper, Telesat), there are still many unanswered questions regarding the performance and design of these networks. Literature around LEO systems’ analysis is mostly limited to the analysis of few satellites with deterministic locations and coverage areas. The uplink outage probability in the presence of interference was evaluated for two LEO constellations through time-domain simulations in [6]. The effect of traffic non-uniformity was studied in [7] by assuming hexagonal service areas for satellites.

A general expression for a single LEO satellite’s visibility time was provided in [8], but it is incapable of concluding the general distribution of visibility periods for any arbitrarily positioned user. The deterministic model in [8] was then developed via statistical analysis of coverage time in mobile LEO during a satellite visit [9]. In [10], the Doppler shift magnitude of a LEO network is characterized for a single spotbeam by using tools from stochastic geometry. Resource control of a hybrid satellite–terrestrial network was performed

in [11] with two objectives of maximizing the delay-limited capacity and minimizing the outage probability. A hybrid satellite–terrestrial network to assist 5G infrastructure has been analyzed by considering only one spotbeam [12], [13]. In [14], the outage probability of a satellite-based IoT network, in which the LEO satellites relay the data to the ground stations, is derived in closed form by assuming a low number of satellites at the known locations.

Only recently, more research based on stochastic geometry of LEO networks has started emerging. In our seminal study [15], generic performance of satellite networking without resorting to explicit orbit simulations and the actual geometry of any specific constellation has been formulated by assuming uniform distribution for satellites. Due to the fact that satellites in practical constellations are distributed unevenly along different latitudes [16], i.e., the number of satellites on the inclination limits is greater than on equatorial regions, the density of practical deterministic constellations is typically not uniform. In [15], [16], we compensated for this mismatch by derivation of a new parameter called effective number of satellites. In [17], stochastic geometry is utilized to derive the coverage probability of a LEO network, where satellite gateways act as relays between the satellites and users. Unlike in [15], the satellites are assumed to be placed at different altitudes. The uplink communication scenario is characterized by considering interfering terrestrial transmitters in [18].

In this paper, downlink and uplink coverage probability and data rate of inclined LEO constellations are analyzed under a general shadowing and fading propagation model. Unlike in [15]–[17], the satellites’ positions are assumed to be distributed as a nonhomogeneous Poisson point process (NPPP), which models the actual distribution of satellites along different latitudes more precisely by selecting the proper intensity. Finally, the mathematical expressions are verified through simulations and the main findings of this paper are demonstrated for different network parameters, e.g., altitude, inclination angle, user’s latitude, and minimum elevation angle required for a satellite to be visible to the user.

The organization of the remainder of this paper is as follows. Section II describes the system model as well as the mathematical preliminaries for modeling a LEO network as an NPPP. Performance analysis of a LEO network in terms of coverage probability and average data rate is provided in Section III. This is followed by the numerical results in Section IV. Finally, the paper is concluded in Section V.

## II. SYSTEM MODEL

The studied network model in this paper is a massive LEO communication satellite constellation, as shown in Fig. 1, that consists of  $N$  satellites distributed uniformly on low circular orbits with inclination angle,  $\iota$ , and altitude denoted by  $r_{\min}$ . The altitude parameter  $r_{\min}$  has the peculiar subscript because it specifies also the minimum possible distance between a satellite and a user on Earth (that is realized when it is at the zenith). The satellites' coordinates in terms of their latitude and longitude are denoted by  $(\phi_s, \lambda_s)$ .

User terminals are located on a specific latitude, denoted by  $\phi_u$ , on the surface of Earth with radius  $r_{\oplus} \approx 6371$  km. The wireless transmissions propagate to/from a user from/to all and only the satellites that are elevated above the horizon to an angle of  $\theta_s \geq \theta_{\min}$ . Smaller values for  $\theta_{\min}$  result in a more drastic path loss due to the greater distance between a user and a satellite. Correspondingly,  $r_{\max}$  denotes the maximum possible distance at which a satellite and a user may be able to communicate without terrain blockage (that is realized when  $\theta_s = \theta_{\min}$ ):

$$\frac{r_{\max}}{r_{\oplus}} = \sqrt{\frac{r_{\min}}{r_{\oplus}} \left( \frac{r_{\min}}{r_{\oplus}} + 2 \right) + \sin^2(\theta_{\min})} - \sin(\theta_{\min}). \quad (1)$$

We assume an association policy where the user communicates with its nearest satellite that is referred to as the serving satellite in what follows. The network performance can be considered as noise-limited due to implementing resource scheduling and co-channel interference mitigation properly. The distances from the user to the serving satellite and the other satellites are denoted by  $r_0$  and  $r_n$ ,  $n = 1, 2, \dots, N-1$ , respectively, while  $G_0$  and  $G_n$  represent the corresponding channel gains. Shadowing effect is modeled by the random variable  $\mathcal{X}_n$ , where  $n = 0, 1, \dots, N-1$ . Obviously,  $\mathcal{X}_n = G_n = 0$  if  $r_n > r_{\max}$  for some  $n = 0, 1, \dots, N-1$ .

Based on the described system model, the signal-to-noise ratio (SNR) at the receiver can be expressed as

$$\text{SNR} = \begin{cases} \frac{p_s G_0 \mathcal{X}_0 r_0^{-\alpha}}{\sigma^2}, & r_0 \leq r_{\max}, \\ 0, & \text{otherwise,} \end{cases} \quad (2)$$

where  $p_s$  is the transmission power of the serving satellite. We assume that the user's receiver is subject to additive white Gaussian noise with constant power  $\sigma^2$ , and the parameter  $\alpha$  is a path loss exponent.

In the satellite constellation described earlier, the satellites are distributed unevenly along different latitudes which means that there are more visible satellites for a user located close to inclination limits than for a user on equatorial region. In order to model the latitude-dependent distribution of satellites, we assume that  $N$  satellites are distributed according to an NPPP,  $\xi$ , on a sphere with radius  $r_{\oplus} + r_{\min}$ . The void probability on some bounded surface area  $\mathcal{A}$  on the sphere is given by

$$\begin{aligned} \mathbb{P}(\xi(\mathcal{A}) = 0) & \\ &= \exp\left(-\iint_{\mathcal{A}} \delta(\phi_s, \lambda_s) (r_{\min} + r_{\oplus})^2 \cos(\phi_s) d\phi_s d\lambda_s\right), \end{aligned} \quad (3)$$

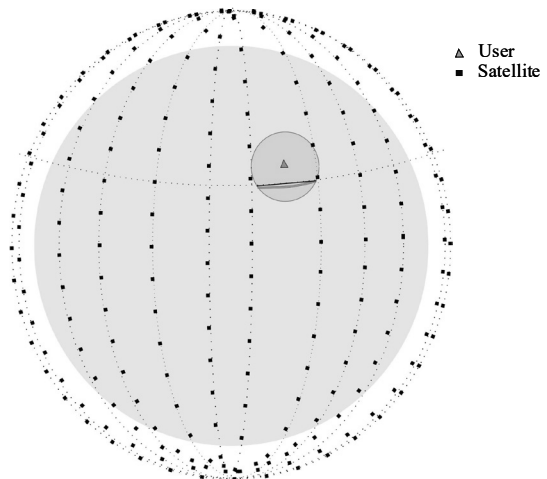


Fig. 1. System model for  $N$  satellites distributed uniformly over inclined orbits (polar orbits with  $\iota = 90^\circ$  inclination in this example).

where  $\delta(\phi_s, \lambda_s)$  is the intensity function of the NPPP at latitude  $\phi_s$  and longitude  $\lambda_s$ .

**Lemma 1.** *When satellites are distributed uniformly on low circular orbits with the same inclination angle,  $\iota$ , and altitude,  $r_{\min}$ , the intensity function of the NPPP is given by*

$$\delta(\phi_s) = \frac{N}{\sqrt{2\pi^2}(r_{\min} + r_{\oplus})^2} \cdot \frac{1}{\sqrt{\cos(2\phi_s) - \cos(2\iota)}}, \quad (4)$$

and we can denote  $\delta(\phi_s, \lambda_s) = \delta(\phi_s)$  since it does not depend on  $\lambda_s$ , for  $\phi_s \in [-\iota, \iota]$ .

*Proof.* For any longitude  $\lambda_s$ , the intensity function is equivalent to the actual density of the satellites on a sphere surface element at latitude  $\phi_s$  that can be written as

$$\delta(\phi_s) = \frac{N f_{\Phi_s}(\phi_s) d\phi_s}{2\pi(r_{\min} + r_{\oplus})^2 \cos(\phi_s) d\phi_s}, \quad (5)$$

where the nominator and denominator represent the number of satellites resided in the surface element and its surface area, respectively. Substituting the probability density  $f_{\Phi_s}(\phi_s)$  of random latitude  $\Phi_s$  [16, Lemma 2] completes the proof.  $\square$

## III. PERFORMANCE ANALYSIS

In order to contribute expressions for coverage probability and average achievable rate, we model the satellite network as a nonhomogeneous Poisson point process with intensity given in Lemma 1. Towards this, we need first to characterize some basic distance distributions that stem from the geometry of the considered system model.

### A. Distance to the Serving Satellite

We express the probability density function (PDF) of the distance to the nearest satellite in the following lemma. The



functions are required for the derivation of the studied performance metrics in the following subsections.

**Lemma 2.** *The PDF of the random serving distance  $R_0$  when the satellites are distributed according to a nonhomogeneous PPP with intensity  $\delta(\phi_s, \lambda_s)$ , is given by*

$$f_{R_0}(r_0) = 2r_0 \left( \frac{r_{\min}}{r_{\oplus}} + 1 \right) \int_{\max(\phi_u - \theta_0, -\iota)}^{\min(\phi_u + \theta_0, \iota)} \delta(\phi_s) \cos(\phi_s) \frac{1}{\sqrt{\cos^2(\phi_s - \phi_u) - \cos^2(\theta_0)}} d\phi_s \times \exp \left( -2(r_{\min} + r_{\oplus})^2 \int_{\max(\phi_u - \theta_0, -\iota)}^{\min(\phi_u + \theta_0, \iota)} \delta(\phi_s) \cos(\phi_s) \times \cos^{-1} \left( \frac{\cos(\theta_0)}{\cos(\phi_s - \phi_u)} \right) d\phi_s \right) \quad (6)$$

for  $r_0 \in [r_{\min}, 2r_{\oplus} + r_{\min}]$  while  $f_{R_0}(r_0) = 0$  otherwise. The polar angle difference between the serving satellite and the user is  $\theta_0 = \cos^{-1} \left( 1 - \frac{r_0^2 - r_{\min}^2}{2(r_{\min} + r_{\oplus})r_{\oplus}} \right)$ .

*Proof.* For a nonhomogeneous PPP, the CDF of  $R_0$  can be written as

$$F_{R_0}(r_0) = 1 - \mathbb{P}(R_0 > r_0) = 1 - \mathbb{P}(\xi(\mathcal{A}) = 0) \quad (7)$$

where  $\mathbb{P}(\xi(\mathcal{A}) = 0)$  is the void probability of PPP given in (3) and  $\mathcal{A}$  is the shaded cap above the user shown in Fig. 1. According to (3), by integrating from the intensity over the spherical cap above the user, we have

$$F_{R_0}(r_0) = 1 - \exp \left( - \int_{\max(\phi_u - \theta_0, -\iota)}^{\min(\phi_u + \theta_0, \iota)} \beta(\phi_s) \delta(\phi_s) (r_{\min} + r_{\oplus})^2 \cos(\phi_s) d\phi_s \right) \stackrel{(a)}{=} 1 - \exp \left( -2(r_{\min} + r_{\oplus})^2 \int_{\max(\phi_u - \theta_0, -\iota)}^{\min(\phi_u + \theta_0, \iota)} \delta(\phi_s) \cos(\phi_s) \times \cos^{-1} \left( \frac{\cos(\theta_0)}{\cos(\phi_s - \phi_u)} \right) d\phi_s \right), \quad (8)$$

where  $\beta(\phi_s)$  is the longitude range of the red surface element in Fig. 1 and (a) follows from substitution of  $\beta(\phi_s)$  using the basic geometry. Taking the derivative of (8) with respect to  $r_0$  completes the proof of Lemma 2.  $\square$

**Lemma 3.** *The PDF of the serving distance  $R_0$  when the satellites are distributed uniformly with constant intensity  $\delta = \frac{N}{4\pi(r_{\min} + r_{\oplus})^2}$ , is given by*

$$f_{R_0}(r_0) = \frac{Nr_0}{2r_{\oplus}(r_{\min} + r_{\oplus})} \exp \left( -N \left( \frac{r_0^2 - r_{\min}^2}{4r_{\oplus}(r_{\min} + r_{\oplus})} \right) \right) \quad (9)$$

for  $r_0 \in [r_{\min}, 2r_{\oplus} + r_{\min}]$  while  $f_{R_0}(r_0) = 0$  otherwise.

*Proof.* The proof follows the same principles as the proof of Lemma 2. However, the integration from a constant density over the cap will reduce to a simple expression. Thus,  $F_{R_0}(r_0) = 1 - \exp \left( -N \left( \frac{r_0^2 - r_{\min}^2}{4r_{\oplus}(r_{\min} + r_{\oplus})} \right) \right)$ . Taking the derivative of the CDF with respect to  $r_0$  completes the proof.  $\square$

## B. Coverage Probability and Average Data Rate

The following performance analysis in terms of coverage probability and average data rate holds for both downlink and uplink communication directions. Furthermore, it is presented under general shadowing and fading distributions so that any specific scenario can be covered by appropriate choice of  $f_{\mathcal{X}_0}(x_0)$  and  $F_{G_0}(g_0)$ , respectively, e.g., Rician fading with lognormal shadowing in our numerical results.

Let us first derive the coverage probability of the LEO satellite network for a user in an arbitrary location on Earth. The performance measure of coverage probability is defined as the probability of having at least the minimum SNR required for successful data transmission. Thus, the coverage probability is defined as

$$P_c(T) \triangleq \mathbb{P}(\text{SNR} > T) = \mathbb{P} \left( \frac{p_s G_0 R_0^{-\alpha}}{\sigma^2} > T \right), \quad (10)$$

where  $\sigma^2$  is additive noise with constant power, and  $\alpha$  represents exponent of path loss.

**Proposition 1.** *The probability of coverage for an arbitrarily located user under general shadowing and fading is*

$$P_c(T) \triangleq \mathbb{P}(\text{SNR} > T) = \int_{r_{\min}}^{r_{\max}} \int_0^{\infty} f_{\mathcal{X}_0}(x_0) f_{R_0}(r_0) \left( 1 - F_{G_0} \left( \frac{Tr_0^{\alpha} \sigma^2}{p_s x_0} \right) \right) dx_0 dr_0, \quad (11)$$

where  $f_{R_0}(r_0)$  is given in Lemma 2 or Lemma 3 and  $f_{\mathcal{X}_0}(x_0)$  is the PDF of  $\mathcal{X}_0$ .

*Proof.* To obtain (11),  $\delta$  from the definition of coverage probability:

$$P_c(T) = \mathbb{E}_{R_0} [\mathbb{P}(\text{SNR} > T | R_0)] = \int_{r_{\min}}^{r_{\max}} \mathbb{P}(\text{SNR} > T | R_0 = r_0) f_{R_0}(r_0) dr_0 = \int_{r_{\min}}^{r_{\max}} \mathbb{P} \left( G_0 \mathcal{X}_0 > \frac{Tr_0^{\alpha} \sigma^2}{p_s} \right) f_{R_0}(r_0) dr_0. \quad (12)$$

The upper limit for the integral is due to the fact that the satellites with smaller than  $\theta_{\min}$  elevation angle have no visibility to the user. The proof is completed by substitution of the product distribution of two independent random variables in (12).  $\square$

The average achievable data rate (in bit/s/Hz) of an arbitrary user over generalized fading channels and shadowing can be derived in the following proposition.

**Proposition 2.** *The average rate (in bits/s/Hz) of an arbitrarily located user and its serving satellite under general shadowing and fading assumption is*

$$\bar{C} \triangleq \mathbb{E} [\log_2(1 + \text{SNR})] = \frac{1}{\ln(2)} \int_{r_{\min}}^{r_{\max}} \int_0^{\infty} \int_0^{\infty} f_{\mathcal{X}_0}(x_0) \left( 1 - F_{G_0} \left( \frac{r_0^{\alpha} \sigma^2}{p_s} (e^t - 1) \right) \right) \times f_{R_0}(r_0) dx_0 dt dr_0. \quad (13)$$

TABLE I  
SIMULATION PARAMETERS

Parameters	Values
Path loss exponent, $\alpha$	2
Rician factor, $K$	100
Transmission power, $p_s$ (W)	10
Noise power, $\sigma^2$ (dBm)	-103
User's latitude, $\phi_u$ (degrees)	61.5
Mean and standard deviation of lognormal distribution: $\mu_s$ (dB), $\sigma_s$ (dB)	0, 9

*Proof.* Taking the expectation over serving distance and channel gain, we have

$$\begin{aligned}
 \bar{C} &= \mathbb{E}_{G_0, \mathcal{X}_0, R_0} [\log_2(1 + \text{SNR})] \\
 &= \frac{1}{\ln(2)} \int_{r_{\min}}^{r_{\max}} \mathbb{E} \left[ \ln \left( 1 + \frac{p_s G_0 \mathcal{X}_0 r_0^{-\alpha}}{\sigma^2} \right) \right] f_{R_0}(r_0) dr_0 \\
 &\stackrel{(a)}{=} \frac{1}{\ln(2)} \int_{r_{\min}}^{r_{\max}} \int_0^{\infty} \mathbb{P} \left[ \ln \left( 1 + \frac{p_s G_0 \mathcal{X}_0 r_0^{-\alpha}}{\sigma^2} \right) > t \right] f_{R_0}(r_0) dt dr_0 \\
 &= \frac{1}{\ln(2)} \int_{r_{\min}}^{r_{\max}} \int_0^{\infty} \mathbb{P} \left[ G_0 \mathcal{X}_0 > \frac{r_0^\alpha \sigma^2}{p_s} (e^t - 1) \right] f_{R_0}(r_0) dt dr_0,
 \end{aligned} \tag{14}$$

where (a) follows from the fact that for a positive random variable  $X$ ,  $\mathbb{E}[X] = \int_{t>0} \mathbb{P}(X > t) dt$ .  $\square$

#### IV. NUMERICAL RESULTS

In this section, we corroborate our analytical findings through Monte Carlo simulations. The propagation model takes into account the large-scale attenuation with path loss exponent  $\alpha = 2$ , the small-scale Rician fading with parameter  $K = 100$ , and lognormal shadowing. As a result, the corresponding channel gains,  $G_n$ , (being the square of the Rice random variable) have a noncentral chi-squared distribution,  $\chi^2$ , with two degrees of freedom and non-centrality parameter  $2K$ . Therefore, the CDF in Propositions 1 and 2 is  $F_{G_0}(g_0) = 1 - Q_1(\sqrt{2K}, \sqrt{g_0})$ , where  $Q_1(\cdot, \cdot)$  denotes the Marcum Q-function. The lognormal shadowing is represented as  $\mathcal{X}_0 = 10^{X_0/10}$  such that  $X_0 \sim \mathcal{N}(\mu_s, \sigma_s)$ , where  $\mathcal{N}$  is a normal distribution with  $\mu_s$  and  $\sigma_s$  being its mean and standard deviation in decibels. Thus, the PDF of lognormal shadowing is  $f_{\mathcal{X}_0}(x_0) = \frac{10}{\ln(10)\sqrt{2\pi}\sigma_s x_0} \exp\left(-\frac{1}{2}\left(\frac{10 \log_{10}(x_0) - \mu_s}{\sigma_s}\right)^2\right)$ . The simulation parameters are given in Table I.

Figure 2 verifies the coverage expression given in Proposition 1, considering different altitudes for  $N = 648$  and  $\iota = 90^\circ$ . The user is assumed to be at Tampere, Finland ( $\phi_u = 61.5^\circ$ ). As shown in Fig. 2, the simulation results (markers) are perfectly matched with the analytical expression (lines) given in Proposition 1. With increasing the altitude, coverage decreases accordingly due to more drastic path loss for larger distances. The effect of shadowing on coverage probability is ambiguous. As it is shown in the figure, as the chance of the user being in outage increases, shadowing affects the coverage probability more positively, the reason being that shadowing randomness increases the chance of a user with poor SNR to be in coverage. It can be also interpreted that

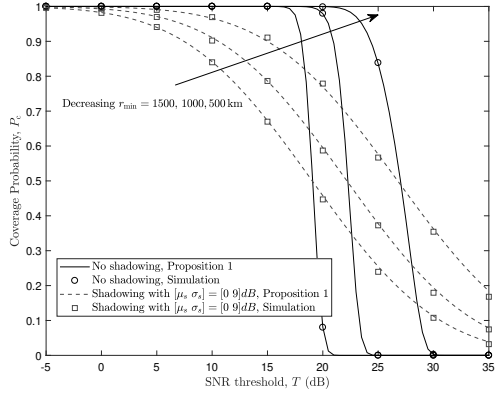


Fig. 2. Verification of Proposition 1 with simulations when  $K = 100$ ,  $\iota = 90^\circ$ ,  $r_{\min} \in \{500, 1000, 1500\}$  km,  $\phi_u = 61.5^\circ$ , and  $\theta_{\min} = 10^\circ$ .

user association techniques based on maximum received signal are able to considerably improve the coverage probability.

Validation of data rate given by Proposition 2 is shown in Fig. 3 for different minimum elevation angles. The data rate decreases with increasing the minimum elevation angle due to a reduction in the chance of satellite visibility to the user. For smaller values of  $\theta_{\min}$ , the data rate increases by decreasing the altitude due to the reduction in path loss. However, as  $\theta_{\min}$  increases, the higher altitudes result in a higher data rate since the visibility probability increases by rising the altitude.

Coverage probability and data rate versus altitude for different users' latitudes, satellites' inclination angles, and minimum required elevation angles are depicted in Figs. 4 and 5, respectively. Starting from very low altitudes, coverage probability and data rate improve with increasing the altitude since a better chance of line-of-sight is attained for the serving satellite which is then followed by a decline caused by more severe path loss in higher altitudes. In both plots, the optimum altitude increases with rising the minimum elevation angle while the maximum achieved coverage and rate decrease accordingly. Moreover, smaller inclination angles result in a superior performance due to the higher density of satellites and, therefore, the existence of a stronger serving channel.

#### V. CONCLUSIONS

In this paper, we studied the performance of low Earth orbit satellite networks in a more generic form comparing with the existing literature on this topic. The satellite network is modeled as a nonhomogeneous Poisson point process which models the uneven distribution of satellites along different latitudes with its intensity being a function of satellites' actual distributions. Utilizing such a model for satellites' locations facilitates derivation of the coverage probability and data rate of an arbitrary user under general fading and shadowing. The proposed analysis paves the way for a more reliable integration of the LEO networks and the existing cellular network in 6G.

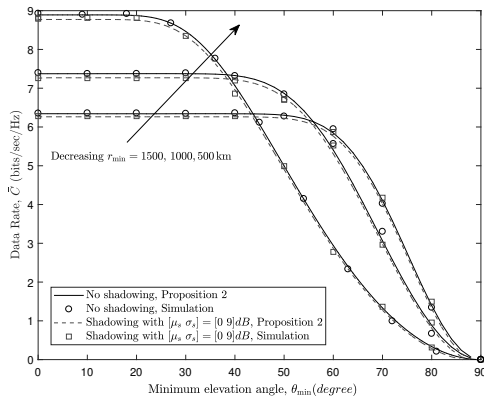


Fig. 3. Verification of Proposition 2 with simulations when  $K = 100$ ,  $\iota = 90^\circ$ ,  $r_{\min} \in \{500, 1000, 1500\}$  km,  $\phi_u = 61.5^\circ$ , and  $\theta_{\min} = 10^\circ$ .

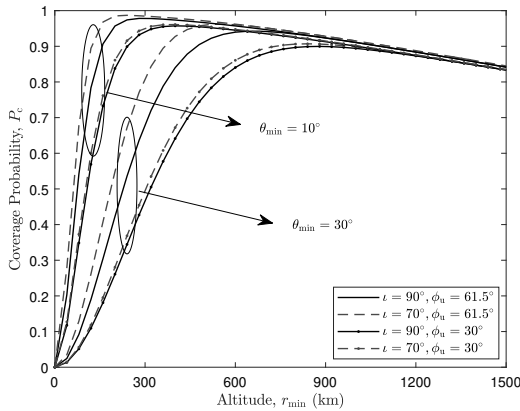


Fig. 4. Coverage probability for different altitudes when  $K = 100$ ,  $T = 10$  dB, and  $\iota = \{90^\circ, 70^\circ\}$ .

#### ACKNOWLEDGMENT

This research work was supported by a Nokia University Donation.

#### REFERENCES

- [1] M. Giordani and M. Zorzi, "Non-terrestrial communication in the 6G era: Challenges and opportunities," available online: <https://arxiv.org/abs/1912.10226v2>, 2019.
- [2] Z. Jia, M. Sheng, J. Li, D. Zhou, and Z. Han, "Joint HAP access and LEO satellite backhaul in 6G: Matching game based approaches," *IEEE Journal on Selected Areas in Communications*, Aug. 2020.
- [3] M. Giordani, M. Polese, M. Mezzavilla, S. Rangan, and M. Zorzi, "Toward 6G networks: Use cases and technologies," *IEEE Communications Magazine*, vol. 58, no. 3, pp. 55–61, Mar. 2020.
- [4] J. L. Grubb, "The traveler's dream come true," *IEEE Communications Magazine*, vol. 29, no. 11, pp. 48–51, Nov. 1991.
- [5] A. Mokhtar and M. Azizoglu, "On the downlink throughput of a broadband LEO satellite network with hopping beams," *IEEE Communications Letters*, vol. 4, no. 12, pp. 390–393, Dec. 2000.

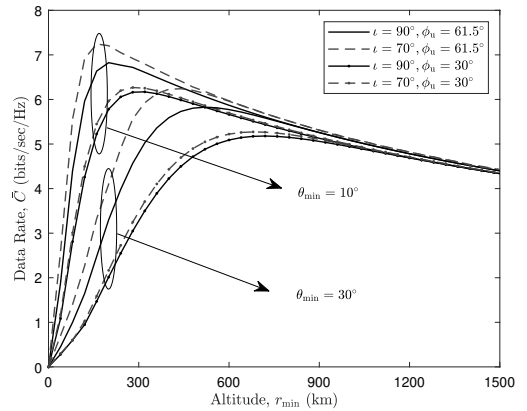


Fig. 5. Data rate for different altitudes when  $K = 100$  and  $\iota = \{90^\circ, 70^\circ\}$ .

- [6] F. Vatalaro, G. E. Corazza, C. Caini, and C. Ferrarelli, "Analysis of LEO, MEO, and GEO global mobile satellite systems in the presence of interference and fading," *IEEE Journal on Selected Areas in Communications*, vol. 13, no. 2, pp. 291–300, Feb. 1995.
- [7] H. M. Mourad, A. A. M. Al-Bassiouni, S. S. Emam, and E. K. Al-Hussaini, "Generalized performance evaluation of low Earth orbit satellite systems," *IEEE Communications Letters*, vol. 5, no. 10, pp. 405–407, Oct. 2001.
- [8] I. Ali, N. Al-Dhahir, and J. E. Hershey, "Predicting the visibility of LEO satellites," *IEEE Transactions on Aerospace and Electronic Systems*, vol. 35, no. 4, pp. 1183–1190, Oct. 1999.
- [9] Y. Seyedi and S. M. Safavi, "On the analysis of random coverage time in mobile LEO satellite communications," *IEEE Communications Letters*, vol. 16, no. 5, pp. 612–615, May 2012.
- [10] T. A. Khan and M. Afshang, "A stochastic geometry approach to Doppler characterization in a LEO satellite network," in *IEEE International Conference on Communications (ICC)*, Jun. 2020.
- [11] J. Hu, G. Li, D. Bian, L. Gou, and C. Wang, "Optimal power control for cognitive LEO constellation with terrestrial networks," *IEEE Communications Letters*, vol. 24, no. 3, pp. 622–625, Mar. 2020.
- [12] J. Zhang, B. Evans, M. A. Imran, X. Zhang, and W. Wang, "Performance analysis of C/U split hybrid satellite terrestrial network for 5G systems," in *20th IEEE International Workshop on Computer Aided Modelling and Design of Communication Links and Networks (CAMAD)*, Sep. 2015.
- [13] A. J. Roumeliotis, C. I. Kourgiorgas, and A. D. Panagopoulos, "Optimal dynamic capacity allocation for high throughput satellite communications systems," *IEEE Wireless Communications Letters*, vol. 8, no. 2, pp. 596–599, Apr. 2019.
- [14] A. K. Dwivedi, S. P. Chokkarapu, S. Chaudhari, and N. Varshney, "Performance analysis of novel direct access schemes for LEO satellites based IoT network," in *Proc. IEEE 31st Annual International Symposium on Personal, Indoor and Mobile Radio Communications*, Sep. 2020.
- [15] N. Okati, T. Riihonen, D. Korpi, I. Angervuori, and R. Wichman, "Downlink coverage and rate analysis of low Earth orbit satellite constellations using stochastic geometry," *IEEE Transactions on Communications*, vol. 68, no. 8, pp. 5120–5134, Aug. 2020.
- [16] N. Okati and T. Riihonen, "Stochastic analysis of satellite broadband by mega-constellations with inclined LEOs," in *Proc. IEEE 31st Annual International Symposium on Personal, Indoor and Mobile Radio Communications*, Sep. 2020.
- [17] A. Talgat, M. A. Kishk, and M. S. Alouini, "Stochastic geometry-based analysis of LEO satellite communication systems," in *Proc. IEEE Communications Letters*, Oct. 2020.
- [18] A. Yastrebova, I. Angervuori, N. Okati, M. Vehkaperä, M. Höyhtyä, R. Wichman, and T. Riihonen, "Theoretical and simulation-based analysis of terrestrial interference to LEO satellite uplinks," in *Proc. IEEE Global Communications Conference (GLOBECOM)*, Dec. 2020.



## PUBLICATION 4

**Nonhomogeneous Stochastic Geometry Analysis of Massive LEO  
Communication Constellations**

N. Okati and T. Riihonen

*IEEE Transactions on Communications*, vol. 70, no. 3, pp. 1848–1860

**Publication reprinted with the permission of the copyright holders.**



# Nonhomogeneous Stochastic Geometry Analysis of Massive LEO Communication Constellations

Niloofer Okati  and Taneli Riihonen , *Member, IEEE*

**Abstract**—Providing truly ubiquitous connectivity requires development of low Earth orbit (LEO) satellite Internet, whose theoretical study is lagging behind network-specific simulations. In this paper, we derive analytical expressions for the downlink coverage probability and average data rate of a massive inclined LEO constellation in terms of total interference power's Laplace transform in the presence of fading and shadowing, ergo presenting a stochastic geometry-based analysis. We assume the desired link to experience Nakagami- $m$  fading, which serves to represent different fading scenarios by varying integer  $m$ , while the interfering channels can follow any fading model without an effect on analytical tractability. To take into account the inherent non-uniform distribution of satellites across different latitudes, we model the LEO network as a nonhomogeneous Poisson point process with its intensity being a function of satellites' actual distribution in terms of constellation size, the altitude of the constellation, and the inclination of orbital planes. From the numerical results, we observe optimum points for both the constellation altitude and the number of orthogonal frequency channels; interestingly, the optimum user's latitude is greater than the inclination angle due to the presence of fewer interfering satellites. Overall, the presented study facilitates general stochastic evaluation and planning of satellite Internet constellations without specific orbital simulations or tracking data on satellites' exact positions in space.

**Index Terms**—Massive communication satellite networks, Low Earth orbit (LEO) Internet constellations, interference, coverage probability, average achievable data rate, stochastic geometry, Poisson point process.

## I. INTRODUCTION

Recent advances towards 6th generation (6G) wireless networks require progression and development of non-terrestrial networks to provide seamless connections with high transmission capacity [1]–[4]. Among non-terrestrial networks, low Earth orbit (LEO) satellite Internet constellations have gained increasing popularity as they provide global connectivity for unserved or underserved regions, where the deployment of terrestrial networks is not feasible or economically reasonable [5], [6]. Deploying thousands of satellites will ensure that every single person or appliance on Earth could be connected and no location is left in outage.

While the performance of many LEO constellations (e.g., Starlink, OneWeb, Kuiper) has been evaluated through

network-specific simulations to put the commercial plans forward, a general scientific understanding of their performance is limited in the open literature. Conventional simulation-based studies are restricted to few number of satellites with deterministic locations which is not capable of evaluating the general performance of a massive satellite network consisting of thousands of satellites. Moreover, in most of the literature, the coverage regions are assumed to have fixed circular footprints, while selecting smaller inclination angles and simultaneous consolidated operation of several LEO networks render a not-so-regular Voronoi tessellation.

In this paper, downlink coverage probability and average data rate of inclined LEO constellations are analyzed under general shadowing and fading propagation models. The satellites' positions are assumed to be distributed as a non-homogeneous Poisson point process (NPPP), which models the satellites distribution across varying latitudes precisely by setting the intensity function to be the actual density of satellites in an actual constellation.

### A. Related Works

The literature around LEO networks is mostly limited to deterministic and simulation-based analyses. In [7], the performance of two different LEO constellations was simulated assuming specific constellation sizes. The probability of average call drop and the distribution of the number of handoffs were studied for the Iridium constellation in [8]. A deterministic model to characterize the visibility time of one LEO satellite was presented in [9]. Since the model in [9] is not valid for any arbitrarily located user, authors in [10] contributed statistical analysis of coverage time in a mobile LEO constellation. In [11], a LEO-based Internet-of-Things architecture was presented so as to supply network access for devices distributed in remote areas.

Stochastic geometry is an area of mathematics, which deals with the study of random objects on Euclidean space. In the area of telecommunication, stochastic geometry has been extensively utilized to model, evaluate, and develop the wireless communication networks with irregular topologies [12]–[14], especially for two-dimensional (planar) terrestrial networks [12]–[20]. Various studies in stochastic geometry modeling of multi-tier and cognitive networks were reviewed in [15]. Observations in [16] have shown that the Poisson point process (PPP) and a regular grid model provide lower and upper bounds on the network performance metrics, respectively, with the same deviation from the actual network performance. The research in [17], [18], being an extension to

Manuscript received June 2, 2021; revised October 21, 2021 and December 22, 2021; accepted January 3, 2022. The work of authors was supported by a Nokia University Donation. The associate editor coordinating the review of this paper and approving it for publication was N. Lee. (*Corresponding author: Niloofer Okati.*)

The authors are with Unit of Electrical Engineering, Faculty of Information Technology and Communication Sciences, Tampere University, FI-33720 Tampere, Finland (e-mail: niloofer.okati@tuni.fi; taneli.riihonen@tuni.fi).

[16], modeled a multi-tier network considering the limitations for the achievable quality-of-service. The coverage of uplink was studied in [19] assuming base stations and devices are distributed as independent PPPs.

The application of stochastic geometry to three-dimensional wireless networks has gained remarkable attention in the literature [21], [22]. In [21], a PPP model was applied to model and analyze the coverage in three-dimensional cellular networks. Since the PPP, despite providing tractable analysis, is not accurate when applied to networks with limited nodes in a finite area [23], a binomial point process (BPP) can be utilized instead to capture the characteristics of such networks [24], [25]. A finite network of unmanned aerial vehicles was modeled as a BPP in [22], [26]. In [24], [27], a planar network with an arbitrary shape was studied assuming the transmitter is positioned at a fixed distance. The results were then generalized in [20], by using two protocols for selecting the transmitter.

On the literature around the LEO satellite networks, the analysis is limited to few number of satellites with known locations and/or coverage spots. In [28], with tools from stochastic geometry, authors have developed a method to characterize the magnitude of Doppler shifts in a LEO network. Resource control of a satellite–terrestrial network was investigated in [29], in order to minimize the outage probability and maximize the data rate. Focusing on only a single spotbeam, the hybrid satellite–terrestrial network supporting 5G infrastructure has been presented in [30], [31]. In [32], the outage probability of a satellite-based Internet-of-Things, in which LEO satellites relay uplink data to ground stations, is derived in closed form by assuming a low number of satellites at deterministic locations.

Recently, more research on LEO networks using stochastic geometry has started emerging. The generic coverage and rate analysis of satellite networking have been formulated in our study [33], by modeling the satellites as a BPP on a spherical shell and using the tools from stochastic geometry, without considering any deterministic model of orbits. However, the approach used in [33] is unable to include the varying density of satellites over different latitudes, except through numerical computations, to adjust the performance deviation in the actual and the uniformly modeled constellations. In fact, in practical constellations, the satellites are not evenly distributed across different latitudes [34], i.e., as the user gets farther from the equator towards the poles, more satellites are visible to it. In [34], we derived a mathematical expression, named as effective number of satellites, based on the actual constellation geometry to compensate for the performance mismatch caused by non-uniform distribution of satellites on the orbital shell.

The satellites' positions are modeled as a nonhomogeneous Poisson point process (NPPP) in [35] to analyze the coverage and rate of a noise-limited *interference-free* LEO network. Utilizing NPPP not only enables us to tractably analyze the LEO network performance, but also models the actual distribution of satellites precisely by setting its intensity to be the physical density of satellites along different latitudes. Similar contributions on performance evaluation of a LEO network were also presented in [36] using a homogeneous

PPP without considering the varying density of satellites on different latitudes. The results were then used in [37] to optimize the constellation altitude.

The work in [38] characterizes the distance distribution in two different communication links in a LEO satellite network: link between a user on Earth and the nearest satellite to it and the link between a satellite and its nearest neighboring satellite. Unlike in [33], the satellites are assumed to be placed at different known altitudes, i.e., on multiple orbital shells. Stochastic geometry and the results from [38] were then utilized in [39] to obtain the downlink probability of coverage for a LEO network, where satellite gateways act as relays between the satellites and users on Earth. An uplink communication scenario was characterized by considering interfering terrestrial transmitters in [40].

This paper, unlike our prior works [33], [34], adopts non-homogeneous Poisson point process to model the satellites' locality, for which the varying density along different latitudes is embedded in the PPP's intensity function. Moreover, a more general fading model, i.e., Nakagami- $m$ , transceivers' antenna patterns, and shadowing attenuation due to the blockage of the signals by obstacles surrounding the user, are considered in our analysis. This paper also includes interference analysis in a generic form which was neglected in [35] and the performance metrics are evaluated in terms of the Laplace function of interference.

## B. Contributions and Paper Organization

We model the satellites' positions in a LEO network as a nonhomogeneous PPP which facilitates not only using the tools from stochastic geometry, but also capturing the exact characteristics of the actual constellations, i.e., the uneven distribution of satellites across different latitudes. Unlike in [33], [34], [39], by selecting the intensity of NPPP to fit the actual distribution of satellites on an orbital shell, there is no mismatch between the performance of theoretical stochastic constellations and actual deterministic LEO networks. We derive the intensity of NPPP in closed form in terms of the constellation parameters: the total number of satellites, altitude of the constellation, latitude of the satellites, and the inclination of the orbits. The model is extensible to develop an analysis on satellite-to-satellite communication, similar to what was proposed in [41] for three-dimensional wireless sensor networks.

As the main contributions, we utilize stochastic geometry to formulate the coverage and average achievable rate of a user served by a LEO constellation in terms of the derivative of Laplace transform of interference power.<sup>1</sup> Our derivations do not rely on exact location of every single satellite and are applicable for performance analysis of any given constellation as long as the constellation parameters are known. Modeling the satellites' locality as a NPPP, the analytical expressions obtained from a stochastic constellation geometry can be particularly used to analyze the actual deterministic constellations.

<sup>1</sup>Thus, the present study, unlike the preliminary results presented in [35] that are limited to the special case of scheduling an orthogonal channel for every satellite, includes the cumulative interference from all other satellites that are visible to the user and share the same channel.



In propagation modelling, unlike most of literature on this topic, we take into account the effect of shadowing caused by the presence of the obstacles surrounding the user. To retain analytical tractability and still cover different fading scenarios, we assume Nakagami- $m$  fading with integer  $m$  as well as shadowing with any desired distribution for the propagation model of desired links.<sup>2</sup> For interfering signals, any arbitrarily distributed fading and shadowing can be considered, since the analytical tractability is unaffected. Frequency reuse has been also taken into account by randomly assigning the frequency channels to the satellites. Random channel assignment preserves the tractability of our analytical derivations since it can be modeled by thinning the original nonhomogeneous Poisson point process.

In this paper, antenna pattern, despite the conventional approach, is formulated and included in the performance analysis by representing the antenna gain as a function of the relative distances between the user and the satellites. Finally, we evaluate two critical performance metrics, i.e., coverage and data rate, in terms of several key design parameters, such as altitude of the constellation and the number of frequency channels. From the numerical results, we are able to observe optimal points for these parameters for some specific network setup. Counter-intuitively, the user which resides in higher latitudes, away from the constellation borders, has the best performance due to existence of fewer interfering satellites in that region. Some constellation design guidelines, e.g., on orbital inclination and altitude, are also provided through the numerical results.

The remainder of this paper is organized as follows. Section II describes the system model and the mathematical preliminaries for modeling a LEO network as a NPPP. The main outcome of this study, which is the derivation of analytical expressions for downlink coverage probability and average achievable rate of a terrestrial user, is presented in Section III, which involves also the analysis of the Laplace transform of interference power. We provide numerical results in Section IV for the verification of our derivations and studying the effect of key system parameters such as the size of the constellation and its altitude as well as the channel parameters on the network performance. Finally, we conclude the paper in Section V.

## II. SYSTEM MODEL

In this section, first, we present the characteristics and geometries of actual low Earth orbit satellite constellations. Next, we will introduce the mathematical preliminaries for modeling the actual network as a stochastic point process.

### A. Actual Inclined Constellations

As shown in Fig. 1, we consider a LEO communication satellite constellation consisting of  $N$  satellites launched uniformly on circular orbits with inclination angle,  $\iota$ , and altitude that is denoted by  $r_{\min}$  — the subscript indicates the minimum possible distance between a satellite and a ground user (as

<sup>2</sup>Varying the value of  $m$ , we are able to control the multi-path fading severity. For instance,  $m = 1$  corresponds to Rayleigh fading environment while  $m \rightarrow \infty$  represents non-fading channels.

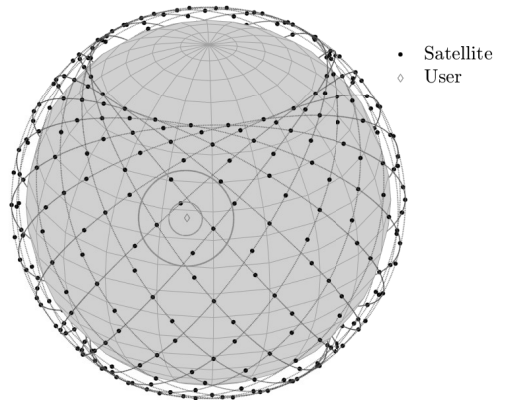


Fig. 1. A constellation in an example case of  $N = 400$  satellites flying on  $\iota = 53^\circ$  inclined orbits. The borders of two spherical caps above the user are shown: the outer one covers all visible satellites to the user while the inner one is empty of satellites and the serving satellite is located on its border.

measured at the zenith). Satellites' spherical coordinates in terms of their latitude and longitude are denoted by  $(\phi_s, \lambda_s)$ .

A user terminal is located on any specific latitude, denoted by  $\phi_u$ , on the surface of Earth that is approximated as a perfect sphere with radius  $r_\oplus \approx 6371$  km. Satellites rising above the horizon at an angle of  $\theta_s \geq \theta_{\min}$  are the only ones capable of transmitting signals to the users. As such,  $r_{\max}$  refers to the maximum distance at which a satellite and a user are able to communicate (and it occurs when  $\theta_s = \theta_{\min}$ ), and

$$\frac{r_{\max}}{r_\oplus} = \sqrt{\frac{r_{\min}}{r_\oplus} \left( \frac{r_{\min}}{r_\oplus} + 2 \right) + \sin^2(\theta_{\min})} - \sin(\theta_{\min}). \quad (1)$$

In this paper, the serving satellite is the one with the shortest distance to the user. We perform frequency reuse by assuming  $K$ , with  $K \leq N$ , orthogonal frequency channels available for the network. The satellites are distributed randomly among the channels, which potentially causes co-channel interference to the user from  $\frac{N}{K} - 1$  satellites which share the same frequency channel. All satellites on the same channel that are elevated above the horizon to an angle of  $\theta_s \geq \theta_{\min}$  cause interference to reception of the user.

The variables  $R_0$  and  $R_n$ ,  $n = 1, 2, \dots, N$ , represent the distances from the user to the serving satellite and the other interfering satellites, respectively, while  $H_0$  and  $H_n$  denote the corresponding channel gains to model fading. Shadowing effect is modeled by random variables  $\mathcal{X}_n$ ,  $n = 1, 2, \dots, N$ , correspondingly. It is worth noting that losses caused by near-ground obstacles in the last few meters of the signal path, named as excess path loss in [36], can be approximated by properly setting the shadowing distribution and its corresponding parameters. On the other hand, our analysis is also capable of including the effect of elevation angle on the shadowing by expressing it as a function of the relative distances between the user and the satellites. However, in this

paper, we do not explicitly formulate that to simplify the expressions. Obviously,  $H_n = \mathcal{X}_n = 0$  if  $R_n > r_{\max}$  for some  $n = 1, \dots, N$ . The attenuation due to atmospheric gases is insignificant for frequencies below 20 GHz (at least, or even at higher bands below the oxygen absorption peak at 60 GHz) [42, Fig. 10], which is the practical range for downlink LEO communication in well-known constellations [43].

For the serving channel, we adopt Nakagami- $m$  fading which will enable not only to consider a wide range of multipath fading conditions but also to maintain the tractability of our derivations. On the other hand, for the interfering channels, we consider arbitrary fading distributions since they have no effect on the tractability of our analysis and, hence there is no need to limit our results to some specific fading models. Following the same logic, we also obtain more general results by assuming arbitrarily distributed shadowing for all — the serving and the interfering — channels.

To simplify notation, when  $N_I > 0$ , we let indices  $n = 1, 2, \dots, N_I$  correspond to those  $N_I \leq N/K - 1$  satellites with  $\theta_s \geq \theta_{\min}$  that cause co-channel interference. The user and the satellites are equipped with directional antennas having gains denoted by  $G_u(\theta_u)$  and  $G_s(\theta_n)$ , respectively, while  $\theta_u$  and  $\theta_n$  are the angles between the line-of-sight path and their corresponding antennas' boresight. We assume that the user's antenna boresight is directed towards the sky, perpendicular to Earth's surface, and the satellites' antennas' boresight always radiates towards the center of Earth. When all antennas have symmetrical radiation patterns, using the law of cosines, we obtain  $\theta_u$  and  $\theta_n$  as

$$\theta_u(R_n) = \pi - \cos^{-1} \left( \frac{r_{\oplus}^2 + R_n^2 - (r_{\oplus} + r_{\min})^2}{2r_{\oplus}R_n} \right) \quad (2)$$

and

$$\theta_n(R_n) = \cos^{-1} \left( \frac{R_n^2 - r_{\oplus}^2 + (r_{\oplus} + r_{\min})^2}{2R_n(r_{\oplus} + r_{\min})} \right), \quad (3)$$

respectively. As can be seen from (2) and (3), the antennas' radiation patterns are one-to-one functions of the relative distances between the user and the satellites. Thus, in the rest of this paper, we will denote the user's and the satellites' antenna gains directly as  $G_u(R_n)$  and  $G_s(R_n)$ , respectively, and  $G_t(R_n) = G_u(R_n)G_s(R_n)$  is the overall antenna gain.

According to the described model, the signal-to-interference-plus-noise ratio (SINR) of the link is given by

$$\text{SINR} = \frac{p_t G_t(R_0) H_0 \mathcal{X}_0 R_0^{-\alpha}}{I + \sigma^2}, \quad (4)$$

where  $p_t$  is the transmit power of satellites, the constant  $\sigma^2$  is the additive noise power, the parameter  $\alpha$  is a path loss exponent, which should be set to  $\alpha = 2$  for satellite communication since the signal travels through free space for most of its path, and

$$I \triangleq \sum_{n=1}^{N_I} p_t G_t(R_n) H_n \mathcal{X}_n R_n^{-\alpha} \quad (5)$$

is the cumulative interference power from all  $N_I$  other satellites above the user's horizon that share the same frequency

channel with the serving satellite. The distance from the user to its nearest satellite is

$$R_0 = \min_{n=1,2,\dots,N_{\text{vis}}} R_n, \quad (6)$$

where  $N_{\text{vis}}$  is a variable representing the number of visible satellites to the user (cf. the outer cap in Fig. 1).

### B. Nonhomogeneous PPP Model

In the constellation described earlier, the satellites appear unevenly along the lines of latitudes, which means, e.g., that there are more visible satellites for a user located close to inclination limits than for one on equatorial region. In order to model the latitude-dependent distribution of satellites, we assume that the satellites are distributed according to a *nonhomogeneous* PPP,  $\xi$ , on a spherical surface with radius  $r_{\oplus} + r_{\min}$ . The NPPP is characterized with its intensity,  $\delta(\phi_s, \lambda_s)$ , which varies according to the satellites' latitude (and/or longitude).

By the definition of a NPPP, the number of points in some bounded region  $\mathcal{A}$  of the orbital shell is a Poisson-distributed random variable denoted by  $\mathcal{N}$ . Thereby, the probability to have  $n$  satellites in  $\mathcal{A}$  is given by

$$\begin{aligned} P_n(\mathcal{A}) &\triangleq \mathbb{P}(\mathcal{N} = n) \\ &= \frac{1}{n!} \left( \iint_{\mathcal{A}} \delta(\phi_s, \lambda_s) (r_{\min} + r_{\oplus})^2 \cos(\phi_s) d\phi_s d\lambda_s \right)^n \\ &\quad \times \exp \left( - \iint_{\mathcal{A}} \delta(\phi_s, \lambda_s) (r_{\min} + r_{\oplus})^2 \cos(\phi_s) d\phi_s d\lambda_s \right), \end{aligned} \quad (7)$$

where  $\delta(\phi_s, \lambda_s)$  is the intensity function of nonhomogeneous PPP at latitude  $\phi_s$  and longitude  $\lambda_s$ . Based on the given system model,  $\mathcal{A}$  is the spherical cap where viewable satellites to the user exist (cf. the outer one in Fig. 1), with surface area  $(\delta\pi (r_{\max}^2 - r_0^2)) / (1 - \frac{r_{\min}}{r_{\oplus} + r_{\min}})$  (See [33, Appendix A]).

In order to precisely model a LEO network as a NPPP, we first need to characterize the intensity function based on the actual physical network as follows. The preliminaries obtained herein will be used shortly towards contributing expressions for probability of coverage and average achievable rate.

**Lemma 1.** *When satellites are distributed uniformly on low circular orbits with the altitude,  $r_{\min}$ , and the inclination angle,  $\iota$ , the intensity function of the nonhomogeneous PPP is a function of latitude,  $\phi_s$ , only and given by*

$$\delta(\phi_s) = \frac{N}{\sqrt{2\pi^2 (r_{\min} + r_{\oplus})^2}} \cdot \frac{1}{\sqrt{\cos(2\phi_s) - \cos(2\iota)}}, \quad (8)$$

and we can denote  $\delta(\phi_s, \lambda_s) = \delta(\phi_s)$  since it does not depend on  $\lambda_s$ , for  $\phi_s \in [-\iota, \iota]$ .

*Proof.* The intensity function is equivalent to the actual density of the satellites on an orbital shell element created by spanning the azimuthal angle from  $0^\circ$  to  $360^\circ$  on the orbital shell at latitude  $\phi_s$ , that is calculated as

$$\delta(\phi_s) = \frac{N f_{\Phi_s}(\phi_s) d\phi_s}{2\pi (r_{\min} + r_{\oplus})^2 \cos(\phi_s) d\phi_s}, \quad (9)$$

TABLE I  
SUMMARY OF MATHEMATICAL NOTATION

Notation	Description
$r_{\oplus}; r_{\min}; r_{\max}$	Earth radius (6371 km); Constellation altitude; Maximum possible distance between a user and a visible satellite
$R_0; R_n$	Serving distance; Distance to the $n^{\text{th}}$ satellite
$N; N_I; K$	Constellation size; The number of interfering satellites; The number of frequency channels
$G_u; G_s; G_t$	Antenna gain of the user; Antenna gain of the $n^{\text{th}}$ satellite; Overall antenna gain
$H_0; H_n$	Channel fading gain of the serving link; Channel fading gain of the $n^{\text{th}}$ link
$\mathcal{X}_0; \mathcal{X}_n$	Shadowing component of the serving link; Shadowing component of the $n^{\text{th}}$ link
$\alpha$	Path loss exponent
$p_t$	Transmission power satellites
$\sigma^2$	Additive noise power
$T$	SINR threshold for coverage probability
$P_C; C$	Coverage probability; Average achievable rate

which is the ratio of the number of satellites resided on the surface element to the element's area. Substituting the probability density  $f_{\Phi_s}(\phi_s)$  of random latitude  $\Phi_s$  [34, Lemma 2] completes the proof.  $\square$

If the intensity of satellites is simplistically presumed to be uniform all over the orbital shell, it can be written as follows.

**Lemma 2.** *When satellites are uniformly distributed on a sphere, the point process turns into a homogeneous Poisson point process with a constant intensity given by*

$$\delta = \frac{N}{4\pi(r_{\min} + r_{\oplus})^2}, \quad (10)$$

which does not depend on latitudinal/longitudinal parameters.

Thus, for the special case when satellites are distributed uniformly on the orbital shell, by substitution from Lemma 2, the probability given in (7) can be expressed in closed form as

$$P_n(\mathcal{A}) = \frac{1}{n!} \left( \frac{N(r_{\max}^2 - r_{\min}^2)}{4r_{\oplus}(r_{\oplus} + r_{\min})} \right)^n \exp\left(-\frac{N(r_{\max}^2 - r_{\min}^2)}{4r_{\oplus}(r_{\oplus} + r_{\min})}\right). \quad (11)$$

### III. PERFORMANCE ANALYSIS

In this section, we focus on the performance analysis of a LEO satellite network in terms of coverage probability and data rate of a user in an arbitrary location on Earth. We utilize stochastic geometry in order to formulate coverage probability and rate as a function of the network and the propagation parameters. Two main components of our analytical derivations are the distribution of the distance to the nearest satellite and the Laplace function of interference which will be presented throughout this section.

#### A. The Distance to The Nearest Satellite

In this paper, the serving satellite is assumed to be the nearest one to the user. Therefore, an important parameter for coverage and rate analysis is the probability density function (PDF) of the distance to the nearest satellite,  $R_0$ , which is given as follows.

**Lemma 3.** *The PDF of the serving distance  $R_0$ , when the satellites are distributed according to a nonhomogeneous PPP with a latitude-dependent intensity,  $\delta(\phi_s)$ , is*

$$\begin{aligned} f_{R_0}(r_0) &= 2r_0 \left( \frac{r_{\min}}{r_{\oplus}} + 1 \right) \exp(-\gamma(r_0)) \int_{\max(\phi_u - \phi_0, -\iota)}^{\min(\phi_u + \phi_0, \iota)} \delta(\phi_s) \\ &\quad \times \frac{\cos(\phi_s)}{\sqrt{\cos^2(\phi_s - \phi_u) - \cos^2(\phi_0)}} d\phi_s, \end{aligned} \quad (12)$$

where

$$\begin{aligned} \gamma(r_0) &= 2(r_{\min} + r_{\oplus})^2 \\ &\times \int_{\max(\phi_u - \phi_0, -\iota)}^{\min(\phi_u + \phi_0, \iota)} \delta(\phi_s) \cos(\phi_s) \cos^{-1} \left( \frac{\cos(\phi_0)}{\cos(\phi_s - \phi_u)} \right) d\phi_s \end{aligned} \quad (13)$$

and  $\phi_0$  is the polar angle difference between the serving satellite and the user which is given by  $\phi_0 = \cos^{-1} \left( 1 - \frac{r_0^2 - r_{\min}^2}{2(r_{\min} + r_{\oplus})r_{\oplus}} \right)$ . Equation (12) is valid for  $\phi_0 \geq |\phi_u| - \iota$  and  $r_0 \in [r_{\min}, 2r_{\oplus} + r_{\min}]$  while  $f_{R_0}(r_0) = 0$  otherwise.

*Proof.* See Appendix A.  $\square$

We validate the PDF of the serving distance given in Lemma 3 (lines) by Monte Carlo simulations (markers) in Fig. 2. As shown in the figure, for larger number of satellites, it is more likely that the serving distance has a value close to the constellation altitude. The PDF becomes more uniform and its maximum point diverges from the constellation altitude for fewer number of satellites. For user's latitudes greater than the inclination angle, e.g.,  $\phi_u = 65^\circ$  in the figure, the serving distance has a value greater than the altitude depending the constellation size and its altitude.

When the density of satellites is presumed to be uniform, i.e., it is not a function of latitude, the PDF of the serving distance can be obtained in closed form as follows.

**Lemma 4.** *The PDF of the serving distance  $R_0$  when the satellites are distributed uniformly with constant intensity*

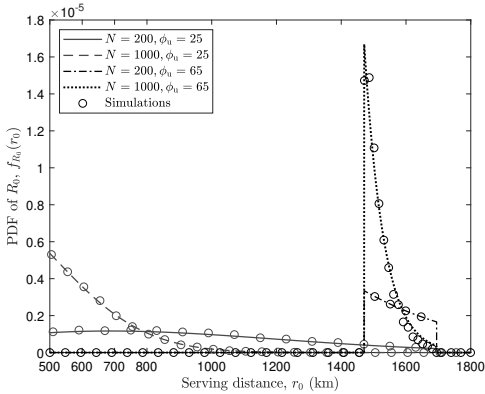


Fig. 2. PDF of the serving distance,  $R_0$ , given in Lemma 3, for  $r_{\min} = 500$  km,  $l = 53^\circ$ , and  $\theta_{\min} = 10^\circ$ . The lines and the markers show the theoretical and simulation results, respectively.

given in Lemma 2 is

$$f_{R_0}(r_0) = \frac{Nr_0}{2r_\oplus(r_{\min} + r_\oplus)} \exp\left(-N\left(\frac{r_0^2 - r_{\min}^2}{4(r_{\min} + r_\oplus)r_\oplus}\right)\right) \quad (14)$$

for  $r_0 \in [r_{\min}, 2r_\oplus + r_{\min}]$  while  $f_{R_0}(r_0) = 0$  otherwise.

*Proof.* In this proof, the same principles are used as in Lemma 3. However, the integration from a constant density over the cap sphere will reduce to a simple expression. Thus,  $F_{R_0}(r_0) = 1 - \exp\left(-N\left(\frac{r_0^2 - r_{\min}^2}{4(r_{\min} + r_\oplus)r_\oplus}\right)\right)$ . Calculating the derivative of the CDF w.r.t.  $r_0$  completes the proof.  $\square$

The PDF of the serving distance is also derived in [33] assuming satellites are uniformly distributed as a BPP. It is worth noting that the Taylor series expansion of Lemma 4 and the serving distance distribution given in [33, Lemma 2] are the same for the first two terms. The difference between the serving distance in a uniformly distributed constellation given in [33] and the homogeneous Poisson point process in Lemma 4 is insignificant since the argument of exponential function in (14), i.e.,  $N\left(\frac{r_0^2 - r_{\min}^2}{4(r_{\min} + r_\oplus)r_\oplus}\right)$ , is small.

### B. Coverage Probability and Average Data Rate

The coverage probability is the probability that the SINR at the receiver is higher than the minimum SINR required to successfully transmit the data. The coverage probability is defined as

$$P_c(T) \triangleq \mathbb{P}(\text{SINR} > T) = \mathbb{P}\left(\frac{p_t G_t(R_0) H_0 \mathcal{X}_0 R_0^{-\alpha}}{I + \sigma^2} > T\right), \quad (15)$$

where  $T$  is the SINR threshold.

Using the above definition, we express the coverage probability of a user in the following theorem.

**Theorem 1.** *The coverage probability for an arbitrarily located user under a Nakagami fading serving channel while*

*both shape parameter and rate parameter of gamma distribution<sup>3</sup> are  $m_0$ , is*

$$P_c(T) \triangleq \mathbb{P}(\text{SINR} > T) = \int_{r_{\min}}^{r_{\max}} \int_0^\infty f_{\mathcal{X}_0}(x_0) f_{R_0}(r_0) \left[ e^{-s\sigma^2} \sum_{k=0}^{m_0-1} \frac{\sum_{l=0}^k \binom{k}{l} (s\sigma^2)^l (-s)^{k-l} \frac{\partial^{k-l}}{\partial s^{k-l}} \mathcal{L}_I(s)}{k!} \right]_{s=\frac{m_0 T r_0^{-\alpha}}{p_t G_t(r_0) x_0}} dx_0 dr_0, \quad (16)$$

where the PDF  $f_{R_0}(r_0)$  is given in Lemma 3 (or Lemma 4),  $f_{\mathcal{X}_0}(x_0)$  is the PDF of  $\mathcal{X}_0$  and  $\mathcal{L}_I(s)$  is the Laplace transform of interference power  $I$  calculated in the next section.

*Proof.* See Appendix B.  $\square$

Let us then move on the average achievable data rate (in bit/s/Hz), which is the ergodic capacity for a fading communication link derived from Shannon-Hartley theorem normalized to unit bandwidth. The average achievable rate is defined as

$$\bar{C} \triangleq \frac{1}{K} \mathbb{E}[\log_2(1 + \text{SINR})]. \quad (17)$$

Unlike for the coverage probability, frequency reuse affects the average rate in two opposite directions. One direction is the improvement in SINR due to the reduction in the number of interfering satellites which use the same channel. The other direction which results in lower data rate is induced by a reduction in the availability of the frequency band shared among a group of satellites.

In the following theorem, we calculate the expression for the average rate of a user over Nakagami fading serving channel. The interfering channel gains may follow any arbitrary distribution.

**Theorem 2.** *The average data rate of an arbitrarily located user under a Nakagami fading serving channel and any fading or shadowing distribution for interfering channels is given by*

$$\bar{C} = \frac{1}{K} \int_{r_{\min}}^{r_{\max}} \int_0^\infty \int_0^\infty f_{\mathcal{X}_0}(x_0) f_{R_0}(r_0) \left[ e^{-s\sigma^2} \sum_{k=0}^{m_0-1} \frac{\sum_{l=0}^k \binom{k}{l} (s\sigma^2)^l (-s)^{k-l} \frac{\partial^{k-l}}{\partial s^{k-l}} \mathcal{L}_I(s)}{k!} \right]_{s=\frac{m_0(2^l-1)r_0^{-\alpha}}{p_t G_t(r_0) x_0}} dt dx_0 dr_0, \quad (18)$$

where  $m_0$  is the parameter of Nakagami fading, and  $\mathcal{L}_I(s)$  will be given in Lemma 5 and its corresponding corollaries, which cover some special cases.

*Proof.* See Appendix C.  $\square$

### C. Interference Analysis

In this subsection, we derive the Laplace function of interference which is a key element of the performance expressions in Theorems 1 and 2. We, first, obtain the expression

<sup>3</sup>Channel gain, being the square of Nakagami random variable, follows a gamma distribution.

considering a general propagation model which means that no assumption is made regarding the specific expressions of  $f_{\mathcal{X}_n}(x_n)$  and  $f_{H_n}(h_n)$ .

**Lemma 5.** *When the server is at distance  $r_0 \geq r_{\min}$  from the user and interfering channels experience an arbitrary distributed fading, the Laplace transform of random variable  $I$  is*

$$\mathcal{L}_I(s) \triangleq \mathbb{E}_I[e^{-sI}] = \sum_{n=0}^{\infty} P_n(\mathcal{A}(r_{\max}) - \mathcal{A}(r_0)) \quad (19)$$

$$\times \left( \int_{r_0}^{r_{\max}} \int_0^{\infty} \mathcal{L}_{H_n}(s p_t G_t(r_n) x_n r_n^{-\alpha}) f_{\mathcal{X}_n}(x_n) f_{R_n|R_0}(r_n|r_0) dx_0 dr_n \right)^n,$$

where

$$f_{R_n|R_0}(r_n|r_0) = \frac{d\gamma(r_n)/dr_n}{\gamma(r_{\max}) - \gamma(r_0)} \quad (20)$$

is the probability density function of the distance from any visible satellite to the user conditioned on the serving distance [33, Lemma 3]. The parameter  $\mathcal{A}(r_{\max})$  represents the spherical cap where all satellites that can be viewed by the user exist while  $\mathcal{A}(r_0)$  is the cap above the user, empty of satellites and with the serving satellite on its border (base of the cap). The function  $f_{\mathcal{X}_n}(x_n)$  denotes the shadowing PDF for the  $n$ th interfering channel.

*Proof.* See Appendix D.  $\square$

In the special cases, where channels experience Nakagami fading without any shadowing, Lemma 5 can be reduced into the following corollary. The expression thereof is obtained by substituting the Laplace function of a gamma random variable, i.e.,  $\mathcal{L}_{H_n}(z) = \frac{m_n^{m_n}}{(m_n + z)^{m_n}}$ , where  $m_n$  stands for both shape parameter and rate parameter of gamma distribution for the  $n$ th link.

**Corollary 1.** *When the interfering channels experience only Nakagami fading (no shadowing), the Laplace function of interference can be written as*

$$\mathcal{L}_I(s) = \sum_{n=0}^{\infty} P_n(\mathcal{A}(r_{\max}) - \mathcal{A}(r_0))$$

$$\times \left( \int_{r_0}^{r_{\max}} \frac{m_n^{m_n}}{(m_n + s p_t G_t(r_n) r_n^{-\alpha})^{m_n}} f_{R_n|R_0}(r_n|r_0) dr_n \right)^n, \quad (21)$$

where  $\mathcal{A}(r_{\max})$  and  $\mathcal{A}(r_0)$  are the visible cap and the null cap above the user, respectively. The PDF  $f_{R_n|R_0}(r_n|r_0)$  is given in (20), and  $m_n$  is the Nakagami fading parameter for  $n$ th link.

When the intensity of the PPP is presumed to be constant (regardless of the latitude), the Laplace function can be obtained from the following corollary by simply substituting  $\gamma(\cdot)$  in (20) by the product of the density in Lemma 2 and the surface area of the spherical cap formed by the distance between the user and the given interfering satellite.

**Corollary 2.** *The Laplace function of interference when the satellites are distributed uniformly with constant intensity, and their channels experience Nakagami fading, is given by*

$$\mathcal{L}_I(s)$$

$$= \sum_{n=0}^{\infty} \frac{1}{n!} \left( \frac{N(r_{\max}^2 - r_0^2)}{4r_{\oplus}(r_{\oplus} + r_{\min})} \right)^n \exp\left(-\frac{N(r_{\max}^2 - r_0^2)}{4r_{\oplus}(r_{\oplus} + r_{\min})}\right)$$

$$\times \left( \int_{r_0}^{r_{\max}} \int_0^{\infty} \frac{2r_n m_n^{m_n} f_{\mathcal{X}_n}(x_0)}{(r_{\max}^2 - r_0^2)(m_n + s p_t G_t(r_n) r_n^{-\alpha})^{m_n}} dx_0 dr_n \right)^n, \quad (22)$$

where  $f_{\mathcal{X}_n}(x_n)$  is the PDF of the shadowing component and  $m_n$  is the fading parameter for Nakagami fading.

The following corollary presents the Laplace function of interference in closed-form, under the assumptions given in Corollary 2 and additionally excluding shadowing from the propagation model.

**Corollary 3.** *Assuming constant antenna gains, the Laplace function of interference, when the satellites are distributed uniformly with constant intensity and their channels experience only Nakagami fading (no shadowing), is given by*

$$\mathcal{L}_I(s)$$

$$= \sum_{n=0}^{\infty} \frac{1}{n!} \left( \frac{N(r_{\max}^2 - r_0^2)}{4r_{\oplus}(r_{\oplus} + r_{\min})} \right)^n \exp\left(-\frac{N(r_{\max}^2 - r_0^2)}{4r_{\oplus}(r_{\oplus} + r_{\min})}\right)$$

$$\times \frac{1}{(r_{\max}^2 - r_0^2)} \left[ r_{\max}^2 {}_2F_1\left(-\frac{2}{\alpha}, m_n; \frac{\alpha - 2}{\alpha}; -\frac{s p_t G_t r_{\max}^{-\alpha}}{m_n}\right)^n \right.$$

$$\left. - r_0^2 {}_2F_1\left(-\frac{2}{\alpha}, m_n; \frac{\alpha - 2}{\alpha}; -\frac{s p_t G_t r_0^{-\alpha}}{m_n}\right)^n \right], \quad (23)$$

where  ${}_2F_1(\cdot, \cdot; \cdot; \cdot)$  is the Gauss's hyper-geometric function and  $m_n$  is the fading parameter.

Finally, using the function given in [44, Eq. 9.100] and substitution from special parameter values, the above can be reduced to elementary functions. For instance, when  $m = 1$  and  $\alpha = 2$ , we have

$$\mathcal{L}_I(s)$$

$$= \sum_{n=0}^{\infty} \frac{1}{n!} \left( \frac{N(r_{\max}^2 - r_0^2)}{4r_{\oplus}(r_{\oplus} + r_{\min})} \right)^n \exp\left(-\frac{N(r_{\max}^2 - r_0^2)}{4r_{\oplus}(r_{\oplus} + r_{\min})}\right)$$

$$\times \left( 1 + \frac{s p_t G_t}{(r_{\max}^2 - r_0^2)} \ln\left(\frac{k + r_0^2}{k + r_{\max}^2}\right) \right)^n. \quad (24)$$

To perform frequency reuse, we assign each satellite randomly and independently to a particular frequency channel. Therefore, the satellites assigned to each of the orthogonal frequency channels form a thinned version of the original PPP with intensity  $\delta(\phi_s)/K$ . Since thinning preserves the Poisson point process according to the thinning theorem of PPP [13], we can take into account the effect of frequency reuse by substitution  $\delta(\phi_s) \rightarrow \delta(\phi_s)/K$  in Laplace function of interference (in Lemma 5 or the corresponding corollaries). Since the same frequency channel is used by the user and its nearest satellite, the frequency reuse has no effect on the original value of

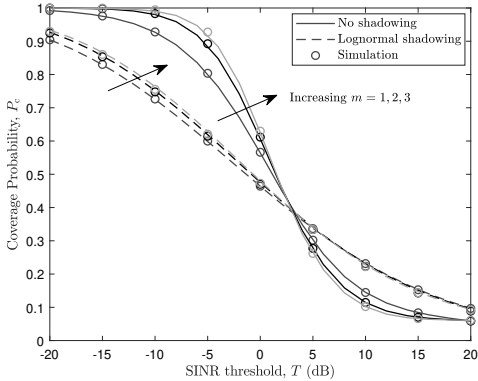


Fig. 3. Theorem 1 verification with simulations when  $\phi_u = 25^\circ$ ,  $\iota = 53^\circ$ ,  $m \in \{1, 2, 3\}$ , and  $\theta_{\min} = 10^\circ$ . The lines and the markers show the theoretical and simulation results, respectively.

intensity that is used to obtain the PDF of the distance from the user to the server in Lemma 3.

#### IV. NUMERICAL RESULTS

In this section, we provide numerical results to study the effect of different network parameters on coverage probability and average data rate using the analytical expressions obtained in Section III. The performance of the network is evaluated in terms of satellite altitude and the number of orthogonal frequency channels, which provides important guidelines into the satellite network design. Furthermore, our analytical derivations are all verified through Monte Carlo simulations.

We consider the large-scale attenuation with path loss exponent  $\alpha = 2$ , and the small-scale Nakagami- $m$  fading with integer  $m \in \{1, 2, 3\}$ . The choice of the fading parameter corresponds to several cases when a dominant line-of-sight component is not available for the user due to being in highly dense urban areas or at higher latitudes compared to the inclination limits. We assume lognormal shadowing which is represented as  $\mathcal{X}_0 = 10^{X_0/10}$  such that  $X_0$  has a normal distribution with mean  $\mu_s = 0$  and standard deviation  $\sigma_s = 9$  dB. Thus, the PDF of lognormal shadowing is

$$f_{\mathcal{X}_0}(x_0) = \frac{10}{\ln(10)\sqrt{2\pi}\sigma_s x_0} \exp\left(-\frac{1}{2}\left(\frac{10 \log_{10}(x_0) - \mu_s}{\sigma_s}\right)^2\right). \quad (25)$$

The number of orthogonal channels is set to  $K = 10$  in all the numerical results unless otherwise stated. We assume ideal isotropic antennas for the satellites as well as the user. The equivalent isotropic radiated power (EIRP) and the noise power are set to 40 dBm, and -103 dBm, respectively. The operating frequency is assumed to be 2 GHz. For the reference simulations, satellites are placed uniformly on orbits centered at Earth's center with radius  $r_{\oplus} + r_{\min}$ .

Figure 3 verifies our derivations given in Theorem 1 for  $53^\circ$  inclined orbits and a user located at  $25^\circ$  latitude. The

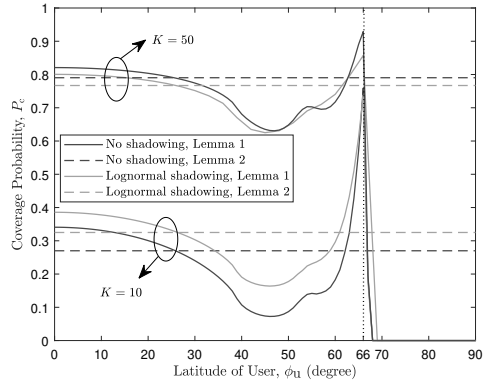


Fig. 4. Theoretical coverage probability on different users' latitudes,  $T = 5$  dB,  $r_{\min} = 500$  km,  $\iota = 53^\circ$ ,  $m = 2$ , and  $\theta_{\min} = 10^\circ$ . The expression given in Theorem 1 is used to plot this figure.

total number of satellites and constellation altitude are chosen to be 2000 and 500 km, respectively. As shown in the figure, the markers that depict the Monte Carlo simulation results are completely matched with the lines that represent our theoretical expressions. Shadowing, as a random phenomenon, may cause an increase or decrease in the received SINR at the user's place. As a result, a varying effect of shadowing on the coverage probability can be observed for different SINR threshold values in Fig. 3. Obviously, this behaviour is thoroughly affected by the mean and variance of lognormal shadowing. Larger values of  $m$  correspond to higher elevation angles and, consequently, less multi-path distortion, which result in slightly better coverage, but shadowing masks the effect of fading at large.

The effect of user's latitude on coverage probability is depicted in Fig. 4 for  $K = 10$  and 50. The coverage probability when satellites form a NPPP with intensity given in Lemma 1 is shown by solid lines. Since the intensity increases as the user moves to higher latitudes, the performance becomes more unreliable due to increase in the density of satellites that share the same frequency channel with the user's serving satellite. When the user is in higher latitudes than the constellation inclination limits, the coverage probability starts increasing due to the reduction in the number of visible interferers. The coverage reaches its maximum at about  $66^\circ$  where the serving satellite is the only visible satellite to the user, i.e., the performance becomes noise-limited. For latitudes larger than  $66^\circ$ , the coverage converges to zero quickly, since there are no satellites above horizon to serve the user. When the intensity of satellites is selected according to Lemma 2, the coverage probability remains constant (dashed lines) all over the Earth for any latitude.

Figure 5 illustrates the probability of coverage at different altitudes. For all propagation environments, the coverage probability increases to reach its maximum value as the altitude increases which is then followed by a decline due to the rise

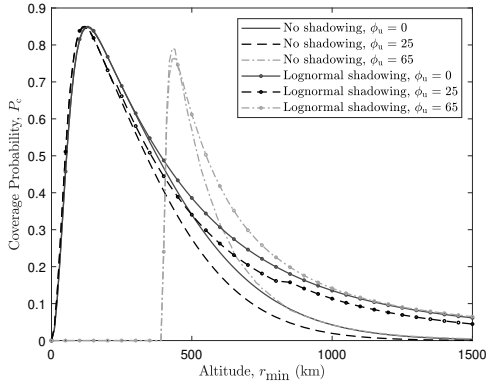


Fig. 5. Effect of altitude on coverage probability when  $T = 5$  dB,  $\phi_u = \{0^\circ, 25^\circ, 65^\circ\}$ ,  $\iota = 53^\circ$ ,  $m = 2$ , and  $\theta_{\min} = 10^\circ$ . The expression given in Theorem 1 is used to plot this figure.

in the number of visible interfering satellites. The optimum altitude for  $\phi_u = 0^\circ$  is slightly larger than  $\phi_u = 25^\circ$ , the reason being that the intensity of satellites, and consequently the number of interferers, is higher at upper latitudes. When the user's latitude is set to  $\phi_u = 65^\circ$ , which means that the user is located out of the constellation borders ( $\phi_u > \iota = 53^\circ$ ), a larger altitude is crucial for the constellation so that the user can be served by a satellite within its visible range. As a result, for altitudes lower than about 400 km, no visible satellite is available to serve the user which results in zero coverage probability.

Several constellation design guidelines can be extracted from Figs. 4 and 5, e.g., regarding the orbital inclination and altitude. The inclination angle does not need to be necessarily greater than the maximum latitude of the intended service area and it may even result in better performance for some latitudes out of the constellation's borders as long as there are visible satellites to the user. On the other hand, increasing the inclination angle to avoid outage on higher latitudes necessitates more satellites to maintain the same density and, consequently, the same performance all over the service area. Similar compromise should be also considered for the altitude. Higher altitudes provide better chance of visibility for the users. However, the overall performance is degraded due to larger path attenuation at those altitudes.

Besides from the performance evaluation, the derivations in Theorems 1 and 2 can be utilized to determine different constellation parameters for a desired performance criterion. For instance, in Table II, we illustrate the minimum number of satellites needed to provide a coverage probability of at least 0.9 for a noise-limited LEO network in three different cities. The inclination angle is assumed to be  $53^\circ$ . As the user gets closer to the inclination limits ( $53^\circ$ ), fewer satellites can provide the desired performance. Moreover, a larger constellation size is required for higher altitudes in order to compensate for the greater path loss. For Helsinki, being on

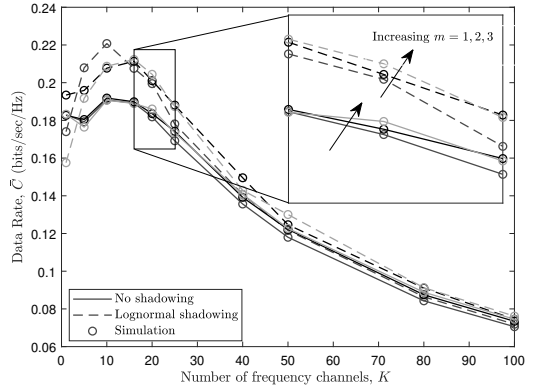


Fig. 6. Theorem 2 verification with simulations when  $\phi_u = 25^\circ$ ,  $\iota = 53^\circ$ ,  $m \in \{1, 2, 3\}$ , and  $\theta_{\min} = 10^\circ$ . The lines and the markers show the theoretical and simulation results, respectively.

TABLE II  
MINIMUM CONSTELLATION SIZE TO PROVIDE 90% COVERAGE  
PROBABILITY IN DIFFERENT CITIES

Cities	Helsinki ( $\phi_u \approx 60^\circ$ N)		Singapore ( $\phi_u \approx 1^\circ$ N)		Sydney ( $\phi_u \approx 34^\circ$ S)	
	Altitude (km)	Constellation size	Altitude (km)	Constellation size	Altitude (km)	Constellation size
	500	1500	500	1500	500	1500
	380	560	230	300	165	210

a higher latitude than the inclination angle, more satellites are required to achieve the same performance.

Figure 6 verifies the derivations for average data rate of a user at the latitude of  $25^\circ$ . As shown in the figure, the simulation results are perfectly in line with theoretical expressions in Theorem 2. The disparate behaviour of the curves is caused by the two opposite effects of frequency reuse on the average achievable rate. As the number of frequency bands increases, the total number of interfering satellites on the same frequency band declines which results in an increase in the data rate. On the other hand, by increasing the number of frequency channels, the bandwidth shared among a group of satellites is reduced. An increase in the plot is observed at first as a result of the decrease in interference received power, followed by a drop which is due to comprising only  $\frac{1}{K}$  of frequency band.

Figure 7, as a counterpart for Fig. 4, illustrates the variation of data rate over different latitudes when the intensity of Poisson point process is chosen to be according to Lemma 1 or, for comparison, Lemma 2. With intensity being as in Lemma 1, data rate varies over the different user's latitudes as shown in Fig. 7. For  $53^\circ$  inclined orbits, there is a minor decline in data rate which is followed by a sharp rise due to a decrease in the number of visible interfering satellites when the user leaves the inclination limits.

The effect of altitude on data rate is depicted in Fig. 8 for  $K = 10$ . Similar to Fig. 5, from the minimum altitude at which the user is able to visit at least one satellite, the data rate increases rapidly until reaches a maximum point. After

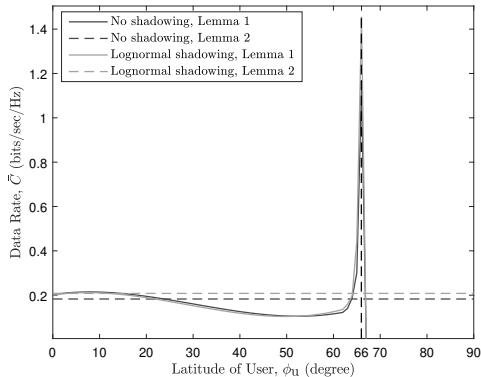


Fig. 7. Data rate on different users' latitudes,  $K = 10$ ,  $r_{\min} = 500$  km,  $\iota = 53^\circ$ ,  $m = 2$ , and  $\theta_{\min} = 10^\circ$ . The expression given in Theorem 2 is used to plot this figure.

the maximum point, the data rate decreases more slowly due to the increase in the number of interfering satellites as well as satellites being at a farther distance from the user. The altitude which maximizes the data rate varies with the user's latitude and, obviously, it has similar value which results in the maximum coverage probability.

## V. CONCLUSIONS

In this paper, a generic approach to obtain the analytical performance of a massive low Earth orbit network was presented by modeling the satellites' locations as a nonhomogeneous Poisson point process and utilizing the tools from stochastic geometry. The density of the nonhomogeneous Poisson point process is derived from the actual geometry of the constellation which enables us to take into account the non-uniform distribution of satellites across different latitudes. Our next step was to apply this model to derive analytical expressions for the coverage probability and average data rate of an arbitrarily located user in terms of the distribution of fading and shadowing as well as the Laplace function of interference. From the numerical results, we concluded that, depending on the shadowing parameters, the effect of shadowing on the network performance is ambivalent. Furthermore, we showed how the analytical results allow one to find — without involved orbital simulations — optimum values for altitude, the number of orthogonal frequency channels, and user's latitude which result in the largest coverage and/or throughput, given the constellation parameters.

## APPENDIX

### A. Proof of Lemma 3

For a NPPP, the CDF of  $R_0$  can be written as

$$F_{R_0}(r_0) = 1 - \mathbb{P}(R_0 > r_0) = 1 - \mathbb{P}(\mathcal{N} = 0), \quad (26)$$

where  $\mathbb{P}(\mathcal{N} = 0)$  is the void probability of PPP in  $\mathcal{A}(r_0)$  that can be obtained from (7) by setting  $n = 0$ . According to (7),

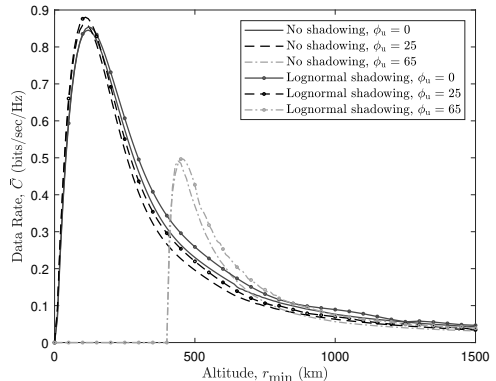


Fig. 8. Effect of altitude on data rate when  $K = 10$ ,  $\phi_u = \{0^\circ, 25^\circ, 65^\circ\}$ ,  $\iota = 53^\circ$ ,  $m = 2$ , and  $\theta_{\min} = 10^\circ$ . The expression given in Theorem 2 is used to plot this figure.

by integrating from the intensity over the spherical cap above the user, we have

$$\begin{aligned} F_{R_0}(r_0) &= 1 - \exp\left(-\int_{\max(\phi_u - \phi_0, -\iota)}^{\min(\phi_u + \phi_0, \iota)} \beta(\phi_s) \delta(\phi_s) (r_{\min} + r_{\oplus})^2 \cos(\phi_s) d\phi_s\right) \\ &\stackrel{(a)}{=} 1 - \exp\left(-2(r_{\min} + r_{\oplus})^2 \int_{\max(\phi_u - \phi_0, -\iota)}^{\min(\phi_u + \phi_0, \iota)} \delta(\phi_s) \cos(\phi_s) \right. \\ &\quad \left. \times \cos^{-1}\left(\frac{\cos(\phi_0)}{\cos(\phi_s - \phi_u)}\right) d\phi_s\right), \quad (27) \end{aligned}$$

where  $\beta(\phi_s)$  is the longitude range inside the spherical cap above the user at latitude  $\phi_s$ . Equality (a) follows from substitution of  $\beta(\phi_s)$  using the basic geometry. Taking the derivative of (27) with respect to  $r_0$  completes the proof of Lemma 3. Note that for  $\phi_0 \leq |\phi_u| - \iota$  the CDF given in (27) is zero since the spherical cap formed by polar angle  $\phi_0$  above the latitude  $\phi_u$  is much farther from the constellation's borders to contain any satellite.

### B. Proof of Theorem 1

To obtain the expression given (16), let us begin with the definition of coverage probability:

$$\begin{aligned} P_c(T) &= \mathbb{E}_{R_0}[\mathbb{P}(\text{SINR} > T | R_0)] \quad (28) \\ &= \int_{r_{\min}}^{r_{\max}} \mathbb{P}(\text{SINR} > T | R_0 = r_0) f_{R_0}(r_0) dr_0 \\ &= \int_{r_{\min}}^{r_{\max}} \mathbb{P}\left(\frac{p_t G_t(r_0) H_0 \mathcal{X}_0 r_0^{-\alpha}}{I + \sigma^2} > T\right) f_{R_0}(r_0) dr_0 \\ &= \int_{r_{\min}}^{r_{\max}} \mathbb{E}_I \left[ \mathbb{P}\left(H_0 \mathcal{X}_0 > \frac{T r_0^\alpha (I + \sigma^2)}{p_t G_t(r_0)} \mid I > 0\right) \right. \\ &\quad \left. \times f_{R_0}(r_0) dr_0. \right. \end{aligned}$$



Since satellites with elevation angles smaller than  $\theta_{\min}$  are not visible to the user, the integral has an upper limit. Then,

$$\begin{aligned}
P_c(T) & \stackrel{(a)}{=} \int_{r_{\min}}^{r_{\max}} \mathbb{E}_I \left[ \int_0^\infty f_{\mathcal{X}_0}(x_0) \left( 1 - F_{H_0} \left( \frac{Tr_0^\alpha (I + \sigma^2)}{p_t G_t(r_0) x_0} \right) \right) \right. \\
& \quad \left. \times f_{R_0}(r_0) dx_0 dr_0 \right] \\
& \stackrel{(b)}{=} \int_{r_{\min}}^{r_{\max}} \mathbb{E}_I \left[ \int_0^\infty f_{\mathcal{X}_0}(x_0) \left( \frac{\Gamma \left( m_0, m_0 \frac{Tr_0^\alpha (I + \sigma^2)}{p_t G_t(r_0) x_0} \right)}{\Gamma(m_0)} \right) \right. \\
& \quad \left. \times f_{R_0}(r_0) dx_0 dr_0 \right] \\
& \stackrel{(c)}{=} \int_{r_{\min}}^{r_{\max}} \int_0^\infty f_{\mathcal{X}_0}(x_0) f_{R_0}(r_0) e^{-\frac{m_0 Tr_0^\alpha \sigma^2}{p_t G_t(r_0) x_0}} \mathbb{E}_I \left[ e^{-\frac{m_0 Tr_0^\alpha I}{p_t G_t(r_0) x_0}} \right. \\
& \quad \left. \sum_{k=0}^{m_0-1} \frac{\sum_{l=0}^k \binom{k}{l} \left( m_0 \frac{Tr_0^\alpha \sigma^2}{p_t G_t(r_0) x_0} \right)^l \left( m_0 \frac{Tr_0^\alpha I}{p_t G_t(r_0) x_0} \right)^{k-l}}{k!} \right] dx_0 dr_0 \\
& = \int_{r_{\min}}^{r_{\max}} \int_0^\infty f_{\mathcal{X}_0}(x_0) f_{R_0}(r_0) \left[ e^{-s\sigma^2} \right. \\
& \quad \left. \sum_{k=0}^{m_0-1} \frac{\sum_{l=0}^k \binom{k}{l} (s\sigma^2)^l (-s)^{k-l} \frac{\partial^{k-l}}{\partial s^{k-l}} \mathcal{L}_I(s)}{k!} \right]_{s=\frac{m_0 Tr_0^\alpha}{p_t G_t(r_0) x_0}} dx_0 dr_0. \tag{29}
\end{aligned}$$

The substitution in (a) follows from the product distribution of two independent random variables, (b) follows from the distribution of gamma random variable  $H_0$  (being the square of the Nakagami random variable), and (c) is calculated by applying the incomplete gamma function for integer values of  $m_0$  to (b).

### C. Proof of Theorem 2

Most of the steps in derivation of the data rate expression, given in Theorem 2, are similar to those given in Appendix B. According to the definition of the average data rate given in (17), we have

$$\begin{aligned}
\bar{C} & = \mathbb{E}_{I, H_0, \mathcal{X}_0, R_0} [\log_2(1 + \text{SINR})] \\
& = \int_{r_{\min}}^{r_{\max}} \mathbb{E}_{I, H_0, \mathcal{X}_0} \left[ \log_2 \left( 1 + \frac{p_t G_t(r_0) H_0 \mathcal{X}_0 r_0^{-\alpha}}{\sigma^2 + I} \right) \right] f_{R_0}(r_0) dr_0 \\
& \stackrel{(a)}{=} \int_{r_{\min}}^{r_{\max}} \int_0^\infty \mathbb{E}_{I, H_0, \mathcal{X}_0} \left[ \mathbb{P} \left( \log_2 \left( 1 + \frac{p_t G_t(r_0) H_0 \mathcal{X}_0 r_0^{-\alpha}}{\sigma^2 + I} \right) > t \right) \right. \\
& \quad \left. \times f_{R_0}(r_0) dt dr_0 \right] \\
& = \int_{r_{\min}}^{r_{\max}} \int_0^\infty \mathbb{E}_{I, H_0, \mathcal{X}_0} \left[ \mathbb{P} \left( H_0 \mathcal{X}_0 > \frac{r_0^\alpha (\sigma^2 + I)}{p_t G_t(r_0)} (2^t - 1) \right) \right. \\
& \quad \left. \times f_{R_0}(r_0) dt dr_0 \right] \tag{30}
\end{aligned}$$

where (a) follows from the fact that for a positive random variable  $X$ ,  $\mathbb{E}[X] = \int_{t>0} \mathbb{P}(X > t) dt$ . Thus, we have

$$\begin{aligned}
\bar{C} & \stackrel{(a)}{=} \int_{r_{\min}}^{r_{\max}} \int_0^\infty \mathbb{E}_I \left[ \int_0^\infty f_{\mathcal{X}_0}(x_0) \right. \\
& \quad \left. \times \left( 1 - F_{H_0} \left( \frac{r_0^\alpha (I + \sigma^2) (2^t - 1)}{p_t G_t(r_0) x_0} \right) \right) dx_0 \right] f_{R_0}(r_0) dt dr_0 \\
& \stackrel{(b)}{=} \int_{r_{\min}}^{r_{\max}} \int_0^\infty \mathbb{E}_I \left[ \int_0^\infty f_{\mathcal{X}_0}(x_0) \right. \\
& \quad \left. \times \left( \frac{\Gamma \left( m_0, m_0 \frac{r_0^\alpha (I + \sigma^2) (2^t - 1)}{p_t G_t(r_0) x_0} \right)}{\Gamma(m_0)} \right) dx_0 \right] f_{R_0}(r_0) dt dr_0 \\
& \stackrel{(c)}{=} \int_{r_{\min}}^{r_{\max}} \int_0^\infty \int_0^\infty f_{\mathcal{X}_0}(x_0) f_{R_0}(r_0) e^{-\frac{m_0 (2^t - 1) r_0^\alpha \sigma^2}{p_t G_t(r_0) x_0}} \\
& \quad \times \mathbb{E}_I \left[ e^{-\frac{m_0 (2^t - 1) r_0^\alpha I}{p_t G_t(r_0) x_0}} \right. \\
& \quad \left. \sum_{k=0}^{m_0-1} \frac{\sum_{l=0}^k \binom{k}{l} \left( \frac{m_0 (2^t - 1) r_0^\alpha \sigma^2}{p_t G_t(r_0) x_0} \right)^l \left( \frac{m_0 (2^t - 1) r_0^\alpha I}{p_t G_t(r_0) x_0} \right)^{k-l}}{k!} \right] dt dx_0 dr_0 \\
& = \int_{r_{\min}}^{r_{\max}} \int_0^\infty \int_0^\infty f_{\mathcal{X}_0}(x_0) f_{R_0}(r_0) \left[ e^{-s\sigma^2} \right. \\
& \quad \left. \sum_{k=0}^{m_0-1} \frac{\sum_{l=0}^k \binom{k}{l} (s\sigma^2)^l (-s)^{k-l} \frac{\partial^{k-l}}{\partial s^{k-l}} \mathcal{L}_I(s)}{k!} \right]_{s=\frac{m_0 (2^t - 1) r_0^\alpha}{p_t G_t(r_0) x_0}} dt dx_0 dr_0. \tag{31}
\end{aligned}$$

Similar to the proof of Theorem 1, (a) follows from the product distribution of two independent random variables, (b) follows from the gamma distribution of serving channel gain  $H_0$ , and (c) is calculated by applying the incomplete gamma function for integer values of  $m_0$  to (b).

### D. Proof of Lemma 5

In this appendix, we derive the expression for Laplace function of interference assuming arbitrary distributions for fading and shadowing. Let us start with the definition of Laplace function for random variable  $I$  which is

$$\begin{aligned}
\mathcal{L}_I(s) & \triangleq \mathbb{E}_I [e^{-sI}] \\
& = \mathbb{E}_{\mathcal{N}, R_n, \mathcal{X}_n, H_n} \left[ \exp \left( -s \sum_{n \in \mathcal{E} \setminus \{s\}} p_t G_t(R_n) H_n \mathcal{X}_n R_n^{-\alpha} \right) \right] \\
& = \mathbb{E}_{\mathcal{N}, R_n, \mathcal{X}_n, H_n} \left[ \prod_{n \in \mathcal{E} \setminus \{s\}} \exp(-s p_t G_t(R_n) H_n \mathcal{X}_n R_n^{-\alpha}) \right]. \tag{32}
\end{aligned}$$

Due to i.i.d. distribution of  $H_n$  and  $\mathcal{X}_n$  as well as their independence from  $\mathcal{N}$  and  $R_n$ , we have

$$\mathcal{L}_I(s) = \mathbb{E}_{\mathcal{N}, R_n} \left[ \prod_{n \in \xi \setminus \{s\}} \mathbb{E}_{\mathcal{X}_n, H_n} \left[ \exp(-s p_t G_t(R_n) H_n \mathcal{X}_n R_n^{-\alpha}) \right] \right] \quad (33)$$

$$\stackrel{(a)}{=} \mathbb{E}_{\mathcal{N}} \left[ \prod_{n \in \xi \setminus \{s\}} \int_{r_0}^{r_{\max}} \mathbb{E}_{\mathcal{X}_n, H_n} \left[ \exp(-s p_t G_t(r_n) H_n \mathcal{X}_n r_n^{-\alpha}) \right] \times f_{R_n|R_0}(r_n|r_0) dr_n \right], \quad (34)$$

where (a) is obtained by taking the expectation over the random variable  $R_n$  conditioned on  $R_0$ . Then

$$\begin{aligned} \mathcal{L}_I(s) &\stackrel{(b)}{=} \sum_{n=0}^{\infty} P_n (\mathcal{A}(r_{\max}) - \mathcal{A}(r_0)) \\ &\times \left( \int_{r_0}^{r_{\max}} \mathbb{E}_{\mathcal{X}_n, H_n} \left[ \exp(-s p_t G_t(r_n) H_n \mathcal{X}_n r_n^{-\alpha}) \right] \right. \\ &\quad \left. \times f_{R_n|R_0}(r_n|r_0) dr_n \right)^n \\ &\stackrel{(c)}{=} \sum_{n=0}^{\infty} P_n (\mathcal{A}(r_{\max}) - \mathcal{A}(r_0)) \\ &\times \left( \int_{r_0}^{r_{\max}} \int_0^{\infty} \mathcal{L}_{H_n}(s p_t G_t(r_n) x_n r_n^{-\alpha}) \right. \\ &\quad \left. \times f_{\mathcal{X}_n}(x_n) f_{R_n|R_0}(r_n|r_0) dx_n dr_n \right)^n, \end{aligned} \quad (35)$$

where  $\mathcal{A}(r_{\max}) - \mathcal{A}(r_0)$  indicates the region above the user where satellites which are more distanced from the user than the serving satellite exist, (b) is obtained by taking the average over the Poisson random variable  $\mathcal{N}$ , and applying the law of total expectation on independent random variables  $H_n$  and  $\mathcal{X}_n$  results in (c).

## REFERENCES

- [1] M. Giordani and M. Zorzi, "Non-terrestrial networks in the 6G era: Challenges and opportunities," *IEEE Network*, vol. 35, no. 2, pp. 244–251, Mar. 2021.
- [2] Z. Jia, M. Sheng, J. Li, D. Zhou, and Z. Han, "Joint HAP access and LEO satellite backhaul in 6G: Matching game-based approaches," *IEEE Journal on Selected Areas in Communications*, vol. 39, no. 4, pp. 1147–1159, Apr. 2021.
- [3] M. Giordani and M. Zorzi, "Satellite communication at millimeter waves: a key enabler of the 6G era," in *Proc. International Conference on Computing, Networking and Communications*, Feb. 2020.
- [4] M. Giordani, M. Polese, M. Mezzavilla, S. Rangan, and M. Zorzi, "Toward 6G networks: Use cases and technologies," *IEEE Communications Magazine*, vol. 58, no. 3, pp. 55–61, Mar. 2020.
- [5] J. L. Grubb, "The traveler's dream come true," *IEEE Communications Magazine*, vol. 29, no. 11, pp. 48–51, Nov. 1991.
- [6] A. Mokhtar and M. Azizoglu, "On the downlink throughput of a broadband LEO satellite network with hopping beams," *IEEE Communications Letters*, vol. 4, no. 12, pp. 390–393, Dec. 2000.
- [7] F. Vatalaro, G. E. Corazza, C. Caini, and C. Ferrarelli, "Analysis of LEO, MEO, and GEO global mobile satellite systems in the presence of interference and fading," *IEEE Journal on Selected Areas in Communications*, vol. 13, no. 2, pp. 291–300, Feb. 1995.
- [8] A. Ganz, Y. Gong, and B. Li, "Performance study of low Earth-orbit satellite systems," *IEEE Transactions on Communications*, vol. 42, no. 234, pp. 1866–1871, Feb. 1994.
- [9] I. Ali, N. Al-Dhahir, and J. E. Hershey, "Predicting the visibility of LEO satellites," *IEEE Transactions on Aerospace and Electronic Systems*, vol. 35, no. 4, pp. 1183–1190, Oct. 1999.
- [10] Y. Seyedi and S. M. Safavi, "On the analysis of random coverage time in mobile LEO satellite communications," *IEEE Communications Letters*, vol. 16, no. 5, pp. 612–615, May 2012.
- [11] Z. Qu, G. Zhang, H. Cao, and J. Xie, "LEO satellite constellation for Internet of Things," *IEEE Access*, vol. 5, pp. 18 391–18 401, Sep. 2017.
- [12] M. Haenggi, *Stochastic geometry for wireless networks*. Cambridge University Press, 2012.
- [13] B. Błaszczyszyn, M. Haenggi, P. Keeler, and S. Mukherjee, *Stochastic geometry analysis of cellular networks*. Cambridge University Press, 2018.
- [14] M. Haenggi, J. G. Andrews, F. Baccelli, O. Dousse, and M. Franceschetti, "Stochastic geometry and random graphs for the analysis and design of wireless networks," *IEEE Journal on Selected Areas in Communications*, vol. 27, no. 7, pp. 1029–1046, Sep. 2009.
- [15] H. ElSawy, E. Hossain, and M. Haenggi, "Stochastic geometry for modeling, analysis, and design of multi-tier and cognitive cellular wireless networks: A survey," *IEEE Communications Surveys and Tutorials*, vol. 15, no. 3, pp. 996–1019, Jun. 2013.
- [16] J. G. Andrews, F. Baccelli, and R. K. Ganti, "A tractable approach to coverage and rate in cellular networks," *IEEE Transactions on Communications*, vol. 59, no. 11, pp. 3122–3134, Nov. 2011.
- [17] H. S. Dhillon, R. K. Ganti, F. Baccelli, and J. G. Andrews, "Modeling and analysis of k-tier downlink heterogeneous cellular networks," *IEEE Journal on Selected Areas in Communications*, vol. 30, no. 3, pp. 550–560, Apr. 2012.
- [18] D. Cao, S. Zhou, and Z. Niu, "Optimal combination of base station densities for energy-efficient two-tier heterogeneous cellular networks," *IEEE Transactions on Wireless Communications*, vol. 12, no. 9, pp. 4350–4362, Sep. 2013.
- [19] H. S. Dhillon, T. D. Novlan, and J. G. Andrews, "Coverage probability of uplink cellular networks," in *Proc. IEEE Global Communications Conference*, Dec. 2012.
- [20] M. Afshang and H. S. Dhillon, "Fundamentals of modeling finite wireless networks using binomial point process," *IEEE Transactions on Wireless Communications*, vol. 16, no. 5, pp. 3355–3370, May 2017.
- [21] Z. Pan and Q. Zhu, "Modeling and analysis of coverage in 3-D cellular networks," *IEEE Communications Letters*, vol. 19, no. 5, pp. 831–834, May 2015.
- [22] V. V. Chetlur and H. S. Dhillon, "Downlink coverage analysis for a finite 3-D wireless network of unmanned aerial vehicles," *IEEE Transactions on Communications*, vol. 65, no. 10, pp. 4543–4558, Oct. 2017.
- [23] S. Srinivasa and M. Haenggi, "Distance distributions in finite uniformly random networks: Theory and applications," *IEEE Transactions on Vehicular Technology*, vol. 59, no. 2, pp. 940–949, Feb. 2010.
- [24] J. Guo, S. Durrani, and X. Zhou, "Outage probability in arbitrarily-shaped finite wireless networks," *IEEE Transactions on Communications*, vol. 62, no. 2, pp. 699–712, Feb. 2014.
- [25] Z. Khalid and S. Durrani, "Distance distributions in regular polygons," *IEEE Transactions on Vehicular Technology*, vol. 62, no. 5, pp. 2363–2368, Jun. 2013.
- [26] X. Wang, H. Zhang, Y. Tian, and V. C. M. Leung, "Modeling and analysis of aerial base station-assisted cellular networks in finite areas under LoS and NLoS propagation," *IEEE Transactions on Wireless Communications*, vol. 17, no. 10, pp. 6985–7000, Oct. 2018.
- [27] J. Guo, S. Durrani, and X. Zhou, "Performance analysis of arbitrarily-shaped underlay cognitive networks: Effects of secondary user activity protocols," *IEEE Transactions on Communications*, vol. 63, no. 2, pp. 376–389, Feb. 2015.
- [28] T. A. Khan and M. Afshang, "A stochastic geometry approach to Doppler characterization in a LEO satellite network," in *Proc. IEEE International Conference on Communications*, Jul. 2020.
- [29] J. Hu, G. Li, D. Bian, L. Gou, and C. Wang, "Optimal power control for cognitive LEO constellation with terrestrial networks," *IEEE Communications Letters*, vol. 24, no. 3, pp. 622–625, Mar. 2020.
- [30] J. Zhang, B. Evans, M. A. Imran, X. Zhang, and W. Wang, "Performance analysis of C/U split hybrid satellite terrestrial network for 5G systems," in *Proc. 20th IEEE International Workshop on Computer Aided Modelling and Design of Communication Links and Networks*, Sep. 2015.

- [31] A. J. Roumeliotis, C. I. Kourgiorgas, and A. D. Panagopoulos, "Optimal dynamic capacity allocation for high throughput satellite communications systems," *IEEE Wireless Communications Letters*, vol. 8, no. 2, pp. 596–599, Apr. 2019.
- [32] A. K. Dwivedi, S. P. Chokkarapu, S. Chaudhari, and N. Varshney, "Performance analysis of novel direct access schemes for LEO satellites based IoT network," in *Proc. IEEE 31st Annual International Symposium on Personal, Indoor and Mobile Radio Communications*, Sep. 2020.
- [33] N. Okati, T. Riihonen, D. Korpi, I. Angervuori, and R. Wichman, "Downlink coverage and rate analysis of low Earth orbit satellite constellations using stochastic geometry," *IEEE Transactions on Communications*, vol. 68, no. 8, pp. 5120–5134, Aug. 2020.
- [34] N. Okati and T. Riihonen, "Stochastic analysis of satellite broadband by mega-constellations with inclined LEOs," in *Proc. IEEE 31st Annual International Symposium on Personal, Indoor and Mobile Radio Communications*, Sep. 2020.
- [35] —, "Modeling and analysis of LEO mega-constellations as nonhomogeneous Poisson point processes," in *Proc. IEEE 93rd Vehicular Technology Conference*, Apr. 2021.
- [36] A. Al-Hourani, "An analytic approach for modeling the coverage performance of dense satellite networks," *IEEE Wireless Communications Letters*, vol. 10, no. 4, pp. 897–901, Apr. 2021.
- [37] —, "Optimal satellite constellation altitude for maximal coverage," *IEEE Wireless Communications Letters*, vol. 10, no. 7, pp. 1444–1448, Mar. 2021.
- [38] A. Talgat, M. A. Kishk, and M.-S. Alouini, "Nearest neighbor and contact distance distribution for binomial point process on spherical surfaces," *IEEE Communications Letters*, vol. 24, no. 12, pp. 2659–2663, Dec. 2020.
- [39] —, "Stochastic geometry-based analysis of LEO satellite communication systems," *IEEE Communications Letters*, vol. 25, no. 8, pp. 2458–2462, Oct. 2020.
- [40] A. Yastrebova, I. Angervuori, N. Okati, M. Vehkaperä, M. Höyhty, R. Wichman, and T. Riihonen, "Theoretical and simulation-based analysis of terrestrial interference to LEO satellite uplinks," in *Proc. IEEE Global Communications Conference*, Dec. 2020.
- [41] Z. Khalid and S. Durrani, "Connectivity of three dimensional wireless sensor networks using geometrical probability," in *Proc. Australian Communications Theory Workshop (AusCTW)*, May 2013.
- [42] P. Series, "Attenuation by atmospheric gases and related effects," *Recommendation ITU-R*, pp. 676–12, Aug. 2019.
- [43] I. del Portillo, B. G. Cameron, and E. F. Crawley, "A technical comparison of three low Earth orbit satellite constellation systems to provide global broadband," *Acta Astronautica*, vol. 159, pp. 123–135, Jun. 2019, available online: <https://www.sciencedirect.com/science/article/pii/S0094576518320368>.
- [44] I. S. Gradshteyn and I. M. Ryzhik, *Table of Integrals, Series, and Products*. Academic Press, 2014.



**Taneli Riihonen** (S'06–M'14) received the D.Sc. degree in electrical engineering (with distinction) from Aalto University, Helsinki, Finland, in August 2014. He is currently an Assistant Professor (tenure track) at the Faculty of Information Technology and Communication Sciences, Tampere University, Finland. He held various research positions at Aalto University School of Electrical Engineering from September 2005 through December 2017. He was a Visiting Associate Research Scientist and an Adjunct Assistant Professor at Columbia University in the City of New York, USA, from November 2014 through December 2015. He has been nominated eleven times as an Exemplary/Top Reviewer of various IEEE journals and is serving as an Editor for IEEE WIRELESS COMMUNICATIONS LETTERS since May 2017. He has previously served as an Editor for IEEE COMMUNICATIONS LETTERS from October 2014 through January 2019. He received the Finnish technical sector's award for the best doctoral dissertation in 2014 and the EURASIP Best PhD Thesis Award 2017. His research activity is focused on physical-layer OFDM(A), multiantenna, relaying and full-duplex wireless techniques with current interest in the evolution of beyond 5G systems.



**Niloofar Okati** received the B.Sc. degree in electrical engineering from Shiraz University of Technology, Iran, in 2013, and M.Sc. degree in communications engineering from Iran University of Science and Technology (IUST), Iran, in 2016. She is currently a Ph.D. researcher at the Faculty of Information Technology and Communication Sciences, Tampere University, Finland. Her research interests include stochastic geometry, wireless communication and satellite networks. She was one of the 200 young researchers in mathematics and computer

science selected worldwide to participate in the 7th Heidelberg Laureate Forum (HLF), in 2019.



## **PUBLICATION 5**

**Coverage and Rate Analysis of Mega-Constellations Under Generalized  
Serving Satellite Selection**

**N. Okati and T. Riihonen**

*In Proc. IEEE Wireless Communications and Networking Conference (WCNC), Apr. 2022*

**Publication reprinted with the permission of the copyright holders.**



# Coverage and Rate Analysis of Mega-Constellations Under Generalized Serving Satellite Selection

Niloofer Okati and Taneli Riihonen

Faculty of Information Technology and Communication Sciences, Tampere University, Finland

e-mail: {niloofer.okati, taneli.riihonen}@tuni.fi

**Abstract**—The dream of having ubiquitous and high-capacity connectivity is coming true by emerging low Earth orbit (LEO) Internet constellations through several commercial plans, e.g., Starlink, Telesat, and OneWeb. The analytical understanding of these networks is crucial for accurate network assessment and, consequently, acceleration in their design and development. In this paper, we derive the coverage probability and the data rate of a massive LEO network under arbitrarily distributed fading and shadowing. The conventional user association techniques, based on the shortest distance between the ground terminal and the satellite, result in a suboptimal performance of the network since the signal from the nearest server may be subject to severe shadowing due to the blockage by nearby obstacles surrounding the ground terminal. Thus, we take into account the effect of shadowing on the serving satellite selection by assigning the ground terminal to the satellite which provides the highest signal-to-noise ratio at the terminal's place, resulting in a more generalized association technique, namely the best server policy (BSP). To maintain tractability of our derivations and consider the latitude-dependent distribution of satellites, we model the satellites as a nonhomogeneous Poisson point process. The numerical results reveal that implementing the BSP for serving satellite selection leads to significantly better performance compared to the conventional nearest server policy (NSP).

## I. INTRODUCTION

Low Earth orbit (LEO) Internet constellations are gaining increasing popularity all around the world due to providing seamless connectivity, especially for isolated regions where deployment of terrestrial networks is not economically feasible or for countries with restricted access to Internet. To keep pace with the commercial progress of LEO networks and accelerate their development, analytical modeling and understanding of these networks — without time consuming and network-specific orbital simulations — are of great importance.

Although several aspects of massive LEO constellations have been investigated recently in the literature [1]–[10], little attention was paid to the effect of shadowing on the selection of the serving satellite, which noticeably affects the network performance. The server association used in the literature is based on the shortest distance, i.e., the so-called the *nearest server policy* (NSP), which is the most simplistic association technique and is rarely used in practice since it is unable to include the effect of the large-scale attenuation, i.e., shadowing, on the variation of the received signal. In this work, we will implement the more realistic association technique, the *best server policy* (BSP), which includes the shadowing effect on the serving satellite selection by assigning

the ground terminal to a satellite that provides the highest signal-to-noise ratio (SNR) at the terminal's place.

The best server policy is frequently used to evaluate the performance of terrestrial networks [11]–[13], and proved to provide more reliable network performance. Moreover, the best server policy is more in line with practical association techniques since, in reality, the SNR at the receiver is a major criterion to determine the server [13].

The literature on LEO network analysis has been mostly limited to simulation-based deterministic analyses [14]–[16] until recently that the application of stochastic geometry and statistical models for tractable analysis of massive wireless networks [17]–[22] was extended to LEO networks' analysis. Utilization of stochastic geometry enables characterization of the serving distance which is a key parameter in performance evaluation of these networks. However, the serving distance for analytical modeling of LEO networks is mostly assumed to be the shortest distance between the user and the satellites.

In [1], we derived the coverage probability and the data rate of a massive LEO network in presence of co-channel interference by modeling the network as a binomial point process (BPP). Since the satellites' locations in actual constellations barely follow a uniform distribution, we adjusted the inherent performance mismatch numerically in [1]. The mismatch was also compensated in [2] and [3] through analytically finding the effective number of satellites for every user's latitude and modeling the network as a nonhomogeneous Poisson point process (PPP) with a latitude-dependent intensity, respectively. Unlike [1], [2], shadowing was included in the propagation model in [3], but it had no effect on the association rule and the user connects to its nearest satellite. A more generalized system model was studied by inclusion of interference in [4].

The contact angle, i.e., the minimum angular distance between the satellites and the user, is characterized in [5] to evaluate the performance of a LEO network without considering the effect of shadowing attenuation. The results were then used in [6] to find the altitude that maximizes coverage probability. The uplink performance of a LEO network in presence of terrestrial interferers was characterized in [7]. In [10], the distribution of conditional coverage probability was derived, given the nodes' positions, for a satellite–terrestrial relay network in order to evaluate the percentage of ground users that may reach a target SINR threshold.

In [8], essential distance distributions were formulated for LEO networks assuming satellites are distributed on multiple

concentric spheres, each of which has a known specific radius. The results were then used to analyze the coverage probability in [9] when satellite gateways relay the data between the satellites and the terrestrial users. Despite assuming shadowed Rician channels in [9], [10], they had no effect on the contact distances.

According to the literature review, the best server policy has not yet been characterized for analytical evaluation of LEO networks, in spite of the fact that it is the most frequently used association technique in practice. Moreover, the shadowing effect, which enables the characterization of the best server policy, was not considered in most of the literature.

In this paper, we formulate new analytical expressions to evaluate the coverage probability and rate of a LEO network, assuming that the server is selected based on the best server policy. Including shadowing in the propagation model, we assume that the ground terminal associates with the satellite that provides the highest received SNR for the terminal. We corroborate our derivations through Monte Carlo simulations, and compare them with the conventional nearest server policy, which was presented in [3]. As our numerical results illustrate, the best server policy results in significantly better performance in both coverage probability and data rate compared with the nearest server policy.

The remainder of this paper is organized as follows. Section II introduces the studied system model and the mathematical preliminaries to model a LEO network as a nonhomogeneous PPP. Distance distributions required to characterize the coverage probability and the data rate of a LEO network are presented in Section III. The numerical results are provided in Section IV. Finally, the paper is concluded in Section V.

## II. SYSTEM MODEL

In this section, firstly, we describe the actual LEO constellation that will be studied in this paper. Secondly, we present the (re)modeled nonhomogeneous PPP which not only captures all the characteristics of the actual physical network, but also enables us to tractably analyze and derive the network performance metrics. One should note that the study holds for both downlink and uplink directions equivalently although some of the following system aspects are specified from the downlink perspective for simplicity.

The actual network studied in this paper is a massive LEO Internet constellation, as shown in Fig. 1, consisting of  $N$  satellites which are distributed uniformly on circular orbits at a given altitude,  $r_{\min}$ . The orbital planes are all inclined to an angle, denoted by  $\iota$ . The ground terminals (GTs), i.e., users and/or gateways, are located on Earth's surface at an arbitrary latitude denoted by  $\phi_u$ . Earth is assumed to be a perfect sphere with radius  $r_{\oplus} \approx 6371$  km.

A satellite is visible to a ground terminal, i.e., it can receive from or transmit to it, if it is elevated above the user's horizon to a minimum angle of  $\theta_{\min}$ . The distances from the satellites to the ground terminal, their corresponding channel gains, and the shadowing coefficients are denoted by  $R_n$ ,  $G_n$ , and  $\mathcal{X}_n$ , where  $n = 0, 1, \dots, N - 1$ . Throughout the paper, we reserve

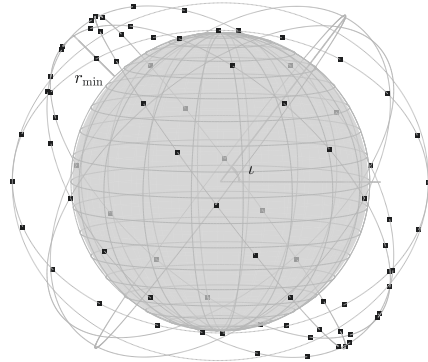


Fig. 1. A LEO constellation in an example case of  $N = 1000$  satellites flying on  $\iota = 53^\circ$  inclined orbits at  $r_{\min} = 1800$  km. Only 6 example orbital planes are shown for clarity.

index zero for the serving link, i.e.,  $R_0$ ,  $G_0$ , and  $\mathcal{X}_0$  represent the distance to the server, its corresponding fading gain and its shadowing coefficient, respectively. A satellite and GT may be able to communicate only if  $R_n \leq r_{\max}$ , where  $r_{\max}$  is the distance between the satellite and GT when the satellite is at the minimum elevation angle, i.e.,  $\theta_{\min}$ . Obviously,  $r_{\max}$  is a function of  $\theta_{\min}$  and is given as [3]

$$\frac{r_{\max}}{r_{\oplus}} = \sqrt{\frac{r_{\min}}{r_{\oplus}} \left( \frac{r_{\min}}{r_{\oplus}} + 2 \right) + \sin^2(\theta_{\min})} - \sin(\theta_{\min}). \quad (1)$$

The signal-to-noise ratio at the receiver, based on the above system model, can be expressed as

$$\text{SNR} = \begin{cases} \frac{p_s G_0 \mathcal{X}_0 R_0^{-\alpha}}{\sigma^2}, & R_0 \leq r_{\max}, \\ 0, & \text{otherwise,} \end{cases} \quad (2)$$

where  $p_s$  is the constant transmission power. The parameter  $\alpha = 2$  is a path loss exponent and the power of the additive noise is denoted by  $\sigma^2$ .

In this paper, we implement the best server policy to select the serving satellite. Accordingly, the serving satellite will be the one which provides the strongest SNR for the receiver. Since fading coefficients,  $G_n$ , vary quickly over the time, we assume that they have no effect on the association technique. Therefore, when implementing the best server policy, the serving link must satisfy the following equation:

$$\mathcal{X}_0^{-\frac{1}{\alpha}} R_0 = \min_n \left( \mathcal{X}_n^{-\frac{1}{\alpha}} R_n \mid R_n < r_{\max} \right). \quad (3)$$

We then remodel the actual network, described earlier, as a nonhomogeneous PPP which allows us to take into account the varying density of satellites along different latitudes while maintaining the tractability of our derivations [3]. Ergo, we assume that the satellites are distributed according to a nonhomogeneous PPP, on a spherical shell with radius  $r_{\oplus} + r_{\min}$ .



By the definition of a nonhomogeneous PPP, the number of points in some bounded region  $\mathcal{A}$  of the orbital shell is a Poisson-distributed random variable denoted by  $\mathcal{N}$ . Thereby, the probability to have  $n$  satellites in  $\mathcal{A}$  is given by

$$\begin{aligned} P_n(\mathcal{A}) &\triangleq \mathbb{P}(\mathcal{N} = n) \\ &= \frac{1}{n!} \left( \iint_{\mathcal{A}} \delta(\phi_s, \lambda_s) (r_{\min} + r_{\oplus})^2 \cos(\phi_s) d\phi_s d\lambda_s \right)^n \\ &\times \exp \left( - \iint_{\mathcal{A}} \delta(\phi_s, \lambda_s) (r_{\min} + r_{\oplus})^2 \cos(\phi_s) d\phi_s d\lambda_s \right), \end{aligned} \quad (4)$$

where  $\delta(\phi_s, \lambda_s)$  is the intensity function of nonhomogeneous PPP at latitude  $\phi_s$  and longitude  $\lambda_s$ . Based on the given system model,  $\mathcal{A}$  is any spherical cap in the area where visible satellites to the user exist.

The intensity of nonhomogeneous PPP, when satellites are distributed uniformly on inclined low Earth orbits, is a function the satellites' latitudinal element,  $\phi_s$ , which is characterized in [3] as

$$\begin{aligned} \delta(\phi_s, \lambda_s) &= \delta(\phi_s) \\ &= \frac{N}{\sqrt{2\pi^2} (r_{\min} + r_{\oplus})^2 \sqrt{\cos(2\phi_s) - \cos(2\iota)}}. \end{aligned} \quad (5)$$

As implied above, the intensity is inherently independent of the satellites' longitudinal element,  $\lambda_s$ .

### III. PERFORMANCE ANALYSIS

In this section, we find mathematical expressions for the coverage probability and the data rate of the described LEO constellation under the best server policy. Modeling the satellites locality as a nonhomogeneous PPP, we are able to find the distance distributions, in terms of their cumulative distribution function (CDF) and probability density function (PDFs), which will contribute to arriving at our main derivations in this paper, i.e., coverage probability and data rate.

#### A. Distance Distributions

In the following lemma, we derive the distribution of the distance from the user to any visible satellite,  $R_n^{\text{vis}}$ , in terms of its CDF.

**Lemma 1.** *The CDF of the distance from any visible satellite in the constellation  $R_n^{\text{vis}}$  to the ground terminal is given by*

$$\begin{aligned} F_{R_n^{\text{vis}}}(r_n) &\triangleq \mathbb{P}(R_n < r_n | R_n < r_{\max}) \\ &= \frac{\iint_{\mathcal{A}(r_n)} \delta(\phi_s, \lambda_s) (r_{\min} + r_{\oplus})^2 \cos(\phi_s) d\phi_s d\lambda_s}{\iint_{\mathcal{A}(r_{\max})} \delta(\phi_s, \lambda_s) (r_{\min} + r_{\oplus})^2 \cos(\phi_s) d\phi_s d\lambda_s} \end{aligned} \quad (6)$$

for  $r_{\min} \leq r_n \leq r_{\max}$ .  $\mathcal{A}(r_n)$  and  $\mathcal{A}(r_{\max})$  are the cap area where all satellites therein have a distance less than or equal to  $r_n$  and  $r_{\max}$  to the GT, respectively.

*Proof.* The CDF of the distance from any visible satellite to the GT is equal to the CDF of surface integral of  $\delta(\phi_s, \lambda_s)$  over the spherical cap  $\mathcal{A}(r_n)$ . Conditioning on the visibility, the CDF is trivially calculated as in (6).  $\square$

**Corollary 1.** *The CDF of  $R_n^{\text{vis}}$ , when the satellites are distributed according to a nonhomogeneous PPP with a latitude-dependent intensity,  $\delta(\phi_s)$ , is*

$$\begin{aligned} F_{R_n^{\text{vis}}}(r_n) &= \frac{\int_{\max(\phi_u - \theta(r_n), -\iota)}^{\min(\phi_u + \theta(r_n), \iota)} \delta(\phi_s) \cos(\phi_s) \cos^{-1} \left( \frac{\cos(\theta)}{\cos(\phi_s - \phi_u)} \right) d\phi_s}{\int_{\max(\phi_u - \theta(r_{\max}), -\iota)}^{\min(\phi_u + \theta(r_{\max}), \iota)} \delta(\phi_s) \cos(\phi_s) \cos^{-1} \left( \frac{\cos(\theta)}{\cos(\phi_s - \phi_u)} \right) d\phi_s}, \end{aligned} \quad (7)$$

where  $\theta(r) = \cos^{-1} \left( 1 - \frac{r^2 - r_{\min}^2}{2(r_{\min} + r_{\oplus})r_{\oplus}} \right)$  is the polar angle difference between a satellite and the ground terminal.

*Proof.* Corollary is obtained by calculating the longitude range inside the spherical cap and with the aid of the basic geometry (for more details see [3, Lemma 2]), and substitution in Lemma 1.  $\square$

Considering the effect of shadowing on BSP association, let us define  $\tilde{R}_0 \triangleq \min_n \mathcal{X}_n^{-\frac{1}{\alpha}} R_n^{\text{vis}}$  as the nearest effective distance from the visible satellites to the user. The following lemma gives the PDF distribution of  $\tilde{R}_0$ .

**Lemma 2.** *The PDF of the nearest effective distance  $\tilde{R}_0$  is given by*

$$\begin{aligned} f_{\tilde{R}_0}(\tilde{r}_0) &= \sum_{n=0}^{\infty} n P_n(\mathcal{A}(r_{\max})) \\ &\times \int_0^{\infty} \alpha z_n^{-\alpha-1} f_{\mathcal{X}_n}(z_n^{-\alpha}) F_{R_n^{\text{vis}}}\left(\frac{\tilde{r}_0}{z_n}\right) dz_n \\ &\times \left( 1 - \int_0^{\infty} \alpha z_n^{-\alpha-1} f_{\mathcal{X}_n}(z_n^{-\alpha}) F_{R_n^{\text{vis}}}\left(\frac{\tilde{r}_0}{z_n}\right) dz_n \right)^{n-1}, \end{aligned} \quad (8)$$

where the PDF of the random variable  $\mathcal{Z}_n \triangleq \mathcal{X}_n^{-\frac{1}{\alpha}}$  is evaluated at point  $z_n$ .

*Proof.* See Appendix A.  $\square$

If satellites were distributed according to a homogeneous PPP with constant density  $\delta = \frac{N}{4\pi(r_{\min} + r_{\oplus})^2}$ , the distribution of the nearest effective distance would be simplified as in the following lemma. This requires compensating for the density mismatch by replacing  $N$  by the effective number of satellites.

**Lemma 3.** *The PDF of the nearest effective distance  $\tilde{R}_0$  when the satellites are distributed uniformly with constant intensity,  $\tilde{\delta} = \frac{N}{4\pi(r_{\min} + r_{\oplus})^2}$ , is*

$$\begin{aligned} f_{\tilde{R}_0}(\tilde{r}_0) &= \sum_{n=0}^{\infty} \frac{1}{(n-1)!} \left( \frac{\delta\pi (r_{\max}^2 - r_{\min}^2)}{1 - \frac{r_{\min}^2}{r_{\oplus} + r_{\min}}} \right)^n \\ &\times \exp \left( - \frac{\delta\pi (r_{\max}^2 - r_{\min}^2)}{1 - \frac{r_{\min}^2}{r_{\oplus} + r_{\min}}} \right) \\ &\times \left( 1 - \int_0^{\infty} \alpha z_n^{-\alpha-1} f_{\mathcal{X}_n}(z_n^{-\alpha}) \left( \frac{\left( \frac{\tilde{r}_0}{z_n} \right)^2 - r_{\min}^2}{r_{\max}^2 - r_{\min}^2} \right) dz_n \right)^{n-1} \\ &\times \int_0^{\infty} \alpha z_n^{-\alpha-3} f_{\mathcal{X}_n}(z_n^{-\alpha}) \left( \frac{2\tilde{r}_0 - r_{\min}^2}{r_{\max}^2} \right) dz_n. \end{aligned} \quad (9)$$

TABLE I  
SIMULATION PARAMETERS

Parameters	Values
Path loss exponent, $\alpha$	2
Rician factor, $K$	10
Transmit power, $p_s$	50 dBm
Noise power, $\sigma^2$	-120 dBm
Frequency	13.5 GHz
Mean and standard deviation of lognormal distribution: $\mu_s, \sigma_s$	0 dB, 9 dB

*Proof.* Since the intensity function  $\delta$  is constant,  $P_n(\mathcal{A}(r_{\max}))$  is obtained simply by multiplying  $\delta$  by the surface of the spherical cap,  $\mathcal{A}(r_{\max})$ , where the visible satellites can reside. Using Lemma 1, we have  $F_{R_n^{\text{vis}}}\left(\frac{\tilde{r}_0}{z_n}\right) = \frac{\mathcal{A}\left(\frac{\tilde{r}_0}{z_n}\right)}{\mathcal{A}(r_{\max})} = \frac{\left(\frac{\tilde{r}_0}{z_n}\right)^2 - r_{\min}^2}{r_{\max}^2 - r_{\min}^2}$ , since the density is constant over the spherical shell.  $\square$

### B. Coverage Probability

In this subsection, we utilize the distance distributions obtained in the previous section to derive the coverage probability of a LEO constellation for an arbitrarily located ground terminal under the best server policy. The coverage probability is the probability of having a greater SNR than a minimum threshold,  $T > 0$ , at the receiver. In other words, whenever the received SNR is above the threshold level, the receiver is considered to be within the coverage and the data is transmitted successfully.

**Proposition 1.** *The probability of network coverage for an arbitrarily located GT, under generally distributed fading and shadowing as well as BSP association is*

$$P_c(T) \triangleq \mathbb{P}(\text{SNR} > T) = \int_0^\infty \left(1 - F_{G_0}\left(\frac{T\tilde{r}_0^\alpha \sigma^2}{p_s}\right)\right) f_{\tilde{R}_0}(\tilde{r}_0) d\tilde{r}_0, \quad (10)$$

where  $F_{G_0}(\cdot)$  is the CDF of the channel gain  $G_0$  and  $f_{\tilde{R}_0}(\tilde{r}_0)$  is given in Lemmas 2 and 3.

*Proof.* To obtain (10), we start with the definition of coverage probability:

$$\begin{aligned} P_c(T) &= \mathbb{E}_{\tilde{R}_0} \left[ \mathbb{P}(\text{SNR} > T | \tilde{R}_0) \right] \\ &= \int_0^\infty \mathbb{P}(\text{SNR} > T | \tilde{R}_0 = \tilde{r}_0) f_{\tilde{R}_0}(\tilde{r}_0) d\tilde{r}_0 \\ &= \int_0^\infty \mathbb{P}\left(G_0 > \frac{T\tilde{r}_0^\alpha \sigma^2}{p_s}\right) f_{\tilde{R}_0}(\tilde{r}_0) d\tilde{r}_0, \end{aligned} \quad (11)$$

The proof is completed by substituting the complementary CDF of  $G_0$ .  $\square$

Note that the effect of the shadowing distribution in the coverage probability is embedded in the PDF of the nearest effective distance,  $f_{\tilde{R}_0}(\tilde{r}_0)$ , given in Lemmas 2 and 3.

### C. Average Data Rate

Let us then turn to the average achievable data rate (in bits per channel use), which states the ergodic capacity derived

from the Shannon–Hartley theorem over a fading communication link normalized to unit bandwidth.

**Proposition 2.** *The average rate (in bits/s/Hz) of an arbitrarily located GT, under BSP association, and generally distributed fading and shadowing is*

$$\begin{aligned} \bar{C} &\triangleq \mathbb{E}[\log_2(1 + \text{SNR})] = \\ &= \int_0^\infty \int_0^\infty \log_2\left(1 + \frac{p_s g_0 \tilde{r}_0^{-\alpha}}{\sigma^2}\right) f_{G_0}(g_0) f_{\tilde{R}_0}(\tilde{r}_0) dg_0 d\tilde{r}_0, \end{aligned} \quad (12)$$

where  $f_{G_0}(g_0)$  represents the PDF of channel gain  $G_0$  and  $f_{\tilde{R}_0}(\tilde{r}_0)$  is given in Lemmas 2 and 3.

*Proof.* Taking the expectation over the serving distance and the channel gain, we have

$$\begin{aligned} \bar{C} &= \mathbb{E}_{G_0, R_0}[\log_2(1 + \text{SNR})] \\ &= \int_0^\infty \mathbb{E}_{G_0} \left[ \log_2\left(1 + \frac{p_s G_0 \tilde{r}_0^{-\alpha}}{\sigma^2}\right) \right] f_{\tilde{R}_0}(\tilde{r}_0) d\tilde{r}_0. \end{aligned} \quad (13)$$

The inner integral comes from the expectation w.r.t.  $G_0$ .  $\square$

## IV. NUMERICAL RESULTS

In this section, we evaluate and compare the effect of the two association policies, i.e., the best server policy (BSP) which is analyzed above in this paper and the nearest server policy (NSP) in [3], on the performance of a LEO network. We also corroborate our analytical derivations through Monte Carlo simulations on the actual constellations.

Since most of the signal path is through the free space, we set the path loss exponent to  $\alpha = 2$ . The small-scale fading around the GT is assumed to be Rician with parameter  $K = 10$ . The CDF and the PDF of  $G_0$ , required to evaluate Propositions 1 and 2, are

$$F_{G_0}(g_0) = 1 - Q_1\left(\sqrt{2K}, \sqrt{g_0}\right) \quad (14)$$

and

$$f_{G_0}(g_0) = \frac{1}{2} e^{-\frac{g_0 + 2K}{2}} I_0\left(\sqrt{2Kg_0}\right), \quad (15)$$

respectively, where  $Q_1(\cdot, \cdot)$  denotes the Marcum Q-function and  $I_0(\cdot)$  is the modified Bessel function of the first kind. Shadowing is assumed to have a lognormal distribution which is represented as  $\mathcal{X}_0 = 10^{X_0/10}$  such that  $X_0$  has a normal distribution with mean  $\mu_s = 0$  and standard deviation  $\sigma_s = 9$  dB. Thus, the PDF of lognormal shadowing is

$$\begin{aligned} f_{\mathcal{X}_0}(x_0) &= \\ &= \frac{10}{\ln(10)\sqrt{2\pi}\sigma_s x_0} \exp\left(-\frac{1}{2}\left(\frac{10 \log_{10}(x_0) - \mu_s}{\sigma_s}\right)^2\right). \end{aligned} \quad (16)$$

The ground terminal is located on 25° latitude. The transmit power and the noise power are set to 50 dBm and -120 dBm, respectively. The operating frequency is assumed to be 13.5 GHz. For the reference simulated constellation, satellites are placed uniformly on circular orbits centered at Earth's center with radius  $r_\oplus + r_{\min}$ . Table I summarizes the simulation parameters used to generate the numerical results.

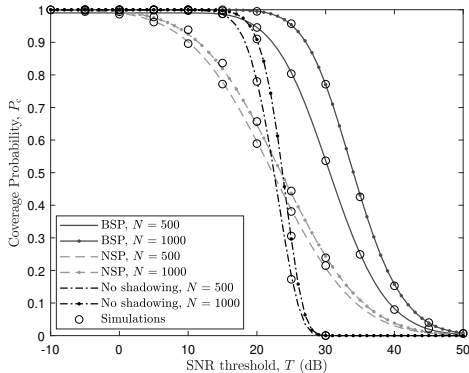


Fig. 2. Verification of Proposition 1 with simulations when  $K = 10$ ,  $\phi_u = 25^\circ$ ,  $\iota = 53^\circ$ ,  $r_{\min} = 500$  km, and  $\theta_{\min} = 10^\circ$ . The lines and the markers represent the analytical results and simulations, respectively.

Figure 2 depicts the coverage probability versus SNR threshold for BSP, NSP, and non-shadowing environment for  $N = 500$  and 1000 satellites. A fair match between the theory (plotted by lines) and the simulations (plotted by markers) is observed in the figure. As can be seen in the figure, the BSP results in a significantly better coverage probability compared to NSP, since the overall SNR at the receiver is improved by inclusion of shadowing in association policy. It is obvious that when shadowing is assumed to be zero, the two association techniques become the same.

The same as for the coverage probability, the BSP provides more reliable data rate compared to the NSP as shown in Fig. 3. We verify the expression given in Proposition 2 (depicted with lines) with simulations (depicted with markers). The data rate slightly decreases with increasing the inclination angle since the satellites' density decreases accordingly. Larger constellation size results in higher data rates due to more chance of being connected to the best possible server.

The effect of constellation size on coverage probability for BSP and NSP association techniques and two inclination angles of  $\iota = 53^\circ$  and  $\iota = 90^\circ$  are illustrated in Fig. 4. The SNR threshold is set to 10 dB. As expected, BSP shows a superior performance compared to NSP and the performance difference rises with increasing the constellation size. Smaller inclination angles result in higher coverage probability due to providing a higher density for a given number of satellites, especially when the constellation size is not too large. As the number of satellites exceeds a certain limit, the coverage probability saturates to a certain value, implying that increasing the constellation size does not always improve the performance (i.e., no better serving channel can be associated).

The data rate for different total number of satellites and inclination angles is depicted in Fig. 5. The curves follow the same behaviour as those in Fig. 4, which illustrates the better performance of BSP. As can be seen, when  $\sigma_s = 9$  dB,

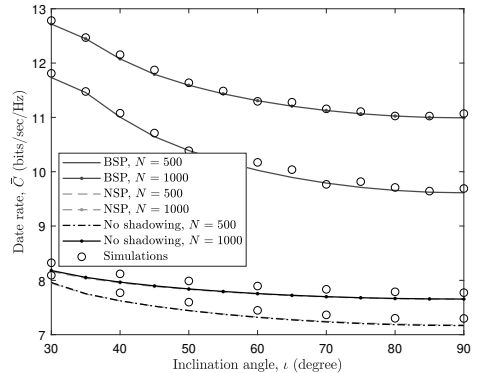


Fig. 3. Data rate versus inclination angle when  $K = 10$ ,  $\phi_u = 25^\circ$ ,  $r_{\min} = 500$  km, and  $\theta_{\min} = 10^\circ$ . The lines and the markers represent the analytical results and simulations, respectively.

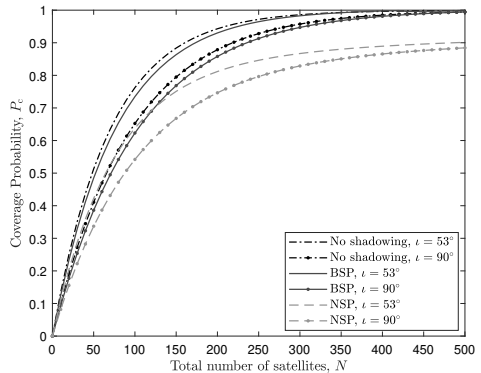


Fig. 4. Coverage probability versus constellation size when  $T = 10$  dB,  $K = 10$ ,  $\phi_u = 25^\circ$ ,  $\iota = 53^\circ$ ,  $r_{\min} = 500$  km, and  $\theta_{\min} = 10^\circ$ .

the effect of shadowing on NSP association is insignificant. Thus, we skipped plotting the results for non-shadowing case in Fig. 5 since they overlap the results of NSP.

## V. CONCLUSIONS

In this paper, the best server policy to assign a ground terminal to the best LEO satellite, which provides the highest SNR at the receiver, is studied and compared with conventional association techniques that only consider the distance between transceivers. Utilizing a nonhomogeneous Poisson point process to model the satellites' locality, enabled us to tractably analyze a LEO network for its two main performance metrics, i.e., the coverage probability and the data rate, while precisely capturing the characteristics of the actual physical network. As a result, the distribution of the serving distance based on BSP is derived mathematically which is a crucial parameter in network performance assessment. From the nu-

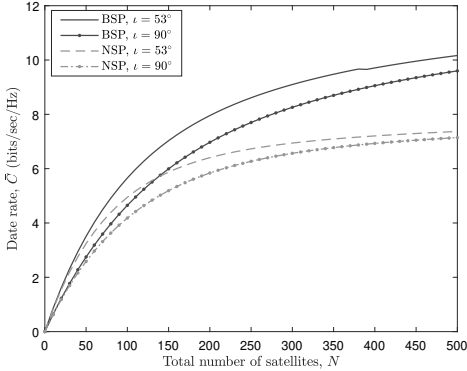


Fig. 5. Data rate versus constellation size when  $K = 10$ ,  $\phi_u = 25^\circ$ ,  $r_{\min} = 500$  km, and  $\theta_{\min} = 10^\circ$ .

merical results, other than verification of our derivations, we presented the coverage probability and the data rate in terms of different network parameters, e.g., inclination angle and the constellation size. The best serving policy resulted in a significantly better performance compared to the conventional nearest server policy for different network parameter settings.

## APPENDIX

### A. Proof of Lemma 2

The CDF of  $\tilde{R}_0$  is defined as

$$\begin{aligned}
 F_{\tilde{R}_0}(\tilde{r}_0) &= \mathbb{P}(\tilde{R}_0 < \tilde{r}_0) = \mathbb{E}_{\mathcal{N}} \left[ \mathbb{P}(\tilde{R}_0 < \tilde{r}_0) \mid \mathcal{N} = n \right] \\
 &= \sum_{n=0}^{\infty} P_n(\mathcal{A}(r_{\max})) \mathbb{P} \left( \min_n \left\{ \mathcal{X}_n^{-\frac{1}{\alpha}} R_n^{\text{vis}} \right\} < \tilde{r}_0 \right) \\
 &= \sum_{n=0}^{\infty} P_n(\mathcal{A}(r_{\max})) \\
 &\times \left( 1 - \mathbb{P} \left( \mathcal{X}_1^{-\frac{1}{\alpha}} R_1^{\text{vis}} > \tilde{r}_0, \dots, \mathcal{X}_n^{-\frac{1}{\alpha}} R_n^{\text{vis}} > \tilde{r}_0 \right) \right) \\
 &\stackrel{(a)}{=} \sum_{n=0}^{\infty} P_n(\mathcal{A}(r_{\max})) \left( 1 - (1 - F_{\tilde{R}_n}(\tilde{r}_0))^n \right), \quad (17)
 \end{aligned}$$

where  $\tilde{R}_n = \mathcal{X}_n^{-\frac{1}{\alpha}} R_n^{\text{vis}}$  and (a) follows from  $\{\tilde{R}_n\}$  being i.i.d. random variables. Since each  $\tilde{R}_n$  is the product of independent random variables  $R_n^{\text{vis}}$  and  $\mathcal{X}_n \triangleq \mathcal{X}_n^{-\frac{1}{\alpha}}$ , the product distribution is given by

$$F_{\tilde{R}_n}(\tilde{r}_0) = \int_0^{\infty} f_{Z_n}(z_n) F_{R_n^{\text{vis}}}\left(\frac{\tilde{r}_0}{z_n}\right) dz_n. \quad (18)$$

Substituting  $f_{Z_n}(z_n) = \alpha z_n^{-\alpha-1} f_{\mathcal{X}_n}(z_n^{-\alpha})$  and taking the derivative with respect to  $\tilde{r}_0$ , the CDF of  $\tilde{R}_0$  is obtained as given in Lemma 2.

## ACKNOWLEDGMENT

This research work was supported by a Nokia University Donation.

## REFERENCES

- [1] N. Okati, T. Riihonen, D. Korpi, I. Angervo, and R. Wichman, "Downlink coverage and rate analysis of low Earth orbit satellite constellations using stochastic geometry," *IEEE Transactions on Communications*, vol. 68, no. 8, pp. 5120–5134, Aug. 2020.
- [2] N. Okati and T. Riihonen, "Stochastic analysis of satellite broadband by mega-constellations with inclined LEOs," in *Proc. IEEE 31st Annual International Symposium on Personal, Indoor and Mobile Radio Communications*, Sep. 2020.
- [3] —, "Modeling and analysis of LEO mega-constellations as nonhomogeneous Poisson point processes," in *Proc. IEEE 93rd Vehicular Technology Conference*, Apr. 2021.
- [4] —, "Nonhomogeneous stochastic geometry analysis of massive LEO communication constellations," *IEEE Transactions on Communications*, Jan. 2022, early access.
- [5] A. Al-Hourani, "An analytic approach for modeling the coverage performance of dense satellite networks," *IEEE Wireless Communications Letters*, vol. 10, no. 4, pp. 897–901, Apr. 2021.
- [6] —, "Optimal satellite constellation altitude for maximal coverage," *IEEE Wireless Communications Letters*, vol. 10, no. 7, pp. 1444–1448, Mar. 2021.
- [7] A. Yastrebova *et al.*, "Theoretical and simulation-based analysis of terrestrial interference to LEO satellite uplinks," in *Proc. IEEE Global Communications Conference*, Dec. 2020.
- [8] A. Talgat, M. A. Kishk, and M.-S. Alouini, "Nearest neighbor and contact distance distribution for binomial point process on spherical surfaces," *IEEE Communications Letters*, vol. 24, no. 12, pp. 2659–2663, Dec. 2020.
- [9] —, "Stochastic geometry-based analysis of LEO satellite communication systems," *IEEE Communications Letters*, vol. 25, no. 8, pp. 2458–2462, Aug. 2021.
- [10] H. Lin *et al.*, "Fine-grained analysis on downlink LEO satellite-terrestrial mmWave relay networks," *IEEE Wireless Communications Letters*, vol. 10, no. 9, pp. 1871–1875, May 2021.
- [11] M. Mühleisen and B. Walke, "Analytical evaluation of LTE uplink performance in the IMT-Advanced Indoor Hotspot scenario," in *Proc. IEEE 22nd International Symposium on Personal, Indoor and Mobile Radio Communications*, Sep. 2011.
- [12] H. S. Dhillon and J. G. Andrews, "Downlink rate distribution in heterogeneous cellular networks under generalized cell selection," *IEEE Wireless Communications Letters*, vol. 3, no. 1, pp. 42–45, Nov. 2014.
- [13] D. Ohmann, A. Awada, I. Viering, M. Simsek, and G. P. Fettweis, "Best server SINR models for single- and multi-point transmission in wireless networks," in *Proc. IEEE Global Communications Conference*, Dec. 2015.
- [14] F. Vatalaro, G. E. Corazza, C. Caini, and C. Ferrarelli, "Analysis of LEO, MEO, and GEO global mobile satellite systems in the presence of interference and fading," *IEEE Journal on Selected Areas in Communications*, vol. 13, no. 2, pp. 291–300, Feb. 1995.
- [15] A. Ganz, Y. Gong, and B. Li, "Performance study of low Earth-orbit satellite systems," *IEEE Transactions on Communications*, vol. 42, no. 234, pp. 1866–1871, Feb. 1994.
- [16] H. M. Mourad, A. A. M. Al-Bassiouni, S. S. Emam, and E. K. Al-Hussaini, "Generalized performance evaluation of low Earth orbit satellite systems," *IEEE Communications Letters*, vol. 5, no. 10, pp. 405–407, Oct. 2001.
- [17] X. Lu, M. Salehi, M. Haenggi, E. Hossain, and H. Jiang, "Stochastic geometry analysis of spatial-temporal performance in wireless networks: A tutorial," *IEEE Communications Surveys and Tutorials*, Aug. 2021.
- [18] M. Haenggi, *Stochastic geometry for wireless networks*. Cambridge University Press, 2012.
- [19] B. Błaszczyszyn *et al.*, *Stochastic geometry analysis of cellular networks*. Cambridge University Press, 2018.
- [20] J. G. Andrews, F. Baccelli, and R. K. Ganti, "A tractable approach to coverage and rate in cellular networks," *IEEE Transactions on Communications*, vol. 59, no. 11, pp. 3122–3134, Nov. 2011.
- [21] H. S. Dhillon, R. K. Ganti, F. Baccelli, and J. G. Andrews, "Modeling and analysis of K-tier downlink heterogeneous cellular networks," *IEEE Journal on Selected Areas in Communications*, vol. 30, no. 3, pp. 550–560, Apr. 2012.
- [22] V. V. Chetlur and H. S. Dhillon, "Downlink coverage analysis for a finite 3-D wireless network of unmanned aerial vehicles," *IEEE Transactions on Communications*, vol. 65, no. 10, pp. 4543–4558, Oct. 2017.

## PUBLICATION 6

**Downlink and Uplink Low Earth Orbit Satellite Backhaul for Airborne  
Networks**

N. Okati and T. Riihonen

In *Proc. IEEE International Conference on Communications Workshops (ICC Workshops)*,  
May 2022

**Publication reprinted with the permission of the copyright holders.**



# Downlink and Uplink Low Earth Orbit Satellite Backhaul for Airborne Networks

Niloofer Okati and Taneli Riihonen

Faculty of Information Technology and Communication Sciences, Tampere University, Finland

e-mail: {niloofer.okati, taneli.riihonen}@tuni.fi

**Abstract**—Providing backhaul access for airborne networks ensures their seamless connectivity to other aerial or terrestrial users with sufficient data rate. The backhaul for aerial platforms (APs) has been mostly provided through geostationary Earth orbit satellites and the terrestrial base stations (BSs). However, the former limits the achievable throughput due to significant path loss and latency, and the latter is unable to provide full sky coverage due to existence of wide under-served regions on Earth. Therefore, the emerging low Earth orbit (LEO) Internet constellations have the potential to address this problem by providing a thorough coverage for APs with higher data rate and lower latency. In this paper, we analyze the coverage probability and data rate of a LEO backhaul network for an AP located at an arbitrary altitude above the ground. The satellites' locality is modeled as a nonhomogeneous Poisson point process which not only enables tractable analysis by utilizing the tools from stochastic geometry, but also considers the latitude-dependent density of satellites. To demonstrate a compromise on the backhaul network's selection for the airborne network, we also compare the aforementioned setup with a reference terrestrial backhaul network, where AP directly connects to the ground BSs. Based on the numerical results, we can conclude that, for low BS densities, LEO satellites provide a better backhaul connection, which improves by increasing the AP's altitude.

## I. INTRODUCTION

Connecting aerial platforms (APs), e.g., airplanes, unmanned aerial vehicles (UAVs), high altitude platforms (HAPs), etc. to the ground users or other APs is envisioned as a significant aspect in 6G airborne-terrestrial integration [1]. To satisfy the high demands of APs for data rate, a high quality backhaul connection is required to ensure the collection of data from/to the APs. One approach to provide backhaul for the airborne network is through geostationary satellites, which provide full sky coverage for most of the regions [2]–[4]. However, other than considerable delay caused by traveling the signal over a large distance, the received signal is subject to severe path loss which limits the achievable data rate significantly. Terrestrial base stations (BSs) can also serve as backhaul for the airborne network with considerably smaller path attenuation and latency [5]–[8]. The main drawback of the terrestrial network is the lack of full sky coverage due to huge under-served regions, e.g., oceans and deserts. Moreover, local operators may restrict the service for some global APs.

The emerging low Earth orbit (LEO) mega-constellation networks, with the primary intention to provide connectivity for remote and under-connected regions, have a great potential

to serve as backhuls for the APs due to offering less path attenuation and delay w.r.t. satellites on the geostationary orbit, and a better sky coverage w.r.t. the terrestrial network.

Along with rapid commercial progress of LEO mega-constellations, e.g., Starlink, OneWeb, Kuiper, and Telesat, their performance analysis when serving a ground gateway and/or user has attracted significant attention recently [9]–[15]. Stochastic geometry was deployed as the most promising tool for analytical understanding of such ultra-dense LEO networks. The first key step for stochastic geometry-based analysis is modeling the satellites' locality with a proper point process which not only facilitates the tractability of the derivations, but also captures the physical characteristics of the network. A Binomial point process (BPP) was used in [9], [10] to model a LEO constellation and derive the downlink coverage probability and data rate. Since the satellites' locations in actual constellations barely follow a uniform distribution, the inherent performance mismatch was adjusted numerically in [9], and analytically through finding the effective number of satellites for every user's latitude in [10].

To better address the uneven distribution of satellites on orbits, in [11] and [12], a nonhomogeneous Poisson point process (PPP) with a latitude-dependent intensity, was utilized to model the satellites' locations. In [13], [14], distance distributions and the coverage probability were formulated for a LEO network comprised of multiple concentric orbital shells, each of which has a known specific radius. The contact angle, i.e., the minimum angular distance between the satellites and the ground user, is characterized in [15] to evaluate the performance of a LEO network without considering the effect of shadowing attenuation. In [16], the distribution of conditional coverage probability was derived, given the nodes' positions, for a satellite-terrestrial relay network to evaluate the percentage of users that may reach a target SINR threshold. Estimation and characterization of Doppler shift is addressed in downlink LEO communication in [17].

Despite the significant utilization of stochastic geometry for UAV-to-ground communication analysis [5]–[8], its application on the study of LEO-backhauled APs has remained unrecognized. In [18], a LEO backhaul, by considering only a single orbit with few satellites at pre-determined positions, is studied for both terrestrial and aerial BSs. The throughput of both backhaul and access links is maximized jointly through radio resource management and UAV trajectory optimization. In [19], capacity and range of air-to-air and satellite networks

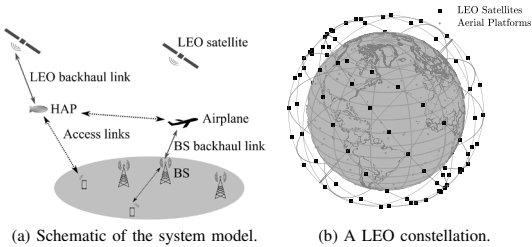


Fig. 1: An airborne network backhauled by either LEO or terrestrial network for uplink and/or downlink connections.

are evaluated as a backhaul for APs through simulations only. It was shown that integration of air-to-air communication and LEO satellites improves the data rate of APs significantly. Revenue maximization in LEO satellites in case of cooperation of LEO satellites and HAPs as data backhaul is studied in [20] for remote regions.

In this paper, we analyze the performance of a LEO satellite backhaul for an airborne network in terms of the coverage probability and the data rate. We model the satellites' locality as a nonhomogeneous PPP which leads to tractable analytical derivations as well as compensation for the latitude-dependent distribution of satellites over the spherical shell. Unlike the existing literature, the satellites are assumed to have directional antennas with their boresight radiating towards the AP. Moreover, we compare the performance of the described setup with the performance of the terrestrial backhaul which provides noteworthy criteria on the selection of the best backhaul for APs, depending on the constellation parameters, the density of ground BSs, and AP's location. Using the numerical results, we verify our derivations and illustrate the performance of both backhaul networks in terms of different system parameters.

## II. SYSTEM MODEL

Let us consider an airborne network, as in Fig. 1(a), which can be backhauled by either a LEO satellite network or the terrestrial BSs for both uplink and downlink directions. A high quality backhaul connection may facilitate the connectivity of APs in the airborne network to other APs or ground users via access links. Each AP is located at an arbitrary altitude and latitude, represented by  $a_{AP}$  and  $\phi_{AP}$ , respectively, above the Earth's surface, which is assumed to be a perfect sphere with radius  $r_{\oplus} \approx 6371$  km. Each AP may select the best backhaul connection, i.e., the one which provides better coverage and rate, between the LEO and the terrestrial network.

A LEO satellite backhaul to serve the airborne network is shown in Fig. 1(b). The satellite network comprises  $N$  satellites distributed uniformly on circular inclined orbits with altitude and inclination angle denoted by  $a_s$  and  $\iota$ , respectively. Obviously,  $a_s > a_{AP}$  or actually  $a_s \gg a_{AP}$ . The maximum distance at which an AP may communicate with a LEO

satellite (that is when the signal is not blocked by Earth) is

$$r_{\max} = \sqrt{2r_{\oplus}a_s + a_s^2} + \sqrt{2r_{\oplus}a_{AP} + a_{AP}^2}. \quad (1)$$

The satellites and APs are equipped with directional antennas with their main beam radiating towards the transceiver. The satellites' and the AP's antenna gains are denoted by  $G_s$  and  $G_{AP}$ , respectively, and  $G_t = G_{AP}G_s$  is the overall antenna gain. For terrestrial backhaul, the BS's antenna gain is denoted by  $G_{BS}$ , and  $G_t = G_{AP}G_{BS}$ . It is worth noting that the AP's antenna gain is different for LEO- and BS-backhauled connections. In this paper, we assume that APs connect to their nearest satellite/BS which will be referred to as the serving satellite/BS. As the network is equipped with directional antennas, the performance is assumed to be noise-limited. The signal-to-noise ratio (SNR) at the receiver can be expressed as

$$\text{SNR} = \begin{cases} \frac{p_s G_t H_s R_s^{-\alpha}}{\sigma^2}, & R_s \leq u, \\ 0, & \text{otherwise,} \end{cases} \quad (2)$$

where  $p_s$  is the transmission power and  $R_s$  is the distance between the AP and the serving satellite or BS with  $H_s$  being its corresponding channel gain. The constant  $\sigma^2$  is the additive noise power and  $\alpha$  is a path loss exponent. The upper limit  $u = r_{\max}$  for LEO backhaul and  $u \rightarrow \infty$  for terrestrial backhaul.

To facilitate tractable performance analysis of the described LEO backhaul network, we model the satellites as a nonhomogeneous Poisson point process. Such model not only enables us to tractably analyze the performance of a LEO backhaul network, but also models the varying density of satellites across different latitudes in the actual physical network by setting the intensity of nonhomogeneous PPP,  $\delta(\phi_s, \lambda_s)$ , to the actual distribution of satellites along different latitudes [11], [12]. When satellites are distributed uniformly on low Earth orbits, the intensity of nonhomogeneous PPP is a function of the satellites' latitudinal element,  $\phi_s$ , which is given as [11], [12]

$$\delta(\phi_s, \lambda_s) = \delta(\phi_s) = \frac{N}{\sqrt{2\pi^2(a_s + r_{\oplus})^2 \sqrt{\cos(2\phi_s) - \cos(2\iota)}}}. \quad (3)$$

By the definition of a nonhomogeneous PPP, the number of points in a bounded region  $\mathcal{A}$  of the orbital shell is a Poisson-distributed random variable denoted by  $\mathcal{N}$ . Therefore, the probability of existing  $n$  satellites in  $\mathcal{A}$  is given by

$$\begin{aligned} P_n(\mathcal{A}) &\triangleq \mathbb{P}(\mathcal{N} = n) \\ &= \frac{1}{n!} \left( \iint_{\mathcal{A}} \delta(\phi_s, \lambda_s) (a_s + r_{\oplus})^2 \cos(\phi_s) d\phi_s d\lambda_s \right)^n \\ &\quad \times \exp \left( - \iint_{\mathcal{A}} \delta(\phi_s, \lambda_s) (a_s + r_{\oplus})^2 \cos(\phi_s) d\phi_s d\lambda_s \right), \end{aligned} \quad (4)$$

where  $\delta(\phi_s, \lambda_s)$  is the intensity function of nonhomogeneous PPP at latitude  $\phi_s$  and longitude  $\lambda_s$ .

Following the conventional approach for modeling the locations of terrestrial BSs [21], we assume that the BSs are distributed as a homogeneous PPP with constant intensity, given by  $\delta_{BS}$ , on a flat plane.



### III. PERFORMANCE ANALYSIS

In this section, we derive analytical expressions for the coverage probability and data rate of the backhaul network. The distribution of the shortest distance between AP and the backhaul server, in terms of its cumulative density function (CDF) and probability density function (PDF), is a key parameter to evaluate the SNR characteristics, which is expressed in the following subsections.

#### A. Distance to the Serving Satellite or Base Station

In the following lemmas, we will obtain the PDF of the shortest distance between an AP and a LEO satellite or a terrestrial BS.

**Lemma 1.** *The PDF of the nearest distance between an AP with  $a_{\text{AP}} < a_s$  and a LEO satellite, when the satellites are distributed according to a nonhomogeneous PPP with intensity  $\delta(\phi_s)$ , is given by*

$$f_{R_s}(r_s) = 2r_s \left( \frac{a_s}{r_{\oplus}} + 1 \right) \exp(-\gamma(r_s)) \int_{\max(\phi_{\text{AP}} - \phi_{\text{max}}, -l)}^{\min(\phi_{\text{AP}} + \phi_{\text{max}}, l)} \delta(\phi_s) \frac{\cos(\phi_s)}{\sqrt{\cos^2(\phi_s - \phi_{\text{AP}}) - \cos^2(\phi_{\text{max}})}} d\phi_s, \quad (5)$$

where

$$\gamma(r_s) = 2(a_s + r_{\oplus})^2 \times \int_{\max(\phi_{\text{AP}} - \phi_{\text{max}}, -l)}^{\min(\phi_{\text{AP}} + \phi_{\text{max}}, l)} \delta(\phi_s) \cos(\phi_s) \cos^{-1} \left( \frac{\cos(\phi_{\text{max}})}{\cos(\phi_s - \phi_{\text{AP}})} \right) d\phi_s, \quad (6)$$

and  $r_s \in [a_s - a_{\text{AP}}, r_{\text{max}}]$  while  $f_{R_s}(r_s) = 0$  otherwise. The polar angle difference between the serving satellite and the AP is  $\phi_{\text{max}} = \cos^{-1} \left( \frac{(a_s + r_{\oplus})^2 + (a_{\text{AP}} + r_{\oplus})^2 - r_s^2}{2(a_s + r_{\oplus})(a_{\text{AP}} + r_{\oplus})} \right)$ .

*Proof.* For a nonhomogeneous PPP, the CDF of  $R_s$  can be written as

$$F_{R_s}(r_s) \triangleq 1 - \mathbb{P}(R_s > r_s) = 1 - \mathbb{P}(\mathcal{N} = 0),$$

where  $\mathbb{P}(\mathcal{N} = 0)$  is the void probability of PPP in  $\mathcal{A}(r_s)$  that can be obtained from (4) by setting  $n = 0$ . Thus,

$$F_{R_s}(r_s) = 1 - \exp \left( - \int_{\max(\phi_{\text{AP}} - \phi_{\text{max}}, -l)}^{\min(\phi_{\text{AP}} + \phi_{\text{max}}, l)} \beta(\phi_s) \delta(\phi_s) (a_s + r_{\oplus})^2 \cos(\phi_s) d\phi_s \right) = 1 - \exp \left( - 2(a_s + r_{\oplus})^2 \int_{\max(\phi_{\text{AP}} - \phi_{\text{max}}, -l)}^{\min(\phi_{\text{AP}} + \phi_{\text{max}}, l)} \delta(\phi_s) \cos(\phi_s) \times \cos^{-1} \left( \frac{\cos(\phi_{\text{max}})}{\cos(\phi_s - \phi_{\text{AP}})} \right) d\phi_s \right), \quad (7)$$

where  $\beta(\phi_s)$  is the longitude range inside the spherical cap above AP at latitude  $\phi_s$ . The latter equality follows from substitution of  $\beta(\phi_s)$  using the basic geometry. Taking the derivative of (7) with respect to  $r_s$  completes the proof. Note

that for  $\phi_{\text{max}} \leq |\phi_{\text{AP}}| - l$  the CDF given in (7) is zero since the spherical cap formed by polar angle  $\phi_{\text{max}}$  above the latitude  $\phi_{\text{AP}}$  is much farther from the constellation's borders to contain any satellite.  $\square$

Let us then derive the serving distance distribution of a reference setup, where an AP is served by the nearest terrestrial BS. The scenario corresponds to the case when there is a sufficient availability of BSs that can provide a high quality backhaul connection for APs. The following lemma represents the distribution of the shortest distance between an AP and a ground BS. Similar approach was used to obtain the nearest distance distribution for terrestrial networks [21] and UAV networks [5].

**Lemma 2.** *The PDF of the nearest distance between an AP and a ground BS, when the BSs are distributed according to a homogeneous PPP with constant intensity  $\delta_{\text{BS}}$ , is given by*

$$f_{R_s}(r_s) = 2\pi\delta_{\text{BS}}r_s \exp(-\pi\delta_{\text{BS}}(r_s^2 - a_{\text{AP}}^2)). \quad (8)$$

*Proof.* Assuming  $a_{\text{AP}} \ll r_{\oplus}$ , Earth is approximately seen as a flat plane from AP's point of view. Thus, using the definition of CDF and basic geometry, we have

$$F_{R_s}(r_s) \triangleq \mathbb{P}(R_s < r_s) = \mathbb{P} \left( \sqrt{a_{\text{AP}}^2 + D_s^2} < r_s \right) = F_{D_s} \left( \sqrt{r_s^2 - a_{\text{AP}}^2} \right), \quad (9)$$

where  $D_s$  is the distance from the serving BS to the projection of AP onto the ground plane. The complementary CDF of  $D_s$  at  $\sqrt{r_s^2 - a_{\text{AP}}^2}$  equals the null probability of the homogeneous PPP on a circle with radius  $\sqrt{r_s^2 - a_{\text{AP}}^2}$ , i.e.,  $F_{R_s}(r_s) = 1 - \exp(-\pi\delta_{\text{BS}}(r_s^2 - a_{\text{AP}}^2))$ . Taking the derivation with respect to  $r_s$  returns the PDF expression given in the lemma.  $\square$

In the following subsections, we utilize the distribution of the serving distance given in Lemmas 1 and 2 to obtain analytical derivations for the probability of coverage and the data rate of a LEO- or BS-backhauled airborne network.

#### B. Coverage Probability

The probability of SNR at the receiver being above a certain threshold value,  $T > 0$ , is named as coverage probability in telecommunication systems. Thus, whenever the received SNR is greater than the threshold level, the data can be transmitted successfully with error control coding.

**Proposition 1.** *The probability of network coverage for an arbitrarily located AP at an altitude, such that  $a_{\text{AP}} < a_s$ , under generally distributed fading is*

$$P_c(T) \triangleq \mathbb{P}(\text{SNR} > T) = \int_l^u \left( 1 - F_{H_s} \left( \frac{T r_s^\alpha G_t^{-1} \sigma^2}{p_s} \right) \right) f_{R_s}(r_s) dr_s, \quad (10)$$

where  $F_{H_s}(\cdot)$  is the CDF of the serving channel gain  $H_s$ . For LEO-backhauled AP,  $f_{R_s}(r_s)$  is given in Lemma 1,  $u = r_{\text{max}}$

TABLE I: Simulation Parameters

Parameters	Values
Path loss exponent, $\alpha$	2
Rician factor for LEO-backhauled channel, $K$	20
Rician factor for BS-backhauled channel, $K$	5
Transmit power for LEO-backhauled connection, $p_s$	50 dBm
Transmit power for BS-backhauled connection, $p_s$	40 dBm
Noise power, $\sigma^2$	-120 dBm
Carrier frequency for LEO-backhauled connection	13.5 GHz
Carrier frequency for BS-backhauled connection	2 GHz
AP altitude	10 km

and  $l = a_s - a_{AP}$ , while for BS-backhauled AP,  $f_{R_s}(r_s)$  is given in Lemma 2,  $u = \infty$  and  $l = a_{AP}$ .

*Proof.* To obtain (10), we start with the definition of coverage probability:

$$\begin{aligned}
 P_c(T) &= \mathbb{E}_{R_s} [\mathbb{P}(\text{SNR} > T | R_s)] \\
 &= \int_l^u \mathbb{P}(\text{SNR} > T | R_s = r_s) f_{R_s}(r_s) dr_s \\
 &= \int_l^u \mathbb{P}\left(H_s > \frac{T r_s^\alpha G_t^{-1} \sigma^2}{p_s}\right) f_{R_s}(r_s) dr_s, \quad (11)
 \end{aligned}$$

The proof is completed by substituting the complementary CDF of  $H_s$ .  $\square$

### C. Average Data Rate

In the following proposition, we will derive the average achievable data rate (in bits per channel use) which is defined as the ergodic capacity derived from the Shannon–Hartley theorem over a fading communication link normalized to unit bandwidth, i.e.,  $\bar{C} \triangleq \mathbb{E}[\log_2(1 + \text{SNR})]$ .

**Proposition 2.** *The average rate (in bits/s/Hz) of an arbitrarily located AP at an altitude, such that  $a_{AP} < a_s$ , under generally distributed fading is*

$$\bar{C} = \int_l^u \int_0^\infty \log_2\left(1 + \frac{p_s G_t h_s r_s^{-\alpha}}{\sigma^2}\right) f_{H_s}(h_s) f_{R_s}(r_s) dh_s dr_s, \quad (12)$$

where  $f_{H_s}(h_s)$  represents the PDF of the serving channel gain  $H_s$ . For LEO-backhauled AP,  $f_{R_s}(r_s)$  is given in Lemma 1,  $u = r_{\max}$  and  $l = a_s - a_{AP}$ , while for BS-backhauled AP,  $f_{R_s}(r_s)$  is given in Lemma 2,  $u = \infty$  and  $l = a_{AP}$ .

*Proof.* Taking the expectation over the serving distance and the channel gain, we have

$$\begin{aligned}
 \bar{C} &= \mathbb{E}_{H_s, R_s} [\log_2(1 + \text{SNR})] \\
 &= \int_l^u \mathbb{E}_{H_s} \left[ \log_2\left(1 + \frac{p_s G_t H_s r_s^{-\alpha}}{\sigma^2}\right) \right] f_{R_s}(r_s) dr_s, \quad (13)
 \end{aligned}$$

and the expectation renders the inner integration in (12).  $\square$

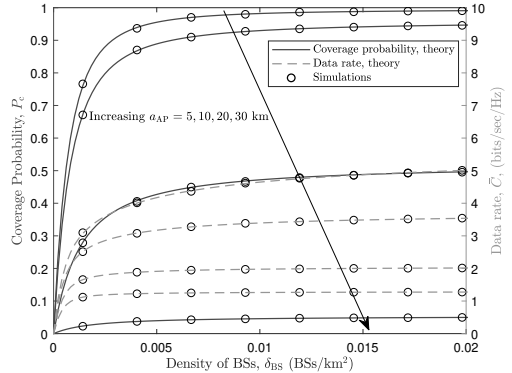


Fig. 2: Coverage probability and data rate provided by a terrestrial backhaul for some aerial platforms at different altitudes.

## IV. NUMERICAL RESULTS AND DISCUSSION

In this section, we provide numerical results to study the effect of different network parameters on coverage probability and average data rate of the LEO and terrestrial backhaul networks for APs, using the analytical expressions obtained in Section III. Furthermore, we verify all the analytical derivations through Monte Carlo simulations in Matlab.

We consider the large-scale attenuation with path loss exponent  $\alpha = 2$ , and the small-scale fading is assumed to be Rician with parameter  $K$ . Thus, the CDF and the PDF of  $H_s$ , required to evaluate Propositions 1 and 2, are  $F_{H_s}(h_s) = 1 - Q_1(\sqrt{2K}, \sqrt{h_s})$  and  $f_{H_s}(h_s) = \frac{1}{2} e^{-\frac{h_s + 2K}{2}} I_0(\sqrt{2K h_s})$ , respectively, where  $Q_1(\cdot, \cdot)$  denotes the Marcum Q-function and  $I_0(\cdot)$  is the modified Bessel function of the first kind.

The altitude of AP is set to 10 km, unless stated otherwise. The satellites' antenna gains within their beamwidth are approximated by a constant gain of 34 dBi. For LEO-backhauled connection, APs are equipped with antennas which radiate towards the sky with constant gain of 3 dBi, while for BS-backhauled communication, both AP and BS are assumed to have unity gain antennas.

The transmit power is set to 40 dBm and 50 dBm for terrestrial and satellite backhauled, respectively, and their corresponding operating frequency is assumed to be 2 GHz and 13.5 GHz. The noise power is set to -120 dBm. For the reference simulations, satellites are placed uniformly on orbits centered at Earth's center with radius  $r_\oplus + a_s$ . The simulation parameters are summarized in Table I.

Figure 2 illustrates the coverage probability and data rate provided by the terrestrial backhaul for APs at different altitudes. The BSs are assumed to be distributed according to a homogeneous PPP on a disc with radius 30 km. As can be seen, for higher density of BSs and lower APs' altitudes, the terrestrial backhaul provides better probability of coverage and data rate. However, for very low densities, which correspond to

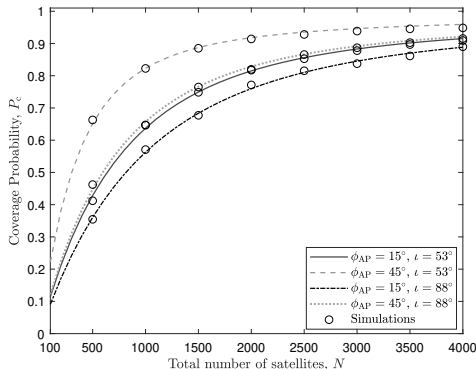


Fig. 3: Coverage probability versus the total number of satellites when  $a_s = 500$  km,  $a_{AP} = 10$  km, and  $T = 5$  dB.

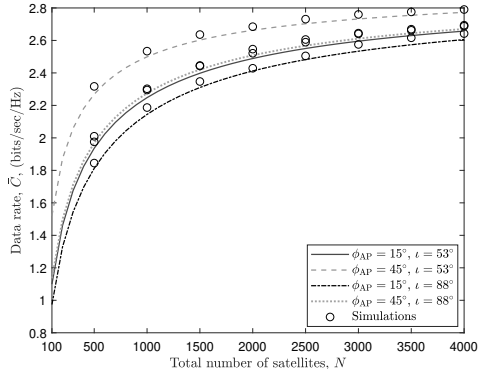


Fig. 4: Data rate versus the total number of satellites when  $a_s$  and  $a_{AP}$  are 500 km and 10 km, respectively.

under-served regions, as well as for high altitudes of APs, the performance of the terrestrial network degrades considerably, especially in terms of the coverage probability.

The effect of the total number of satellites on the coverage probability and data rate of a LEO-backhauled AP are illustrated in Figs. 3 and 4, respectively. The performance is depicted for different AP's latitudes and constellation inclination angles. A better visibility is provided by increasing the constellation size which leads to more promising performance in terms of both metrics. For higher AP's latitude the performance is better due to higher density of satellites at those latitudes and, consequently, the availability of closer satellites to serve the AP. As shown in the figures, lower inclination angles also provide higher rate and coverage due to higher density for those constellations, i.e., the same amount of satellites are distributed on a smaller region of the spherical shell. Since  $a_s \gg a_{AP}$ , the performance is only slightly affected by varying the altitude of AP.

The probability of coverage and the data rate of a LEO backhaul network versus the altitude of the constellation are depicted in Figs. 5 and 6, respectively. As can be seen in the figures, the smallest inclination angle and the highest AP's latitude provide better performance in terms of both performance metrics due to the availability of more visible satellites to the AP. Since the signal is exposed to more severe path loss when traveling over a larger distance, the performance degrades accordingly by increasing the constellation altitude.

The effect of AP's altitude on the data rate of both terrestrial and LEO backhauls are shown in Fig. 7. Despite the terrestrial backhaul, the data rate for LEO backhaul slightly improves by rising the AP's altitude due to the increase in visibility and the decrease in the serving distance, which results in smaller path loss. However, since the altitude of AP is notably smaller than the constellation altitude, the variation in the data rate is not significant. The altitude range over which the LEO backhaul outperforms the terrestrial backhaul is highly affected by the

density of BSs.

Based on the numerical results, it can be interpreted that both terrestrial and LEO networks have the potential to serve as the backhaul for the airborne network. Selecting the best backhaul depends on several factors such as the LEO constellation parameters, the BS density, and AP's location. For instance, terrestrial backhaul can provide higher data rate than the LEO satellites, when the BS density is large or when the AP is located at very high latitudes, out of the constellation inclination limits. On the other hand, the AP is better to be LEO-backhauled if the density of BS is extremely low or the AP's altitude is excessively high. It is also worth noting that in highly dense urban areas where the transmission from the BSs is subject to severe blockage due to the surrounding obstacles, a LEO backhaul can provide better connectivity to the AP due to having a higher probability of line-of-sight.

## V. CONCLUSIONS

In this paper, we studied the performance of LEO mega-constellation as a backhaul for an airborne network. Modeling the satellites locality as a nonhomogeneous Poisson point process enabled us to tractably analyze the performance of a LEO backhaul network, while precisely capturing the characteristics of the actual physical network by setting the intensity of PPP to the actual density of satellites along different latitudes. For sake of comparison, we also evaluated the performance when APs are backhauled by terrestrial networks. From the numerical results, other than verification of our derivations, we presented the coverage probability and the data rate in terms of different system parameters, e.g., constellation altitude, total number of satellites, inclination angle, and AP's location. Based on the results, it is concluded that a LEO backhaul can provide more promising performance in terms of both coverage probability and data rate when the terrestrial BSs' density is low and/or APs' altitude is significantly high.

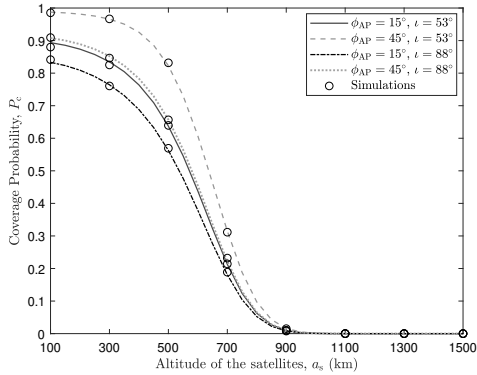


Fig. 5: Coverage probability versus the altitude of the constellation when  $N = 1000$ ,  $a_{AP} = 10$  km, and  $T = 5$  dB.

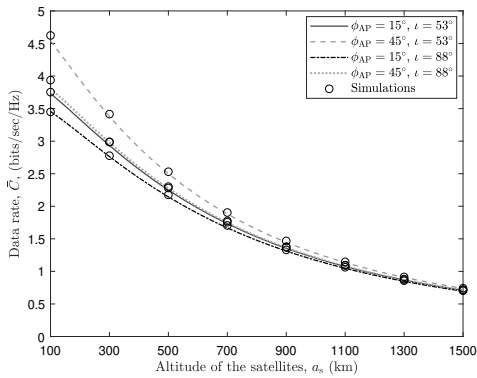


Fig. 6: Data rate versus the altitude of the constellation when  $N = 1000$  and  $a_{AP} = 10$  km.

## REFERENCES

- [1] S. Kota and G. Giambene, "6G integrated non-terrestrial networks: Emerging technologies and challenges," in *Proc. IEEE International Conference on Communications Workshops (ICC Workshops)*, Jul. 2021.
- [2] Y. Zhu, W. Bai, M. Sheng, J. Li, D. Zhou, and Z. Han, "Joint UAV access and GEO satellite backhaul in IoRT networks: Performance analysis and optimization," *IEEE Internet of Things Journal*, vol. 8, no. 9, pp. 7126–7139, May 2021.
- [3] J. Wang, C. Jiang, Z. Wei, C. Pan, H. Zhang, and Y. Ren, "Joint UAV hovering altitude and power control for space-air-ground IoT networks," *IEEE Internet of Things Journal*, vol. 6, no. 2, pp. 1741–1753, Oct. 2019.
- [4] Y. Wang, Y. Xu, Y. Zhang, and P. Zhang, "Hybrid satellite-aerial-terrestrial networks in emergency scenarios: a survey," *China Communications*, vol. 14, no. 7, pp. 1–13, Aug. 2017.
- [5] V. V. Chetlur and H. S. Dhillon, "Downlink coverage analysis for a finite 3-D wireless network of unmanned aerial vehicles," *IEEE Transactions on Communications*, vol. 65, no. 10, pp. 4543–4558, Oct. 2017.
- [6] A. Al-Hourani, S. Chandrasekharan, G. Kaandorp, W. Glenn, A. Jamalipour, and S. Kandeepan, "Coverage and rate analysis of aerial base stations," *IEEE Transactions on Aerospace and Electronic Systems*, vol. 52, no. 6, pp. 3077–3081, Dec. 2016.
- [7] M. M. Azari, F. Rosas, K.-C. Chen, and S. Pollin, "Ultra reliable UAV communication using altitude and cooperation diversity," *IEEE Transactions on Communications*, vol. 66, no. 1, pp. 330–344, Jan. 2018.

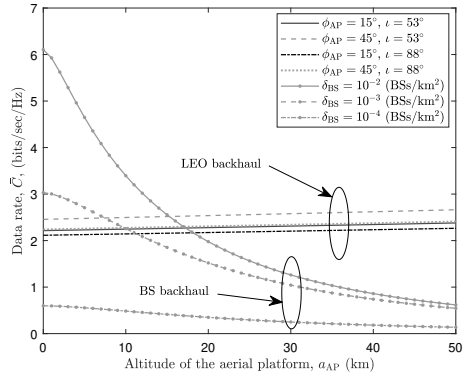


Fig. 7: Data rate versus the altitude of the aerial platform (AP) for LEO and BS backhaul networks. The LEO constellation size and altitude are set to 1000 and 500 km, respectively.

- [8] P. S. Bithas, V. Nikolaidis, A. G. Kanatas, and G. K. Karagiannidis, "UAV-to-ground communications: Channel modeling and UAV selection," *IEEE Transactions on Communications*, vol. 68, no. 8, pp. 5135–5144, May 2020.
- [9] N. Okati, T. Riihonen, D. Korpi, I. Angervo, and R. Wichman, "Downlink coverage and rate analysis of low Earth orbit satellite constellations using stochastic geometry," *IEEE Transactions on Communications*, vol. 68, no. 8, pp. 5120–5134, Aug. 2020.
- [10] N. Okati and T. Riihonen, "Stochastic analysis of satellite broadband by mega-constellations with inclined LEOs," in *Proc. IEEE 31st Annual International Symposium on Personal, Indoor and Mobile Radio Communications*, Sep. 2020.
- [11] —, "Modeling and analysis of LEO mega-constellations as nonhomogeneous Poisson point processes," in *Proc. IEEE 93rd Vehicular Technology Conference*, Apr. 2021.
- [12] —, "Nonhomogeneous stochastic geometry analysis of massive LEO communication constellations," *IEEE Transactions on Communications*, Jan. 2022, early access.
- [13] A. Talgat, M. A. Kishk, and M.-S. Alouini, "Stochastic geometry-based analysis of LEO satellite communication systems," *IEEE Communications Letters*, Oct. 2020.
- [14] —, "Nearest neighbor and contact distance distribution for binomial point process on spherical surfaces," *IEEE Communications Letters*, vol. 24, no. 12, pp. 2659–2663, Dec. 2020.
- [15] A. Al-Hourani, "An analytic approach for modeling the coverage performance of dense satellite networks," *IEEE Wireless Communications Letters*, vol. 10, no. 4, pp. 897–901, Apr. 2021.
- [16] H. Lin, C. Zhang, Y. Huang, R. Zhao, and L. Yang, "Fine-grained analysis on downlink LEO satellite-terrestrial mmWave relay networks," *IEEE Wireless Communications Letters*, May 2021.
- [17] I. Ali, N. Al-Dhahir, and J. Hershey, "Doppler characterization for LEO satellites," *IEEE Transactions on Communications*, vol. 46, no. 3, pp. 309–313, Mar. 1998.
- [18] A. H. Arani, P. Hu, and Y. Zhu, "Re-envisioning space-air-ground integrated networks: Reinforcement learning for link optimization," in *Proc. IEEE International Conference on Communications (ICC)*, Aug. 2021.
- [19] M. Vondra, M. Ozger, D. Schupke, and C. Cavdar, "Integration of satellite and aerial communications for heterogeneous flying vehicles," *IEEE Network*, vol. 32, no. 5, pp. 62–69, Sep. 2018.
- [20] Z. Jia, M. Sheng, J. Li, D. Zhou, and Z. Han, "Joint HAP access and LEO satellite backhaul in 6G: Matching game-based approaches," *IEEE Journal on Selected Areas in Communications*, vol. 39, no. 4, pp. 1147–1159, Apr. 2021.
- [21] J. G. Andrews, F. Baccelli, and R. K. Ganti, "A tractable approach to coverage and rate in cellular networks," *IEEE Transactions on Communications*, vol. 59, no. 11, pp. 3122–3134, Nov. 2011.

## PUBLICATION 7

**Stochastic Coverage Analysis for Multi-Altitude LEO Satellite Networks**

N. Okati and T. Riihonen

*IEEE Communications Letters*, under review after major revision

**Publication reprinted with the permission of the copyright holders.**





